

3rd International Conference on Science, Ecology and Technology

ICONSETE'2017

Rome, ITALY • August 14-16, 2017

**3rd INTERNATIONAL CONFERENCE ON SCIENCE
ECOLOGY AND TECHNOLOGY
(ICONSETE'2017)
Rome, ITALY**

August 14-16, 2017

PROCEEDINGS BOOK



**3rd INTERNATIONAL CONFERENCE ON
SCIENCE, ECOLOGY AND TECHNOLOGY
(ICONSETE'2017)**

PROCEEDINGS BOOK



**Rome-ITALY
14-16 August, 2017**

EDITORS

Prof. Dr. Uğur USLU
Assist. Prof. Dr. Deniz ULUKUŞ
Assist. Prof. Dr. İbrahim UYANIK
Assoc. Prof. Dr. Adem Alpaslan ALTUN

© Her hakkı saklıdır. Bu kitabın tamamı ya da bir kısmı, yazarlarının izni olmaksızın, elektronik, mekanik, fotokopi ya da herhangi bir kayıt sistemi ile çoğaltılamaz, yayınlanamaz, depolanamaz. Bu kitaptaki bilgilerin her türlü sorumluluğu yazarına aittir.

ISBN: 978-605-2338-04-9

© Konya, Aralık 2017
PALET YAYINLARI
Mimar Muzaffer Caddesi Rampalı Çarşı No. 42 Konya
Tel. 0332 353 62 27
e-mail: paletyayinevi@gmail.com
www.paletyayinlari.com

COMMITTEES

General Coordinator of Conference

Prof. Dr. Uğur USLU, Selçuk University, TURKEY

Conference Co-Chairman

Assoc. Prof. Dr. Adem Alpaslan ALTUN, Selçuk University, TURKEY

Organizing Committee

Prof. Dr. Mehmet TÜMAY, Adana Science and Technology University, TURKEY

Prof. Dr. Ahmet Kağan KARABULUT, Selçuk University, TURKEY

Prof. Dr. Cristiano POLETO, Federal University of Technology - Parana (UTFPR), BRAZIL

Prof. Dr. Fahrettin TILKI, Artvin Çoruh University, TURKEY

Prof. Habil. Dr. Arūnas Ramanavičius, Vilnius University, LITHUANIAN

Prof. Dr. Jose A. Lopez-Sanchez, The University of Liverpool, UNITED KINGDOM

Prof. Dr. Xiaoxi WANG, Henan University of Technology, CHINA

Prof. Dr. Wale ADENIRAN, Osun State University, NIGERIA

Assist. Prof. Dr. Berrin OKKA, Konya University, TURKEY

Conference Secretary

Assist. Prof. Dr. Deniz ULUKUŞ, Selçuk University, Konya, TURKEY

Scientific Committee

Prof. Dr. Amir Khalaf Aziz AL, DARVWAH, University of Baghdad, IRAQ

Prof. Dr. Cristiano POLETO, Federal University of Technology - Parana (UTFPR), BRAZIL.

Prof. Dr. Enrico CILIBERTO, Catania University, ITALY.

Prof. Dr. Fernando SA Neves SANTOS, Guarda Politechnic Institute, Guarda PORTUGAL.

Prof. Dr. Ferruh YILDIZ, Selçuk University, TURKEY

Prof. Dr. George VARVOUNIS, Organic Chem. & Biochem. Sec., Department of Chemistry, University of Ipannia, GREECE.

Prof. Dr. Harold M. Van ES, Cornell University, USA.

Prof. Dr. Jesus SIMAL-GANDARA, Analy. Chem. & Food Sci. Dep. Food Sci. & Tech. Fac. University of Vigo, Ourense, SPAIN.

Prof. Dr. Jiri BAREK, Charles University, Prague, CZECH REPUBLIC.

Prof. Dr. Juraj LADOMERSKY, Technical University in Zvolen, SLOVAKIA.

Prof. Dr. M. Kemal ÇİFTÇİ, Selçuk University, TURKEY.

Prof. Dr. M. Tariq JAVED, University of Agriculture, PAKISTAN.

Prof. Dr. Markuz ARBENZ, IFOAM, FRANCE.

Prof. Dr. Mehmet OKKA, Selçuk University, TURKEY

Prof. Dr. Mohammed RIHANI, University Chouaib Doukkali of El Jadida, MOROCCO.

Prof. Dr. Mohd Marsin SANAGI, University Teknologi Malaysia, MALAYSIA.

Prof. Dr. Muhammad ASHFAQ, University of Agriculture, PAKISTAN.

Prof. Dr. Muhammad Subhan QURESHI, Agricultural University, PAKISTAN.

Prof. Dr. Mustafa KÜÇÜKÖDÜK, Selçuk University, TURKEY.

Prof. Dr. Ong Say LEONG, The National University of Singapore, SINGAPORE.

Prof. Dr. Piotr WARSZYNSKI, J. Haber Institute of Catalysis and Surface Chemistry, Krakow, POLAND.

Prof. Dr. Prosun BHATTACHARYA, KTH Royal Institute of Technology, SWEDEN.

Prof. Dr. Said WAHAB, The University of Agriculture, PAKISTAN.

Prof. Dr. Sherin Ahmed SHERIF, Alexandria University, EGYPT.

Prof. Dr. Spase SHUMKA, Agriculture Univesity, ALBANIA.

Prof. Dr. Tahir BALEVİ, Selçuk University, TURKEY.

Prof. Dr. Teodor RUSU, University of Agricultural Sciences and Veterinary Medicine Cluj, ROMANIA.

Prof. Dr. Victor A. DRYBAN, Head of Department of Rock Pressure National Academy of Sciences of Ukraine, UKRAINE.

Prof. Dr. Victor STAROV, Loughborough University, UK.

Prof. Dr. Victoria DUTSCHK, Twente University, NETHERLANDS.

Prof. Dr. Wan Aini Wan IBRAHIM, Universiti Teknologi Malaysia, MALAYSIA.

Prof. Dr. Zdravka LAZAROVA, AIT Austrian Institute of Tecnology Gmbh, AUSTRIA.

Assoc. Prof. Dr. Adem Alpaslan ALTUN, Selçuk University, TURKEY.

Assoc. Prof. Dr. Fetullah ARIK, Selçuk University, TURKEY.

Assoc. Prof. Dr. Hakan ERTİN, İstanbul University, TURKEY.

Dr. Bonga ZUMA, Rhodes University, (ENGLAND), SOUTH AFRICA.

Dr. Darlina Md. NAİM, Universiti Sains Malaysia, MALAYSIA.

Dr. David M. SAXOWSKY, North Dakota State University, USA.

Dr. İbrahim UYANIK, Selçuk University, TURKEY.

Dr. Kokom KOMARIAH, Sebelas MaretUniversity, INDONESIA.

Dr. Rabha BENNAMA, University of Mostaganem, ALGERIA.

Dr. Muhammed Kamil ÖDEN, Selçuk University, TURKEY

Dr. Reza Shahriyar KAMRAI, School of Medicine, Tehran University of Medical Sciences, IRAN.

Dr. Rudi Hari MURTI, Gadjah Mada University, Yogyakarta, INDONESIA.

Dr. Seema DHAIL, JayotiVidyapeeth Womens University, INDIA.

Dr. Shazia SHAFIQUE, Institute of Agricultural Sciences University of the Punjab, PAKISTAN.

Dr. Sutrisno Hadi PURNOMO, Sebelas Maret University, INDONESIA.

CONFERENCE INFORMATION

Conference Date

The ICONSETE'2017 – Rome conference is held between August 14-16, 2017.

Conference Venue

Yunus Emre Enstitüsü Rome/ITALY

Language

The official language of the conference is **English**.

Conference Website

Further information and updates about the conference can be found at

[http:// http://www.2017.iconsete.org](http://http://www.2017.iconsete.org)

About Presentations:

Oral Presentations

A slide projector and a computer will be available in the presentation rooms. Each presenter will have 10 minutes for his/her presentation and 5 minutes for discussions.

Poster Presentations

Poster should be prepared according to the poster template (80 cm width and 120 cm height).

The poster presenters are kindly requested to stand in front of their own posters during the poster sessions to answer arising questions. The posters should be hanged/withdrawn by the presenters.

Contact:

info@2017.iconsete.org

iconsete2017@gmail.com

İÇİNDEKİLER / CONTENTS

Numerical Investigation on Thermal Analysis of Military Helmet with PCM

Erhan Akyol, Çiğdem Susantez, Kamil Kahveci, Oktay Hacihafizoğlu.....1

Changes in the Midday Water Potential in Anatolian Black Pine After the Late Precommercial Thinning

A. Deligoz, E. Bayar, Y. Karatepe, M. Genc, F.G. Cankara.....15

Comparison Of Gripper Designs For Robotic Kiwi Fruit Harvesting

Erhan Kahya , Selçuk Arın.....23

Variation of total soluble sugar content in Anatolian Black Pine stands applied precommercial thinning

E. Bayar, A. Deligoz..... 33

Performance Analysis of EEG Signal Classification and SSVEP in OpenVibe

Harun ÇİĞ, M. Fatih TÜYSÜZ.....40

Thermodynamic Analysis of a Gas Turbine

Ugur Akyol, Ercan Özdemir.....54

Flow Rate Estimation Modelling in a Transmission Pipeline Using Response Surface Methodology (RSM)

Ugur Akyol, Tuğrul Akyol, A. Deniz Karaoğlan, Bedri Yüksel Asiye Aslan.....63

Environmental Impact of No-Till Farming

Davut Karayel76

The Applications of No-tillage in Turkey

S. Altikat, E. Kus, H.K. Kucukerdem, Z. Gozubuyuk.....85

Short-Term Load Forecasting Model Using Flower Pollination Algorithm

Volkan ATEŞ Murat LÜY Necaattin BARIŞÇI3 Ertuğrul ÇAM.....98

Characterization of Volatile Compounds of Shade-Dried Lavender (*Lavandula stoechas*) Flowers by Purge & Trap Technique

Onur Sevindik, Ahmet Salih Sonmezdag, Gamze Guclu, Hasim Kelebek, Serkan Selli.....110

Assessment of Genetic Diversity of *Psephellus aucherianus* complex in Turkey using SSR Markers

Meryem BOZKURT.....118

Investigation of Physical and Chemical Properties of Drinking Water of Iğdir University Sehit Bülent Yurtseven Campus

Bingul Z., Ozturk E., Yigit A., Turhan Irak Z., Altikat A..... 128

Improving Water Leaching Resistance of Fire Retardants in Wood	
Suat ALTUN	137
Energy and Exergy Analysis of an Organic Rankine Cycle Using Different Working Fluids from Waste Heat Recovery	
E. Ozdemir, M. Kilic.....	149
Finding the Overlapping Modules in Weighted Complex Networks	
Yılmaz Atay, Murat Aslan, Halife Kodaz.....	163
Colour Feature-Based Classification of Wheat Grain Using ANN with Bayesian Regularization Learning Algorithm	
A. Kayabasi, B. Yildiz, K. Sabanci, E. Yigit, A. Toktas, M. Tekbas	174
Photovoltaic (PV) Covered Electricity Demand Of A Building With Non-Optimal Inclination And Orientation	
Rustu Eke, Cihan Demircan.....	187
An Approach Based on Recursive Largest First (RLF) Algorithm to Solving the Graph Coloring Problem Using a Hybrid Selection Strategy	
Murat Aslan, Yılmaz Atay.....	201
Effect of Surface Roughness on Wettability of Adhesive on Wood Substrates	
H. Yorur, A. M. Erer, S. Oğuz.....	217
Classification of Bread and Durum Wheat Using ELM and ANN	
K. Sabanci, M. F. Aslan, E. Yigit, A. Kayabasi, A. Toktas, H. Duysak.....	224
Engineering Materials For The Improvement Of Thermal Comfort During Immersion	
Vesna Marija Potočić Matković, Ivana Salopek Čubrić, Goran Čubrić.....	236

NUMERICAL INVESTIGATION ON THERMAL ANALYSIS OF MILITARY HELMET WITH PCM

Erhan Akyol*¹, Çiğdem Susantez², Kamil Kahveci³ and Oktay Hacıhafizoğlu⁴

^{1, 2, 3, 4} Department of Mechanical Engineering, Engineering Faculty, Trakya University,
TURKEY.

(E-mail: erhanakyol@trakya.edu.tr, cigdemsusantez@trakya.edu.tr, kamilk@trakya.edu.tr,
oktayh@trakya.edu.tr)

Corresponding Author's e-mail: erhanakyol@trakya.edu.tr

ABSTRACT

During hot days, soldiers may suffer because of temperature rise inside their helmet. On the other hand, taking out helmet has risks especially during operations. Phase change materials (PCM) are substances which can start melting relatively at low temperatures with respect to other materials which are solid in room temperature and provide cooling effect due to its latent heat. Phase change materials with their high thermal energy storage capacity have extensive usage area in free cooling applications. Using PCM inside the helmet enables the soldier to be in thermal comfort for a certain time interval. In this study, a new military helmet with PCM, heat collector and gel pad was designed. This study also includes the thermal analysis inside the military helmet with PCM for different external air temperatures and convection heat transfer coefficients. Results show that the time interval when the soldier is in thermal comfort is considerably affected from convection heat transfer coefficient and external air temperature. After the PCM completely liquidized, inner surface temperature of the helmet increases rapidly. In that case in order to have thermal comfort conditions again, the portable PCM pouch can easily be removed and solidified in an appropriate cold medium.

Keywords: Helmet, latent heat, phase change material (PCM), thermal comfort

1. INTRODUCTION

During recent years the attraction on the use of phase change materials (PCMs) for thermal energy storage has been increased considerably due to their high thermal energy storage capacity. They can also store or release thermal energy at the desired temperatures and this causes it is practical for many applications. The usage of PCMs for thermal applications is considerably wide such as air conditioning, electronic cooling, free cooling applications in building and automobiles.

PCMs can be classified according to types of compound (organic, inorganic and eutectic PCMs), their operating temperatures (low, medium and high temperature PCMs) [13]. Organic PCMs are paraffin and non-paraffin. Although organic PCM's are chemically stable and have a high latent heat of fusion, their low thermal conductivity limits their applications. Inorganic PCMs are salt hydrates and metallic. They not only have high latent heat of fusion and good thermal conductivity, but also they are not flammable and expensive.

Because of its wide usage area PCMs have been the subject of many studies. Hosseini *et al.* [1] performed a numerical and experimental study on the heat transfer pipe with PCM. They obtained the result that heat transfer from the heat transfer pipe to the PCM is considerably effected by natural convection at the melting layer section. Moreover, increasing the inlet water temperature decreases the total melting time considerably. Darzi *et al.* [2] numerically investigated melting behavior of PCM in a concentric and eccentric cylindrical tubes. In their study they considered inner cylindrical tube as hot wall and outer tube is isolated. When the inner cylinder tube moves toward down the center of the cylinder, it has been observed that the speed of melting increased rapidly because of dominance of natural convection heat transfer in the PCM. Shatikian [3] studied on the process of melting and solidification of paraffin wax with fins. He presented how the melting rate, melting front profile and heat transfer effected by the boundary conditions and geometry of the system as a result. In the review paper of Sharma *et al.* [4], they focused thermal energy storages (TES) systems with PCM and mentioned melt fraction studies related to the PCMs. Kahveci and Akal [13] numerically investigated heat transfer and fluid flow in a heat exchanger with a plate type storage including phase change material. They found that the cooling performance is considerably depends on the mass flow rate.

There is a limited number of study about the thermal analysis of the helmet in the literature. Ghani *et al.* [5] performed numerical and experimental study on the miner's helmet cooling performance at different environmental conditions. In their study, they take account the effects of the solar radiation, forced convection and PCM on the helmet's thermal performance. They also investigated that influence of sweating on mass and heat transfer of the modeled head. They observed the temperature of the helmet internal air channel decreased from 47 °C to 40.6 °C. Tan and Fok [6] proposed design of a PCM cooled motorcycle helmet by using thermal resistance networks. Their design is substantially practical because of the detachable PCM porch and cooling effect of the head up to 2h. Sharifpour *et al.* [7] have numerically investigated the thermal comfort of the motorcycle helmet using $\text{CaCl}_2 \cdot 6\text{H}_2\text{O}$ as PCM. According to their results the melting period of PCM improves with the thickness of the PCM section.

It is important that for soldier to be in thermal comfort especially during operation. As it can be seen from literature that there is no enough study about design and cooling of military helmet. Therefore, in this study a new design of military helmet with PCM has been proposed to ensure the soldier to be in thermal comfort for a time interval.

2. MATERIAL AND METHODS

In this study, a new design of helmet has been proposed. It consists of gel cushion, Aluminium as heat collector, PCM and Kevlar 49 from the inside to the outside of the helmet respectively. The coordinate system and the geometry with dimensions used in this study are given in Fig. 1. Geometric dimensions of the helmet and thermophysical properties of materials composing the helmet are given in Table 1 and Table 2 respectively. Thermophysical properties of the materials are assumed to be constant. As it has been known that phase change materials (PCM) are substances which can start melting relatively at low temperatures with respect to other materials which are solid in room temperature, it is possible to design a helmet which enables the soldier to be in thermal comfort for a certain time interval by using PCMs with high latent heat and melting temperature near the 22°C. RT22HC corresponds these needs and is has been used for this study.

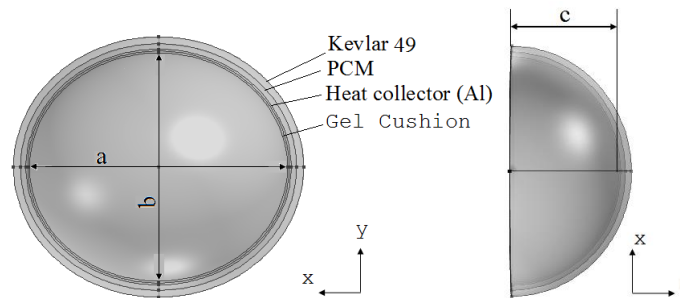


Figure 1. Geometry and the coordinate system

Table 1. Geometric dimensions

a	$283 \cdot 10^{-3} \text{ m}$	[8]
b	$250 \cdot 10^{-3} \text{ m}$	[8]
c	$134 \cdot 10^{-3} \text{ m}$	[8]
Thickness of Kevlar 49	$t_{\text{KEVLAR}} = 7.6 \cdot 10^{-3} \text{ m}$	[8]
Thickness of PCM	$t_{\text{PCM}} = 6 \cdot 10^{-3} \text{ m}$	
Thickness of Al	$t_{\text{Al}} = 2 \cdot 10^{-3} \text{ m}$	
Thickness of gel cushion	$t_{\text{gel}} = 2 \cdot 10^{-3} \text{ m}$	

Table 2. Thermophysical properties of the materials

Material	k (W/mK)	ρ (kg/m ³)	c (J/kgK)	Ref.
Kevlar 49	0.04	1440	1420	[9]
PCM (RT22HC, T _s =20°C, T _i =23°C)	0.2	760	2000	[10]
Al (Alloy 2024-T6)	177	2770	875	[11]
Gel cushion (Gel 8010)	3	2700	1000	[12]

The temperature distribution inside the helmet has been investigated for different convection heat transfer coefficients ($h=5, 10, 15, 20 \text{ W/m}^2\text{K}$) and external air temperatures ($T_{\text{air}}=30, 35, 40, 45^\circ\text{C}$). It was assumed that convection heat transfer coefficient was same for the whole helmet geometry exposed to external air. The inside of the helmet has a boundary condition of constant heat flux. Because the heat generated by the wearer head is 116W/m^2 [6]. Latent heat for the RT22HC is 170 kJ/kg [13]. The proposed three dimensional model for the military helmet has been solved by using Comsol Multiphysics finite element and simulation software.

Governing equations are as followings.

$$\rho_{gel}c_{gel}\frac{\partial T}{\partial t} = \vec{\nabla} \cdot (k_{gel}\vec{\nabla}T) \quad \text{for gel cushion} \quad (1)$$

$$\rho_{Al}c_{Al}\frac{\partial T}{\partial t} = \vec{\nabla} \cdot (k_{Al}\vec{\nabla}T) \quad \text{for heat collector} \quad (2)$$

$$\rho_{PCM}c_{PCM}\frac{\partial T}{\partial t} = \vec{\nabla} \cdot (k_{PCM}\vec{\nabla}T) + S_H \quad \text{for PCM} \quad (3)$$

$$\rho_{Kev}c_{Kev}\frac{\partial T}{\partial t} = \vec{\nabla} \cdot (k_{Kev}\vec{\nabla}T) \quad \text{for Kevlar 49} \quad (4)$$

where ρ , c , k and T are density, specific heat, thermal conductivity and temperature respectively. The source term for the PCM layer is defined as following.

$$S_H = -\rho_{PCM} L \frac{\partial \beta}{\partial T} \frac{\partial T}{\partial t} \quad (5)$$

where L is latent heat for the RT22HC and β is melt fraction. It can be defined as follows.

$$\beta = \begin{cases} 0 & \text{if } T \leq T_s \\ \frac{T - T_s}{T_l - T_s} & \text{if } T_s < T < T_l \\ 1 & \text{if } T \geq T_l \end{cases} \quad (6)$$

The entire geometry was assumed initially at a constant temperature of 18 °C. This means PCM is at the solid phase before the soldier wear the helmet. Boundary conditions on the contact surfaces of materials arises from the continuity of the heat flux and thermal equilibrium on these surfaces.

Initial and boundary conditions are given as followings.

$$T_0 = 18 \text{ } ^\circ\text{C} \quad (7)$$

$$-\vec{n} \cdot (-k_{Kev} \vec{\nabla} T) = h(T_{air} - T) \quad \text{on the outer surface of the helmet} \quad (8)$$

$$-\vec{n} \cdot (-k_i \vec{\nabla} T) = h(T_{air} - T) \quad \text{on the thin surface (on xy plane in Fig.1)} \quad (9)$$

$i = gel, Al, PCM, Kev$

$$-\vec{n} \cdot (-k_{gel} \vec{\nabla} T) = q_o = 116 \text{ W/m}^2 \quad \text{on the inner surface of the helmet} \quad (10)$$

$$\vec{n} \cdot (\vec{q}_1 - \vec{q}_2) = 0, \quad \text{on contact surfaces (Gel-Al, Al-PCM and PCM-Kevlar 49)} \quad (11)$$

$$T_1 = T_2$$

1 and 2 subscripts show the inner and outer mediums respectively and \vec{n} is the unit normal vector.

As the thickness of the PCM layer is thin, the effect of the fluid flow in the liquid phase due to buoyancy forces to the temperature distribution is neglected. Surface average values of the helmet inner temperature have been calculated and presented for all investigated parameters.

$$T_{ave} = \frac{1}{A_{in}} \int_{A_{in}} T dA \quad (12)$$

3. RESULTS AND DISCUSSION

The numerical results were obtained for convection heat transfer coefficient values of 5, 10, 15, 20 W/m²K and external air temperature values of 30, 35, 40, 45°C by Comsol Multiphysics finite element and simulation software. GMRES (Generalized Minimal Residual) solver has been used. Physics-controlled mesh has been applied for the geometry. The related properties of the mesh used for the new designed military helmet with PCM are presented in Table 3.

Table 3. Mesh properties

Number of tetrahedral elements	Number of triangular elements	Number of edge elements	Number of degrees of freedom
866113	169322	7848	115284

Gel cushion has been preferred for the inner layer of the helmet in order to primarily provide comfort and create a heat transfer medium between head and Aluminium layer. Aluminium layer serves as a heat collector, it transfers heat generated from the head to the PCM layer by conduction. In the design of the military helmet, the geometry has been simplified by subtracting the parts which are not in contact with the head and without changing any dimensions taken from the Edirne Provincial Gendarmerie Command.

The temperature simulations after 1 hour for $h=5$ W/m²K and $h=20$ W/m²K have been presented on Fig. 2 and 3 respectively. One can conclude from the results that temperature inside the helmet increases with h and T_{air} . But this small bottom area of the helmet shown on Fig. 2 and 3 is exposed to convective heating by the medium at the temperature of T_{air} . Because of that reason these figures can cause mistakable results for the sensitive prediction of the temperature inside the material composing the helmet. On the other hand, it has been exactly concluded from the Fig. 2 and 3 that the inner temperature inside the helmet maintains around 22°C after 1 h and this means that the soldier head is in thermal comfort. In Fig. 4,

volume average temperatures of each material have been computed for $h=20 \text{ W/m}^2\text{K}$ and $T_{\text{air}}=40^\circ\text{C}$. It has been

observed from Fig. 4 that while volume average values of the gel cushion and Al layer temperatures are exactly same with the surface average value of the helmet inner temperature, that of PCM layer temperature is a bit lower than the surface average value of the helmet inner temperature and that of Kevlar 49 layer temperature is higher than the surface average value of the helmet inner temperature. The volume average temperature value of Kevlar 49 intersects with the surface average value of the helmet inner temperature at about 38°C . It is expected result that the volume average temperature value of Kevlar 49 higher than others. Because it is in contact with the surrounding hot air and because of its low thermal conductivity it is relatively less effected by the cooling effect of the PCM layer. On the other hand, PCM layer has the lowest value of the average temperature. Because it is at the origin of the cooling effect.

$$T_{vol.ave} = \frac{1}{V} \int_V T dV \quad (13)$$

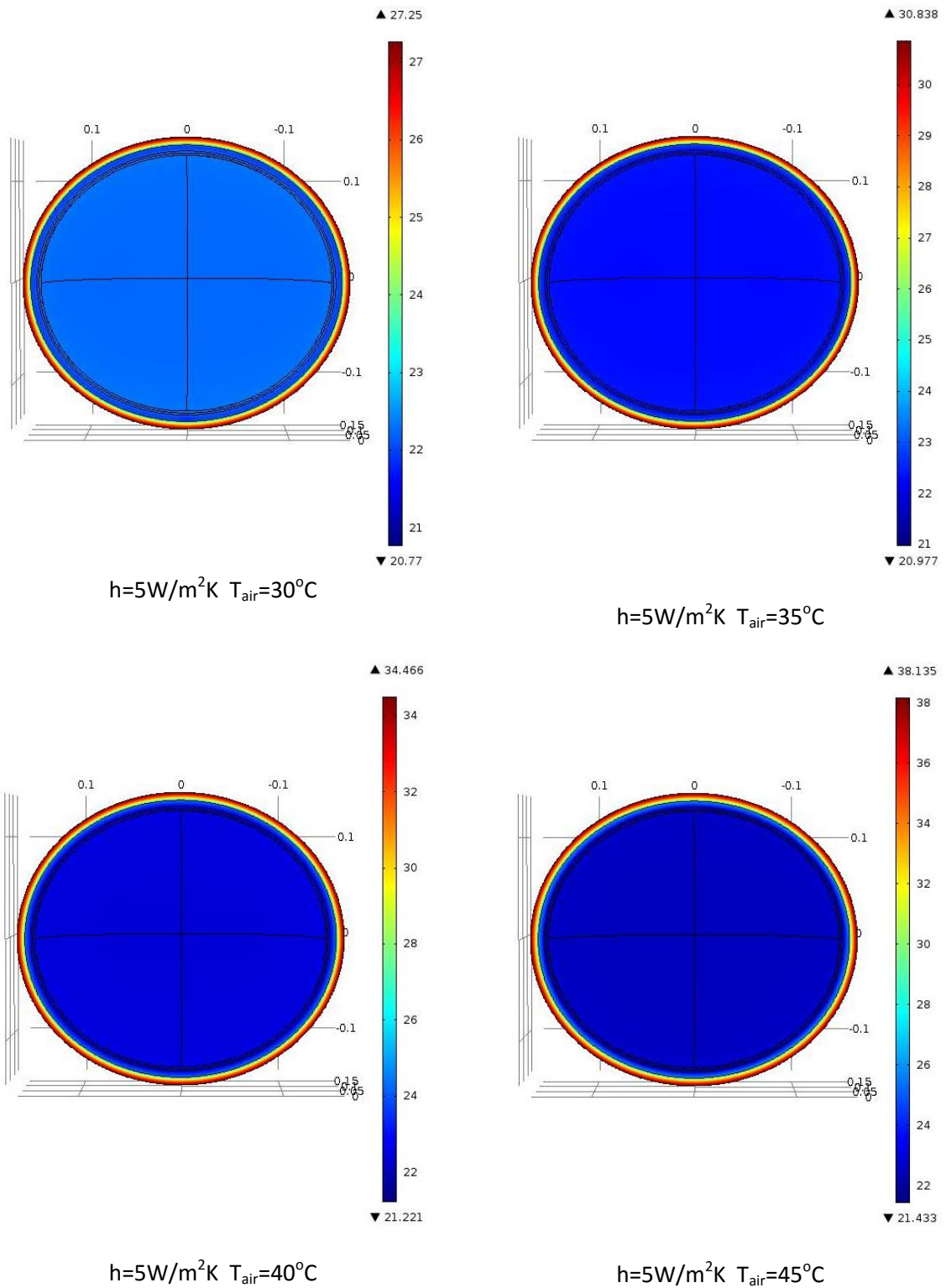


Figure 2. Temperature distribution inside the helmet after 1h for $h=5\text{W/m}^2\text{K}$

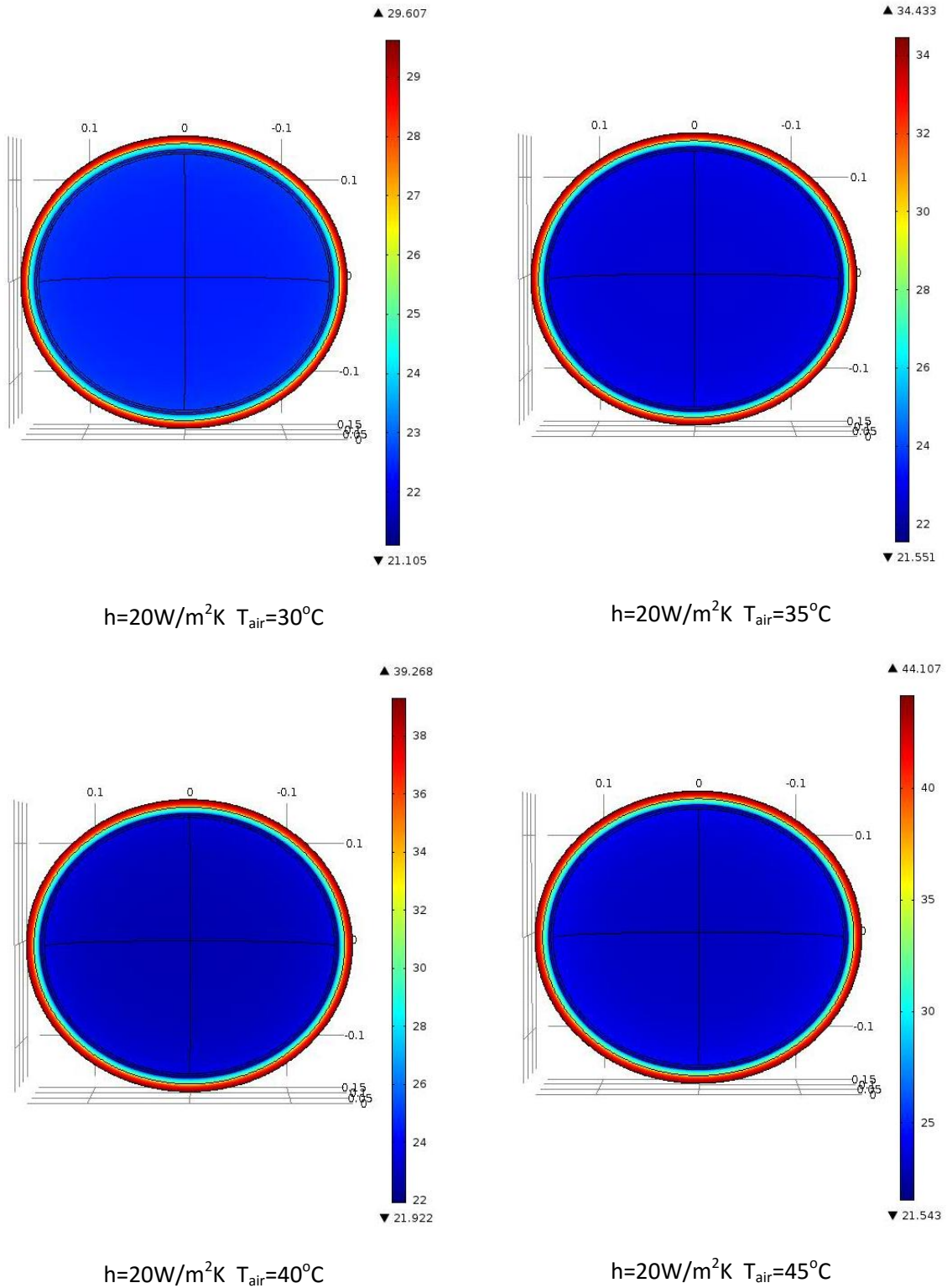


Figure 3. Temperature distribution inside the helmet after 1h for $h=20\text{W/m}^2\text{K}$

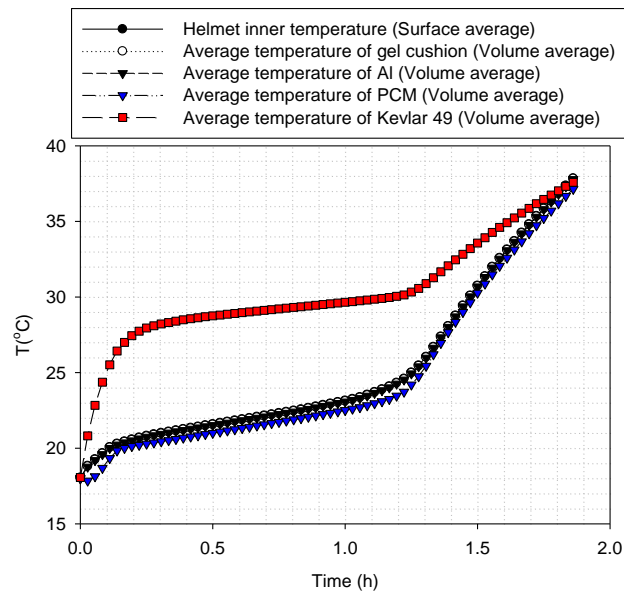


Figure 4. Volume average temperatures of gel, Al, PCM and Kevlar 49 with average temperature of the inner surface of the helmet for $h=20 \text{ W/m}^2\text{K}$ and $T_{\text{air}}=40^\circ\text{C}$.

According to the presented results in Fig. 5-8, one can conclude that surface average values of the helmet inner temperature with PCM increases with the convection heat transfer coefficient and external air temperature. After the PCM completely liquidized, inner surface temperature of the helmet increases rapidly. As human sweats to keep his or her core head temperature below 39°C by cooling effect of evaporation [5], the presented results for the average temperature of the inner surface of the helmet don't exceed 38°C in this study. Although sweating depends on many factors as metabolism rate, relative humidity of the air other than external air temperature, it has been also assumed that the person doesn't sweat at lower temperatures than 38°C .

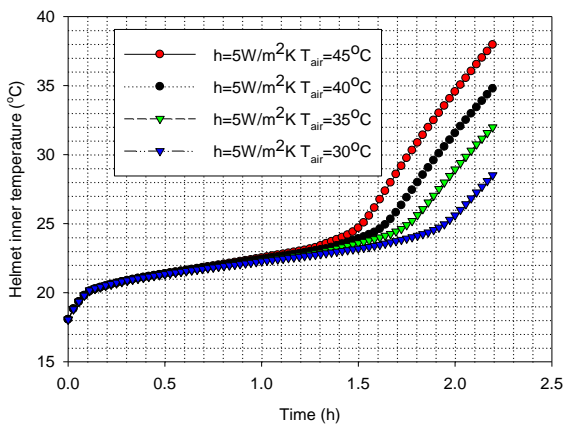


Figure 5. Average values of helmet inner temperature with PCM for $h=5\text{W/m}^2\text{K}$

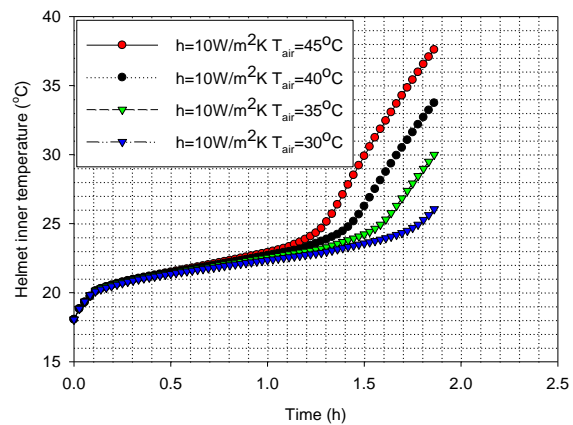


Figure 6. Average values of helmet inner temperature with PCM for $h=10\text{W/m}^2\text{K}$

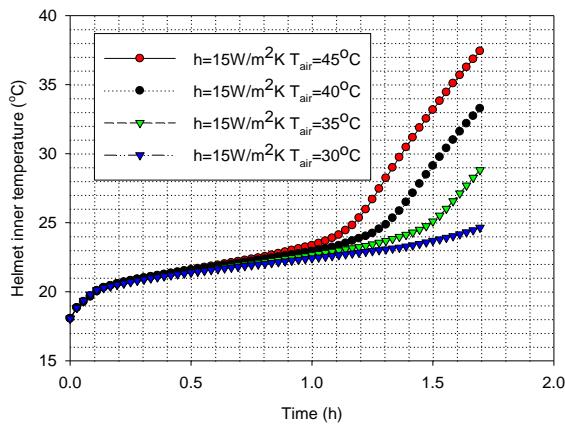


Figure 7. Average values of helmet inner temperature with PCM for $h=15W/m^2K$

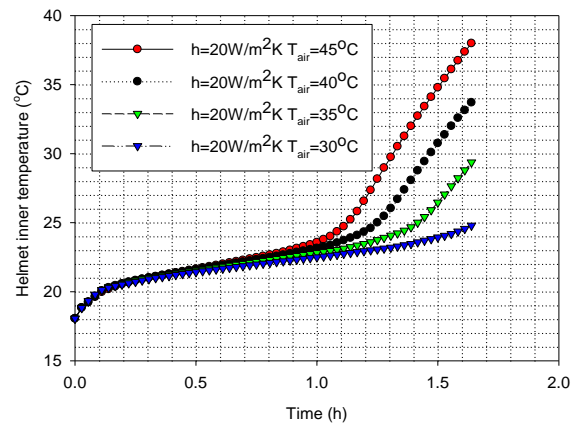


Figure 8. Average values of helmet inner temperature with PCM for $h=20W/m^2K$

On the other hand, same analyses have been performed for the helmet without PCM layer by keeping the thickness of the other materials and inner dimensions of the helmet same as the helmet with PCM. Presented results in Fig. 9 show that using PCM inside the helmet prolong considerably the time interval when the soldier head is in thermal comfort.

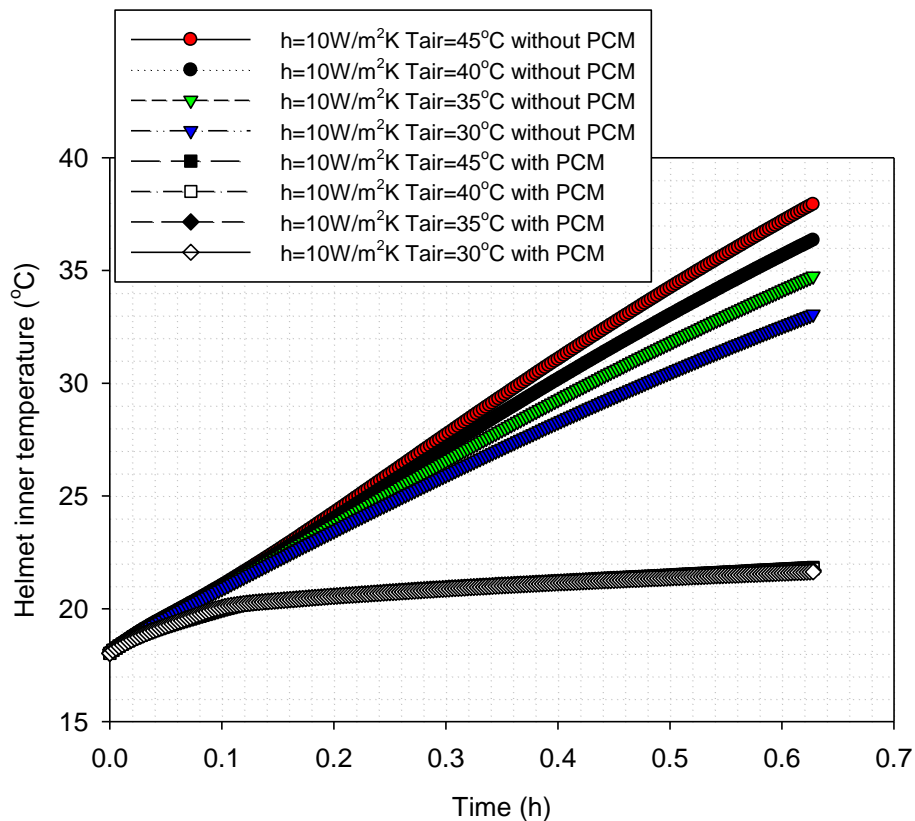


Figure 9. Comparison of the average values of helmet inner temperature with and without PCM

4. CONCLUSION

Heat transfer inside the new designed military helmet with and without PCM has been numerically investigated. It has been concluded that using PCM inside the helmet considerably increases the time interval when the the soldier is in thermal comfort. Results also show that the time interval for the thermal comfort is strongly affected by convection heat transfer coefficient and external air temperature. A soldier wearing this new designed helmet will be in thermal comfort for a longer time when the convection heat transfer coefficient and external air temperature are relatively low.

NOMENCLATURE

a, b, c: Geometric dimensions for the helmet (m)
c: Specific heat (J/kgK)
h: Convection heat transfer coefficient (W/m²K)
k: Thermal conductivity (W/mK)
L: Latent heat (J/kg)
 \vec{n} : Unit normal vector
S_H: Source term (W/m³)
T: Temperature (°C)
T₀: Initial temperature (°C)
T_l: Liquefied temperature (°C)
T_s: Solidified temperature (°C)
 \vec{q} : Heat flux vector (W/m²)
q_o: Heat flux from the inner surface of the helmet (W/m²)
t: Thickness (mm), time (s)
V: Volume (m³)

Greek symbols

β : Melt fraction
 ρ : Density (kg/m³)

Subscripts

1, 2: represents the inner and outer mediums

A: Area (m²)

air: Air

Al: Aluminium

ave: Average

in: Inner

gel: Gel

KEVLAR: Kevlar 49

PCM: Phase change material

vol. ave: Volume average

ACKNOWLEDGMENT

The authors would like to acknowledge Edirne Provincial Gendarmerie Command for the geometric dimensions of the military helmet.

REFERENCES

- [1] M. J. Hosseini, A. A. Ranjbar, K. Sedighi and M. Rahimi, 2012. A combined experimental and computational study on the melting behavior of a medium temperature phase change storage material inside shell and tube heat exchanger. *International Communications in Heat and Mass Transfer* 39 1416-1424.
- [2] A.A.R. Darzi, M. Farhadi and K. Sedighi, 2012. Numerical study of melting inside concentric and eccentric horizontal annulus. *Applied Mathematical Modelling* 36 4080-4086.
- [3] V. Shatikian, 2004. *Melting And Solidification Of A Phase-Change Material With Internal Fins*, M.Sc. Thesis, Department of Mechanical Engineering, Faculty of Engineering Sciences, Ben-Gurion University of the Negev, Israel.
- [4] A. Sharma, V.V. Tyagi, C.R. Chen and D. Buddhi, 2009. Review on thermal energy storage with phase change materials and applications. *Renewable and Sustainable Energy Reviews* 13 318-345.
- [5] S. Ghani, E.M.A.A. Elbially, F. Bakochristou, S.M.A. Gamaledin and M.M. Rashwan, 2017. The effect of forced convection and PCM on helmets' thermal performance in hot and arid environments. *Applied Thermal Engineering* 111 624–637.
- [6] F.L. Tan and S.C. Fok, 2006. Cooling of helmet with phase change material. *Applied Thermal Engineering*. 26 2067–2072.
- [7] E. Sharifpour, M. Farrokhnia, F. Golzar and Gh. Karimi, 2012. Improving thermal comfort of motorcycle helmet by using phase change materials. *20th Annual International Conference on Mechanical Engineering-ISME2012* ISME2012-3008.

[8] <http://www.tekbim.msb.gov.tr>

[9] Technical Guide Kevlar Aramid Fiber

(http://www.dupont.com/content/dam/dupont/products-and-services/fabrics-fibers-and-nonwovens/fibers/documents/Kevlar_Technical_Guide.pdf)

[10] Rubitherm Phase Change Material, Data Sheet, www.rubitherm.com

(https://www.rubitherm.eu/media/products/datasheets/Techdata_RT22HC_EN_29062016.PDF)

[11] T.L. Bergman, A.S. Lavine, F.P. Incropera and D.P. Dewitt, Fundamentals of Heat and Mass Transfer, John Wiley & Sons, U.S.A. 2011.

[12] Parker Chomerisc, www.parker.com

(<https://www.parker.com/literature/Chomerics/Parker%20ChomericsGel-8010-Gel30.pdf>)

[13] K. Kahveci and D. Akal, 2016. A numerical investigation on free cooling by a PCM-Heat exchanger. *Thermotechnica*. Supliment 1/2016 32-36.

CHANGES IN THE MIDDAY WATER POTENTIAL IN ANATOLIAN BLACK PINE AFTER THE LATE PRECOMMERCIAL THINNING

A. Deligoz¹, E. Bayar¹, Y. Karatepe¹, M. Genc², F.G. Cankara¹

¹ Süleyman Demirel University, Faculty of Forestry, Isparta, TURKEY.

(E-mail: aysedeligoz@sdu.edu.tr, esrabayar@sdu.edu.tr, yasinkaratepe@sdu.edu.tr)

²Giresun University, Faculty of Tourism, Giresun, TURKEY

(E-mail: msgnc61@gmail.com)

Corresponding Author's e-mail: aysedeligoz@sdu.edu.tr

ABSTRACT

In this study, changes midday xylem water potential after late precommercial thinning in the naturally regenerated Anatolian black pine [*Pinus nigra* Arn. subsp. *pallasiana* (Lamb.) Holmboe] stand was studied at Gölhisar forest districts in the Western Mediterranean region of Turkey. Three levels of late precommercial thinning - heavy (spacing varied between 3.0 to 3.5 m), moderate (spacing varied between 2.0 to 2.5 m), and unthinned control - were established in early 2015. Midday xylem water potential, soil moisture and temperature were measured during the first growing seasons following late precommercial thinning. The days were selected to correspond approximately to the beginning, the middle and the end of the growing season. Midday xylem water potential was varied significantly with thinning the beginning and the end of the growing season, but the treatment impact was not significant the middle of the growing season. At the end of the growing season following thinning, thinned trees had higher midday xylem water potential compared with unthinned control. Soil moisture content was generally lower in the unthinned control than the thinned treatments. Soil temperature was always greater on the thinned plots.

Keywords: *Pinus nigra*, soil moisture, stand, thinning, xylem water potential.

1. INTRODUCTION

Turkey has a rich plant biodiversity because of its geographic position, topography and climate. In parallel to this ecological richness, its forests are also rich in term of both species and composition. The total area of forest in Turkey is 22.342.925 hectares, which consists of pure and mixed forests [1]. Anatolian black pine is one of the importance forest tree species in Turkey, because of its great economic, aesthetic and ecological importance. It occurs through Turkey excluding Eastern Black Sea, Eastern and South-eastern geographical and ecological

regions of Turkey [2]. The forests of this species cover an area of 4.2 million hectares in Turkey. There is total 2.727.524 ha of stands suitable for natural regeneration of Anatolian

Black Pine [1]. Regeneration coming from natural regeneration, during especially good seed years, can be very dense. Overstocked stands have greater competition and stress. More competition and stress leads to mortality and lower growth rates. In very dense Anatolian black pine stands, the stands density needs to be regulated and thus requiring precommercial thinning to reduce density.

Precommercial thinning is a silvicultural operation, it primarily used to improve growing conditions of remaining trees in young stands [3]. The timing (i.e. the height of a stand at the time of thinning) and intensity (i.e. the spacing of a stand) of precommercial thinnings affect the yield and quality development of young stands. Precommercial thinning considerably enhanced the diameter development [4], [5]. Thinning has also an important effect on water balance. The increase of the soil water reserve led to a lower duration and level of water stress in the thinned plot [6]. In other words, the water status of trees is generally improved by the thinning [7]. But, its intensity results in greater or lesser changes in the environment of the remaining trees. An understanding of effects of silvicultural treatments such as precommercial thinning on individual trees or whole stand is extremely useful to help the forester to optimise the environmental conditions (water status of the plants, temperature conditions, light) for regional or local area. The objective of this study was to determine the effect of precommercial thinning on midday xylem water potential, soil moisture and temperature a young Anatolian black pine stand.

2. MATERIAL AND METHODS

2.1. Study area and experimental desing

This study was carried out in a young stand of Anatolian black pine [*Pinus nigra* Arn. subsp. *pallasiana* (Lamb.) Holmboe] located within the boundary of Gölhisar District Directorates of Forestry belonging to Isparta Regional Directorate of Forestry. The study area is located between 36° 54' North latitude and 29° 22' East longitudes. The altitude of the area is 1700 m. Its aspects are to the northeast-east. The area was located on conglomerate bedrock. The soil texture ranges from sandy clay loam to sandy loam. The readings taken with a small weather station installed within the study area for the precipitation and air temperature was shown in Figure 1.

The study stand was established by natural regeneration using seed trees of Anatolian black pine. The stand was approximately 21-23 years old and pure. Precommercial thinning treatments were implemented prior to the 2015 growing season. Treatments consisted of two levels of precommercial thinning with an untreated control were established in a randomized complete block design with three replication. There are a total of nine plots in experiment area (3 treatment x 3 replicates). The plot area varied between 150-200 m². Untreated control had

stand density of 4942 trees per hectare. The moderate precommercial thinning (spacing varied between 2.0 to 2.5 m) treatment, stand density was reduced to 2133 trees per hectare. The heavy

precommercial thinning (spacing varied between 3.0 to 3.5 m) treatment was thinned to the density of 1094 trees per hectare.

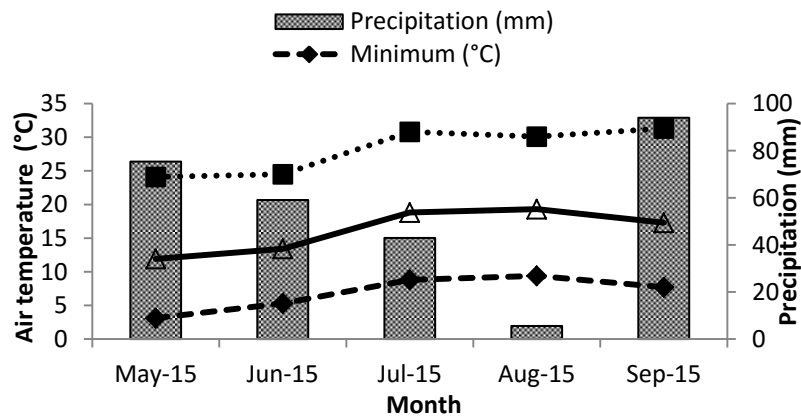


Figure 1. Variations in precipitation and air temperature for the study area during the sampling periods.

2.2. Measurements

Midday xylem water potential (Ψ_{md}) was measured with a pressure chamber [8] in May, July and September during the first growing season following precommercial thinning. The midday measurements were made between 12:30 and 13:30 when tree water stress was highest. Shoot samples were collected with pole pruners from south side and at the same crown positions of 12 trees per treatment (4 trees per replication). To minimize water loss, samples were immediately placed in a cooler in a sealed polythene bags.

In May, July and September, soil samples were collected total of 15 samples per treatment from 0-20 cm depth within each treatment plot (five samples per replication) to determine the soil moisture content by gravimetric method. At the same time, soil temperatures were measured with portable digital thermometer at 0-20 cm depth within each treatment plot (total of 15 samples per treatments).

2.3. Statistical analysis

For statistical analysis, data were subjected to analysis of variance. Means were compared using Duncan's multiple-range test at 5% probability. Data were reported as the mean \pm standard error of mean using the SPSS 20.0 statistical software package.

3. RESULTS AND DISCUSSION

The arrangement of the intensity of the stands affects the properties of both the individual trees and the whole stand [4]. Changes in soil temperature and moisture after thinning are important

in explaining the impacts of this intervention on soil fertility [9]. In the first year after precommercial thinning, the beginning of growing season (May), mean soil moisture content were significantly higher in the thinned plots ($P < 0.001$; Figure 2). Middle of the

growing season (July), soil moisture content of heavy precommercial thinning were significantly higher than the moderate precommercial thinning and untreated control. Mean

soil moisture content were not affected by the precommercial thinning treatment the end of the growing season. Wallentin, [10] found that the heavy thinning increased soil moisture, light transmittance and soil temperature, and hence the nitrogen mineralization in the *Picea abies* forest. In our study, soil temperature significantly differed among precommercial thinning treatments in May and July ($P < 0.001$; Figure 3). On these dates, soil temperature was highest in the moderate and heavy precommercial thinning treatments and lowest in the unthinned control treatment. Also in September, precommercial thinning had effect on soil temperature. In September, the highest soil temperature was determined moderate precommercial thinning treatments. Thibodeau *et al.* [9] studied precommercial thinning in the young balsam fir (*Abies balsamea* (L.) Mill.) stands in Quebec, Canada. They found that precommercial thinning significantly increased soil temperature in the mineral horizon. Another study, in precommercially thinned and unthinned stands of balsam fir (*Abies balsamea* (L.) Mill.), the thinned stand had significantly higher average hourly soil temperature than the unthinned stand [11]. Akburak and Makineci [12] reported that temporal variation of soil temperature was higher in the thinned plots, generally in the summer period from the beginning of April in a coppice-originated *Carpinus betulus* L. stand in Turkey. These results corroborate our findings with Anatolian black pine.

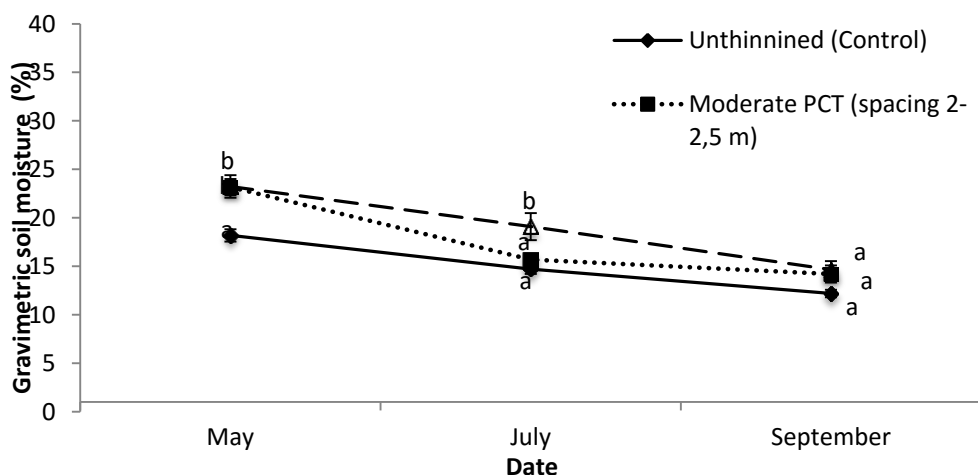


Figure 2. Soil moisture content (%) at 0-20 cm depth in different precommercial thinning (PCT) treatments during the first growing season after thinning. The measurements are averages of n=15.

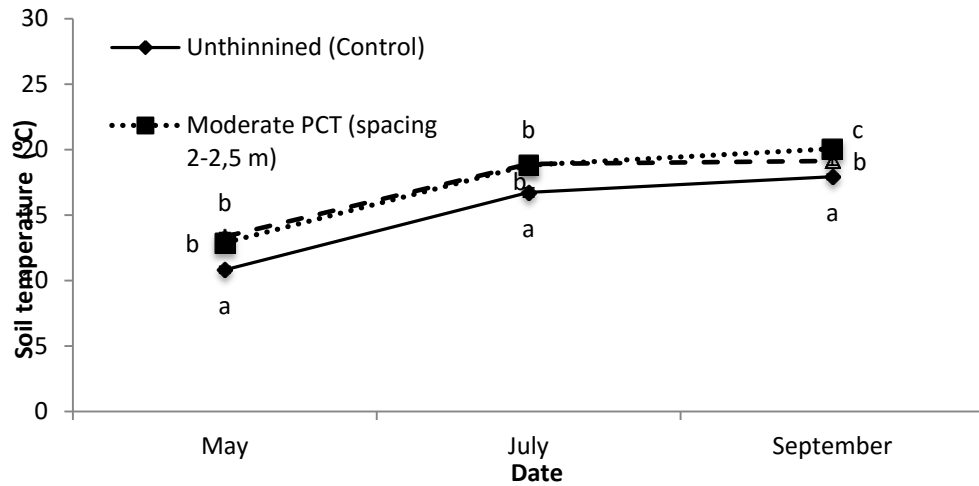


Figure 3. Soil temperature (°C) at 0-20 cm depth in different precommercial thinning (PCT) treatments during the first growing season after thinning. The measurements are averages of n=15.

The changes of midday xylem water potential in shoots of Anatolian black pine trees from all treatments during the growing season were presented in Figure 4. In May and September, midday xylem water potential of the shoots were significantly affected by the precommercial thinning treatment ($P < 0.001$; Figure 4), but the treatment impact was not significant in July. In May, midday xylem water potential of the shoots was highest in trees in the unthinned control, intermediate in trees in the moderate precommercial thinning treatment, and lowest in trees in the heavy precommercial thinning treatment. But, in September, midday water potential of the shoots of trees from the control treatments were significantly lower compared with precommercial thinning treatments. Gauthier and Jacobs [13] found that the mature black walnut (*Juglans nigra* L.) trees, compared with control trees, thinned trees had higher midday leaf water potential 1 year after treatment. Breda *et al.* [14] reported that predawn leaf water potential was significantly higher in trees in the thinned stand than in the closed stand and the improvement in water availability in the thinned stand resulted from decreases in both interception and transpiration an oak forest (*Quercus petraea* (Matt.) Liebl.). It was reported [15] that water availability usually increases as a result of thinning because of the reduction of crown interception or root competition.

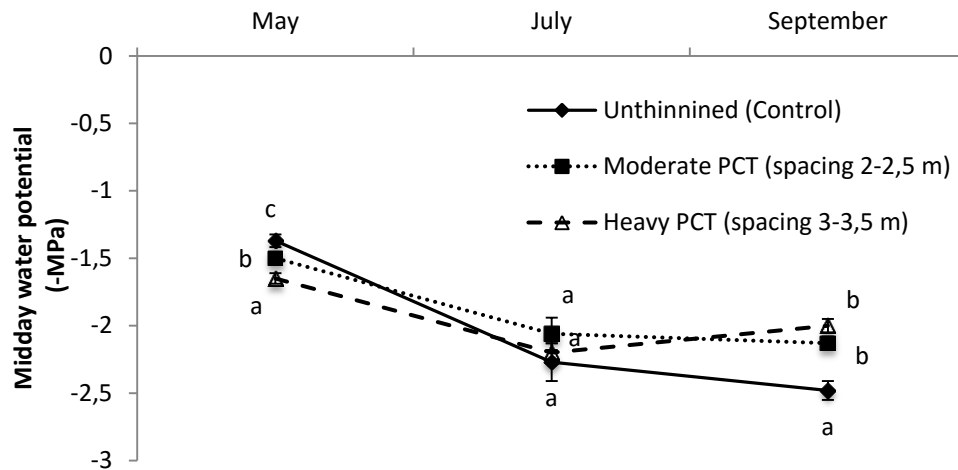


Figure 4. Midday xylem water potential (-MPa) measured in Anatolian black pine trees in different precommercial thinning (PCT) treatments during the first growing season after thinning. The measurements are averages of n=12 trees.

4. CONCLUSION

Precommercial thinning is a silvicultural operation that removes a portion of the canopy to accelerate height and diameter increment of residual trees [16]. The results showed that soil moisture content and soil temperature generally increased in response to precommercial thinning during the first year after thinning. Compared with control trees, thinned trees had higher midday xylem water potential the end of the growing season (September). Precommercial thinning in young Anatolian black pine forests may be beneficial effect on soil fertility due to increasing soil moisture and temperature. In addition, water stress in trees can also reduce by thinning. So, precommercial thinning can contribute to the growth of Anatolian black pine trees.

ACKNOWLEDGMENT

This study is supported by the TUBITAK (The Scientific and Technical Research Council of Turkey) with project number TOVAG-114O659. We thank TUBITAK for this financial support.

REFERENCES

- [1] Anonymous (2015). Orman Varlığımız. T.C. Çevre ve Orman Bakanlığı, Orman Genel Müdürlüğü, Ankara. (in Turkish).
- [2] I. Atalay and R. Efe, Ecology of The Anatolian Black Pine (*Pinus nigra* Arnold subsp. *pallasiana* (Lamb.) Holmboe) and its Dividing into Regions in Terms of Seed Transfer, Forest Tree Seeds and Tree Breeding Research Directorate, 37, Ankara, 2010.
- [3] K. Vestlund, 2005. *Aspects of automation of selective cleaning*. PhD Thesis, Department of Silviculture, Swedish University of Agricultural Sciences, Sweden.
- [4] M. Varmola and H. Salminen, 2004. Timing and intensity of precommercial thinning in *Pinus sylvestris* stands. *Scandinavian Journal of Forest Research*. 19 (2)142-151.
- [5] S. Huuskonen and J. Hynynen, 2006. Timing and intensity of precommercial thinning and their effects on the first commercial thinning in Scots pine stands. *Silva Fennica*. 40(4) 645–662.
- [6] G. Aussenac and A. Granier, 1988. Effects of thinning on water stress and growth in Douglas-fir. *Canadian Journal of Forest Research*. 18(1) 100-105
- [7] G. Aussenac, 2000. Interactions between forest stands and microclimate: ecophysiological aspects and consequences for silviculture. *Annals of Forest Science*. 57: 287-301.
- [8] P. F. Scholander, H. T. Hammel, E. D. Bradstreet and E. A. Hemmingsen. 1965. Sap pressure in vascular plants. *Science*. 148: 339-346.
- [9] L. Thibodeau, P. Raymond, C. Camiré and A.D. Munson, 2000. Impact of precommercial thinning in balsam fir stands on soil nitrogen dynamics, microbial biomass, decomposition, and foliar nutrition. *Canadian Journal of Forest Research*. 30(2) 229-238.
- [10] C. Wallentin 2007. *Thinning of norway spruce*. PhD Thesis, Swedish University of Agricultural Sciences, Sweden.
- [11] U. Hagemann, M. Moroni, P. Carter and F. Makeschin 2008. *Impact of Precommercial Thinning on Soil Respiration, Temperature, and Moisture in Western Newfoundland Balsam Fir*, Information Report M-X-223E, Natural Resources Canada, Canada.
- [12] S. Akburak and E. Makineci, 2016. Thinning effects on soil and microbial respiration in a coppiceoriginated *Carpinus betulus* L. stand in Turkey. *iForest*. 9: 783-790.
- [13] M. Gauthier and D.F. Jacobs, 2009. Short-term physiological responses of Black walnut (*Juglans nigra* L.) to plantation thinning. *Forest Science*. 55(3) 221–229.
- [14] N. Bréda, A. Granier and G. Aussenac, 1995. Effects of thinning on soil and tree water relations, transpiration and growth in an oak forest (*Quercus petraea* (Matt.) Liebl.). *Tree Physiology* 15, 295-306.



3rd International Conference on Science, Ecology and Technology
Rome, ITALY
14-16 August 2017

[15] D. Martín-Benito, M. Del Río, I. Heinrich, G. Helle and I. Cañellas, 2010. Response of climate-growth relationships and water use efficiency to thinning in a *Pinus nigra* afforestation. *Forest Ecology and Management*. 259, 967–975.

[16] D.P. Ostaff, H. Piene, D.T. Quiring, G. Moreau, J.C.G. Farrell, T. Scarr, 2006. Influence of pre-commercial thinning of balsam fir on defoliation by the balsam fir sawfly. *Forest Ecology and Management*. 223, 342–348.

COMPARISON OF GRIPPER DESIGNS FOR ROBOTIC KIWI FRUIT HARVESTING

Erhan Kahya¹, Selçuk Arın²

1. Control and Automation Technology Department, Technical Sciences Vocational School, Namık Kemal University, Tekirdağ, Turkey (E-mail:ekahya@nku.edu.tr)
2. Department of Agriculture Machine, Faculty of Agriculture, Namık Kemal University, Tekirdağ, Turkey (E-mail:sarin@nku.edu.tr)

Corresponding Author's e-mail: ekahya@nku.edu.tr

ABSTRACT

One of the most important pieces of robotic fruit harvest is Gripper, which made the last cutting action. Other parts are robotic arm, image processing and image processing software. In this study, image processing was carried out for fruit harvesting with the robotic system. The position of the fruit on the branch was determined and the cutting operation was performed. Two-dimensional and real-time images were transferred to digital media with a 2D camera. The images of the fruit transferred to the digital medium were processed in real-time image based on shape feature with the help of camera program. The movement of the robotic system is provided by finding the coordinates of the X and Y coordinates on the branches of the fruits according to the received and processed data. The designed Pneumatic shear system and step motorized shear cutter were individually mounted on the end of the robotic arm. 100 pieces of kiwifruit were placed differently on the branch and designs were tried separately. As a result of the experiments, It has been observed that the stem diameter of the fruit and the stem breaking resistor are effective in breaking the fruit over the branch. As a result of experiments on different designs, The cutting success was statistically analyzed. It has been seen that the cutting system working with the pneumatic system can cut through the fruiting branch with %72 success rate. The success rate in the shears system working with the stepper motor is determined as 0% (no cutting). The failure rate of %28 in the shears system working with the pneumatic system and the failure rate in the stepper motor shears system were investigated. In the research results; The reasons for failure in the system of pneumatic system shears are that the fruit stem is at the tip of the shears, It has been shown that shears does not come off the stem of the fruit, but comes to the fruit burl or with the sharp knife, causing an error in the breakout process. It is understood that the cause of the high failure rate in the step motor shears system is due to the engine can not move cutting action with a strong shutdown. According to the results obtained, it is seen that the pneumatic shears system is the most suitable system that can be used for fruits.

Keywords: Robotics Harvest, Cutting, Gripper, kiwi

1. INTRODUCTION

Nowadays, the robot technology is in significant advancement process. The objective of robot technology, which is widely used in many fields from medical practice to agricultural implementations, is to ease the lives of human, to accelerate the processes, and to perform a uniform production. Considering the tasks, which the humans do not want to fulfil, or the tasks, which might result in life-threatening circumstances, it can be seen that the robot technology is used in all of these domains. In this approach, the robotic systems eases the lives of human and eliminates the risks, as well as the most important benefit of robotic systems is to protect the humans from potential damages. For these reasons, the robotic systems are the most popular technology of today. The advancements in robotic systems gained speed with the development of integrated circuits in 1980s, and the costs started to decline during this process. Due to these advancements and decrease in costs, this technology penetrated into all of the industries.

The development of robotic systems continues in parallel with the development of microchip technology. As the technology advances, the configurations required for these systems get smaller. Thus, the robotic structures transformed into more light-weight and more functional structures.

The term “robot” refers to the machines thinking like human, making decisions, and mimicking the human behaviors and motions. The development and design of robots is executed by inspiring from the characteristics the creatures have adopted in order to attune to the life. The best example that can be given about this subject is the similarity between the activity zones of robotic arm and human arm.

The common property of all the robotic systems is that they all work on a platform and the end-effectors at the end are designed in accordance with the tasks. In robotic technology, the gripper units, which are specially designed for fulfilling the defined functions, are needed. The systems that are capable of mimicking the motions, which the human hand can perform, are of significant importance. In design and working principles of these units, the human hand, which is the most functional hand, is taken as base.

The fundamental properties that a robot should have are as follows;

1. Capability of performing a task: The unit should physically or virtually fulfill the task that is expected from it.
2. Capability of determining the consequences of operation: It should be capable of determining the consequences of task expected from the unit.
3. Capability of decision-making: The unit should make decision based on the consequences of task, which it is expected to fulfil, or the external factors.

Any system that is capable of fulfilling a task, determining the consequences, and making decisions can be called robot. But, even though the robots are capable of fulfilling any task that human can do, they actually mimicking the capabilities of human. The robots are capable of performing task, which are assigned by human, in the way programmed by human.

The most important part of the design of a robot is the part that fulfills the final motion of gripper system attached to the tip of end-effector. The most important point to be paid attention in gripper design of robotic system is that the hand should be functional and ready-to-operate in accordance with desired function. In robotic systems used in agricultural operations, the design of gripper used in harvesting plays important role in efficiency of harvest. In order to cut the fruit on the branch, the gripper should perform the cutting operation at highest level. Another factor that should be considered in gripper design is that it should be suitable for the physico-mechanical properties of fruit to be harvested. While being cut from the branch, the fruit should completely fit into the gripper and the stem's breaking resistance should be eliminated.

Scarfe et al. (2009) designed a remote-controlled kiwi-harvesting robot. In this design, it is possible to harvest 14,000 kiwis per hour. Using the infra-rouge camera system attached on the harvesting arms, and they defined the fruit diagnostically. Under favor of arms capable of moving 360°, the fruits are harvested by rotating them around their own axes depending on the penetrometric measurement results.

Zhi-Guo et al. (2009) carried out a study on impact-mechanical properties of robotic fingers used in tomato harvesting. In their study, the effects of input current, and engine speed and position were examined, as well as the control tests of fingers used in tomato harvest grippers. The current values of engine were set between 1200 and 2100 mA, while the engine speed varied between 25 and 3000 RPM. The optimum force for tomato harvesting was sought between these values.

Henten et al. (2010) designed an optimal manipulator for robotic cucumber harvesting. The algorithm used for optimization was the direct algorithm in the Tomlab package. The authors have used 4-connection PPRR type manipulator. They used the values of degree of freedom in cucumber harvesting in the tricyclic system rotating around the vertical axis for the robot. In Figure 1.1, the product selection and motion simulation of harvesting robot is presented.

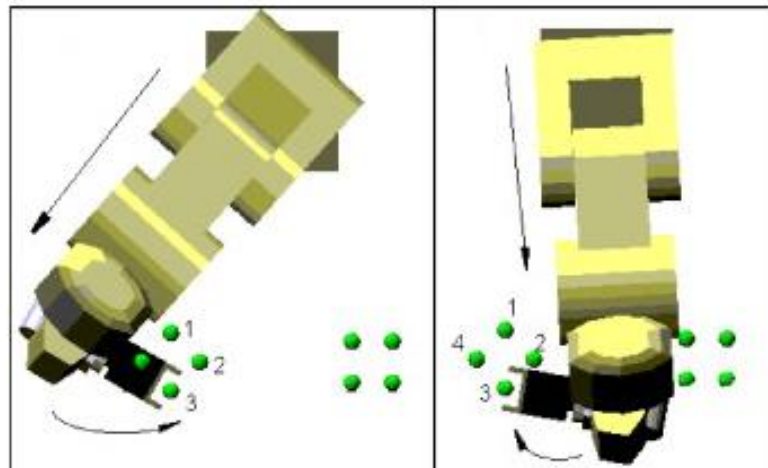


Figure 1.1. The product selection and motion simulation of harvesting robot

The common point of all of these studies is that a different gripper was designed especially for harvesting different fruits. Even though the robotic system structures show certain similarities, they grippers were designed in accordance with physico-mechanical properties of fruits.

2. MATERIAL AND METHODS

2.1. MATERIAL

System design has been done for the creation of the system. The following elements are used for this system. These;

1. 2D camera
2. Robotic arm
3. Gripper
4. Ultrasonic sensor.
5. Robotic Control Card
6. Pneumatic System Control

2.1.1. 2D Camera

The 2D camera has a capture ratio of 30 FPS with a 640x380 pixel black and white sensor. Image processing is done with extended SDRAM memory running on a 1 GHz processor. The camera flash memory and images are stored in memory. In addition, the FPGA optimizes pixel processing. It uses TCP / IP and UDP / IP protocols with 10/100 Mb Fast Ethernet to communicate with the computer. Apart from these connections, the camera has the ability to

communicate with the RS-485 serial port. Triggering feature is made by standard photoelectric switching. It is controlled by its own software.

2.1.2. Robotic Arm

A robot with 4 degrees of freedom (DOF) moving towards the fruit is used according to the coordinates of the image processing method. 4 Springr SM-8166B and 2 Savox SV-0236 MG model servo motors are used to move the 4 axis robot. Arm lengths $L_1 = 20$ cm, $L_2 = 17$ cm, $L_3 = 15$ cm. The parts of the robot arm are shown in Figure.2.1.

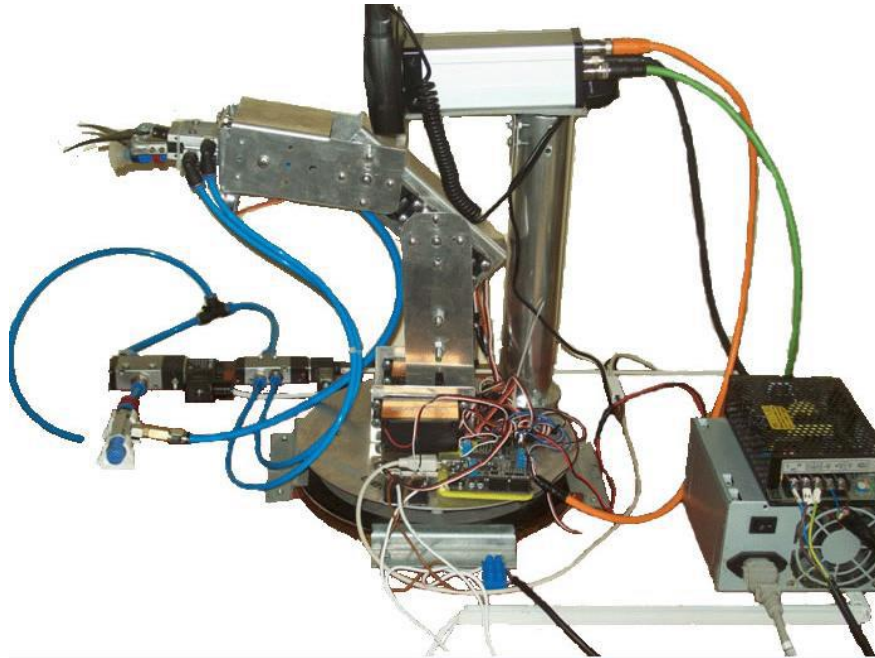


Figure 2.1. Robot kol tasarımı (orjinal)

2.1.3. Gripper

Two different gripper designs were used in the study. The first method is the servo motor controlled system shown in Figure 2.2. The second method is the system controlled by the pneumatic system shown in Figure 2.3.

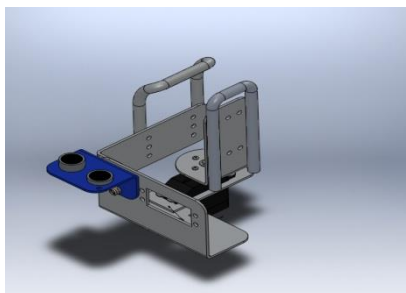


Figure 2.2. System controlled by servo motor

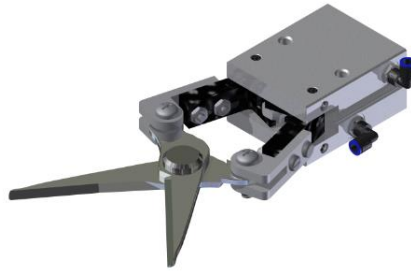


Figure 2.3. Control system with pneumatic system

Cutting apparatus used in the system has a size of 17.5 cm lower jaw and 15 cm upper jaw. A blade of 3 cm length was placed on the ends of the jaws. In the second method, a pneumatic scissors system was installed by combining 1 parallel holder and 1 pruning shear.

2.1.4. Ultrasonic Sensor

Parallax Ping Ultrasonic sensor is used to stop the fruit located on the branch of the robot arm at a certain approach distance. The sensor used calculates the distance as the processing of the sound signals. The sensor is scanning the distance between 2 and 3 meters and detects the obstacles in the front. The ping sensor has an I / O pin and a status LED. There are two sensors on the card and 3 pins (5V, GND and signal).

2.1.5. Robotic Control Card

Arduino Uno has been used as a robotic control card. The ATmega 328 is a microprocessor development card and has 14 digital input / output connections, 6 analog inputs, 16 Mhz crystal oscillator, USB connection, power connection, ICSP connection and reset button.

2.1.6. Pneumatic System Control

Two solenoid valves MVS0-180-4E1 were used to control the pneumatic system in the system.

2.2. METHODS

The servo engine in first method and pneumatic pruner in second method were controlled via a robotic control card, and a program was coded for rotation of servo. The pneumatic system was connected to a compressor, which provides 5-8 Bars of pressure, via 8mm-diameter hoses. The system was controlled by running the control valves via the coded program. The control valves were used for operating the pruner under 5-8 Bars of pressure.

The calculation of cutting pressure of pruner was calculated according to the formula below:

Cutting Stress (D. Dursun, 2001):

$$\tau = \frac{F}{A} \quad (1)$$

τ =Cutting stress (N/ mm²)

A=Cross-section area (mm²)

$$A = \frac{\pi \cdot d^2}{4} \quad (2)$$

d=Stem diameter

Cutting Force (D. Dursun, 2001):

$$F_1 * L_1 = F_2 * L_2 \quad (3)$$

L₁ = Stem length

L₂ = Cutting length

Pneumatic pressure (D. Dursun, 2001):

$$P = F/A \quad (4)$$

P=Pressure (Pascal)

F=Force (N)

A=Cross-section area (mm²)

In order to cut the fruits on the stem, the systems presented in Figures 2.2 and 2.3 were mounted on the robotic system. The cutting stress during cutting the fruits was calculated using Formulas 1, 2, 3, and 4. During the calculations, the stem diameters were measured using a caliper. L₁ and L₂ lengths and the inner diameter of pneumatic hose were measured using a caliper, and the results are presented below.

L₁=20 mm

L₂=25 mm

The inner diameter of hose was 4 mm. The area of hose (A) was calculated to be 12.56 mm².

The pressure values of compressor running the pneumatic system were set between 5 and 8 Bars. The force applied on the lever (F₁) was calculated using Formula 4, while the cutting force (F₂) was calculated by using Formula 3. By putting the values of force applied on lever (F₁) cutting force (F₂) in Formula 1, the stem cutting stress (τ) was calculated. The calculations repeated for 100 times for each fruit species were statistically analyzed.

The pressure of system run by servo engine was calculated to be 0.68 Bar. The force applied on lever (F_1) was calculated using Formula 4, whereas the cutting force (F_2) was calculated according to Formula 3. By putting the values of force applied on lever (F_1) cutting force (F_2) in Formula 1, the stem cutting stress (τ) was calculated. The calculations repeated for 100 times for each fruit species were statistically analyzed.

3.RESULTS AND DISCUSSION

The pressure values of compressor running the pneumatic system varied between 5 and 8 Bars. The force applied on lever (F_1) was calculated using Formula 4, whereas the cutting force (F_2) was calculated according to Formula 3. F_1 and F_2 values are presented in Table 1.

Table 1. Pneumatic cutting system

	Pressure Values (Bar)			
	5	6	7	8
F_1 (N)	6.28	7.53	8.79	10.04
F_2 (N)	5.02	6.03	7.03	8.04

By putting the values of force applied on lever (F_1) cutting force (F_2) in Formula 1, the stem cutting stress (τ) was calculated. The calculations repeated for 100 times for kiwi fruit were statistically analyzed. The statistical analysis was performed according to the cutting status of fruits. The results are summarized in Table 2.

Table 2. Exchanges cutting force for Kiwi

		Sum of Squares	df	Mean of Squares	F	Sig.
a*	Between Groups	6.698	62	.108	4.859E32	.000
	In-Group	.000	38	.000		
	Total	6.698	100			
b*	Between Groups	9.682	62	.156	2.916E33	,000
	In-Group	.000	38	.000		
	Total	9.682	100			
c*	Between Groups	13.132	62	.212	1.905E33	.000
	In-Group	.000	38	.000		

	In-Group	.000	38	.000		
	Total	13.132	100			
d*	Between Groups	17,243	62	.278	2.502E33	.000
	In-Group	.000	38	.000		
	Total	17.243	100			

*a=5 bar, b=6 bar, c=7 bar, d=8 bar

The pressure of system run by servo engine was computed to be 0.68 Bar. The force applied on lever (F_1) was calculated using Formula 4, and the cutting force (F_2) was calculated by using Formula 3. By putting the values of force applied on lever (F_1) cutting force (F_2) in Formula 1, the stem cutting stress (τ) was calculated. No statistical analysis could be performed, since no cutting could be made in 100 attempts made for kiwi fruit.

During the experiments, the percentage of accurate positioning of robotic arm was found to be 83%. The reason for this is that the camera chose the fruit randomly during determining the coordinates when the fruits are collateral or consecutive. It was found that the coordinates of fruit that better fits to the defined shape was given, rather than the fruit with perfect shape.

The rate of cutting was 72%. The reason for difference between finding and cutting was found to be the position of fruit on the pruner. As a result of T-test performed, it was determined that not only x-axis but also y-axis is important for cutting the fruit from branch. During positioning the pruner, it was determined that axis ensured the positioning of pruner on the stem of fruit. The position of fruit stem on the tip of pruner, the position of pruner corresponding to the body of fruit, the fruit, or the beginning of stem rather than the stem, and the position of pruner on the shoot of stem were observed to cause failure during cutting.

According to the results of ANOVA test, the pressure values of pressure varying between 5 and 8 Bars were found to be significant for cutting force. It was determined that the compressor pressure running the pneumatic system provided enough pressure for cutting operation. The pressure values varying between 5 and 8 Bars were observed to be enough for cutting. It was determined that the change in pressure of compressor wouldn't affect the cutting force.

4.CONCLUSION

In experiments carried out with servo engine, the cutting couldn't be accomplished. As servo engine, the servo engines running on AC power that has higher pressure values should be preferred. Since the stem diameters affect the stem's breaking resistance, the system failed. The pressure that was applied was observed to be unsuitable for cutting the fruit stem.

It was determined that the system to be used as gripper providing the final motion of robotic system was the pneumatic one. It was concluded that the success rate of cutting can be increased by pulling the fruit inwards from the tip of blade and keeping it stable in order to improve the plucking success. Specially designing the vacuum pad at the tip of vacuum generator used for pulling the fruit inside is believed to improve the success in keeping fruit stable. In the present study, it was concluded that the most important factor in robotic design is the gripper fulfilling the final motion. Although the determination of fruit's position, all of the parts moving the robotic arm, and all of the software were the same, the higher level of success of system driven by the pneumatic system also corroborates this.

ACKNOWLEDGMENT

This research was supported by Namık Kemal University BAP. Project Number: NKÜBAP.00.24.DR.10.05

REFERENCES

- [1] A. Scarfe , C. Flemmer , R. Flemmer ,2009. *Development of An Autonomous Kiwifruit Picking Robot*. Autonomous Robots and Agents, ICARA 2009. 4th International Conference on, Page Number:380-384,ISBN:978-1-4244-2712-3,New Zealand.
- [2]L. Zhi-Guo, L. Ji-Zhan, L. Ping-Ping, Y. Yin Jian-Jun ,2009. *Study On The Collision Mechanical Properties Of Tomatoes Gripped By Harvesting Robot Fingers*, African Journal of Biotechnology ,Volume 8 (24), 7000-7007, ISSN 1684–5315.
- [3]E.J. Henten, E.J. Schenk, L.G. Willigenburg,J. Meuleman, P.Barreiro ,2010. *Collision-Free Inverse Kinematics Of The Redundant Seven-Link Manipulator Used in a Cucumber Picking Robot*. Biosystems Engineering, Published By Elsevier ,Volume 106(2),112-124.
- [4]D. Dursun,2001. *Cisimlerin Dayanımı Temel Ders Kitabı*.Milli Eğitim Basımevi, ISBN 975-11-1913-8, Ankara

VARIATION OF TOTAL SOLUBLE SUGAR CONTENT IN ANATOLIAN BLACK PINE STANDS APPLIED PRECOMMERCIAL THINNING

E. Bayar¹, A. Deligoz¹

¹ Suleyman Demirel University, Faculty of Forestry, Isparta/TURKEY.

(E-mail: esrabayar@sdu.edu.tr, aysedeligoz@sdu.edu.tr)

Corresponding Author's e-mail: esrabayar@sdu.edu.tr

ABSTRACT

In this study, three different late precommercial thinning (control, moderate and heavy) were applied with three replications using a randomized block design in natural stands of Anatolian Black Pine in Pazarkoy/Isparta. Total soluble sugars were analyzed in May, June, July, August, September and November (2014) during the first growing seasons following late precommercial thinning. The total soluble sugar content was determined by the phenol sulfuric acid method. When the seasonal variations of total soluble sugar content were assessed, significant differences have been determined between in measurement periods. This study showed that total soluble sugar content was relatively higher in May and June, declined by September and then relatively increased in November. In addition, there were no significant differences between the treatments except September and November. The heavy precommercial thinning has the higher total soluble sugar content than the others in September and November.

Keywords: Anatolian black pine, precommercial thinning, total sugar content

1. INTRODUCTION

Precommercial thinning (PCT) are one of the important and an essential silvicultural operation to improve the growth of the remaining trees. It generally described with its intensity, form and timing. The intensity of precommercial thinning is explained as the number of stems. The timing is related to the average tree height and choosing stems (e.g. removal wolf trees). In addition, precommercial thinning with the aim of rising timber quality can be carried out in two steps release the competitive pressure on the main stems with step by step [1].

Nowadays, maintenance work is given importance, but unfortunately, there are many areas that are still delayed to apply precommercial thinning in Turkey. Anatolian black pine [*Pinus nigra* Arn. subsp. *pallasiana* (Lamb.) Holmboe] is one of the species that should be done precommercial thinning on time. It is resistant to frost and drought and also it is widespread

species, so it is important for our country. The Anatolian black pine passes precommercial thinning in the age of 10-15 years depending on the site. This stage continues until the age of 25-40 [2]. The effects of thinning on stand density, basal area, diameter and height [3], [4], [5],

[6], [7], [8], [9], [10] and water relations [11], [12], [13], [14], [15] have been studied for several species.

Thinning is expressed stand density at a given age, but now thinning problems can be determined on a functional basis progress in forest ecophysiology. For example, light, temperature, water, wind ext physiological behaviour is conceivable. If some trees eliminate in the stand, it changes in the microclimate which lead to major changes in the physiological behaviour of the trees like that changing photosynthesis and transpiration, growth, form and size of the remaining crowns [16].

Trees need to reserves their survival during winter and for bud flush and leaf growth in the following spring. In many tree species, these reserves are basically covered by starch. It is degraded to soluble carbohydrates during the dormant season for respiration and in spring during budding [17]. During the growing season, accumulation of carbohydrates is required for survival of plants. Stored carbohydrates play an important role in metabolism, defense, growth, development of cold hardiness, and postponement or suppression of mortality [18]. Carbohydrates accumulate in a variety of tissues and organs, including buds, leaves, branches, stems, roots, seeds, fruits and also sometimes vascular sap. Carbohydrates are the special importance because, first of all they are direct products of photosynthesis and secondly they have the primary energy storage compounds and the basic organic substances [19].

The objective of this study was to evaluate variation of total soluble sugar content in Anatolian Black Pine stands applied late pre-commercial thinning.

2. MATERIAL AND METHODS

2.1 Study area and experimental design

The study area is located within the boundaries of the Isparta Regional Directorate of Forestry /Eğirdir District Directorates of Forestry (37° 43 north latitude, 31° 04 east longitude). Study area has north-northwest aspects. The altitude of the area is 1550 m. The stand was about 25-27 years old and pure. The average slope varies between 40 % and 70 %. The mini-meteorological station was established on the study area for measuring temperature, precipitation and humidity. During 2014, mean annual air temperature, maximum and minimum temperature, and the total precipitation was approximately estimated 14° C, 37° C, 7° C and 720 mm, respectively (Figure 1).

At the end of March 2014, three late precommercial treatments including control were applied in natural stands of Anatolian black pine. These treatments were done 2-2.5 m (moderate) and 3-3.5 m (heavy) spacing with three replications using a randomized block design. Sufficient homogenous structure has been provided and each sample area was taken 400 m² in size. After precommercial thinning, control, moderate (spacing varied between 2.0 to 2.5 m) and heavy

(spacing varied between 3.0 to 3.5 m) treatments had stand density of 4100, 2283 and 1242 trees per hectare, respectively.

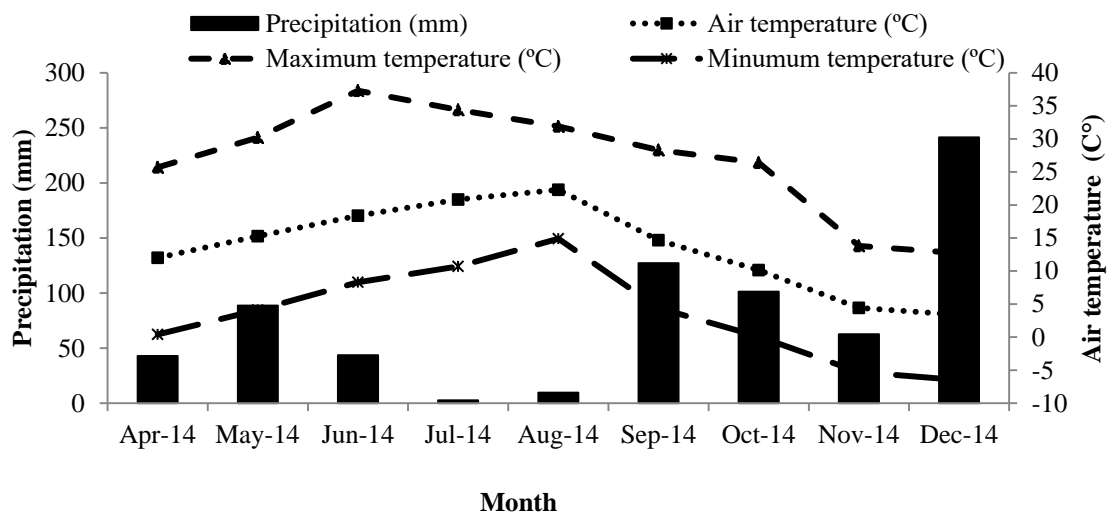


Figure 1. The temperature and precipitation values taken from the mini meteorological station in the study area

2.2. Total sugar contents

Samples were collected a total of six times from May 2014 to November 2014. Needles were taken from each treatment with three replications. Needles were dried in an oven at 65 °C for 48 hours. 0.1 g dry weight of needles was incubated with 10 ml ethanol (80%) for 24 hours in unlighted conditions and then centrifuged 6000 rpm for 10 minutes. 0.05 ml sample and 1 ml 5% phenol solution and 5 ml H₂SO₄ were added in each tube and mixed in vortex and remained at room temperature for an hour. Total soluble sugar analysis was determined according to Dubois et al. [20] and recorded as mg g⁻¹ dried weight by reading absorbance at 490 nm.

2.3. Data analysis

All data was subjected to analysis of variance by using SPSS 20.0 statistical package software. Means comparison was conducted multiple range test at the significant level 5%.

3. RESULTS AND DISCUSSION

Results of total soluble sugar contents that measured from May to November are shown in Figure 2. When the seasonal variations of total soluble sugar content were assessed, significant differences have been determined between in measurement periods. Control, moderate and heavy treatments were the highest value in June and lowest value in September. Total soluble sugar contents were 165 mg/g (control), 183 mg/g (moderate) and 164 mg/g (heavy) dry weight

in June and 70 mg/g (control), 80 mg/g (moderate) and 84 mg/g (heavy) dry weight in September. This study showed that total soluble sugar content was relatively higher in May and June, declined by September and then relatively increased in November. In general, the content of soluble sugars and starch is high during winter and the low during dry summer [21], [22]. Similar results were found *Q. ilex* and *Q. suber*. species. Starch and total

soluble sugars leaf concentrations were lower in summer than autumn [23]. During the cold months, soluble sugars increase when starch concentrations decrease, and they may play a role in cold tolerance [24]. To summarize, the content of carbohydrates in the plants can vary significantly between different seasons [18]. For all that, water stress that is develops gradually difference over periods comprising weeks or months under field conditions can change leaf biochemistry [25].

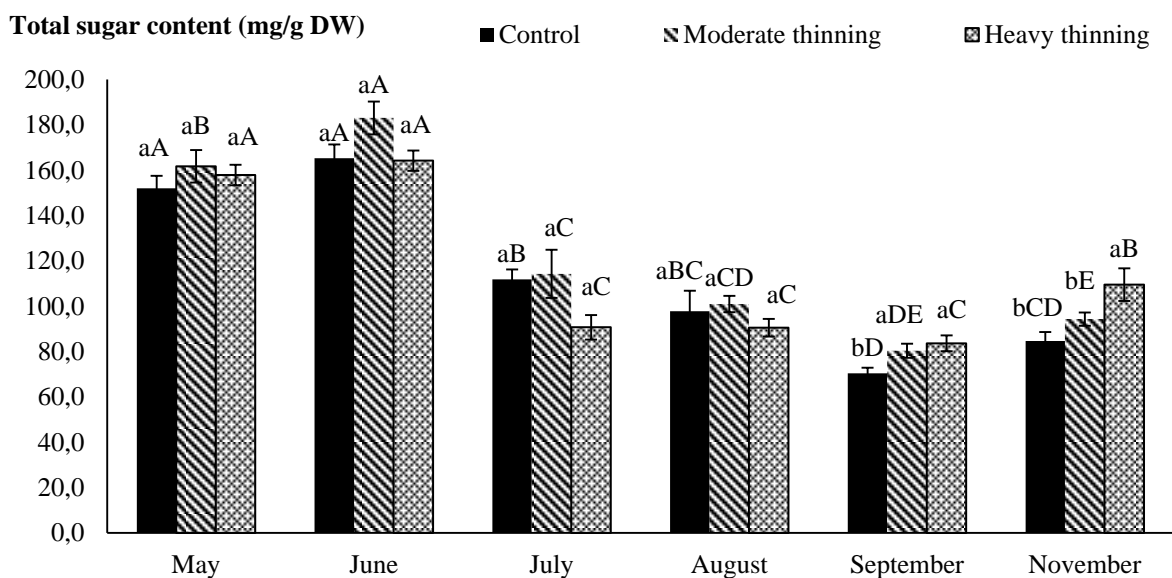


Figure 2. Variations after pre commercial thinning of total soluble sugar contents (mg/g DW, mean value + SE) in needles (Lower case: shows difference between treatments, upper case: shows difference between the months).

When treatments were compared, there were significant differences in September and November in this study. Heavy treatments have the higher total soluble sugar content than the others in September and November. In addition, control treatments have the lowest total soluble sugar content than moderate and heavy treatments. A greater sugar concentration in leaves was an important component of the lower osmotic potentials at full saturation ($\Psi \pi$, sat) of thinned trees [26]. Also, soluble carbohydrates reduce the osmotic potential of the cell sap [19].

4. CONCLUSION

Precommercial thinning (PCT) are one of the important and an essential silvicultural operation to improve the growth of the remaining trees [1]. Carbohydrates are also important organic compounds for survival of plants. Changes in carbohydrate is related to photosynthesis, water relations, low and high temperatures. This study show that after precommercial thinning, total soluble sugar content has the significant differences in measurement periods during the first growing season. In addition, there were not significantly differences between treatments except in September and November in natural Anatolian Black Pine stands. Heavy treatments have the higher total soluble sugar content than the others. However, to make clear decisions about these results, it will be more appropriate to assess the results of two or three years.

ACKNOWLEDGMENT

This study was funded by the ÖYP and BAP (Project Number: ÖYP-05241-DR14 and 4167-ÖYP-D2-14).

REFERENCES

- [1] N. Fahlvik, 2005. *Aspects of precommercial thinning in heterogeneous forests in Southern Sweden*. PhD thesis, Swedish University of Agricultural Sciences, Alnarp Sweden.
- [2] M. Genc, Orman Bakımı, Süleyman Demirel Üniversitesi Orman Fakültesi Yayını, Isparta, 2011.
- [3] Ü. Eler, R. Özçelik, İ. Özdemir, Y. Çatal, 2004. Göller Yöresinde İki Genç Doğal Toros Sediri (*Cedrus libani* A. Rich.) Meşceresinde Gecikilmiş Sıklık Bakımının Gelişme Üzerine Etkileri. *Süleyman Demirel Üniversitesi Fen Bilimleri Enstitüsü Dergisi*. 8(1)1-6.
- [4] H. Mäkinen, A. Isomäki, 2004. Thinning intensity and growth of Scots pine stands in Finland. *Forest Ecology and Management*. 201,311-325.

- [5] S.W. Simard, T. Blenner-Hassett, I.R. Cameron, 2004. Pre-commercial thinning effects on growth, yield and mortality in even-aged paper birch stands in British Columbia. *Forest Ecology and Management*. 190,163-178.
- [6] A. Tüfekçioğlu, S. Güner, M. Küçük, 2005. Thinning Effects on Production, Root Biomass ve Some Soil Properties in a Young *Oriental beech* Stand in Artvin, Turkey. *J. Environ Biol*. 26(1)91-5.
- [7] M.D. Río, R. Calama, I. Canellas, S. Roig, G. Montero, 2008. Thinning intensity and growth response in SW-European Scots pine stands. *Annals of Forest Science*. 65(3)1.
- [8] R. Özçelik, Ü. Eler, 2009. Effects of release cutting on the development of young natural Lebanon cedar (*Cedrus libani* A.Rich.) stands of western Mediterranean region of Turkey. *Journal of Environmental Biology*, 30(2)179-182.
- [9] E. Çiçek, F. Yılmaz, A.K. Özbayram, B. Çetin, 2010. Aralamannın Dişbudak (*Fraxinus angustifolia* ssp. *oxycarpa*) Plantasyonunun Gelişimine Etkisi. III. Ulusal Karadeniz Ormancılık Kongresi. 20-22 Mayıs 2010, 886-894.
- [10] Ö. Öncül, Ç. Uğurlu, M. Köse, F. Tilki, 2016. Sıklık bakımının doğal sarıçam (*Pinus sylvestris* L.) meşcerelerinde çap ve göğüs yüzeyi üzerine etkisi. *Ormancılık Araştırma Dergisi*. 1(3)29-37.
- [11] G. Aussenac, A. Granier, 1988. Effects of thinning on water stress and growth in Douglas-fir. *Can. J. For. Res.* 18,100-105.
- [12] B.M. Cregg, T.C. Hennessey, P.M. Dougherty, 1990. Water relations of loblolly pine trees in southeastern Oklahoma following precommercial thinning. *Can. J. For. Res.* 20,1508-1513.
- [13] N. Bréda, A. Granier, G. Aussenac, 1995. Effects of thinning on soil and tree water relations, transpiration and growth in an oak forest (*Quercus petraea* (Matt.) Liebl.). *Tree Physiol.* 15(5)295-306.
- [14] Z. Tang, J.L. Chambers, M.A., Sword, J. Barnett, 2003. Seasonal photosynthesis and water relations of juvenile loblolly pine relative to stand density and canopy position. *Trees*. 17,424-430.
- [15] M.M. Gauthier, 2008. *Morphological and physiological responses of fine hardwood tree species to plantation thinning*, PhD Thesis, Purdue University Graduate School, Indiana.
- [16] G. Aussenac, 2000. Interactions between forests stands and microclimate: Ecophysiological aspects and consequences for silviculture. *Ann. For. Sci.* 57,287-301.
- [17] N. Regier, S. Streb, S.C. Zeeman, B. Frey, 2010. Seasonal changes in starch and sugar content of poplar (*Populus deltoides* × *nigra* cv. Dorskamp) and the impact of stem girdling on carbohydrate allocation to roots. *Tree Physiology*. 30,979-987.

- [18] T.T. Kozlowski, 1992. Carbohydrate sources and sinks in woody plants. *Bot. Rev.* 58, 107-222.
- [19] T. T. Kozlowski, S. G. Pallardy, *Physiology of Woody Plants*. Second Edition, Academic Press, New York, 1997.
- [20] M. Dubois, K.A. Gilles, J.K. Hamilton, P.A. Rebers, F. Smith, 1956. Calorimetric Method for Determination of Sugars and Related Substances. *Analytical Chemistry*. 28,350-356.
- [21] C.H.A. Little, 1970. Seasonal changes in carbohydrate and moisture content in needles of balsam fir (*Abies balsamea*). *Can J Bot.* 48,2021–2028.
- [22] S. Diamantaoglou, S. Rhizopoulou, A. Herbig, U. Kull, 1989. Seasonal trends in energy content and storage substances in mediterranean shrub *Ephedra*. *Acta Ecologica*, 10:3,263-274.
- [23] M. Vaz, J.S. Pereira, L.C. Gazarini, T.S. David, A. Rodrigues, J. Maroco, M.M. Chaves, 2010. Drought-induced photosynthetic inhibition and autumn recovery in two Mediterranean oak species (*Quercus ilex* and *Quercus suber*). *Tree Physiology*. 30, 946-956.
- [24] B.L. Wong, K.L. Baggett, A.H. Rye, 2003. Seasonal patterns of reserve and soluble carbohydrates in mature sugar maple (*Acer saccharum*). *Can. J. Bot.* 81,780-788.
- [25] M.M.Chaves, M.M. Oliveira, 2004. Mechanisms underlying plant resilience to water deficits: prospects for water-saving agriculture. *J. Exp. Bot.* 55,2365–2384.
- [26] D. Pothier, H.A. Margolis, 1990. Changes in the water relations of balsam fir and white birch saplings after thinning. *Tree Physiology*. 6(4)371:380.

PERFORMANCE ANALYSIS OF EEG SIGNAL CLASSIFICATION AND SSVEP IN OPENVIBE

Harun ÇİĞ¹, M. Fatih TÜYSÜZ²

^{1,2} Department of Computer Engineering, Harran University, Şanlıurfa, Turkey.

(E-mail: ftuysuz@harran.edu.tr, haruncig@harran.edu.tr)

ABSTRACT

OpenVibe is a software platform that makes use of the brain-computer interfaces. It can be used in real time to acquire, filter, process, train, test, classify and display brain signals. It is free and open source, works on Windows and Linux operating systems. OpenVibe also supports Steady State Visual Evoked Potentials (SSVEP), which is a brain response in the visual cortex once focused with visual attention to a light source flickering with frequency between approximately 6 and 100Hz. In this paper, we analyse the EEG signal classification and SSVEP performance of the OpenVibe, utilizing three flickers in a few steps. These steps consist of configuration, training acquisition, Common Spatial Pattern filters (CSP) training, classifier training and online test shooter. Our test results show that offline accuracy rate of 90.33% with LDA, 87% with MLP and 92.56% with SVM has been obtained as the average of three flickers. Online tests carried out through the paper also validates the accuracy of the SSVEP in OpenVibe.

Keywords: OpenVibe, Ssvep, EEG, signal classification

1. INTRODUCTION

OpenVibe is an open source graphical software platform, used as a brain-computer interface (BCI) [1]. The goal of the OpenVibe is to provide an easy-to-use platform; an incentive tool for research, development and use of BCI technology [2]. Throughout this paper, we test the SSVEP-based BCI performance using OpenVibe in a few steps. These steps consist of configuration, training acquisition, Common Spatial Pattern filters (CSP) training, classifier training and online test shooter.

First step must be run at least one time because this will be the scenario utilized by the SSVEP experiment. There are two boxes in the configuration step; Peripheral and Experiment Settings boxes, which contain configuration parameters. Peripheral box should be adjusted according to the screen refresh rate, which is the hardware configuration. Experiment box contains more than one parameter related to general settings of SSVEP. The colors of the flickering boxes on the simulator screen, the frequency value of each box, length of the signal to be used to find the SSVEP response, speed range between the signal segments and

tolerance of the frequency band around the excitation frequency used for classification adjustments are handled in this box.

In the second step, to train the SSVEP classifiers and obtain the necessary training data, simultaneous Electroencephalogram (EEG) signal data of the user (looking at stimuli of different frequencies) is recorded within the determined time. The SSVEP Training Controller has an important role in this step. It contains many parameters, such as Goal Sequence, which represents the target box to be looked at among the flickering boxes at different frequencies, Stimulation Duration, which represents the duration of the sequence in which the targets flicker, Break duration, which represents the length of the period during which the objects on the screen do not flicker and Flickering Delay which represents the delay between the arrow marking the target and the beginning of the flicker index from the subject being viewed by the subject.

Third step includes three different signal processing situation assessment platforms. The first of these processes is based on the first flickering frequency, the second one is based on the second flickering frequency, and the third one is based on the third flickering frequency. The data saved in the previous step is loaded into the generic stream reader in this step. Then, Common Spatial Pattern filter is used, so that it automatically selects which electrode channels are the most efficient combination for the training.

In the fourth step, the processed and saved signal in the third step is used to generate classifiers that can be used in on-line BCI applications. Three different classifiers; Support Vector Machine, Linear Discriminant Analysis and Multi-Layer Perceptron can be utilized in this step. The most efficient channel combinations are used by integrating CSP as a filter. This is done separately for each flicker box. The offline accuracy rate trained on the processed dataset are computed in this step. On the recorded data, accuracy rate of 92% with Linear Discriminant Analysis (LDA), 89% with Multi-Layer Perceptron (MLP) and 97% with Support Vector Machine (SVM) have been obtained for the first flicker. For the second flicker, accuracy rate of 89% with LDA, 87% with MLP and 91.7% with SVM have been obtained. Finally, for the third flicker, accuracy rate of 90% with LDA, 85% with MLP and 89% with SVM have been obtained.

Eventually, game configuration is realized in the fifth step. That is, the raw signal is taken by the acquisition server from the emotive device in real-time, signal is processed at specified time intervals, filtered, passed through the trained network and then it is determined which flicker the Subject is looking at.

1. STEADY STATE VISUALLY EVOKED POTENTIALS (SSVEP)

Steady State Visual Evoked Potential based BCIs use several stable oscillating light sources (e.g. flickering LEDs), each of which vibrates at unique frequencies. SSVEP is a continuous brain response that occurs at a constant frequency in the occipital and parietal cortical regions of the brain under visual stimulation by looking at the constantly pulsing light source at

specific frequencies. SSVEP can be detected automatically by signal processing algorithms such as pre-processing, artefact detection-correction, feature extraction and classification.

The target focused from within the shape group consisting of the continuously shaking visual stimuli shown in Figure 1 is modulated with the frequency corresponding to the brain signals.

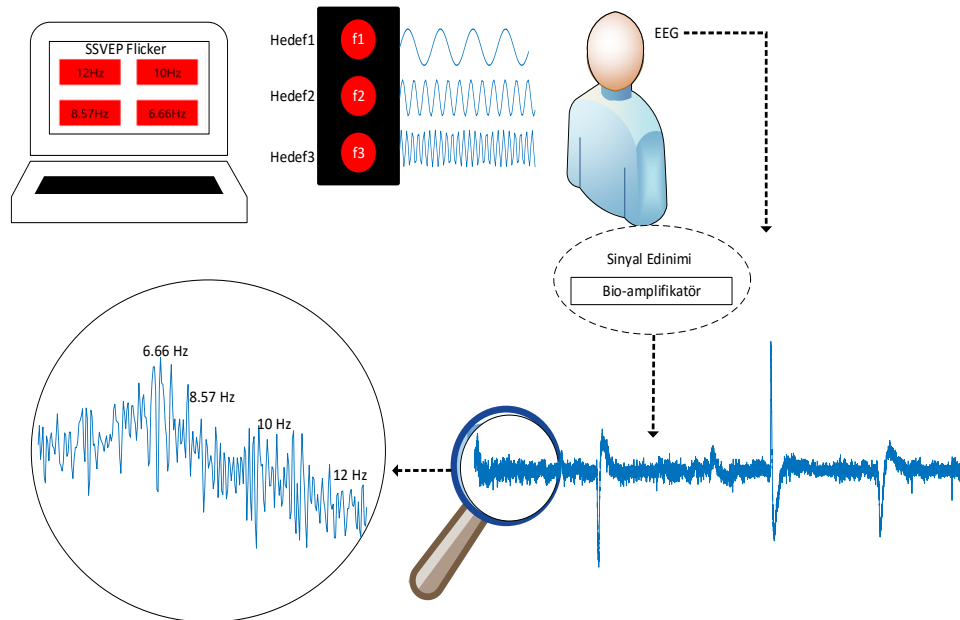


Figure 1. SSVEP Based BCI

These signals are recorded with non-invasive EEG devices in real-time [3]. The OpenVibe editor can be connected to many EEG devices such as Emotiv, Neurosky, OpenBCI, OpenEEG and gTec by loading the necessary libraries and the collection of EEG signal data. Anyone who wants to conduct research in this field with OpenVibe SSVEP can create their own data set. Many signal processing methods such as FFT, CSP, Band Pass filter can be used as ready-made package. LDA, SVM and MLP classifiers can be used for the generated data set. This means that we do not have to process more regularly and quickly on the area being surveyed.

In current SSVEP-based BCI systems, EEG is often used for temporal resolution and simplicity to obtain SSVEP [4], [5]. Several methods have been proposed for extracting SSVEP knowledge from EEG for BCI application [6]. Power Spectrum Density Analysis (PSDA) is often used for frequency-domain detection in BCI systems, which corresponds to SSVEP [7]. Peak power spectral density as considered SSVEP component induced by visual EEG spectrum light source can be estimated by the FFT method. For this method, a long window size is required for spectral estimation with high frequency resolution [8]. Depending on age, changes in SSVEP amplitudes and memory performance delays may occur [9].

2. EEG SIGNAL CLASSIFICATION AND SSVEP IN OPENVIBE

In OpenVibe, 5 steps are required to be processed in an order to test the SSVEP procedure. These steps consist of configuration, training acquisition, CSP filter training, classifier training and online testing.

First, we select Emotiv device in driver section of OpenVibe Acquisition Server, then from drive properties to device configuration pages we fill necessary parameters. Most importantly we add folder directory, where Emotiv sdk file is located in emotiv research sdk directory. This is illustrated in

Figure 2.

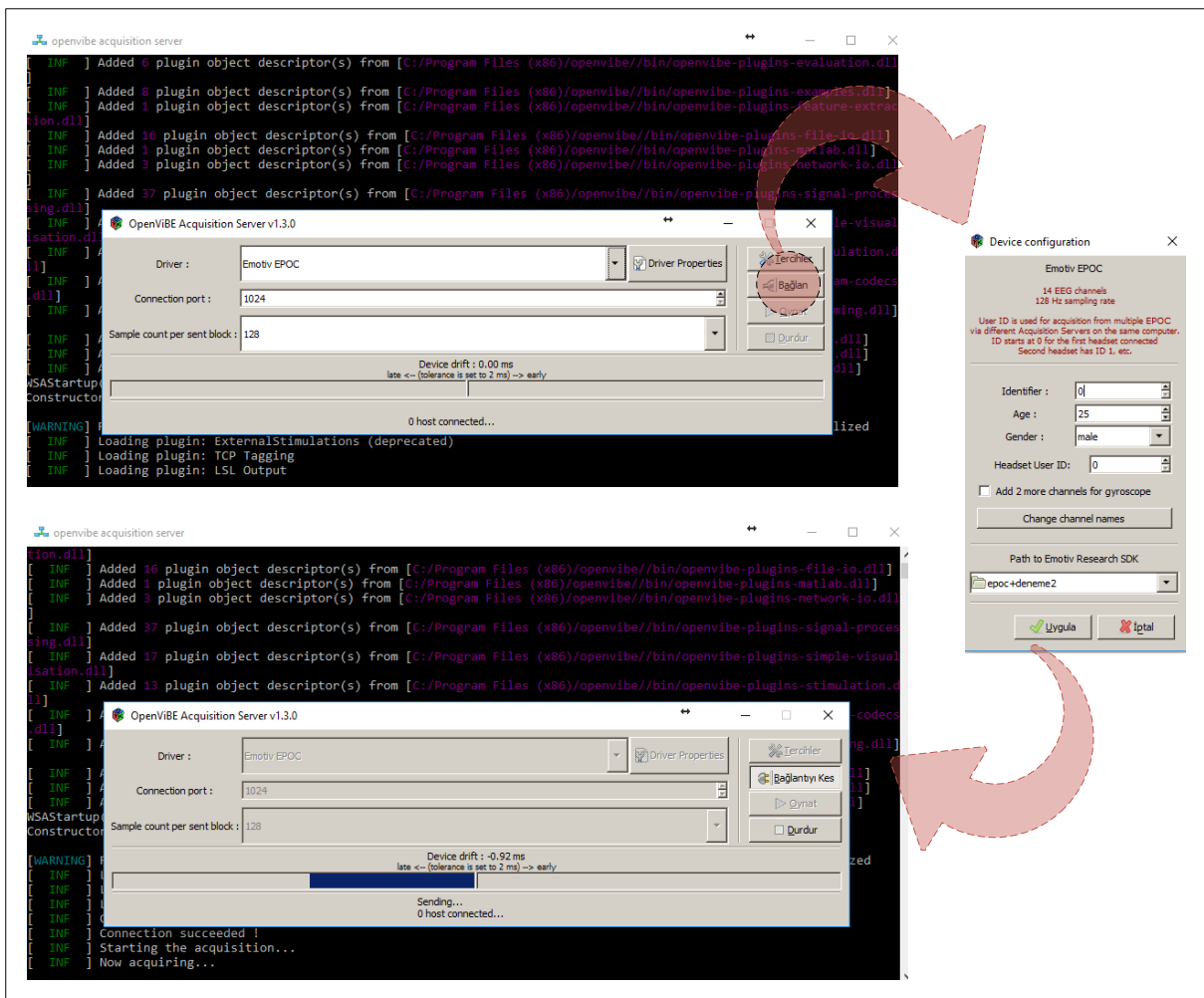


Figure 2. OpenVibe Connection to Emotiv EPOC+

In Figure 3, the OpenVibe instantaneous raw signal, the filtered signal, and the Fast Fourier Transform view of the signal are shown. In this step, OpenVibe provides signals from EPOC+ to the graphical interface through the Acquisition client module. However, a band pass filter is applied to the raw signal obtained from a channel, and a spectrum that varies with time can be

obtained by performing FFT on the other channel, and the results of these operations are displayed instantaneously. On one hand, a filter is applied to the acquired signal and on the

other hand an FFT is applied to obtain a spectrum that varies in time, and the results of these operations are displayed instantaneously.

In addition, Figure 4 shows two boxes, Peripheral and Experiment Setting boxes, containing the configuration parameters. The settings in the peripheral box must be adjusted to the screen refresh rate, which is the hardware configuration. The settings in the experiment box include several parameters related to the general settings of SSVEP. Adjustments are made such as the colours of the flickering boxes on the simulator screen, the frequency value of each box, the signal length to be used to find the SSVEP response, the speed range between the signal ranges, and the tolerance of the frequency band around the stimulus frequency used for classification.

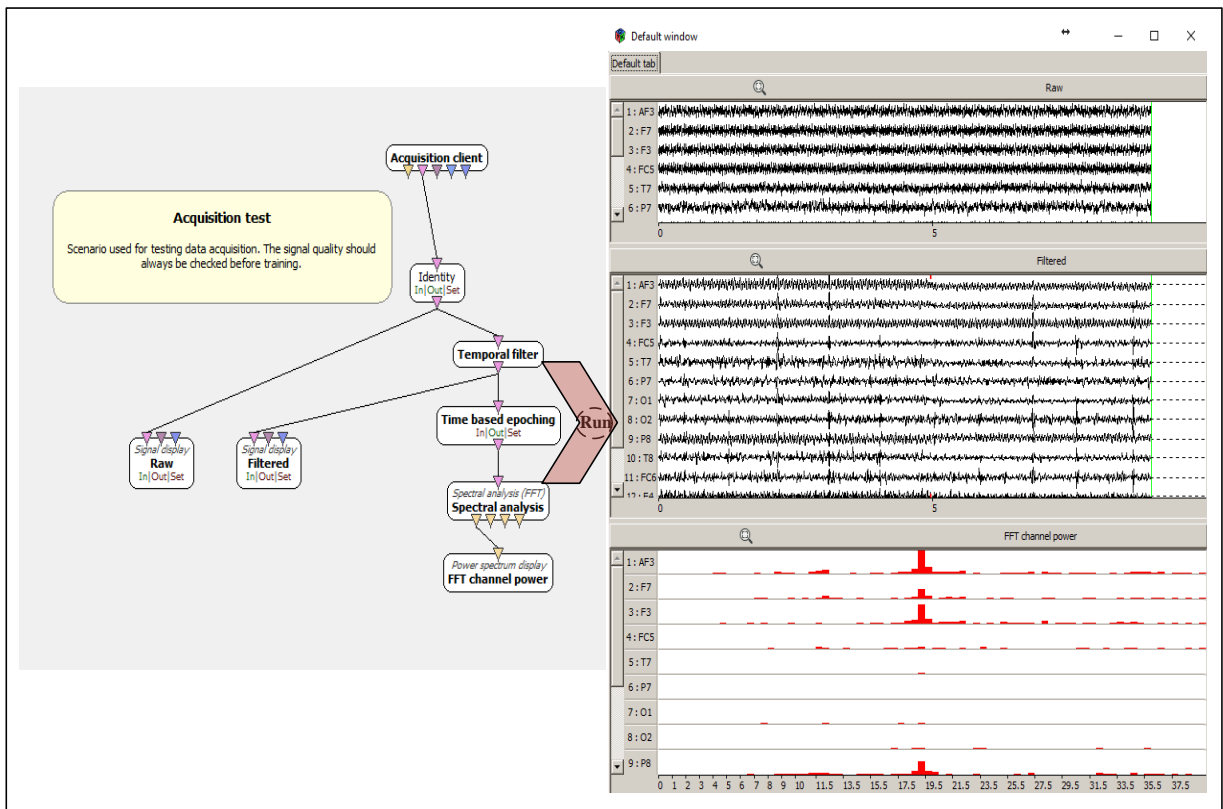


Figure 3. Instant Signal Processing Imaging In OpenVibe

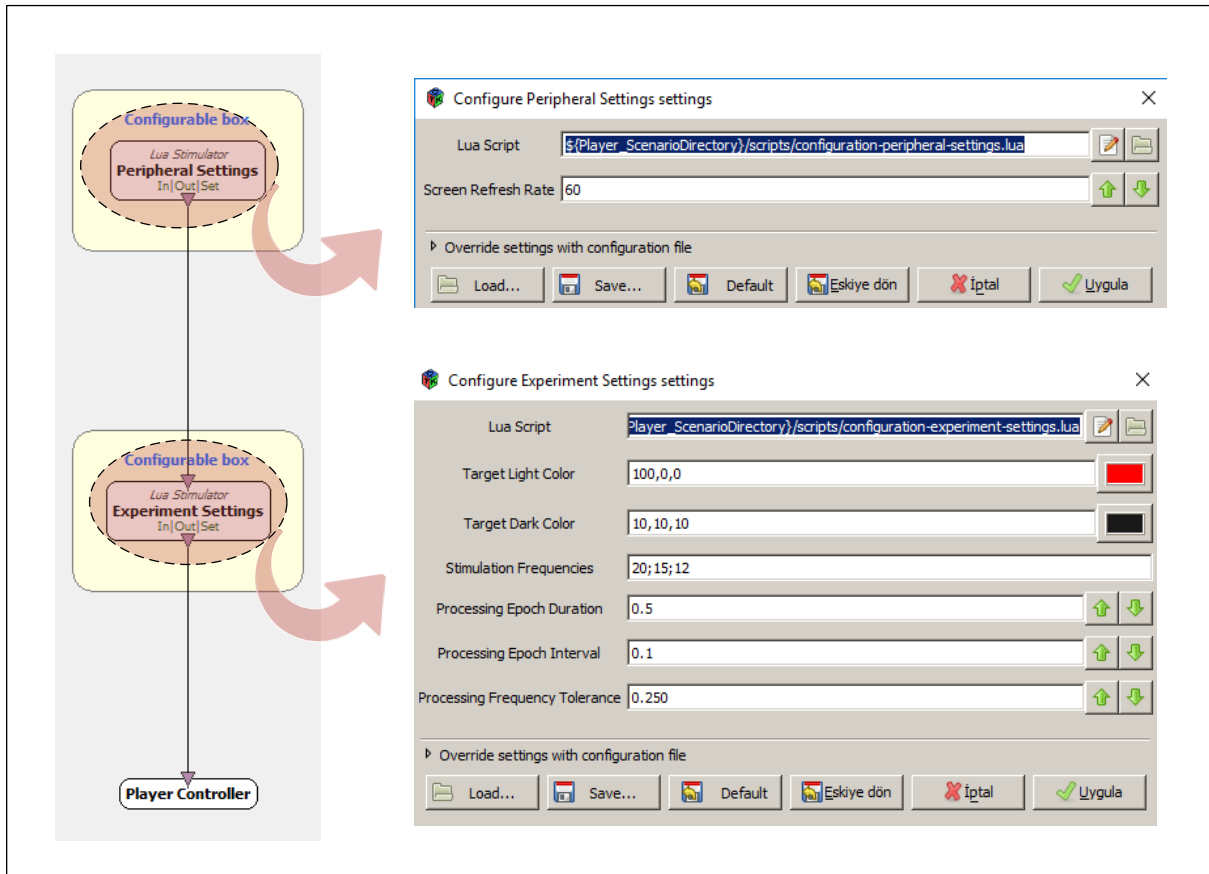


Figure 4. OpenVibe Signal Acquisition Configuration Settings

To train the SSVEP classifiers in this step, the user's concurrent EEG signal, which looks at stimuli vibrating at different frequencies, is recorded within the specified time and the required training data is obtained. The scenario in which the data recorded to be trained is shown in Figure 5. The SSVEP Education Supervisor has an important role in this step.

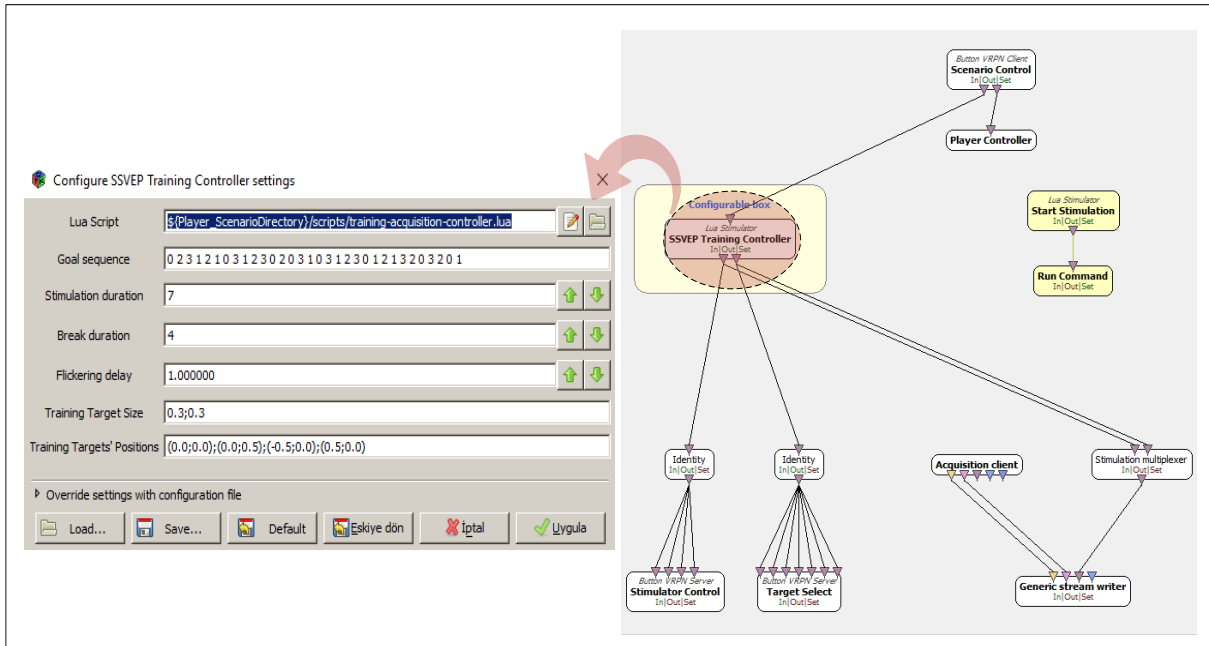


Figure 5. OpenVibe SSVEP Signal Training

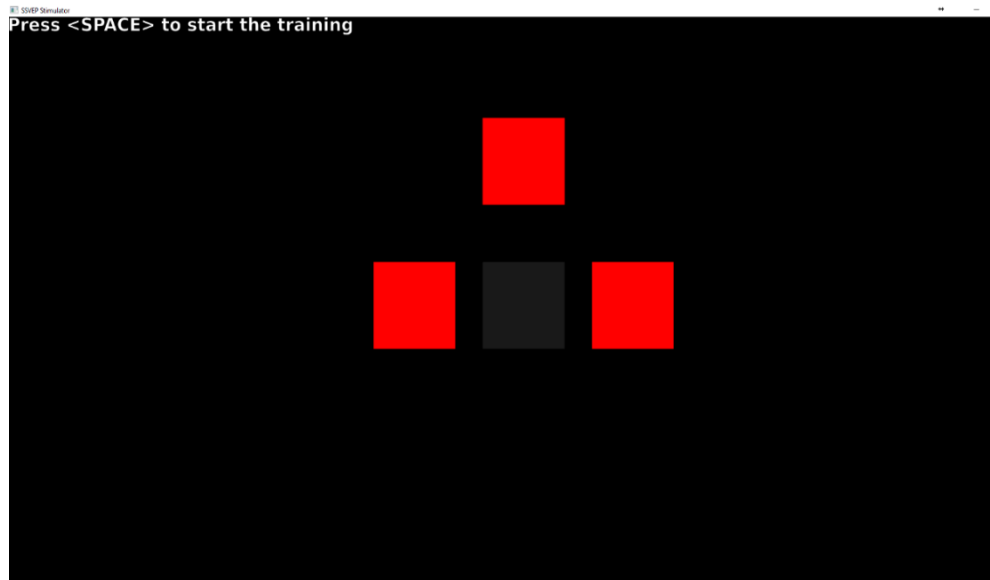


Figure 6. Vibrating Boxes at Different Frequencies

As shown in Figure 6, the flicker stimulator has parameters that need to be set. These can be defined as the target sequence showing the target box to be looked at among the vibrating boxes at different frequencies, the duration of the excitation showing the duration of the sequence of vibrations of the targets, the duration of the rupture representing the duration of the objects, the oscillating delay representing the delay between the arrow indicating the target and the beginning of the oscillation.

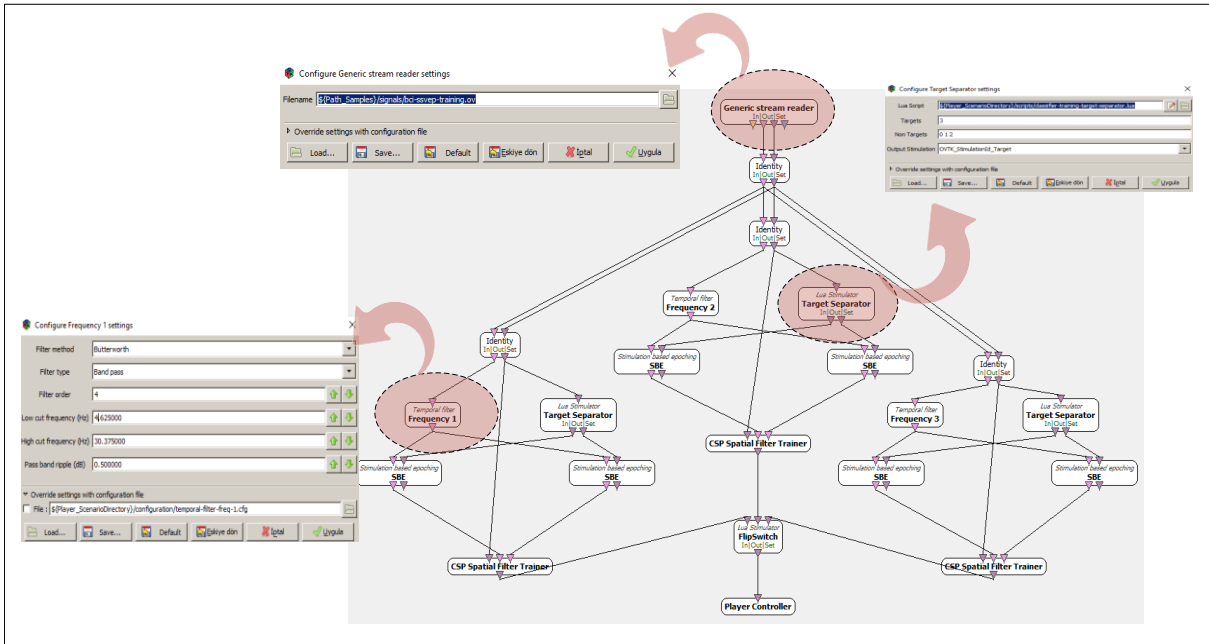


Figure 7. OpenVibe CSP Filter

This step as shown Figure 7, includes three different signal processing situation assessment platforms. The first of these processes is based on the first flickering frequency, the second one is based on the second flickering frequency, and the third one is based on the third flickering frequency. The data saved in the previous step is loaded into the generic stream reader. Then, Common Spatial Pattern filter which automatically selects which electrode channels are the most efficient combination is used for training. The most suitable channels of the Emotiv headset corresponding to the region in which the 3 different brain signal frequency responses are seen intensely in the brain and where the separable essences of these signals dominate are selected. Band pass filter and butterword method are applied to each frequency.

3. PERFORMANCE ANALYSIS OF SSVEP

Three different classifiers, Support Vector Machine, Linear Discriminant Analysis and Multi-Layer Perceptron, are used. *Linear Diskiriminant Analysis* (LDA) is based on searching for a linear combination of variables that best distinguishes between good class (targets). The best way to determine discrimination is to calculate Mahalanobis distance between two groups. The fact that Mahalanobis distance is less than three means that the probability of misclassification is rather small.

Single layer perceptron's are simple and fast, but not sufficient to solve complex problems, since they can only solve uncomplicated linear problems. This is due to the fact that there is only one weight matrix that can be trained. Therefore, multi-layered artificial neural networks are needed to solve complex and non-linear problems. For example, Multilayer-Artificial

Neural Network (ANN) neurons are composed of at least one input layer, one or two hidden layers, and finally at least one output layer. The most important findings in an ANN model are inter-node links. The formation of the network topology is achieved by connecting a certain number of neurons in each layer with neurons in subsequent layers [10].

Multilayer Sensors belong to the advanced feeder of the nerve network. Typical MLP network model consists of a group of neurons with three categories: input neurons, hidden neurons, and output neurons. Each neuron is in a layer and is associated with all neurons of the set layer [11],[12]. In order to achieve good performance, it is important to determine the appropriate neural network model for the problem. A suitable training algorithm is used after the layers and the number of units in each layer have been determined. And we have weight and threshold values that will reduce the guess error of the network to the minimum.

Support Vector Machines is a supervised machine learning algorithm that can be used for both classification and regression difficulties. In this algorithm, each data item is represented as an n-dimensional set of points along with the value of each feature. When used for classification, the classification is performed in such a way that a certain binary-labelled training set is separated by a hyperplane farthest from them. For situations where linear separation is not possible, it can work with the "core" technique.

SVM has a technique called kernel. These are functions that take a low-dimensional input field and transform it into a higher-dimensional area; In other words, transforms the non-decomposable problem into separable problems, which are called the kernel [13]. It is often useful in the problem of nonlinear separation. Briefly stated, it makes highly complex data transformations, then learns the operation that separates data based on tags or output you define.

4. RESULTS AND DISCUSSION

In this study the percentages of success of the network trained on the processed dataset are computed. On the recorded data, accuracy rate of 92% with LDA, 89% with MLP and 97% with SVM have been obtained for the first flicker. For the second flicker, accuracy rate of 89% with LDA, 87% with MLP and 91.7% with SVM have been obtained. Finally, for the third flicker, accuracy rate of 90% with LDA, 85% with MLP and 89% with SVM have been obtained as shown in Table 1.

Table 1 Frequency classification results

Frequencies	LDA	MLP	SVM
<i>Frequency1</i>	92%	89%	97%
<i>Frequency2</i>	89%	87%	91.7%
<i>Frequency3</i>	90%	85%	89%
<i>Mean</i>	90.33%	87%	92.56%

Table 1 shows the post-training classification results of the SSVEP response of the data set generated by the Emotiv Epoc+ device and the personal EEG signals in the openVibe editor. The best classifier has been identified as SVM with 92.56% accuracy, as seen in the Table 1.

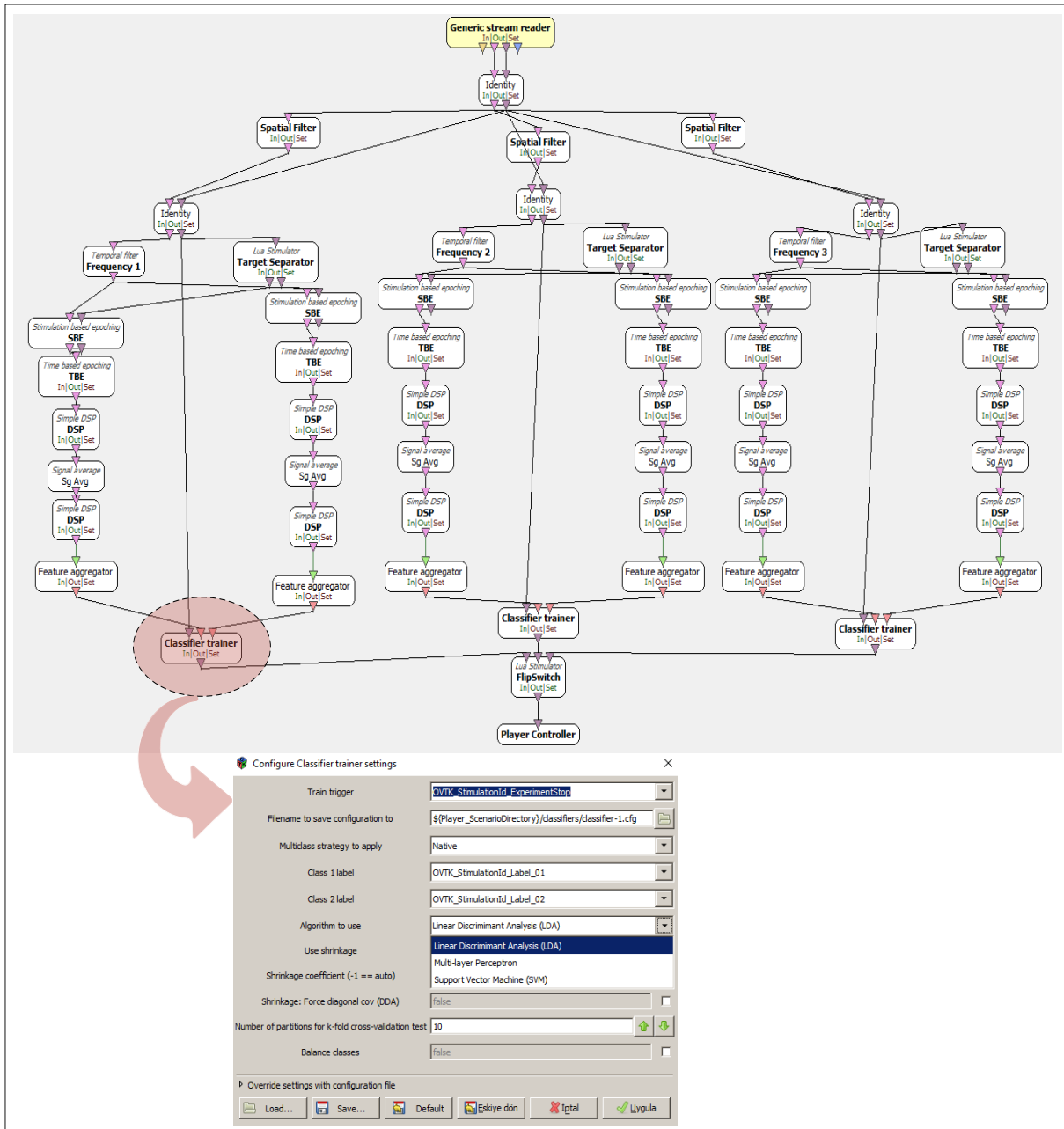


Figure 8. OpenVibe Classifier Trainer

Finally, the amplitude values for the stimulated and non-stimulated periods are received by the classifier and trained to distinguish between the two. One classifier is trained per each stimulation frequency. Each frequency is treated separately. There are two important boxes in the processing chain; Temporal filter extracts a single frequency band. It is configured with a file generated by the configuration processing. Target Separator separates the targets used to separate a frequency from the others and each stimulus response is sent to the corresponding classes according to their frequency.

In Figure , the pre-processed signals recorded for training in the previous steps are shown to be classified by LDA, MLP and SVM. The processed and recorded signals are used to generate classifiers that can be used in online BCI applications.

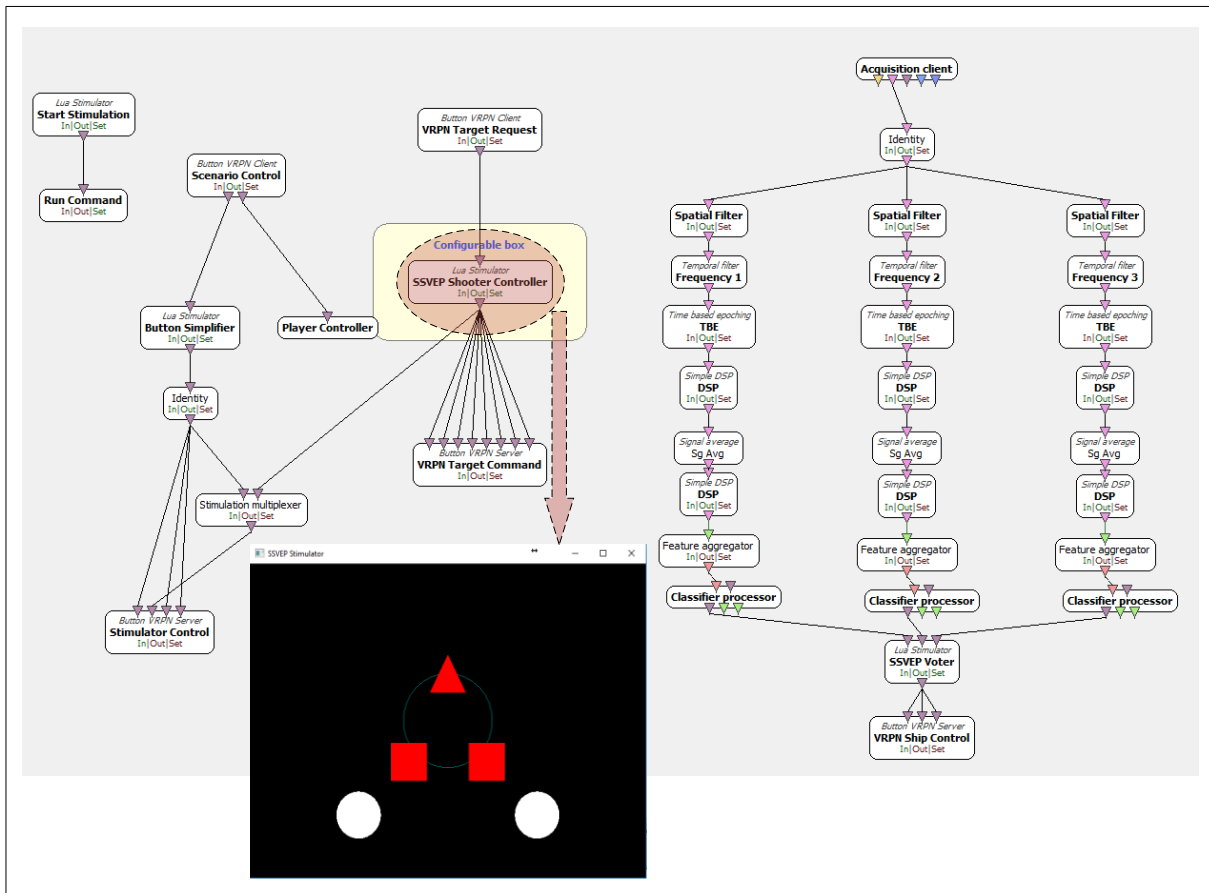


Figure 9. BCI Online Test Shooter

In the last step, the system was tested by shooting the target online using the brain signals recorded momentarily. This is shown in Figure . This step is the online testing setup. We can use it to evaluate the trained network structure of the classifiers in the previous step. The system is simply tested with a game. There are 3 moves in the game. When you look at the left square, it moves clockwise. When you look at the left square, it moves in the opposite direction of the clock. When you look at the triangular shape, the system is shooting. Online tests carried out through the experiments showed a high amount of accuracy rate and hence, it validates the accuracy of the SSVEP in OpenVibe.

5. CONCLUSION

Steady State Visual Evoked Potential based BCIs use several stable oscillating light sources, each of which vibrates at unique frequencies. SSVEP is a continuous brain response that

occurs at a constant frequency in the occipital and parietal cortical regions of the brain under visual

stimulation by looking at the constantly pulsing light source at specific frequencies. SSVEP can be detected automatically by signal processing algorithms such as pre-processing,

artefact detection-correction, feature extraction and classification. In this paper, we analyse the EEG signal classification and SSVEP performance of the OpenVibe, utilizing three flickers in a few steps. These steps consist of configuration, training acquisition, Common Spatial Pattern filters (CSP) training, classifier training and online test shooter. Our test results show that offline accuracy rate of 90.33% with LDA, 87% with MLP and 92.56% with SVM has been obtained as the average of three flickers. Online tests carried out through the paper also validates the accuracy of the SSVEP in OpenVibe.

REFERENCES

- [1] Y. Renard *et al.*, “OpenViBE: An Open-Source Software Platform to Design, Test, and Use Brain–Computer Interfaces in Real and Virtual Environments,” *Presence Teleoperators Virtual Environ.*, vol. 19, no. 1, pp. 35–53, 2010.
- [2] I. Martišius and R. Damaševičius, “A Prototype SSVEP Based Real Time BCI Gaming System,” *Comput. Intell. Neurosci.*, vol. 2016, pp. 1–15, 2016.
- [3] A. A. Ioannides, V. Poghosyan, J. Dammers, and M. Streit, “Real-time neural activity and connectivity in healthy individuals and schizophrenia patients,” *Neuroimage*, vol. 23, no. 2, pp. 473–482, 2004.
- [4] B. Allison, T. Luth, D. Valbuena, A. Teymourian, I. Volosyak, and A. Graser, “BCI Demographics: How Many (and What Kinds of) People Can Use an SSVEP BCI?,” *IEEE Trans. Neural Syst. Rehabil. Eng.*, vol. 18, no. 2, pp. 107–116, 2010.
- [5] Y.-F. Chen, K. Atal, S.-Q. Xie, and Q. Liu, “A new multivariate empirical mode decomposition method for improving the performance of SSVEP-based brain–computer interface,” *J. Neural Eng.*, vol. 14, no. 4, p. 46028, 2017.
- [6] F.-B. Vialatte, M. Maurice, J. Dauwels, and A. Cichocki, “Steady-state visually evoked potentials: Focus on essential paradigms and future perspectives,” *Prog. Neurobiol.*, vol. 90, no. 4, pp. 418–438, 2010.
- [7] H.-J. Hwang, J.-H. Lim, Y.-J. Jung, H. Choi, S. W. Lee, and C.-H. Im, “Development of an SSVEP-based BCI spelling system adopting a QWERTY-style LED keyboard,” *J. Neurosci. Methods*, vol. 208, no. 1, pp. 59–65, 2012.
- [8] T. MISAWA, J. MATSUDA, and S. HIROBAYASHI, “A Single-Trial Multiclass Classification of Various Motor Imagery Tasks for EEG-Based Brain-Computer Interface Communication,” *Electron. Commun. Japan*, vol. 100, no. 1, pp. 18–26, 2016.
- [9] H. Macpherson, A. Pipingas, and R. Silberstein, “A steady state visually evoked potential investigation of memory and ageing,” *Brain Cogn.*, vol. 69, no. 3, pp. 571–



3rd International Conference on Science, Ecology and Technology
Rome, ITALY
14-16 August 2017

- 579, 2009.
- [10] Q. Yang, S. Le Blond, R. Aggarwal, Y. Wang, and J. Li, “New ANN method for multi-terminal HVDC protection relaying,” *Electr. Power Syst. Res.*, vol. 148, pp. 192–201, 2017.
- [11] N. M. Hewahi and E. Abu Hamra, “A Hybrid Approach Based on Genetic Algorithm and Particle Swarm Optimization to Improve Neural Network Classification,” *J. Inf. Technol. Res.*, vol. 10, no. 3, pp. 48–68, 2017.
- [12] N. Mammadova and İ. Keskin, “Application of the Support Vector Machine to Predict Subclinical Mastitis in Dairy Cattle,” *Sci. World J.*, vol. 2013, pp. 1–9, 2013.
- [13] N. Cristianini and J. Shawe-Taylor, *An Introduction to Support Vector Machines and Other Kernel-based Learning Methods*. Cambridge University Press, 2000.

THERMODYNAMIC ANALYSIS OF A GAS TURBINE

Ugur Akyol*¹ and Ercan Özdemir²

¹ Mechanical Engineering Department, Namık Kemal University, TURKEY.

(E-mail: uakyol@nku.edu.tr)

² Trakya Organic Agriculture Livestock and Trade Limited Company, TURKEY.

(E-mail: ercanozdemir1986@hotmail.com)

Corresponding Author's e-mail: uakyol@nku.edu.tr

ABSTRACT

This study involves analyzing of a natural gas turbine system by using the first and second laws of thermodynamics. As a result of the study, the optimal operating conditions of a gas turbine were determined and some information was given on what needs to be done to increase the efficiency. It was determined that an average of 81.1% of the energy produced in the gas turbine was consumed in the compressor while the compressor compression ratio was 10:1; also an average of 78% while the compressor compression ratio was 15:1, an average of 76.2% while the compressor compression ratio was 20:1 and an average of 75.7% while the compressor compression ratio was 25:1 at compressor air inlet temperatures between 270 and 303 K. A 33°C increase in compressor inlet temperature leads to a 6% reduction in thermal efficiency when the compressor pressure ratio is 10:1, and leads to a 4.8% reduction when the compressor pressure ratio is 25:1. The increase in the compressor inlet air temperature reduces the thermal efficiency at all compressor pressure ratios. However, the effect of reducing the thermal efficiency of the increase in compressor inlet air temperature is reduced as the compressor pressure ratio increases. Also the reversible work and the second law efficiency of the compressor of the gas turbine system were calculated at different compressor pressure ratios for different compressor air inlet temperatures.

Keywords: Gas turbine; Compressor; Thermodynamic analysis; Optimal operating conditions.

1. INTRODUCTION

According to other energy sources, natural gas, which is easy to use and has less impact on the environment, is increasingly used as primary energy source in Turkey. Due to its advantages such as high efficiency and short time operation, natural gas-fired gas turbines have been used increasingly in recent years in electricity generation in our country. Natural gas fueled gas turbines can be operated in a shorter period of time with lower installation costs than thermal, nuclear and hydroelectric power plants using other fossil fuel sources. In addition to providing high efficiency and power, gas turbines have working characteristics

that are suitable for flexible operating conditions, can be quick-actuated, can be easily adapted to full load and

variable load conditions, and change their efficiency according to ambient temperature and compressor pressure ratio. Gas turbines are used worldwide for power

generation in many regions. The place of installation of such systems is very important. The interest of the gas turbines in the generation of electricity is very much related to the environmental temperature. The average environmental temperature and humidity from different geographical locations affect power generation and turbine efficiency.

The first law of thermodynamics relates to the quantity of energy and refers to the conservation of energy. The first law does not make any assessment of the nature of the energy. The second law of thermodynamics makes it possible to make evaluations on the quality of the energy. The second law analysis is based on entropy or available energy.

There is considerable work in the literature on the performance of gas turbines. Ünver and Kılıç (2009) studied thermodynamic analysis of a combined cycle power plant. In the study, the changes of the performance parameters of a natural gas-fired combined cycle power plant were investigated with the help of first and second law analysis of thermodynamics [1]. Çetin (2006) has conducted a study on the optimal performance analysis of gas turbines. They theoretically calculated according to the working conditions of gas turbines. As a result of the calculations made, he has interpreted and suggested the optimal performance analyzes of the working conditions of the gas turbines [2]. Alhazmy and Najjar (2004) have conducted a study to improve the gas turbine performance by cooling the compressed air. They used two different types of coolers in their work. These are water-sprayed and cooling coils [3]. Basrawi *et al.* (2011) examined the effect of ambient temperature on the performance of a micro gas turbine system in cold climatic conditions [4].

2. MATERIAL AND METHODS

Gas turbine system

As a gas turbine, a natural gas-operated system was examined in the Caterpillar Tarus 5.7 MW power plant, which is shown in Figure 1. The characteristics of the gas turbine is shown in Table 1.

Table 1. Characteristics of the gas turbine considered in the study [5].

Brand Mark	Installed power (MW)	Length (m)	Width (m)	Height (m)	Weight (kg)
Caterpillar Tarus	5.7 MW	9.8	2.5	2.9	32800

In the Caterpillar Tarus gas turbine, the pressure and temperature of the air taken by the filter are raised by the rotors in the compressor. The pressure and temperature of the compressor are

mixed with the natural gas, and the gas is sent to the combustion chamber of the turbine by the manifold. The combustion air, which is the result of combustion, is propelled by the gas turbine

shaft. The shaft of the gas turbine begins to rotate with this drive and performs the electricity generation by rotating the shaft of the gas turbine generator connected to it. The gases produced as a result of combustion are discharged to the atmosphere through the exhaust outlet system.

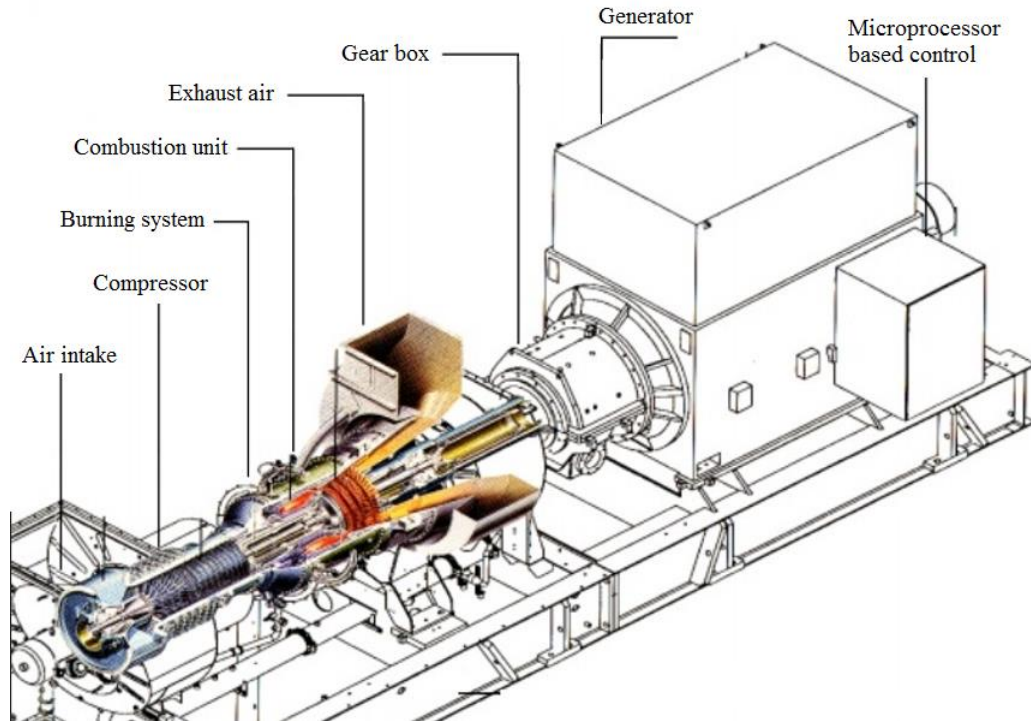


Figure 1. Schematic view of the gas turbine system [5].

Formulation

Thermodynamic analysis was carried out by taking temperature and pressure values at different compressor pressure ratios. The assumptions made for the analysis are: Air and products of combustion are assumed to be ideal gases. It is thought to be a complete combustion reaction. Each of the components that constitute the system is considered as a steady-flow control volume. The combustion gases are considered to be air. First, inlet temperatures and turbine combustion chamber temperatures were taken by the plant during the year at different compressor pressures. The ideal gas table for the air was used in solutions. Figure 2 shows the main components of the gas turbine cycle and the points considered in calculations. The principle of conservation of energy, in other words first law of thermodynamics for a steady-flow open system is expressed as follows [6]:

$$\dot{Q} - \dot{W} = \sum \dot{m}_{out} \left(h_{out} + \frac{V_{out}^2}{2} + gz_{out} \right) - \sum \dot{m}_{in} \left(h_{in} + \frac{V_{in}^2}{2} + gz_{in} \right) \quad (1)$$

where \dot{Q} (kW) is heat transfer rate, \dot{W} (kW) is power, \dot{m} (kg/s) is mass flow rate, h (kJ/kg) is enthalpy, V (m/s) is velocity of the fluid related to the kinetic energy, g (m/s²) is acceleration of gravity and z (m) is elevation related to the potential energy. Also, the subscripts *in* and *out* denotes the fluid entering and leaving the control volume respectively.

The kinetic and potential energy changes between compressor input and output, and the heat transfer at the compressor can be neglected. In this case, according to Figure 2, compressor work w_c (kJ/kg) can be written as;

$$-w_c = h_2 - h_1 \quad (2)$$

The heat given to the system in the combustion chamber is q_{in} (kJ/kg);

$$q_{in} = h_3 - h_2 \quad (3)$$

Turbine work is w_t (kJ/kg);

$$w_t = h_3 - h_4 \quad (4)$$

Net work of the system is w_{net} (kJ/kg);

$$w_{net} = w_t - w_c \quad (5)$$

Thermal efficiency of the cycle is;

$$\eta_{th} = \frac{w_{net}}{q_{in}} \quad (6)$$

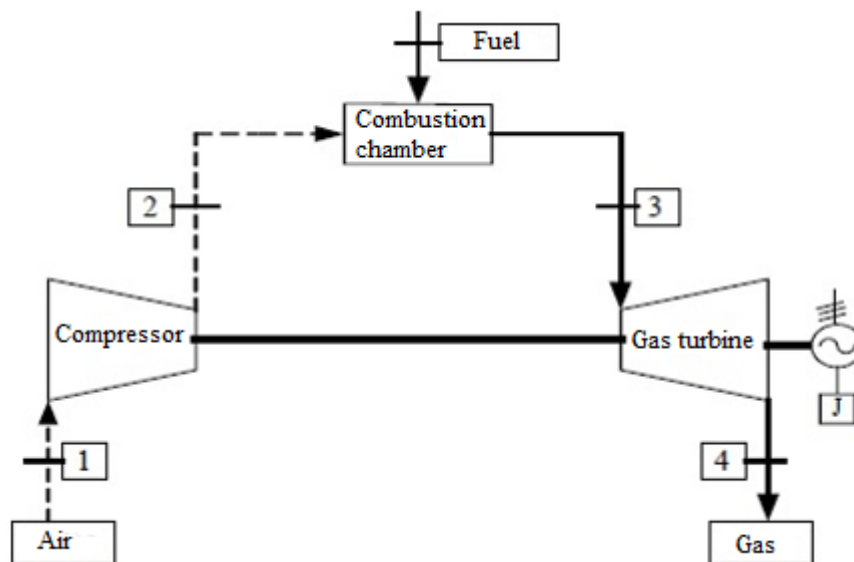


Figure 2. Gas turbine cycle.

The second law of thermodynamics for a steady-flow open system is expressed as follows:

$$\dot{S}_{pro} = \sum \dot{m}_{out} s_{out} - \sum \dot{m}_{in} s_{in} + \frac{\dot{Q}_o}{T_o} \quad (7)$$

where \dot{S}_{pro} (kW/K) is entropy production, \dot{m} (kg/s) is mass flow rate, s (kJ/kg·K) is specific entropy, \dot{Q}_o (kW) is heat transfer rate between the system and the environment, T_o (K) is temperature of the environment.

Reversible work w_{rev} (kJ/kg) for the compressor is;

$$w_{rev} = (h_1 - h_2) - T_o(s_1 - s_2) \quad (8)$$

When calculating the entropy change for an ideal gas considering the variable specific heat, the following relation can be used taking into account both the effect of temperature and pressure on the entropy;

$$s_1 - s_2 = (s_1^o - s_2^o) - R \cdot \ln \frac{P_1}{P_2} \quad (9)$$

where R (kJ/kg·K) is ideal gas constant and P (kPa) is pressure. Second law efficiency for the compressor is as follows:

$$\eta_{c,II} = \frac{w_{rev}}{w_u} \quad (10)$$

where w_{rev} (kJ/kg) is reversible work and w_u (kJ/kg) is useful work.

3. RESULTS AND DISCUSSION

In this study the effect of ambient temperature and the compressor compression ratio on the performance of the gas turbine was determined by using thermodynamic analysis. Specific net work, thermal efficiency of the system, reversible work and second law efficiency of the compressor were calculated. Figure 3 shows the variation of the energy consumed in the compressor according to the pressure ratio in the compressor. When the figure is examined, the energy consumed in the compressor is also increased in proportion to the ambient temperature and compressor pressure ratio.

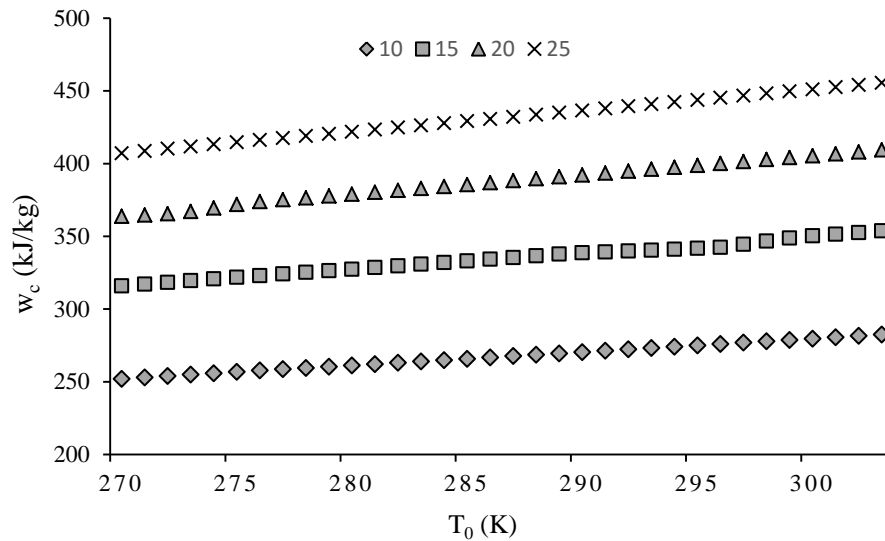


Figure 3. Energy consumed in compressor for different compressor pressure ratio and inlet air temperature values.

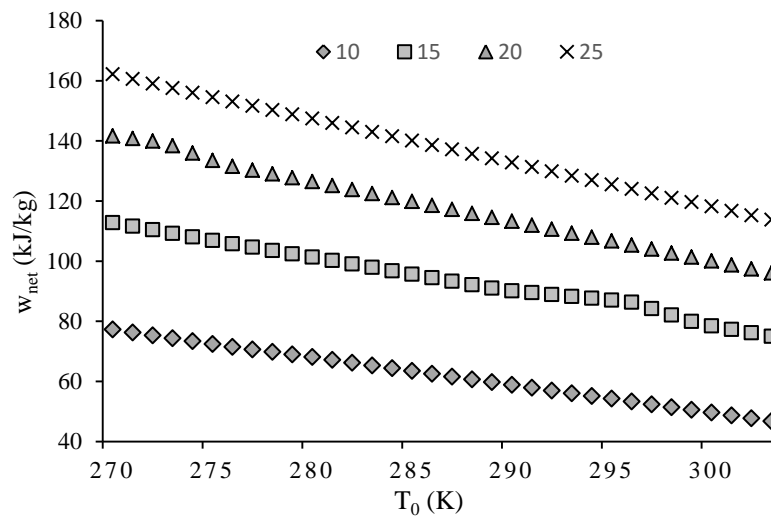


Figure 4. Net work values for different compressor pressure ratio and inlet air temperature values.

Figure 4 shows w_{net} values at different compressor pressure ratios according to T_0 temperature. For example, the pressure ratio is 10:1, $w_{net}=77.3$ kJ/kg at $T_0=270$ K, and $w_{net}=46,7$ kJ/kg at $T_0=303$ K. However, when the pressure ratio is 25:1, $w_{net}=162.1$ kJ/kg at $T_0=270$ K and $w_{net}=113.8$ kJ/kg at $T_0=303$ K. As can be seen from the calculation results, the net work is increasing as the compressor pressure ratio decreases and the ambient temperature decreases.

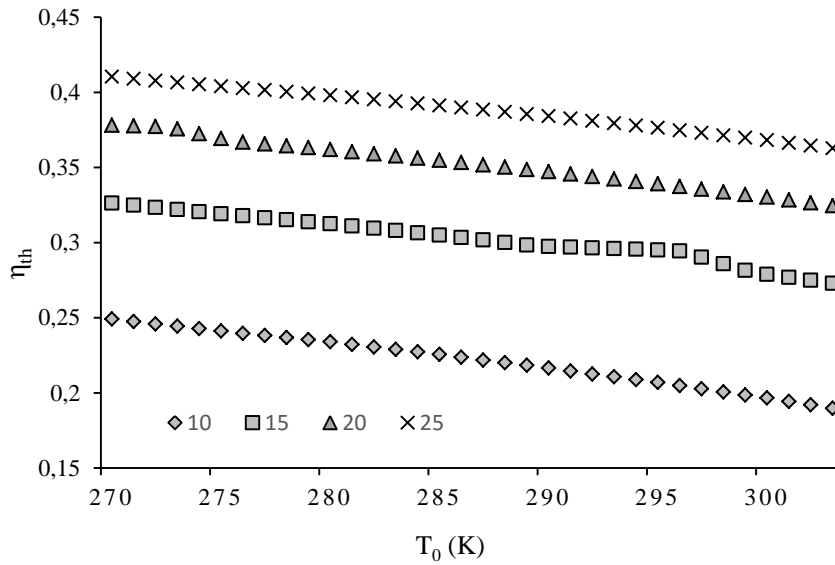


Figure 5. Thermal efficiency for different compressor pressure ratio and inlet air temperature values.

The effect of ambient temperature on thermal efficiency at different pressure ratios can be seen in Figure 5. At any compressor pressure ratio value, as the ambient temperature increases, the thermal efficiency decreases while the decrease in the pressure ratio causes the tendency to decrease at the thermal efficiency. For example, for a 10:1 pressure ratio, the thermal efficiency at $T_0=270$ K is 24.9% and the thermal efficiency at $T_0=303$ K is 18.9%. While the pressure ratio is 10:1, an increase of 33°C at ambient temperature reduces the thermal efficiency by 6%. For a 25:1 pressure ratio, the thermal efficiency at $T_0=270$ K is 41% and the thermal efficiency at $T_0=303$ K is 36.2%. While the pressure ratio is 25:1, an increase of 33°C at ambient temperature reduces the thermal efficiency by 4.8%. As the compressor pressure ratio increases, the effect of the ambient temperature on the thermal efficiency decreases.

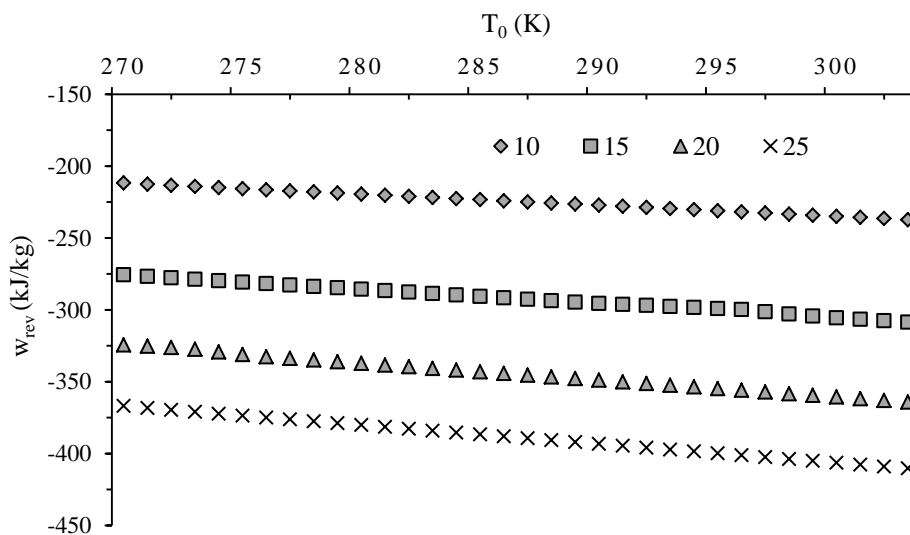


Figure 6. Reversible work of compressor for different compressor pressure ratio and inlet air temperature values.

Figure 6 shows the reversible work of the compressor depending on the air inlet temperature at different compressor pressure ratios. Reversible work represents the most useful work that can be obtained from a system. This happens when the system is totally reversible. In other words, the heat transfer between the system and environment is reversible and there is no irreversibility in the system. As can be seen in this figure, the reversible work is considerably reduced with increasing in the compressor pressure ratio and ambient temperature.

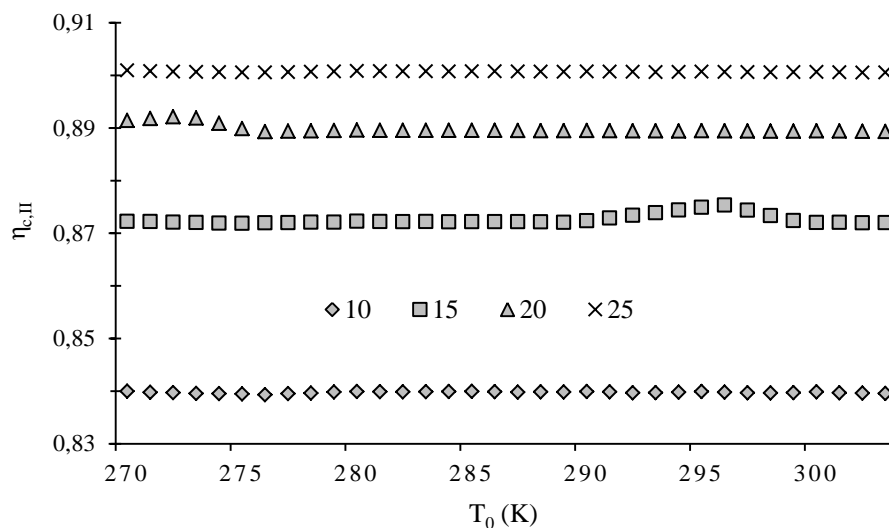


Figure 7. Second law efficiency of the compressor for different compressor pressure ratio and inlet air temperature values.

Figure 7 shows the second law efficiency values calculated for the compressor depending on inlet air temperature at different compressor pressure ratios. The second law is about how much of the business potential is being used. The second law is the ratio of useful work to the least (reversible) work required for compressors. As can be seen from this figure, the second law efficiency increases with increase in compressor pressure ratio. When the compressor pressure ratio is 10, the second law efficiency is approximately 84%, when it is 15, it is between 87-88%, when it is 20 it is about 89% and when the pressure ratio is 25, second law efficiency is slightly over 90%. On the other hand, the second law efficiency does not change considerably depending on the inlet temperature of the compressor inlet air.

4. CONCLUSION

As can be seen from the results obtained, at any pressure ratio value, the net work and thermal efficiency decreases as the ambient temperature increases. As the compressor pressure ratio increases, the energy, net work and thermal efficiency of the compressor is increased. That is, the thermal efficiency and net work are directly proportional to the compressor pressure ratio, while the energy consumed in the compressor is inversely proportional to the compressor pressure ratio.

As the ambient temperature increases, the mass flow of air entering the gas turbine decreases, which causes the net work value to be reduced by affecting the entire system. It is also seen that the pressure ratio of the compressor is higher than the ambient temperature of the effect of the system on the thermal efficiency.

As a result, it is very important to determine the compressor pressure ratio during the first stage of the system installation. Because, as the net work of the system decreases at low pressure ratios, it is necessary to increase the mass load, that is, to design a larger system, in order to obtain the desired power. A larger system may not be economical. Therefore, the most economical system should be determined by the relationship between compressor pressure ratio, ambient temperature change and desired net work. The best choice for this plant is to use a 25:1 compressor. Once the compressor selection has been completed, the annual temperature data at which the system is to be installed should be inspected, and the systems to be used to reduce the temperature of the compressor air entering must be investigated. The cost of the pre-cooling systems should be determined by comparing the income from the increase in the efficiency of the system.

REFERENCES

- [1] Ü. Ünver and M. Kılıç, 2009. Bir Kombine Güç Santralinin Termodinamik Analizi. *Mühendis ve Makina*. 46 (545) 47 - 56.
- [2] B. Çetin, 2006. Gaz Türbinlerinin Optimal Performans Analizi. *Doğuş Üniversitesi Dergisi*. 7 (1) 59 - 71.
- [3] M.M. Alhazmy and Y.S.H. Najjar, 2004. Augmentation of Gas Turbine Performance using Air Coolers. *Applied Thermal Engineering*. 24 (2 - 3) 415 - 429.
- [4] F. Basrawi and T. Yamada, K. Nakanishi and S. Naing, 2011. Effect of Ambient Temperature on the Performance of Micro Gas Turbines with Cogeneration System in Cold Region. *Applied Thermal Engineering*. 31 (6 - 7) 1058 - 1067.
- [5] E. Özdemir, 2017. *Thermodynamic Analysis of a Gas Turbine Cycle*, Ms Thesis, Department of Mechanical Engineering, Graduate School of Natural and Applied Sciences, Namık Kemal University, Turkey.
- [6] Y.A. Çengel and M.A. Boles, *Thermodynamics: An Engineering Approach*, 8th ed. Wiley-McGraw-Hill, New York, 2015.

FLOW RATE ESTIMATION MODELLING IN A TRANSMISSION PIPELINE USING RESPONSE SURFACE METHODOLOGY (RSM)

Ugur Akyol*¹, Tuğrul Akyol², A. Deniz Karaoğlan³, Bedri Yüksel² and Asiye Aslan⁴

¹ Mechanical Engineering Department, Namık Kemal University, TURKEY.

(E-mail: uakyol@nku.edu.tr)

² Mechanical Engineering Department, Balıkesir University, TURKEY.

(E-mail: akyol@balikesir.edu.tr, byuksel@balikesir.edu.tr)

³ Industrial Engineering Department, Balıkesir University, TURKEY.

(E-mail: deniz@balikesir.edu.tr)

⁴ Gönen Vocational School, Bandırma Onyedi Eylül University, TURKEY.

(E-mail: asiye_aslan@yahoo.com)

Corresponding Author's e-mail: uakyol@nku.edu.tr

ABSTRACT

The source of geothermal energy to be used for district heating systems is, in most cases, located some distance from the heating market, although geothermal water may also be found within the market area. A transmission pipeline is therefore needed to transport the geothermal fluid from the geothermal field to the end users. Geothermal fluids can be transported over fairly long distances in thermally insulated pipelines. Transmission pipelines of even 60 km length have been built with acceptable heat loss values, though shorter transmission distances are much more common and clearly more desirable. At flowing conditions, the temperature drop in insulated pipelines is in the range of 0.1 to 1.0°C/km, while in uninsulated lines it is 2 to 5°C/km (in the range of 5 to 15 l/s flow for 15-cm diameter pipe).

In addition to a group of parameters, which are almost constant, such as the length, diameter, thickness, thermal insulation properties and material type of the pipeline, whether above ground or buried and so on, temperature drop rate in transmission pipelines is strongly affected by flow rates. At low flow rates, the temperature drop is higher than that of greater flow rates. The temperature drop depending on the flow rate becomes more apparent for relatively long pipelines.

In this study, the temperature drops in the transmission pipeline of the Bigadiç geothermal district heating system (GDHS), a buried 18 km long pipeline, is investigated for varying flow rates. Response Surface Methodology (RSM) is then used for modelling and estimating the flow rate depending on the temperature drop in the pipeline. The results show that the flow rates given by the model (with R^2 , coefficient of determination, of 96.67%) are in a good agreement with those measured by the flowmeter.

Keywords: District heating system; Flow rate; Response Surface Methodology (RSM); Transmission pipeline.

1. INTRODUCTION

Geothermal energy, which is considered as one of the most promising alternative among renewable energy sources, has proven to be sustainable, clean, and safe. Therefore its worldwide applications are increasing steadily. Turkey is one of the top five countries for the direct geothermal applications [1]. Direct use of geothermal energy in Turkey has focused mainly on district heating. Over 8.5 million m² of indoor space is heated using geothermal energy in more than 20 district heating systems [2]. The total installed capacity of these systems (805 MW_t) accounts for 12% of the estimated worldwide capacity of the geothermal district heating systems (6725 MW_t) [3].

The distance of the geothermal resource from the potential heating market is a very important parameter as regards the technical and economic viability of the heating system. However, geothermal fluids can be transported over fairly long distances in thermally insulated pipelines. Transmission pipelines of even 60 km length have been built with acceptable heat loss values (i.e., the Akranes project in Iceland), though shorter transmission distances are much more common and clearly more desirable [4, 5]. The heat loss occurring in a transmission pipeline, whether above ground or buried underground, constitute one of the main sources of total energy loss in a district heating system, and thus a loss in revenue.

In addition to a group of parameters, which are almost constant, such as the length, diameter, thickness, thermal insulation properties and material type of the pipeline, whether above ground or buried and so on, temperature drop rate in transmission pipelines is strongly affected by flow rates. At low flow rates, the temperature drop is higher than that of greater flow rates. The temperature drop depending on the flow rate becomes more apparent for relatively long pipelines. At flowing conditions, the temperature drop in insulated pipelines is in the range of 0.1 to 1.0°C/km, and in uninsulated lines, it is 2 to 5°C/km (in the approximate range of 5 to 15 l/s flow for 15-cm diameter pipe) [6]. It is less for larger diameter pipes. For example, less than 2°C loss is experienced in the new aboveground 29 km long and 80 and 90 cm diameter pipeline (with 10 cm of rock wool insulation) from Nesjavellir to Reykjavik in Iceland [7]. The flow rate is around 560 l/s and takes seven hours to cover the distance.

Uninsulated pipe costs about half of insulated pipe, and thus, is used where temperature loss is not critical. Pipe material does

not have a significant effect on heat loss; however, the flow rate does. At low flow rates, the heat loss is higher than as greater flows.

Balıkesir is one of the geothermal energy-rich provinces of Turkey with several geothermal fields. These sources are all appropriate for direct use such as space and greenhouse heating, industrial processing and balneology. In addition to individual heating, district heating is a common use of geothermal energy in the city. An estimation of nearly 10000 equivalent residential heating is provided in Balıkesir through five GDHSs, namely Gönen, Edremit, Bigadiç, Güre and Sındırgı. However, almost in all systems, the total amount of geothermal fluids produced cannot be determined correctly during the operation due to the lack of flow meters. Instead of this, the geothermal energy produced by the systems is estimated by taking a group of system parameters into account. These parameters are constant initial flow rate of the wells, operating characteristics of the well pumps, some system related temperatures, and etc.

The above mentioned basic incapability has encouraged the authors to develop a mathematical model to estimate the flow rate of geothermal fluids. Thus, the temperature drop rate in the transmission pipeline of the Bigadiç (GDHS), a buried 18 km long pipeline, is investigated for varying flow rates. Response Surface Methodology (RSM) is then used for modelling and estimating the flow rate depending on the temperature drop in the pipeline. The results show that the flow rates given by the model (with R^2 , coefficient of determination, of 96.67%) are in a good agreement with those measured by the flowmeter.

2. MATERIAL AND METHODS

Bigadiç geothermal district heating system

System description. The Bigadiç geothermal district heating system (GDHS), projected for 3000 equivalent residential heating, is located 38 km south of the city of Balıkesir which is in the west of Turkey. Being one of more than 20 GDHSs in Turkey, it began operation for 300 users in 2004-2005 heating season and reached 1548 equivalent residential heating as of 2016. The heat source of the Bigadiç GDHS, Hisarköy geothermal field, is located 23 km east of Bigadiç, and extends over an area of more than 1 km². The reservoir temperature is taken as 110°C (Figure 1).



Figure 1. General view of Hisarköy geothermal field.

The Bigadiç GDHS has 8 production wells in total ranging in depth from 307 to 750 m. However, only two of them, namely HK-2 and HK-8, are operative while the rest are out of service due to the effects of pressure drops in the geothermal fields, precipitation in the wells and the interactions of the wells. Therefore, a peak power unit (an auxiliary heating support) has to be operated in most cases, almost 70% of the heating period, due to the wells which subsequently became inoperative. Lineshaft pumps are used in both geothermal wells. The pumps are driven by frequency converter to regulate the flow instead of just turning the pump on and off. The mean temperatures and flow rates of the HK-2 and HK-8 wells are 95°C and 100.5°C; 10 kg/s and 15 kg/s, respectively (Figure 2).



Figure 2. Views from the HK-8 well (left) and main gas separator and collection lines (right).

The Bigadiç GDHS consists mainly of three circuits: (a) energy production circuit (EPC), (b) energy distribution circuit (EDC), and (c) energy consumption circuit (ECC). The schematic diagram of the system is given for the heating period in Fig. 3. In the EPC, the thermal water at an average temperature of 95°C and a flow rate range of 20-25 l/s drawn from the production wells in the Hisarköy geothermal field is transported to the heat exchangers

located in the heat centre of the system. A buried transmission pipeline of 18 km is used for the transportation. The

geothermal water moves itself in the transmission pipeline since the elevation difference between the inlet and outlet of the pipeline is approximately 200 m, good enough for a natural flow of 25 l/s water.

The EDC is a closed-loop system with three pairs of independent supply and return pipes in which a secondary fluid circulates in order to transfer the heat to the ECC. The supply/return temperatures for the secondary fluid obtained during the winter operation conditions are on average of 56/44°C. The supply temperature of 56°C is reached in two stages: the return temperature (44°C) is first raised up to 50°C using three flat heat exchangers; Heat Exchanger-I (HE-I), Heat Exchanger-II (HE-II) and Heat Exchanger-III (HE-III), which transfer the heat from the geothermal fluid to the secondary fluid in the heat centre. The secondary fluid is then transferred to the peak power unit, which consists of two liquid fuel boilers, each of which has a nominal power of 2326 kW. The final temperature, 56°C, can be therefore achieved. This auxiliary heating support is provided for only two distribution lines, for HE-2 and HE-3 lines. The buildings which are heated by the HE-1 line are located in high altitudes. This disables the connection of the HE-1 line with the boilers since the high static

pressure will act on the boilers. After its heat is transferred, some part of the geothermal fluid is pumped to the hotels for the hot spring and thermal therapy purposes, while the remainder is discharged to the river. The discharge temperature varies between 40°C and 46°C during the heating period (Figure 3).

The ECC comprises of many closed-loop systems constructed under each building which connect the consumers with the EDC. In the ECC, the closed-loops are designed to have one or two heat exchangers for each building. One heat exchanger is for heating, and the other is for hot water requirements. The supply/return temperatures for the ECC obtained during the winter operation conditions are on average of 43/39°C (Figure 3).

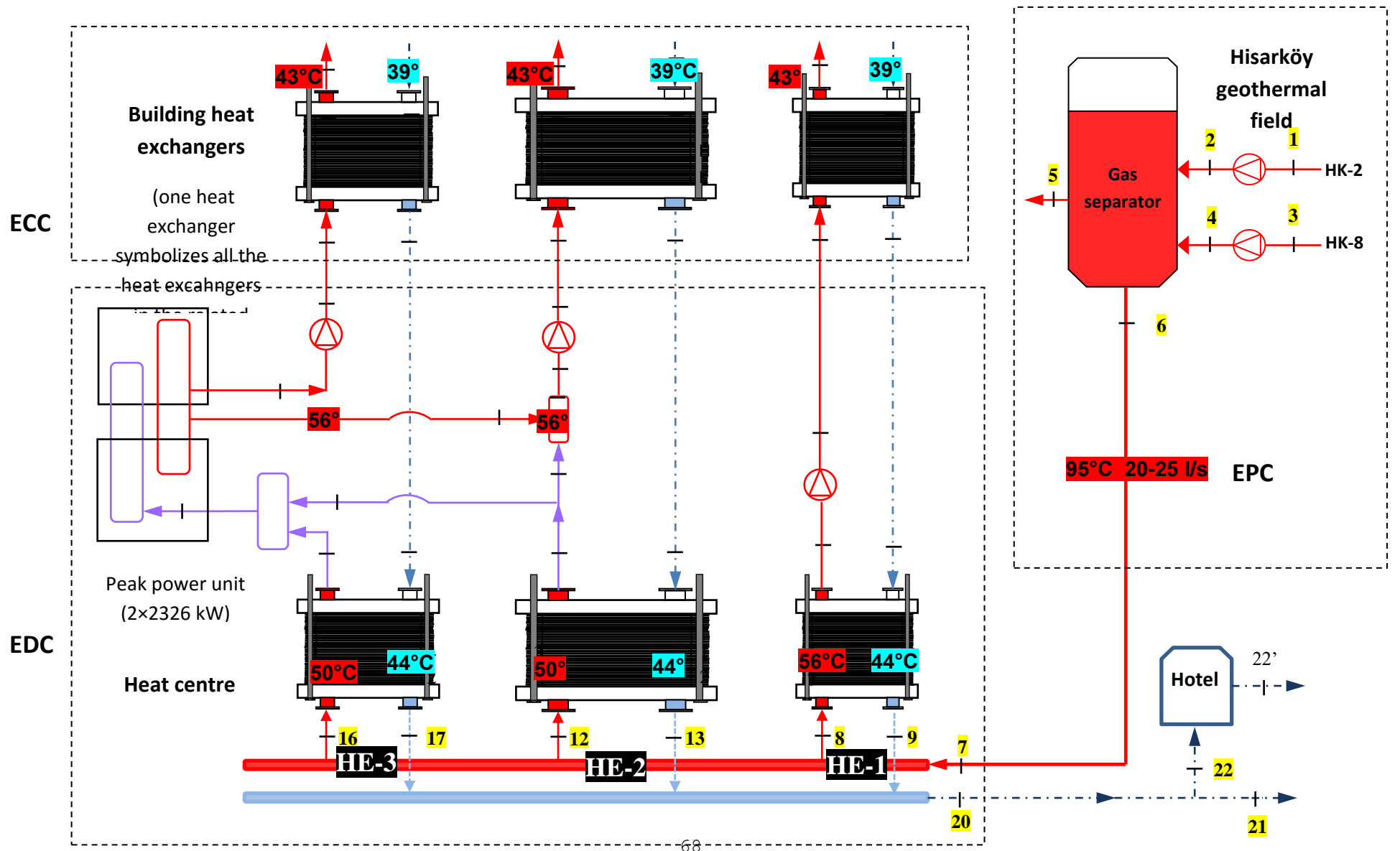


Figure 3. Schematic diagram of the Bigadiç GDHS for winter season.

51-56 °C

40-46 °C

Discharge
to the

Transmission pipeline. In the Bigadiç GDHS, a buried, 18-km-long transmission pipeline at an average depth of 1 m is used to link the Hisarköy geothermal field and the distribution network in Bigadiç town (Figure 4). The transmission line consists of the steel pipes of 250 mm nominal diameter, insulated with 3.54 cm thick polyurethane foam and covered by a protective high density polyethylene layer. The insulation thickness is considerably lower than in similar pipes. Therefore, the pipeline constitutes one of the main sources of the heat losses accounting for 18-24% of the total energy losses. The heat loss rate in the transmission pipeline obtained by applying the energy balance equation varies between 900 kW and 1400 kW depending on the operating conditions in the heating season. This means that 8-12% of the total energy input to the system is lost in the line [8].

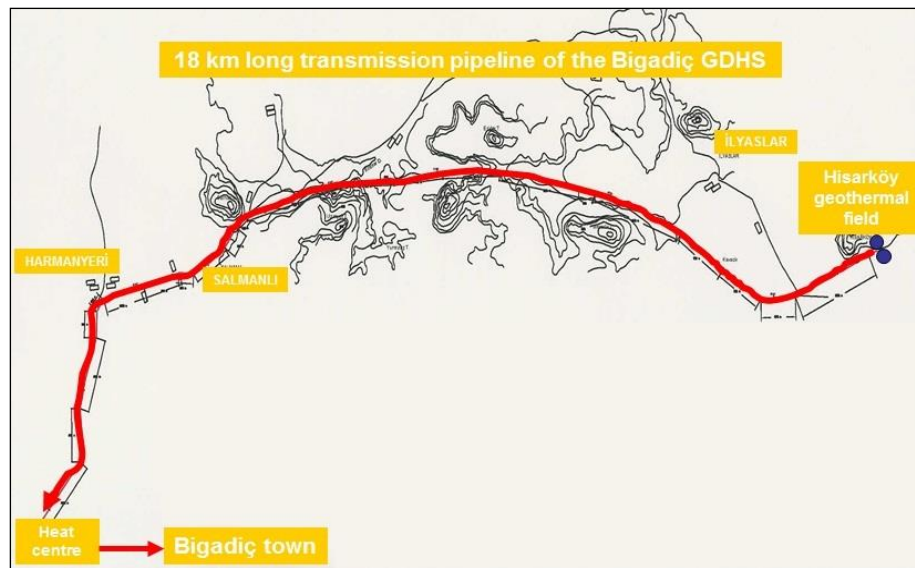


Figure 4. Transmission pipeline of the Bigadiç GDHS.

The high heat losses in the transmission pipeline result in high temperature drops throughout the pipeline. The temperature drop rate, that is, the temperature difference between the inlet and the outlet of the transmission pipeline varies between 9°C and 14°C in the heating season. It takes peak values particularly when the temperature of the ground in which the pipeline lies is the lowest and at lower flow rates (e.g., below 10 l/s) when a single well works. However, the temperature drop rate is below 9°C at relatively high flow rate conditions which are rarely experienced in the system (e.g., 7.45°C at flow rate of 31 l/s and ground temperature of 10.6°C). The well operators take care that the maximum geothermal flow rate produced in the system does not exceed 25 l/s for a long time in order to prevent any failure in the wells. The operation frequencies of the well pumps are therefore kept in the related limits.

Temperature and flow rate measurements

The rate of temperature drop in the transmission pipeline was clearly determined by taking the difference between the entering and leaving temperatures of the geothermal water. Thermal resistive probes were used for the temperature measurements. Since the pipeline had no flowmeter, a bypass line consisting of 150 mm diameter steel pipes was constructed at the

inlet of the pipeline. An electromagnetic flowmeter, appropriate for the bypass line, was also mounted on the bypass line to measure the volumetric flow rate of the geothermal fluid flowing in the pipeline (Figure 5). The bypass line was not designed to work constantly and therefore kept closed except during the flow measurements. This resulted in a relatively few number of flow rate measurements which were used for the RSM modelling. The daily average soil temperatures at a depth of 1 m were obtained from a meteorological station located near the transmission pipeline. The technical data of the measuring instruments used in the study is given in Table 1.



Figure 5. Temperature measurement at the inlet of the transmission pipeline (left), flow rate measurement at the outlet of the transmission pipeline (right).

Table 1. Properties of measuring instruments used in the study.

	Instrument	Technical data		Intended use
Temperature	Thermal resistive probes	Measuring range	$-50 \text{ to } +180 \text{ } ^\circ\text{C}$	
		Sensor	$Pt100, \text{ class A, 4 wires}$	
		Accuracy	$\pm \text{ } ^\circ\text{C} \quad \pm \text{ } \Omega$	
			$-50 \text{ } ^\circ\text{C}$	$0,25$
		$0 \text{ } ^\circ\text{C}$	$0,15$	$0,06$
		$100 \text{ } ^\circ\text{C}$	$0,35$	$0,13$
Flow rate	Electromagnetic flowmeter	Accuracy	$\leq \pm 0,3 \text{ } \% \text{ or } 0,2 \text{ } \% \text{ of } MV$	
		Lining	$Polypropylene$	
		Pipe dimension	$DN150$	
		Process temperatures	$-5 \text{ to } 90^\circ\text{C}$	
			Total volumetric flow rate of the transmission pipeline.	

RSM modelling

RSM is a statistical technique that is used for modelling the relationship between the factors and responses. By this way, results of the unpracticed combinations of different factor levels can be predicted. Equation (1) presents the general full factorial response surface mathematical model for the experimental design which is composed of linear, square and interaction terms [9]:

$$Y = \beta_0 + \sum_{i=1}^n \beta_i X_i + \sum_{i=1}^n \beta_{ii} X_i^2 + \sum_{i < j}^n \beta_{ij} X_i X_j + e \quad (1)$$

where Y is the response (volumetric flow rate of the transmission pipeline in l/s), X_i are coded values of the i th input parameters in $^\circ\text{C}$ (daily average soil temperature, T_{soil} , and temperature drop throughout the pipeline, ΔT), terms, β_0 , β_i , β_{ii} and β_{ij} are the regression coefficients and e is the random error term which is the difference between observed and predicted responses. In this study, because of the uncontrollable factors namely T_{soil} and ΔT (which are selected for the predictor of the flow rate) RSM is not used for designing the experiments. Modeling

and predictions are performed by using the data that is observed in different dates instead of using

a data set obtained from an experimental design. The data set which was obtained in different operation conditions of the transmission pipeline (for different flow rates and soil temperatures) is used for the RSM modelling (Table 2).

Table 2. Flow rate, temperature drop and soil temperature parameters used in RSM modelling.

Date of measurement	Measured flow rate (l/s)	Temperature of the geothermal water entering the pipeline (°C)	Temperature of the geothermal water leaving the pipeline (°C)	Temperature drop, ΔT , (°C)	Daily average soil temperature T_{soil} , (°C)
14.10.2011	25.5	95.27	85.76	9.51	17.8
10.11.2011	23.5	94.52	84.37	10.15	13.9
23.11.2011	22.8	94.61	84.06	10.55	12.2
18.12.2011	22.0	92.92	81.42	11.50	10.0
02.01.2012	26.0	95.48	83.87	11.61	7.8
12.01.2012	25.4	94.70	81.50	13.20	7.2
20.02.2012	24.5	94.44	80.38	14.06	4.4
25.12.2011	10.0	89.42	74.70	14.72	9.4
21.03.2012	9.8	93.50	78.12	15.38	10.6

3. RESULTS AND DISCUSSION

According to the experiments presented in Table 2, mathematical model based on RSM (presented in Equation (2)) for the responses has been established with 95% confidence (type-I error (α)=0.05) by using Minitab Statistical Package. R^2 (coefficient of determination) is calculated as 96.67% which means that ΔT and T_{soil} explain 96.67% of the change in the flow

rate while the rest, 3.33%, is affected by other variables which are not included in the model. According to the results of analysis of variance (ANOVA), P-value for the regression model including lines and quadratic terms is calculated as 0.003, less than $\alpha=0.05$, which means that the given mathematical model is significant.

$$\text{Flow Rate} = -148.100 + 33.902(\Delta T) - 4.554(T_{soil}) - 1.456(\Delta T^2) + 0.204(T_{soil}^2) \quad (2)$$

The experimental flow rates are compared to those estimated by RSM model in Table 3. As seen in the table, the difference between the model and measured values is on average of 4.31%. The test set and corresponding model responses are given in Table 4 and Fig. 6. The difference between the model and measured values is calculated less than 10%.

Table 3. Comparison table of the experimental and model flow rates.

Flow rate (measured, l/s) (Y_i)	Flow rate (obtained from the model, l/s) (\hat{Y}_i)	Prediction error (%) ($e_i = Y_i - \hat{Y}_i / \hat{Y}_i$)
9.8	9.5	3.16
10	10.7	6.54
22	24.1	8.71
22.8	22.3	2.24
23.5	22.1	6.33
24.5	24.6	0.41
25.4	23.5	8.09
25.5	26.2	2.67
26	26.1	0.38

Table 4. Test set for confirmation and corresponding model responses.

Date	Temperature drop in the pipeline, ΔT , (°C)	Daily average soil temperature, T_{soil} , (°C)	Flow rate (measured, l/s) (Y_i)	Flow rate (obtained from the model, l/s) (\hat{Y}_i)	Prediction error (%) (e_i)
17.12.2011	10.52	10.0	21.4	22.3	4.21
10.01.2012	12.54	7.80	25.5	25.0	1.96
02.04.2012	12.55	11.1	20.7	22.6	9.18

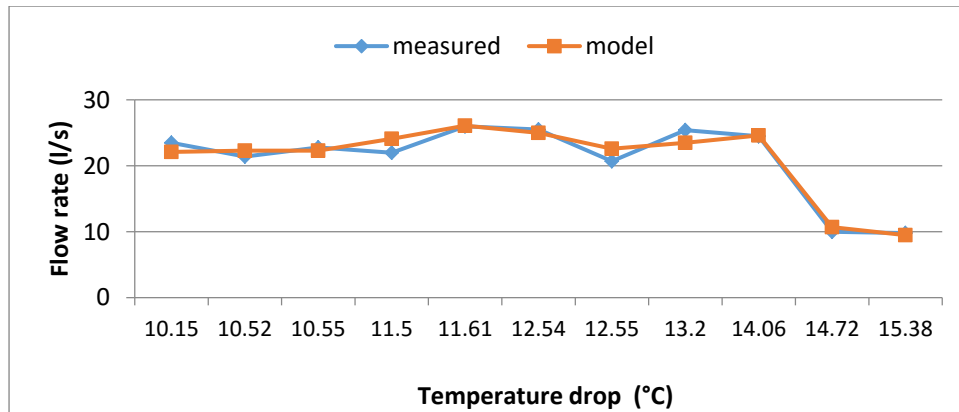


Figure 6. Comparison of the experimental and model flow rates.

4. CONCLUSION

In this study, the transmission pipeline of the Bigadiç GDHS is investigated and a mathematical model based on RSM has been established with R^2 of 96.67% which gives the volumetric flow rate of the geothermal water flowing in the pipeline depending on the rate of temperature drop and soil temperature. The results show that the flow rates given by the model are in a good agreement with those measured by the flowmeter. A test set was used for the model validation. The error rate for the given model is calculated less than 10%. As justified above, the flow meter used in this study, was not appropriate to operate continuously or to collect a wide range of flow rate data. This caused an insufficient number of flow rate measurements used for the RSM modelling and therefore led to high deviations in the model responses from the experimental results. However, the model can be improved considerably and more accurate responses can be obtained by using extensive data set which will better explain the flow characteristics in the pipeline.

REFERENCES

- [1] J.W. Lund, D.H. Freeston and T.L. Boyd, 2005. Direct application of geothermal energy. *Geothermics*. 34, 691-727.
- [2] J.W. Lund and T. Boyd, 2015. Direct Utilization of Geothermal Energy 2015 Worldwide Review. *Proceedings World Geothermal Congress 2015*. Melbourne-Australia.
- [3] M. Parlaktuna, O. Mertoglu, S. Simsek, H. Paksoy and N. Basarir, 2013. Geothermal Country Update Report of Turkey (2010-2013). *European Geothermal Congress*. Pisa- Italy.



3rd International Conference on Science, Ecology and Technology
Rome, ITALY
14-16 August 2017

- [4] A. Ragnarsson and I. Hrolfsson, 1998. Akranes and Borgarfjordur District Heating System. *Geo-Heat Center Quarterly Bulletin*, 19 (4).
- [5] M. H. Dickson, and M. Fanelli (Eds.), Geothermal Energy Utilization and Technology, UNESCO, France, 2003.
- [6] G. P. Ryan, 1981. Equipment Used in Direct Heat Projects. *Geothermal Resources Council Transactions*.5, Davis, CA, pp. 483-485.
- [7] J.W. Lund, 2006. Direct Heat Utilization of Geothermal Resources Worldwide 2005. *ASEG Extended Abstracts 2006: 18th Geophysical Conference*.1-15.
- [8] T. Akyol, 2016. *Energy and Exergy Analysis of Bigadiç-Balıkesir Geothermal District Heating System*, PhD Thesis, Department of Mechanical Engineering, Graduate School of Natural and Applied Sciences, Balıkesir University, Turkey.
- [9] A.D. Karaoglan, N. Celik, 2016. A New Painting Process for Vessel Radiators of Transformer: Wet-on-Wet (WOW). *Journal of Applied Statistics*. 43 (2), 370-386.



ENVIRONMENTAL IMPACT OF NO-TILL FARMING

Davut Karayel

Akdeniz University, Faculty of Agriculture, Department of Agricultural Machinery and Technologies
Engineering, Antalya/TURKEY

(e-mail: dkarayel@akdeniz.edu.tr)

ABSTRACT

No-till sowing practices that promote soil and water conservation and reduce input costs have become an increasingly accepted alternative to conventional tillage systems. Traditional soil cultivation systems in the tropics and subtropics, with intensive soil tillage, will end in soil degradation and loss of crop productivity. This will result in poverty, exodus of farmers from rural areas, resulting in an increase of city slums and marginal populations, and finally in social conflicts. If we are to offer the farm family a chance to survive on the farm and if sustainable agriculture is to be achieved, than the paradigms of soil use and management must be changed and new farming practices must be implemented. FAO called no-tillage 'conservation agriculture', the essence of which is maintaining the soil permanently covered with vegetation, dead or alive, never plowing or tilling the soil and practicing crop rotation including cover crops whenever possible. Because no-tillage has an outstanding effect that it provides for agricultural production, reduces erosion and the consequent pollution of water bodies, increases the water supply of underground aquifers, increases carbon sequestration and contributes to soil biodiversity and it uses less energy than conventional tillage, the practice essentially contributes to sustainable development.

Keywords: Carbon dioxide emissions, Erosion, No-tillage, Environment, Water quality

1. INTRODUCTION

No-tillage, or direct seeding, is generic names describing the sowing of seeds into soil that has not been previously tilled specifically to form a 'seed bed'. No-tillage is the term used in North America while direct-seeding is the term used in England to describe the same process. These terms are used synonymously in most parts of the world. The notation of sowing seeds into untilled soils is very old. The ancient Egyptians practiced it by creating a hole in untilled soil with a stick, dropping seeds into the hole and then closing it again by pressing the sides together with one foot. But it was not until the 1960s, when the weed-controlling chemicals paraquat and disquat were released, that the modern concept of no-tillage was born. For the



preceding decade it had been recognized that for no-tillage to be viable, weeds had to be controlled by some other method than tillage: but the range of agricultural chemicals than available was limited because they all had a residual effect in the soil. This necessitated a

delay of several weeks after spraying before the new crop seeds could be safely sown, which partly negated one of the more noteworthy advantages of no-tillage compared with tillage, i.e. saving time. Paraquat and diquat are almost instantly de-activated upon contact with soil, so they could be sprayed onto susceptible living weeds. The soil beneath the weeds, however, was almost instantly ready to take the new seeds, without risk of injuring those seeds too. This breakthrough in chemical weed control spawned the birth of true no-tillage. Since then, other broader-spectrum non-residual chemicals such as glyphosate have been developed which have expanded the concept even further (Baker *et al.*, 2002) [1].

Research on modern methods of no-tillage agriculture in USA began in earnest during the 1960s. But in Turkey research on no-tillage began in 1980s and attracted continuing academic interest. Researchers soon demonstrated the soil conservation benefits of no-tillage, and economic aspects were later elucidated. Nevertheless, there was limited interest at a practical level, and deep tillage predominated throughout the 1980s.

Conservation tillage and no-tillage systems offer numerous benefits that intensive tillage systems cannot match. These advantages have been summarized as follows:

- More wildlife,
- Reduced release of carbon gases, and air pollution
- Time savings,
- Reduced machinery wear,
- Reduced labor requirements,
- Fuel savings,
- Improved long- term productivity,
- Improved surface water quality,
- Reduced soil erosion,
- Greater soil moisture retention,
- Improved water infiltration,
- Decreased soil compaction and
- Improved soil tilth

No-tillage offers a means to address some of the agronomic and environmental risks presented by conventional tillage, and to improve the overall environmental quality. Birkas *et al.* (2008) [2] identified the main environmental risk factors of soil tillage were: soil compaction, clodding or smearing/puddling or dust formation, inducing water and wind erosion, decreased organic content, increased carbon dioxide emission, and destruction of earthworm habitats.

Tables 1 to 3 summarize the environmental effects of the main risk factors. Tillage or other operations are considered environmentally benign when there are no significant adverse effects during adoption and when the operation's result is likely to fulfill soil conservation and environmental criteria. Environmental and agronomical requirements differ (e.g. farmers do not qualify their plow on the basis of the CO₂ flux).

Table 1. Environmental impacts of planting method on humid soils (Birkas *et al.*, 2008) [2].

Environmental risk factors	No tillage	Strip tillage	Conventional tillage
Soil compaction	0*	-	0
Water/wind erosion	-	-	+
Stubble residues	-	-	+
Moisture loss	-	-	+
Environmental risk	less	least	great

* Impact on environmental risk: – (alleviation); 0 (neutral); + (increase) at the given soil moisture content, and for the respective planting process. Designations of – and 0 indicate a lessened risk, designations of + signifies a greater risk.

Table 2. Environmental impacts of planting methods on dry soils (Birkas *et al.*, 2008) [2].

Environmental risk factors	No tillage	Strip tillage	Conventional tillage
Soil compaction	-*	-	0
Water/wind erosion	-	-	+
Stubble residues	-	-	+
Moisture loss	-	-	+
Environmental risk	least	least	great

* Impact on environmental risk: – (alleviation); 0 (neutral); + (increase)

Table 3. Environmental risk of planting methods on wet soil (Birkas *et al.*, 2008) [2].

Environmental risk factors	No tillage	Strip tillage	Conventional tillage
Soil compaction	0*	0	+
Water/wind erosion	-	-	+
Stubble residues	-	-	+
Moisture loss	0	0	0
Environmental risk	less	less	great

* Impact on environmental risk: – (alleviation); 0 (neutral); + (increase)

2. EFFECT OF NO-TILLAGE ON SOIL PROPERTIES

Near-surface soil aggregate structural properties such as aggregate size distribution, stability, strength, and wettability determine the extent to which a soil will erode under water or wind erosive forces. Knowledge of aggregate structural properties is especially important in semiarid regions, such as the Great Plains, where low precipitation, high evaporation, and variable biomass production coupled with intensive tillage and fallow can accelerate soil's susceptibility to wind and water erosion.

Blanco *et al.*, (2009) [3] revealed that no-tillage farming increased soil aggregate resistance against raindrops and water repellency over plowed systems, particularly at the soil surface (0 to 2.5 cm depth). The kinetic energy of raindrops required to disintegrate 4.75 to 8 mm aggregates from no-tillage soils equilibrated at 0.03 and 155 MPa matric potential was between two and seven times greater than that required for plowed soils. The water drop penetration time in aggregates from no-till soils was between four and seven times greater compared with that in plowed soils. Reduced till was less beneficial than no-till but was more beneficial than conventionally tilled soils. A no-till induced increase in soil organic C concentration partly explained the improvement in aggregate properties. The soil organic C concentration was greater in no-till than in conventionally tilled soils near the surface. Kinetic energy of raindrops required for aggregate disintegration increased positively, while aggregate wettability decreased with the increase in soil organic C concentration. Soils rich in organic C most likely provided organic binding agents to stabilize aggregates. Soil organic C compounds also imparted slight hydrophobic properties, reducing aggregate slaking and the amount of soil that will be eroded. Aggregate wettability was positively correlated ($r=0.70$) with wet aggregate stability. This regional study showed, however, that no-till management



may not improve dry aggregate size distribution and stability, which are sensitive parameters of wind erosion. Aggregates in no-till soils were equally strong or slightly weaker when dry compared with those in plowed soils.

Karlen *et al.* (1994) [4] evaluated several proposed soil quality indicators to determine effects of removing, doubling, or maintaining crop residues for 10 years in a no-tillage, continuous maize production study. Soil aggregate characteristics, penetration resistance, bulk density, volumetric water content, earthworm populations, respiration, microbial biomass, ergosterol concentrations, and several soil-test parameters (pH, P, K, Ca, Mg, Total-N, Total-C, NH₄-N, and NO₃-N) were measured on samples collected from silt loam soils. Soil aggregates from double residue treatments were more stable in water than those from normal and removal treatments. The double and normal residue treatments had higher total carbon concentrations and higher levels of microbial activity as measured by CO₂ evolution. Ergosterol concentrations where crop residues were removed were 8 to 10 times lower suggesting this biochemical measurement of fungal biomass may be a sensitive soil quality indicator. Earthworm populations where crop residues had been removed for 10 years were significantly lower than in either normal or double residue treatments. Measures of force and energy required to crush soil aggregates were extremely variable and showed significant differences only for aggregate size. Several parameters were used to develop a soil quality index that gave ratings of 0.45, 0.68, or 0.86 for removal, normal, or double residue treatments, respectively. This study demonstrates a framework for soil quality evaluation and shows how crop residue management can affect this rating.

3. EFFECT OF NO-TILLAGE ON CARBON DIOXIDE EMISSIONS

Soil is the most valuable natural resource for agriculture. Situated between the lithosphere and atmosphere, it supports a great part of the Earth's biosphere. The difference between soil and other types of non-consolidated matter is the presence in the soil of organisms that produce and degrade organic matter, promoting its transformation. Microorganisms mineralize organic matter from remains of plants and other organisms. In this process, not all organic matter is mineralized. A more resistant part remains as humus, conferring outstanding properties to the soil, such as aggregation, porosity, and water and nutrient retention. This allows the development of plants, which obtain water and mineral nutrients from the soil through their roots. Soil has a central role in nutrient cycling, especially of carbon and nitrogen, neither of which exists in rocks. They are incorporated in soils from the air, by photosynthesis and CO₂ inclusion in organic compounds and by natural nitrogen fixation processes. As a result of the intimate interaction with the biosphere, soil has more carbon than either the atmosphere or the biosphere. On the other hand, soil cultivation results in great losses of organic matter with CO₂ release into the atmosphere, contributing to the greenhouse effect. Curiously, soils are seldom remembered as one of the main sources of CO₂ release into the atmosphere that contributes to the greenhouse effect. Important for this discussion is the fact that no-till preserves soil organic matter, reversing the continuous reduction that occurs in conventional tillage. In other words, besides improving the physical conditions of the soil, a very important improvement, no-till is also providing, by the accumulation of organic matter, a sink of

atmospheric carbon dioxide, thus an important system of carbon sequestration (Mello and Rajj, 2006) [5].

A large number of studies on soil CO₂ emissions from soils have been conducted. However, most have focused on the effects of climate change, mainly temperature and rainfall, on soil respiration. Tillage can also have a major influence on soil C emissions.

Lifeng *et al.*(2007) [6] monitored CO₂ flux on croplands with a winter wheat and maize rotation on plots with conventional tillage, rotary tillage and no-tillage. Soil CO₂ flux was generally greater in conventional tillage than in no-tillage and the rotary tillage CO₂ flux was only slightly smaller than the conventional tillage. Daily soil flux for conventional, rotary, and no tillage averaged 11.30 g CO₂/m²/d, 9.63 g CO₂/m²/d, and 7.99 g CO₂/m²/d, respectively, during the growing period. Peak CO₂ emissions were recorded on the conventional tillage and rotary tillage croplands after tillage operation, demonstrating that the tillage operations result in a rapid physical release of CO₂. At the same time, no obvious increased emission of CO₂ occurred on the no-tillage plot due to no tillage operation.

4. EFFECT OF NO-TILLAGE ON EROSION

Plowing has always been an important practice in agriculture, especially for short cycle or annual crops. It was believed that the soil needed to be loosened and aerated to receive seeds and facilitate the seedling roots to penetrate the soil without difficulty. Plowing also eased weed control. Once the crop was established, weeds had to be removed and the crop kept free to avoid competition for water and nutrients. Only the cultivated plants should occupy the area, all other plants that could compete for water and nutrients should be eliminated. As time went by, this type of soil management was considered inappropriate. Uncovered soil in a slope terrain is a vulnerable soil. Much has been written on the disaggregating power of the water drop, those raindrops falling on the recently plowed soil release the so awaited 'smell of wet land', the starting sign of the rainy season. But those same drops also destroy and disperse soil aggregates. And many water drops follow and soon they cannot be recognized anymore as they become part of a rushing stream of water that moves downhill. When there is erosion, the muddy water takes with it the best part of the soil, the finest portion called clay, which contains most of the organic matter and nutrients. Researchers estimate that soil losses caused by heavy rains falling on unprotected soil can reach tens of tons of lost soil per hectare in a single year. Erosion carries away the best part of the soil resulting in lower productivity of agricultural crops. Erosion can also change the soil surface by digging furrows that hinder the traffic of machines over the land. These furrows acquire, in some soils, great dimensions, forming gullies. The solids in suspension originated by soil erosion fill rivers, lakes and reservoirs; the silt reduces the space for water in reservoirs or rivers, intensifying the risk of floods. The water content of aquifers is reduced because of lesser water infiltration. The capacity of water reservoirs is reduced and the treatment of muddy water for city supply becomes more difficult and expensive (Mello and Rajj, 2006) [5].

Occurrence of erosion can be considered the most important factor causing soil degradation. Under the concept of sustainability, the first negative factor in relation to productivity and



profitability, and the major aggressor of the environment is soil erosion. Consequently, sustainability can only be achieved if soil erosion is stopped completely.

When agriculture is practiced on slopes in undulating topography, and rains of a certain intensity occur, soil preparation especially with disc implements results in bare soil, and this results in water erosion, or in regions of heavy winds in wind erosion (Derpsch and Moriya, 1998) [7].

It is estimated that soil losses in cropland in Latin America reach 10 to 60 t/ha/year (Steiner, 1996; Derpsch *et al.*, 1998) [7]. Average soil losses in the State of Paraná, Brazil, where good soil conservation is practiced, are as high as 16 t/ha/year. In Paraguay, on 4000 m² plots with 6% and 8% slope on high clay content Oxisols, average soil losses of 21.4 t/ha were measured in conventional soil preparation, while only 633 kg/ha of soil loss were measured in no-tillage. For the same experiment after extreme precipitations of 186 mm on June 9 and 18, 1995, soil losses of 46.5 t/ha were measured under conventional tillage, as compared to soil losses of only 99 kg/ha under no-tillage (both plots on 8% slopes). This resulted in 470 times higher soil losses when soil was prepared. In conventional tillage Paraguay is losing on average 9.2 tons of soil for each ton of soybean being produced. In conventional agriculture 23 t of soil are lost on average per ha/year while only 0.53 t/ha/year are lost when using the no-till system, a difference of 22.47 t/ha/year (Venialgo, 1996, cited by Karlen, 2006) [8]. In other words on 1.7 million ha of no-tillage being applied, farmers are saving 38.2 million tons of soil. One has to remember that the damage of lost soil in conventional tillage does not only affect farmers, soil is deposited in creeks and rivers causing sedimentation of rivers, lakes and dams, it blocks roads, often causing accidents, etc. This deposition of sediments in unwanted places has negative implications on the rural road system, hydraulic energy generation, on drinking water production, on recreational areas, resulting in significant expenditures for the State and for society as a whole. These costs are avoided or minimized through application of the no-tillage technology.

5. EFFECT OF NO-TILLAGE ON WATER QUALITY

Movement of phosphorus and nitrogen into surface water and leaching of nitrogen into groundwater are serious environmental concerns. Tillage methods affect the amount of nutrient runoff and leaching. Phosphorus can run off crop fields and move into surface waters and is considered to be the nutrient contaminant of greatest concern to surface waters. In most soils, phosphorus exists in one of four forms: associated with soil particles; in mineral forms as aluminum, iron, or calcium compounds; soluble compounds dissolved in soil water; or incorporated in organic matter.

Phosphorus can move into surface waters associated either with soil particles during erosion or as soluble phosphorus with runoff water. Greater than 75 percent of the phosphorus in surface water is associated with or bound to soil particles. Much less is soluble phosphorus.

The most effective way to reduce phosphorus pollution of surface water is to reduce soil erosion. No-tillage reduces total phosphorus losses. Total phosphorus consists primarily of insoluble phosphorus attached as soil particles, freestanding inorganic compounds, and soluble phosphorus. No-till generally has higher losses of soluble phosphorus than do tilled systems. To reduce losses of soluble phosphorus under no-till systems, phosphorus fertilizers should be deep banded or placed near the seed.

Nitrogen, in the nitrate form, readily moves with soil water and can move downward as water moves down through the soil profile. Eventually, the water and nitrate may leach far enough to enter groundwater and be an environmental concern. The major sources of nitrogen in soils include commercial fertilizer, animal manure, plant residues, soil organic matter, and biological fixation by legumes. More macropores occur in long-term no-till fields than in fields using tillage. Macropores allow greater quantities of water to rapidly infiltrate the soil, causing concerns that the use of no-till may result in greater nitrate leaching to groundwater. However, researches comparing tillage systems and nitrogen leaching has not found higher nitrate movement with no-till. Regardless of tillage system, one should always be concerned about nitrate leaching on environmentally sensitive soils, such as sandy soils overlying groundwater supplies and near water sources for human or livestock consumption (Devlin and Barnes, 2009) [9].

Sharpley and Smith (1994) [10] studied the impact of conventional tillage (moldboard plow or sweeps) and no-tillage wheat management practices on surface and groundwater quality. Concentrations and amounts of sediment, nitrogen (N), and phosphorus (P) in surface runoff, and associated nutrient levels in ground water were determined for seven dryland watersheds at two locations for periods up to 14 years. In general, annual surface runoff was similar for both tillage practices, ranging from 6 to 15 cm. Compared with conventional tillage, no-tillage reduced sediment, N, and P loss an average of 95%, 75%, and 70%, respectively. Concurrently, elevated levels of dissolved P (maximum 3.1 mg/l) in surface runoff, and nitrate-N in ground water (maximum 26 mg/l) were observed. About 25% more available soil water was in the no-tillage soil profiles, but this did not translate into increased grain yield. Instead, no-till grain yields were reduced an average 33% (600 kg/ha) compared with conventional tillage, which is attributed to a lower availability of surface applied fertilizer, and increasing cheat and associated weed problems. From an overall agronomic and environmental standpoint, results indicate that the management of no-tillage systems should include careful fertilizer placement and timing.

6. CONCLUSIONS

Results of some studies find that the recent drought that began after 2000 in the eastern Mediterranean Levant region which comprises Turkey, Syria, Palestine, Jordan, Israel and Lebanon, is likely the worst drought of the past nine centuries. During the past decade, dry years with longer droughty periods have become increasingly frequent in this region. This



may encourage growers to adopt production practices that are adapted to these more extreme climatic conditions. No-till technologies under extensive farming conditions can be easily learned and profitably implemented within a reasonable time period. Some of the environmental risk factors of soil tillage such as soil compaction, clodding or smearing/puddling or dust formation, water and wind erosion, decreased organic content, increased carbon dioxide emission, and destruction of earthworm habitats can be decreased using no-till farming systems.

REFERENCES

- [1] C.J. Baker, K.E. Saxton, W.R. Ritchie, 2002. No-tillage Seeding: Science and Practice. New York: CAB International, 2002.
- [2] M. Birkás, M. Jolánkai, A. Stingli, 2008. Experiences in No-till Farming in Hungary. No-till Farming Systems. Bangkok: World Association of Soil and Water Conservation, P. 201-312. (ISBN:978-974-8391-60-1)
- [3] H. Blanco, M.M. Mikha, J.G. Benjamin, L.R. Stone, A.J. Schlegel, D.J. Lyon, M.F. Vigil, P.W. Stahlman, 2009. Regional study of no-till impacts on near surface aggregate properties that influences soil erodibility. *Soil Sci. Soc. Am. J.*, 73, 1361–1368.
- [4] D.L. Karlen, N.C. Wollenhaupt, D.C. Erbach, E.C. Berry, J.B Swan, N.S. Eash, J.L. Jordahl, 1994. Crop residue effects on soil quality following 10-years of no-till corn. *Soil and Tillage Research*, 31 (2-3), 149-167
- [5] I. Mello, B. Van Raij 2006. No-till for sustainable agriculture in Brazil. Proc. World Assoc. Soil and Water Conserv., P. 49-57
- [6] H. Lifeng, C. Fu, L. Hongwen, Z. Xuemin, L. Lin, L. Wenying, N.J. Kuhn, 2007. Carbon dioxide emissions after application of different tillage systems for loam in Northern China. International Seminar on Enhancing the Extension of Conservation Agriculture Techniques in Asia and the Pacific Zhengzhou, Henan, China
- [7] R. Derpsch, K. Moriya, 1998. Implications of no-tillage versus soil preparation on sustainability of agricultural production. *Advances in Geoecology*, 2, 1179- 1186
- [8] N. Venialgo, 1996: IN: D.L. Karlen, 2011. Istro Info. A Publication of the International Soil Tillage Research Organization, <http://iworx5.webxtra.net/~istroorg/download/ISTRO%20INFO%20October%202006.pdf>, Accessed 25th January 2011
- [9] D.L. Delvin, P.L. Barnes, 2011. Impacts of No-till on Water Quality. <http://www.ksre.ksu.edu/library/crps12/mf2907.pdf>, Accessed 25th January 2017
- [10] A.N. Sharpley, S.J. Smith, 1994. Wheat tillage and water quality in the southern plains, *Soil and Tillage Research*, 30 (1), 33-48

THE APPLICATIONS OF NO-TILLAGE IN TURKEY

S. Altikat*¹, E. Kus², H.K. Kucukerdem³ and Z. Gozubuyuk⁴

^{1, 2, 3} Department of the Biosystem Engineering, Agriculture Faculty, Iğdir University,
(E-mail: sefa.altikat@igdir.edu.tr, emrah.kus@igdir.edu.tr, kaan.kucukerdem@igdir.edu.tr)

⁴ East Anatolian Agricultural Research Institute, Erzurum, TURKIYE.

(E-mail: zgozubuyuk2001@yahoo.com)

Corresponding Author's e-mail: sefa.altikat@igdir.edu.tr

ABSTRACT

No-tillage is economically viable, erosion limiting crop production system in which the crop planted directly into the previous crop's stubble with minimum soil disturbance. When compared to conventional tillage, the no-tillage system provides nitrogen accumulation in the soil and also improves soil aggregation and moisture holding capacity. In addition, the no-tillage increases N and C concentrations, microbial carbon mass, and bacterial and fungal populations. It also reduces CO₂ and NO₂ emissions and fuel consumption, and increases crop yield over long periods. There are several factors that are effective in the success of this system. These factors include the type of no-till seeder, stubble condition, sowing depth and time, crop rotation and the selection of the varieties. When studies on this subject are examined, it can be said that there is a need for more specific researches in order to spread the no-tillage rapidly throughout the country. For the foreseeable future, facilitating national development strategies for up-scaling of no tillage, conducting training course with national organizations remain a high priority to promote no tillage systems. Our purpose in this research is to examine the scientific publications and projects about no-tillage in Turkey and to discuss the difficulties in the implementation phase of the method. It is also one of the goals of trying to discuss the advantages and disadvantages of Turkey for no-tillage and conventional tillage.

Keywords: Benefits, Conventional tillage, No-tillage, Turkey.

1. INTRODUCTION

No-tillage, 'direct drilling' or 'direct seeding' are all terms describing the sowing of seeds into soil that has not been previously tilled in any way to form a 'seedbed'. Direct drilling'

was the first term used, mainly in England, where the modern concept of the technique originated in the 1960s. The most commonly identified feature of no-tillage is that as much as possible of the surface residue from the previous crop is left intact on the surface of the

ground, whether this be the flattened or standing stubble of an arable crop that has been harvested or a sprayed dense sward of grass.

No-tillage has many advantages and disadvantages. The advantages of no-tillage are fuel, time and labor conservation, increased the soil organic matter and soil nitrogen, preservation of soil structure and earthworms, improved aeration and infiltration, reduced irrigation requirements, germination of weeds and pollution of water ways, lower cost and increased crop yields. Disadvantages of no-tillage are risk of crop failure, larger tractors required, new pest and disease problems, and no-tillage seeder selection and weed control in the first years.

In order to be able to see the expected effect from the no-tillage, it is necessary to evaluate a number of factors together during the crop production period. The most important factor for the success of this system is no-till seeder type which used the no tillage. The first step in implementing no-tillage is to place the seeds precisely at the desired depth. It is used specially designed machines to achieve this purpose. No-till seeders have a more specific design than other sowing machines due to their untilled or stubble-covered fields. The most spectacular units of these machines are furrow openers that can plant in untilled soil conditions.

In addition to furrow openers, row cleaners, press wheel and covering chains are among other vital parts of these machines. Row cleaning units remove stubble on the row and a clean row space is obtained. The pressure wheel ensure that the seed- soil contact. Finally, the seeds are covered with soil using covering units and sowing is completed. The sowing depth at the time of sowing should be homogeneous for obtain a good seed emergence. The density and distribution of stubble on the surface of the field is another factor affecting the sowing success. If the moisture content of the stubble is inevitable, furrow opener cannot cut the stubble. Furthermore, if the stubble is not homogeneously distributed on the surface of the field, the seeder cannot sowing to the desired depth. However, furrow opener of no-till seeder should not bury stubble into the soil, because prevent seed-soil contact.

Soil fertilizer at the time of sowing is important for seed germination and crop yield. Without soil tillage to stir and mix applied fertilizer applications, careful attention must be paid to placing the fertilizer in untilled soils to optimize crop uptake and yield. Bands of fertilizer to the side and below the seed have proved to be very effective, sometimes utilizing one fertilizer band for each pair of seed rows. While it is important to place fertilizers far enough away from seeds and seedlings to avoid toxicity problems, it also appears that separation distances can be much closer than those commonly accepted for tilled soils. Fertilizer banding has been found to be optimally accomplished by simultaneously seeding and fertilizing with a combination direct seed drill and fertilizer dispenser, and which is now common practice.



Energy is required for all agricultural operations. Practices that require lower energy inputs, such as no-tillage versus conventional tillage, generally result in lower inputs of fuel and a consequent decrease of CO₂- carbon emissions into the atmosphere per unit of land area under cultivation. Emissions of CO₂ from agriculture are generated from four primary sources: manufacture and use of machinery for cultivation, production and application of fertilizers and pesticides, the soil organic carbon that is oxidized following soil disturbance

(which is largely dependent on tillage practices) and energy required for irrigation and grain drying.

The aim of this research is to examine the problems of the no-tillage method applied in Turkey. For this purpose, we examined that machinery manufacturing companies, stubble management, scientific researches and projects, and Turkey's advantages and disadvantages for no-tillage.

2. MATERIAL AND METHODS

The materials of this study are statistical results, scientific studies and projects and interviews with farmers. As a method, it is considered that the findings obtained from these studies are discussed according to a specific subject line.

Climate properties of Turkey

Turkey is located in the middle Europe, Asia and Africa. Turkey surrounded at north Black Sea, at south Mediterranean Sea and at west Aegean. While the coastal areas have moderate climates, the Anatolian plateau has extremes temperature both in summer and winter. Turkey receives most of the rainfall in the winter season. In this season, mean temperature usually is below 5°C and there is no too much evaporation. Summer season is very limited in terms of rainfall and it is necessary to irrigation in this season. The Aegean and Mediterranean coasts have rainy winters and hot summers, also annual precipitation in these areas varies from 580 to 1300 mm according to the locations. Black Sea coast has great potential of rainfall. The eastern part of this area receives 2200 mm annually. Marmara region is milder climates (winter 4°C and summer 27°C); in winter however the temperatures can drop below zero. In Western Anatolia, there is a mild Mediterranean climate with average temperatures of 9°C in winter and 29°C in summer. On the southern coast of Anatolia has a similar climatic condition. The temperature difference between night and day is very high. It can be seen snow in this region instead of rainfall. The average temperature is 23°C in summer and -2°C in winter. Black Sea area is wet, and humid (summer 23°C, winter 7°C). In the Eastern Anatolia region has a long winter, and snow remains on the ground from November until the end of April (the average temperature in winter is -13 °C and in summer 17 °C). In the South-Eastern Anatolia region, summers are hot and dry, with temperatures above 30°C. Spring and autumn are generally mild, but during both seasons sudden hot and cold spells frequently occur in the region.

Arable area distribution of Turkey

According to Turkish Statistical Institute's data there are 23762572 ha agriculture land in Turkey. In this agricultural area sown area, fallow area, vegetable production, fruit production and Ornamental plant production are done with 15574371 ha, 4049998 ha, 804142 ha, 4844 ha, respectively. Arable area distribution in Turkey was given in Figure 1.

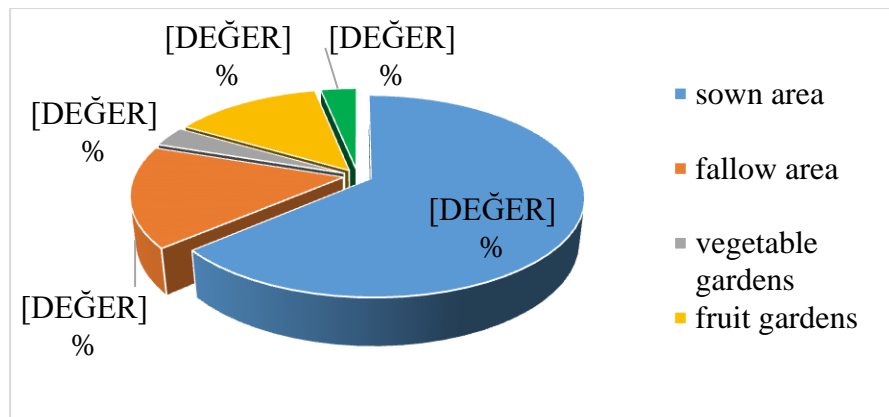


Figure 1. Arable land of Turkey

Turkey has a great agricultural potential. The main farming systems are dry and irrigated farming. According to the results of Crop Production Survey (Turkish Statistical Institute) the most planted crops in 2016 were wheat and sunflower 7687 and 8407 ha respectively. These plants were followed by barley, clover, cotton and maize production (2743, 1900, 1248 and 1105 ha).

No-tillage projects and scientific researches in Turkey

Numerous scientific researches and projects have been carried out in different geographical regions, climatic conditions and rotation systems in Turkey. There are completed and ongoing projects in the country in relation to the subject. As a main factor in these projects, the subjects such as conservation tillage and no-tillage, crop rotations agronomy and weed control have been examined. In the projects, the products were grown in irrigated and not-irrigated soil conditions and got an idea about the efficiency of the conservational tillage and no-tillage. Some projects related to no-tillage and conservation tillage in Turkey are given in Table 1.

As in the case of the projects, the method of conservational tillage and the no-tillage has been the subject of scientific publications. In the scientific researches, soil physical properties, seed



emergence and crop yield parameters were investigated. In the majority of these scientific publications, soil bulk density, porosity, penetration resistance, moisture exchange of soil in seed germination period are evaluated within soil physical properties. In addition, weed control has also been the subject of research in the no-tillage. The problem of weeding must be overcome for the farmers in order to accept the no-tillage. In these publications, it is explained in detail how to make struggle with weed control. In addition, the most effective crop rotation and water management that can be used in areas where research has been conducted is also emphasized in these scientific studies. Numerous scientific studies have been carried out to develop the no-till seeders. In these studies, the designs of furrow-opener are the foreground. In particular, the angles of furrow openers, furrow opener types have been researched and various suggestions have been made. Some scientific publications related to

the subject in Turkey are given in Table 2. Despite the fact that there are many projects and scientific publications about the subject in the whole country, there are still a lot of topics to be investigated. One of the most crucial of these issues is the farmers' adoption and implementation steps. The acceptance of this method in Turkey depends on the practices of the farmers themselves in their fields. For this reason, scientific studies should be carried out in farmers' fields together with farmers. With such an approach, the farmer will be able to learn how to follow the adaptation process.

Soil tillage machinery distribution in Turkey

The majority of the arable land in Turkey is tilled by conventional tillage practices. This unsustainable soil tillage method negatively affects the physical, chemical and biological quality of the soils. In the conventional tillage system soil is tilled by plough, cultivator, disc harrow and land roller. As a result of this intensive tillage, the soil is much more disturbed and thus increases the fuel consumption and soil compaction. Turkey also has farmers who follow and implement innovations in the subject of agriculture. These farmers imitate other farmers by applying new methods. In this respect, progress has been made especially in the field of tillage. In some parts of the country, farmers that has large agricultural lands tend to conservation tillage and no-tillage. Across the country the number of farm machinery that using conventional tillage is 1909524 according to TÜİK's data (2016). The number of no-till seeder in Turkey is less than other conventional sowing machines. However, the number of no-tillage machines has increased over the years. Approximately 40 companies manufacture farm machines throughout the country, but the companies that manufactured no-till seeder is only 7. In the last 15 years there was a government support which covered 50% of the no-till seeder cost and 361 pneumatic no-till seeder was sold. The number of no-till seeders were given in figure 2.

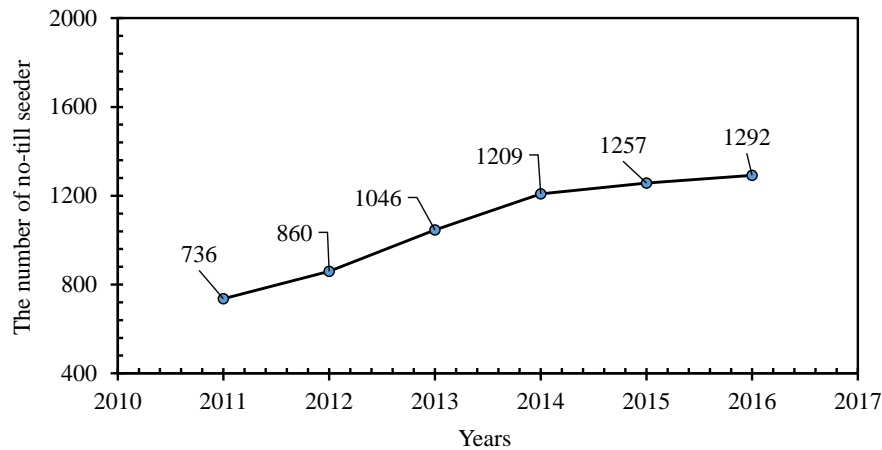


Figure 2. The number of no-till seeders in Turkey

The problems of no-tillage in Turkey

In Turkey, some problems are encountered in the application of conservation and no-tillage. No-tillage may cause reductions in crop yield in the first years. However, when analyzed economically it appears that this decline in crop yield is not serious. The method must be applied for at least 4 years in order to be able to see the expected effect of the no-tillage. During this time, the amount of soil organic matter, microbial population and soil physical properties will improve as a result, an increase in the yield of the product will be observed. Unfortunately, Turkish farmers do not expect the healing process of the soil and think that the method does not work economically.

The weed problem encountered during the application phase of no-tillage is another effect that makes production difficult. In the solution of the problem, herbicides are used effectively. Total herbicide application, especially before sowing, allows sowing to be done smoothly. The weed problem encountered in plant growth period can be solved by chemical and mechanical methods.

Plant rotation is an important parameter in terms of protecting soil fertility and weed control. However, crop rotation that is effective in one region may not give the same results in another region. For this reason, the type of crop rotation appropriate for each region should be decided. Another problem encountered during the production period is rodent damage. This problem can be solved using predators.

In no-tillage system, the soil surface must be covered with stubble. In this way soil is protected against water and wind erosion. The stubble on the soil surface protects the moisture content of the soil and accelerates plant emergencies. In Turkey, however, stubble is used as an animal nutrient. In order to solve this problem, there is a need for scientific studies on stubble management.

Table 1. Some of the past and ongoing conservation agriculture projects in Turkey

Subject	Location	Years	Systems	Crops	Researchers
Conservation tillage	East Anatolia	2003-2005	Rainfed and irrigation	Maize and sunflower	Prof. Dr. Ahmet ÇELİK
No tillage	East Anatolia	2008-2011	Rainfed and Irrigation	Vetch and wheat	Prof. Dr. Ahmet ÇELİK
Conventional tillage and soil compaction	East Anatolia	2003-2005	Rainfed and Irrigation	Wheat	Prof. Dr. Ahmet ÇELİK
Conventional tillage and compaction	East Anatolia	2013-2014	Rainfed and Irrigation	Corn	Prof. Dr. Ahmet ÇELİK
Machinery and	Central Anatolia	2007-2009	Rainfed	Wheat, chickpea	Prof. Dr. Kazım Çarman
Soils and Agronomy	East Mediterranean	2006-2009	Rainfed and irrigation	Wheat, corn, soybean	Prof. Dr. İsmail ÇELİK
Machinery and	Aegean	2001-2002	Irrigation	Cotton as a second crop	Prof. Dr. Erdem Aykas
Tillage and soil	Black sea region	2007-2009	Rainfed	Corn	Prof. Dr. Engin Özgöz
Subject	Location	System	Crops	Researchers	
Machinery 3E	Central Anatolia	Rainfed	Wheat-Fallow	Prof. Dr. Kazım Çarman	
Soil	Central Anatolia	Rainfed	Wheat-legume	Derya Sürek	
Agronomy and soil	Southeastern Anatolia	Rainfed	Wheat-fallow	Ahmet Çıkman	
Weeds Agronomy	South Eastern Anatolia	Rainfed	Lentil	Murat Urgan	
Agronomy, and machinery	Eastern Anatolia	Rainfed	Wheat, vetch and fallow	Zinnur Gözübüyük	

Table 2. Some of the academic publication of no-tillage and conservation tillage

Subject	Location	Years	Crops	Researchers
Performance of no-till seeders	Mediterranean	2006	Maize	Karayel, D, 2009 [1]
Tillage and energy consumption	Mediterranean	2006-2007	Maize	Barut <i>et al.</i> , 2012. [2]
Residue management and crop yield	East Anatolia	2003-2006	Cotton	Gürsoy <i>et al.</i> , 2010 [3]
Soil physical properties and crop yield	Southeastern Anatolia	2003-2004	Maize	Sessiz <i>et al.</i> , 2010 [4]
Tillage systems and economic analyses	Aegean	2004-2005	Wheat	Yalçın <i>et al.</i> , 2005 [5]
Tillage- energy analyses	Mediterranean	1999-2000	Corn	Öztürk <i>et al.</i> , 2008 [6]
Tillage- biomass-nitrogen content	Mediterranean	2007-2008	Soybean	Doğan <i>et al.</i> , 2011 [7]
Tillage-microbial properties	Mediterranean	2006-2009	Wheat	Çelik <i>et al.</i> , 2011 [8]
Tillage-energy analyses-crop yield	Southeastern	2003-2004	Sunflower	Sessiz <i>et al.</i> , 2008 [9]
Tillage-predators	Aegean	2000-2001	Cotton	Gençsoylu and Yalçın 2004 [10]
Tillage hydraulic properties	East Anatolia	2000-2012	Wheat-vetch	Gözübüyük <i>et al.</i> , 2014 [11]
Tillage –compaction-seed emergence	Eastern Anatolia	2006-2007	Red lentil	Altıkat S, and Çelik A., 2011 [12]
Tillage-physical properties-crop yield	Eastern Anatolia	2004-2005	Maize	Çelik A and Altıkat S., 2010 [13]
Tillage-CO2 emission, microbial population	Eastern Anatolia	2005-2006	Common vetch	Altıkat <i>et al.</i> , 2006 [14]
Tillage-stubble-sowing performance-crop yield	Eastern Anatolia	2004-2005	Maize and	Altıkat S., 2012 [15]
Tillage-soil physical properties seed emergence	Eastern Anatolia	2008-2009	Summer vetch-	Altıkat and Çelik 2012 [16]



3rd International Conference on Science, Ecology and Technology
Rome, ITALY
14-16 August 2017

Tillage-soil physical properties-seed emergence	Eastern Anatolia	2008-2009	Vetch-wheat	Altikat S., Çelik A 2012 [17]
Tillage and equipment	Eastern Anatolia	2008-2009	Wheat	Çelik and Altikat 2012 [18]
Tillage – Stubble distribution	Eastern Anatolia	2008-2009	Vetch-wheat	Altikat S, Çelik A., 2012 [19]



3. RESULTS AND DISCUSSION

A large part of the land of Turkey (67%) has erosion risk and thus intensive soil tillage and open channel irrigation systems very dangerous for Turkey's arable land. In the conservation tillage especially no-tillage the soil less distribution and plant water consumption is less compare to conventional tillage. For these reasons the spread of the conservation tillage and no –tillage throughout the country is very important for Turkey's farming.

The number of firms producing direct sowing machines in Turkey is less than that of conventional sowing machines. In some researches, it is stated that the no-till seeder produced in Turkey cannot sow at the desired level. The biggest reason for this is the fact that farmers do not have enough knowledge about the use of these special no-till seeders. These machines must be calibrated to soil conditions before they can be used. Farmers use the machine without any calibration. Thus, the desired effect is not observed. The farmers should buy the type of machine suitable for his soil conditions. Particularly, it should be ensured that the machine's furrow openers, press wheels and closure systems work smoothly at the time of sowing.

Turkish farmers have to use this method personally for their adoption. To this end, demonstration work should be accelerated throughout the country. Livestock is an important source of livelihood in Turkey. In Turkey, stubble is used as a nutrient source in the livestock sector. This is an important problem in terms of the application of conservation agriculture. From this perspective, effective stubble management is inevitable for protective tillage applications.

Another significant trouble for no-tillage in Turkey is weed control and rodent damage. In the short time scale these trouble can be solved with used herbicides and insecticides. At the long time scale crop rotation can be solved these trouble. Effectiveness of the no-tillage can be changed with regionally.

Turkey has some outstanding features compare to others neighbor country about application of no-tillage system. There are sophisticated farm machinery industry across the country. Besides, Turkey has well established agricultural research, developed and extension institutes, widespread agricultural chambers network, widespread farmer machinery ownership, high quality seed registration system and trade, no sanctions or limitations for trade and government support.

4. CONCLUSION

Intensification of agricultural practices in Turkey caused a lot of problems in Turkey's land. At the beginning of these problems are the deterioration of soil properties and inefficiency of



arable land. At the last 10 years a lot of land converted to the arable land. And thus, the number of tilled land rapidly increased. At the result of this this unsustainable increase of agriculture land has been caused risks by monoculture practices, and excessive irrigation and tillage. The most of the Turkey's agriculture land has erosion risk due to dominant steep

slopes (>6%). More than 55% of arable lands in Turkey are severely affected by water erosion. Further to this, 5% of arable lands are subject to wind erosion.

When these factors are considered conservation tillage practices, especially no-tillage must be used by Turkey's farmer. In no-tillage system soils protected from water and wind erosion compare to conventional soil tillage systems because soil's surface cover with stubble and use less water during the growing period.

Farming decision making process is very important for spread no-tillage throughout the country. No-tillage is relatively complex system and involves a wide range of intervening factors. Hence farmers are supported during this complex process. The importance of local farmer discussion groups is critical to successful adoption of new technologies and innovations.

Affordable, dependable and adoptable no-till machinery development is one of the greatest challenge for the agricultural machinery producers. Machinery producers should be given adequate support to fine-tune their no-till drills. Researchers and no-till machinery producers should work in collaborate to address possible site-specific issues.

REFERENCES

- [1] D.Karayel. 2009. Performance of a modified precision vacuum seeder for no-till sowing of maize and soybean. *Soil & Tillage Research* .104(1) 121-125.
- [2] Z. Barut, C.Ertekin and H.Karaağaç, 2011. Tillage effects on energy use for corn silage in Mediterranean Coastal of Turkey. *Energy* 36 5466-5475.
- [3] S. Gürsoy, A. Sessiz and S.S. Malhi, 2010. Short-term effects of tillage and residue management following cotton on grain yield and quality of wheat. *Field Crops Research* 119 :260-268.
- [4] A. Sessiz, A. Alp and S. Gürsoy, 2010. Conservation and conventional tillage methods on selected soil physical properties and corn (*zea mays* l.) Yield and quality under cropping system in turkey. *Bulgarian Journal of Agricultural Science*, 16: 597-608.

- [5] H. Yalçın, E. Çakır and E. Aykas 2005. Tillage parameters and economic analysis of direct seeding, minimum and conventional tillage in wheat. *Journal of Agronomy* 4(4):329-332.
- [6] H. Öztürk, K. Ekinçi and Z. Barut 2017. Energy analysis of the tillage systems in second crop corn production. *Journal of Sustainable Agriculture* 28:3,25-37.
- [7] K. Doğan, I. Çelik, M. Gök and A. Çoskan 2011. Effect of different soil tillage methods on rhizobial nodulation, biyomas and nitrogen content of second crop soybean. *African Journal of Microbiology Research* 5(20):3186-3194.
- [8] I. Çelik, Z. Barut, I. Ortaş, M. Gok, A. Demirtaş, Y. Tulun, and C. Akpınar. Impacts of different tillage practices on some soil microbiological properties and crop yield under semi-arid Mediterranean conditions. *International Journal of Plant Production* 5(3):237-254.
- [9] A. Sessiz, T. Soğut, A. Alp and R. Esgici, 2008. Tillage effects on sunflower (*helianthus annuus*, l.) Emergence, yield, quality, and fuel consumption in double cropping system. *Journal of Central Europe Agriculture*. 4:697-710.
- [10] I. Gençsoylu and I. Yalçın, 2004. The effects of different tillage systems on cotton pests and predators in cotton fields. *Asian Journal of Plant Sciences*. 3(1):39-44.
- [11] Z. Gözübüyük, Ü. Şahin, İ. Öztürk, A. Çelik and M. Adıgüzel, 2014. Tillage effects on certain physical and hydraulic properties of a loamy soil under a crop rotation in a semi-arid region with a cool climate. *Catena*. 118:195-205.
- [12] S. Altıkat and A. Çelik, 2011. The effects of tillage and intra-row compaction on seedbed properties and red lentil emergence under dry land conditions. *Soil & Tillage Research* 114:1-8.
- [13] A. Çelik and S. Altıkat 2010. Effects of various strip widths and tractor forward speeds in strip tillage on soil physical properties and yield of silage corn. *Journal of Agricultural Science*. 16:169-179.
- [14] S. Altıkat, A. Çelik and S. Bilen, 2012. Effects of various tillage systems on soil CO₂-C fluxes and bacteria and fungi populations in *Zea mays*. *African Journal of Agricultural Research* 7(19):2926-2934.
- [15] S. Altıkat, A. Çelik and Z. Gözübüyük, 2013. Effects of various no-till seeders and stubble conditions on sowing performance and see emergence of common vetch. 126:72-77.



- [16] S. Altıkat 2012. Effects of strip width and tractor forward speed on sowing uniformity of maize and sunflower. *Bulgarian Journal of Agricultural Science*. 18:375-382.
- [17] S. Altıkat and A. Çelik 2012. Effects of different no-till seeders and tractor forward speeds on the soil physical properties and seed emergence of summer vetch and winter wheat. *Journal of Agricultural Sciences*. 18:21-30.
- [18] A. Çelik and S. Altıkat, 2012. Seeding performance of no-till seeders equipment with different furrow openers, covering components and forward speeds for winter wheat. 2012. *Journal of Agricultural Science* 18:226-238.
- [19]. S. Altıkat, A. Çelik, 2012. The effects of different no-till seeder and tractor forward speeds on stubble distribution of summer vetch and winter wheat. *Journal of Agricultural Faculty of Atatürk University* 43(2): 149-156.



SHORT-TERM LOAD FORECASTING MODEL USING FLOWER POLLINATION ALGORITHM

Volkan ATEŞ*¹ Murat LÜY² Necaattin BARIŞCI³ Ertuğrul ÇAM⁴

^{1,2,4} Electrical and Electronics Engineering Kırıkkale University, TURKEY

(volkanfire@hotmail.com, muratluy@yahoo.com, ertugrul_cam@yahoo.com)

³ Computer Engineering Faculty of Technology Gazi University, TURKEY.

(nbarsici@hotmail.com)

Corresponding Author's e-mail: volkanfire@hotmail.com

ABSTRACT

Electricity is natural but not a storable resource and has a vital role in modern life. Balancing between consumption and production of the electricity is highly important for power plants and production facilities. Researches show that electricity load consumption characteristic is highly related to exogenous factors such as weather condition, day type (weekdays, weekends and holidays etc.), seasonal effects, economic and politic changes (crisis, elections etc.). In this study, we propose a short-term load forecasting models using artificial intelligence based optimization technique. Proposed 5 different empirical models were optimized using flower pollination algorithm (FPA). Training and testing phase of the proposed models held with historical load and weather temperature dataset for the years between 2011-2014. Forecasting accuracy of the models was measured with Mean Absolute Percentage Error (MAPE) and monthly minimum approximately %1,79 for February 2013. Results showed that proposed load forecasting model is very competent for short-term load forecasting.

Keywords: Short-Term Load Forecasting; Nature-Inspired Optimization; Flower Pollination Algorithm; Artificial Intelligence

1. INTRODUCTION

Electric energy is an energy source produced by using various sources and also having a wide variety of consumption fields. Electric energy consumption has a large share in total energy

consumption because it can easily be converted into basic energy types such as heat, light, motion. The magnitude of the industrial sector volume, which can be expressed as a measure of development, is directly proportional to the consumption of electric energy.

Load consumption forecasting models are essential and vital for planning and production scheduling of the production facilities. These forecasting models and studies help to make important decisions on purchasing, generating electric power, load switching, and infrastructure development. The forecasting studies are also extremely important for suppliers and other participants in production, transmission, distribution and energy markets [1].

Load demand forecasting is very important for planning and production of power plants and production facilities. Load demand forecasts are generally divided into three main divisions: short-term, medium-term and long-term depending on the time periods [2]. Medium and long-term demand forecasts basically are related to what the electricity consumption is based on in total years, what might be in the future. The establishment of new power generation plants and the planning of large-scale energy investments are planned according to this demand. Short-term based approaches are based on optimum usage of existing resources and profiling the consumption characteristics. Basically, short-term methods are used for security and survival of the main system.

When literature is examined, it is seen that, there are several types of models and methods tried out on load consumption and energy demand forecasting. These studies are divided into two main sections as classical statistical based approaches and artificial intelligence based approaches. These models and methods are classified as time series based (univariate) models which are modelled as a function of historical load data and expert systems which are modelled as systems of exogenous factors especially weather and social variables [3].

Traditional statistical models are based on relation on historical load changes. Some of these univariate studies are auto-regressive models [4, 5], dynamic linear, non-linear models [6, 7], non-parametric regressive model [8], structural model [9], curve-fitting procedural model [10]. These models have lower forecasting errors for the routine periods of consumption.

Literature shows that statistic based models are not sufficient for non-linear periods of consumption. Thus, researchers leaned to nature inspired and artificial intelligence based non-linear models. Some of these studies are fuzzy logic and artificial neural networks based forecasting models [11-14]. S. Hassan et al. (2016) proposed fuzzy type-2 based load forecasting model. They also used extreme learning machine (ELM) to optimize and finding optimal fuzzy parameters [15]. D.K. Chatuverdi et al. (2015) proposed a model by using generalized neural networks (GNN) [16]. Song Li et al. (2015) used hybrid load forecasting model. They used ELM and modified artificial bee colony (MABC) to optimize input weights of ELM [17].

In Turkey, there are varying types of studies on short-term load forecasting. E. Yukseltan et al. (2017) proposed a linear model using climatic and econometric dataset. They trained and tested forecasting model for the period 2012-2014 and the weekly, daily horizon was estimated [18]. H.H. Cevik et al. (2015) proposed fuzzy and adaptive neuro-fuzzy models to estimate short-term load consumption of Turkey. They used historical weather information

and seasonal changes in their study [19]. I Esener et al. (2006) proposed an artificial intelligence based model for short-term load forecasting. They used signal processing techniques and ANN with historical weather condition changes [20].

2. MATERIAL AND METHODS

In this paper, we present a hybrid short-term load forecasting model by using structural mathematical models with nature inspired optimization technic. We used historical load consumption and weather temperature changes data set for the period 2011-2014. We used

five different mathematical equation for modelling load consumption and flower pollination algorithm (FPA) was used for finding optimal parameters in equations. Forecasting accuracy of the mathematical models was measured using mean absolute percentage error (MAPE).

Dataset Preparation

Electricity load consumption has linear and non-linear characteristic. Literature shows that there are several types of input variables used to estimate and define load consumption characteristic. These variables are varying to location, model type and other exogenous factors. While having long-term forecasting, globally scaled factors are used such as economic growth depth and population changing for years, in short-term load forecasting, most of the researchers used hourly changing data such as air temperature, raining period, insolation period etc. In this study, we used 4 different input variables. These variables are;

- Last Day Consumption (L_{DC})
- Last Week Consumption (L_{WC})
- Weekly Consumption Trend (L_{CAL})
- Weekly Temperature Trend (T_{EFF})

Last day consumption (L_{DC}) – Last week consumption (L_{WC})

Historical changes of the electricity load consumption are very significant indicator for future demand estimations. Electricity load usually follows a routine path. Actual load consumption values belonging to 2013 is seen in Figure 1. Last day consumption for the time L_{t-24} and last week consumption L_{w-7} may help to estimate future load demand.

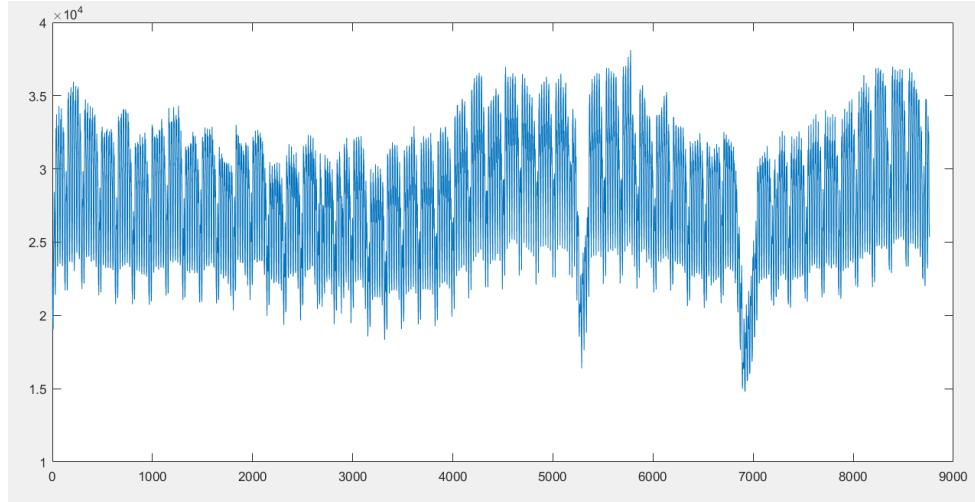


Fig 1. Actual hourly electricity load consumption of 2013

Weekly Consumption Trend (L_{CAL})

Data obtained with the observations of the amount of consumption for a certain period, may give significant information about the future situation of electricity consumption. These observations are not sufficient information enough for a certain forecasting lonely but may be helpful for an accurate estimation indeed. In this study, we tried to understand consumption characteristic using least square trend analysis for 7 days consumption period and used these

results as an input for the mathematical models. Load trend analysis was calculated with using equations 1, 2 and 3.

Load Trend

$$L = a + b_{x_i} \quad (1)$$

Slope

$$b = \frac{\sum_{i=1}^n x_i y_i - n \bar{x} \bar{y}}{\sum_{i=1}^n x_i^2 - n \bar{x}^2} \quad (2)$$

Load Intercept

$$a = \bar{y} - b \bar{x} \quad (3)$$

Sample load trend data using these equations is seen in Table 1.

Table 2. 25.12.2011 - 31.12.2011 Load consumption data

Date	Time Period (Distance)	Load Consumption (MWh)	x²	x²y
25.12.2011	1	26175	1	26175
26.12.2011	2	24386	4	97544
27.12.2011	3	26412	9	237708
28.12.2011	4	26493	16	423888
29.12.2011	5	26345	25	658625
30.12.2011	6	26463	36	952668
31.12.2011	7	26083	49	1278067
1.1.2012		26595		

Weekly Temperature Trend (L_{CAL})

Literature research shows that, air temperature changes are highly related to hourly based load consumption characteristic. Thus, we used historical temperature data set collected from six different location in Turkey between 2011 and 2014 as an input for proposed forecasting models. The weighted average value of temperature collected from different cities of Turkey calculated with using coefficients. these coefficients were defined by using economic development values according to report published by Republic of Turkey Ministry of Science, Industry and Technology in 2013. The effect of each locations is seen in Table 2.

Table 2. Coefficient values of locations

17030 (City-1)	17130 (City-2)	17135 (City-3)	17220 (City-4)	17351 (City-5)	17603 (City-6)
0.02	0.15	0.02	0.10	0.04	0.67

Mathematical Models

In this study, five different linear and non-linear empirical models were developed for load consumption forecasting. Mathematical models were mostly used empirical models in literature. In this study, five different linear and non-linear empirical models were developed for load consumption forecasting. Mathematical equations were empirical models mostly used by researchers in the literature. These are linear, power, exponential, semi-quadratic and quadratic models.

Linear model

$$Lm = w_1L_{dc} + w_2L_{wc} + w_3L_{cal} + w_4T_{eff} + w_5 \quad (4)$$

Power model

$$Km = w_1(L_{dc})^{w_2} + w_3(L_{wc})^{w_4} + w_5(L_{cal})^{w_6} + w_7(T_{eff})^{w_8} \quad (5)$$

Exp. model

$$Em = w_1e^{w_2L_{dc}} + w_3e^{w_4L_{wc}} + w_5e^{w_6L_{cal}} + w_7e^{w_8T_{eff}} + w_9 \quad (6)$$

Qua. model

$$\begin{aligned} Qm = & w_1(L_{dc})^2 + w_2(L_{wc})^2 + w_3(L_{cal})^2 + w_4(T_{eff})^2 + \\ & w_5(L_{dc})(L_{wc}) + w_6(L_{dc})(L_{cal}) + w_7(L_{dc})(T_{eff}) + \\ & w_8(L_{wc})(L_{cal}) + w_9(L_{wc})(T_{eff}) + w_{10}(L_{cal})(T_{eff}) + \\ & w_{11} \end{aligned} \quad (7)$$

Sem-Qua. model

$$\begin{aligned} Sm = & w_1(L_{dc}) + w_2(L_{wc}) + w_3(L_{cal}) + w_4(T_{eff}) \\ & + w_5\sqrt{(L_{dc})(L_{wc})} + w_6\sqrt{(L_{dc})(L_{cal})} \\ & + w_7\sqrt{(L_{dc})(T_{eff})} + w_8\sqrt{(L_{wc})(L_{cal})} \\ & + w_9\sqrt{(L_{wc})(T_{eff})} + w_{10}\sqrt{(L_{cal})(T_{eff})} + w_{11} \end{aligned} \quad (8)$$

Artificial intelligence based flower pollination algorithm was used to improve forecasting accuracy of the empirical models. Accuracy of the empirical models was calculated by using mean absolute percentage error (MAPE) and mean square error (MSE) methods.

MAPE

$$\frac{1}{n} \sum_{t=1}^n \left(\left| \frac{AL_t - FL_t}{AL_t} \right| \times 100 \right) \quad (9)$$

MSE

$$\frac{1}{n} \sum_{t=1}^n (AL_t - FL_t)^2 \quad (10)$$

Flower Pollination Algorithm

Nature inspired optimization algorithms have become very popular in the last 20 years. It can be seen in the literature, these algorithms are frequently used in NP hard problems especially in the solution of complex problems in engineering and industrial field [21]. Flower pollination algorithm (FPA) is a nature inspired optimization algorithm developed by Xie-She Yang in 2012. The algorithm is inspired by the pollination process of the flowery plants. Pollination process is having a vital role for the flowery plants. Pollination can take two major forms: abiotic and biotic. About 90% of flowering plants belong to the biotic pollination group. In biotic pollination process, pollens are transferred by natural transporters such as insects, flies or other animals. The abiotic form of pollination is realized with natural effects such as wind and diffusion. Grass is one of the good examples of abiotic pollination process. From the aspect of view of biological evolution, the main purpose of flower pollination is the survival of the fittest and the optimal reproduction. This may be expressed like an engineering optimization process of flowery plant species.

Optimization process of the FPA is based on four rules. These rules are:

1. Biotic and cross-pollination can be considered processes of global pollination, and pollen-carrying pollinators move in a way that obeys Lévy flights.
2. For local pollination, abiotic pollination and self-pollination are used.
3. Pollinators such as insects can develop flower constancy, which is equivalent to a reproduction probability that is proportional to the similarity of two flowers involved.
4. The interaction or switching of local pollination and global pollination can be controlled by a switch probability $p \in [0, 1]$, slightly biased toward local pollination.

These rules are converted into proper mathematical equations. In biotic process of the pollination, flower pollen gametes are transferred and carried by pollinator animals such as insects and used for global search in algorithm. Therefore rule 1 and rule 3 are represented mathematically as below equation 11.

$$x^{t+1} = x_i^t + \gamma L(\lambda)(g_* - x_i^t) \quad (11)$$

x_i^t is the pollen i , solution vector x_i at iteration t . g_* is the best current solution among all solutions. γ is the scaling factor and used for controlling the step size for each iteration. $L(\lambda)$ is a Lévy-flights based step size parameter and corresponds the strength of the pollination. Levy-flights can be used for mimic of global pollination which is realized by bio-natural agents mentioned before. The local pollination, both Rule 2 and Rule 3 is represented in equation 12.

$$x^{t+1} = x_i^t + \epsilon(x_j^t - x_k^t) \quad (12)$$

$x_j^t - x_k^t$ are pollens from different flowers of same species and ϵ is drawn from uniform distribution [0-1]. The working process of FPA may be represented with pseudo code as below.

1. Initialize a population of n flowers/pollen gametes with random solutions
2. Find the best solution g_* in the initial population. Define a switch probability $p \in [0, 1]$
3. **while** ($t < \text{MaxGeneration}$)
 - for** $i = 1 : n$ (all n flowers in the population)
 - if** $\text{rand} < p$,
 - Draw a (d -dimensional) step vector L from a Levy distribution
 - Global pollination via $x^{t+1} = x_i^t + \gamma L(\lambda)(g_* - x_i^t)$
 - else**
 - Draw from a uniform distribution in [0,1]
 - Do local pollination via $x^{t+1} = x_i^t + \epsilon(x_j^t - x_k^t)$
 - end if**
 - Evaluate new solutions. If new solutions are better, update them in the population
 - end for**
 - Find the current best solution g_*
 - end while**
4. Output the best solution found

3. RESULTS AND DISCUSSION

In this study, we trained and tested 5 different empirical models with historical load consumption and temperature data set. Flower pollination optimization algorithm was used to optimize mathematical models and having accurate load forecasting values. Parameters and pre-defined constraints of the optimization method FPA are given in Table 3.

Table 3. Parameters and constraints for FPA.

Population Limit (Np)	30
Probability Density	0.80
Beta	3/2
Step Size	0.01
Maximum Iteration Limit	2000

Training and testing of the proposed models was used for monthly horizons. Proposed models trained with data of 2012 and 2013 then tested with data of 2014. Training and testing results for the period 2013 and 2014 are seen in Table 4.

Table 4. Training and testing mape results for FPA.

	February 2013	February 2014	March 2013	March 2014	April 2013	April 2014
Linear	1,871	1,816	2,015	2,146	3,436	2,932
Exponential	11,257	11,919	10,156	11,148	10,206	11,141
Power	2,302	2,576	2,938	2,865	3,573	2,949
Quadratic	9,29	10,33	9,241	10,042	9,634	9,924
Semi-Quadratic	1,794	2,068	1,796	1,953	2,535	2,279

As it seen in Table 3, semi-quadratic model generally gives the better forecasting values than the other empirical models. Obtained results of the proposed models for the 12-hour period of 1 February 2013 is given in Table 4 and comparative results for the period between 1-5 February 2013 is seen in Figure 2.

Real (MWh)	Linear	Exp.	Power	Quad.	Sem- Quad.	Error Linear	Error exp.	Error power	Error quad.	Error semi- quad
27114	27654	2781 4	26865	2691 8	2682 2	1,991	2,582	0,917	0,722	1,075
25480	26002	2781 6	25290	2537 5	2517 5	2,048	9,167	0,746	0,411	1,196
24374	24958	2782 1	24374	2448 6	2429 2	2,395	14,142	0,000	0,459	0,335
23783	24416	2781 5	23632	2398 1	2363 7	2,661	16,952	0,633	0,834	0,613
23574	24327	2781 0	23463	2388 4	2357 9	3,195	17,968	0,473	1,315	0,023
24040	24758	2780 9	23860	2421 8	2397 1	2,986	15,679	0,751	0,742	0,285
24376	25434	2781 3	24538	2480 6	2463 1	4,341	14,101	0,666	1,764	1,046
25122	26630	2782 3	25734	2587 4	2595 9	6,001	10,750	2,437	2,993	3,330
29277	30599	2790 8	29921	3028 6	3047 2	4,514	4,676	2,199	3,447	4,082
32054	33055	2797 0	32597	3321 8	3300 0	3,124	12,742	1,695	3,633	2,951
33032	33793	2804 7	33552	3410 4	3368 2	2,303	15,091	1,574	3,245	1,967
33805	34152	2803 7	33975	3443 7	3392 5	1,028	17,064	0,502	1,869	0,354

Table 5. Training and testing mape results for FPA

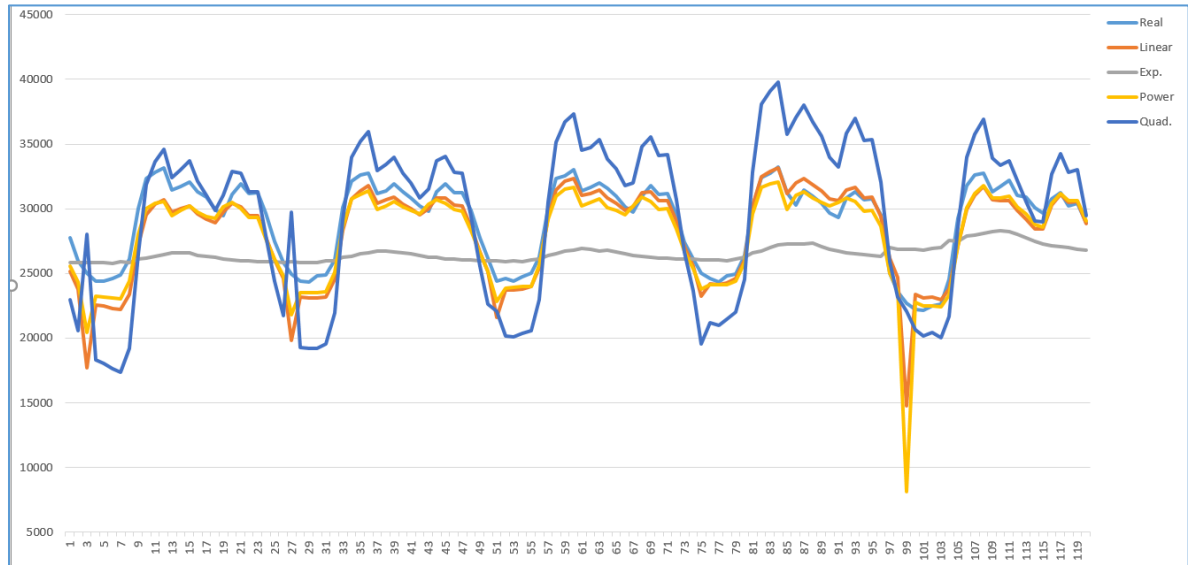


Fig 2. Comparative results of the proposed empirical models for the period between 1-5 February 2013

4. CONCLUSION

Electricity load consumption estimation is having a vital role for official and non-official environments which are responsible for generation and distribution of the resources. From the aspect the view of literature, short-term load forecasting is becoming very popular research area recent years. There are several types of studies and varying of models have been developed for aiming accurate load forecasting. These models and techniques are basically divided into two main categories: classical statistical based models and artificial intelligence or nature inspired models.

In this study, we proposed a hybrid forecasting model which composed classical structural based empirical models and nature-inspired optimization techniques. We used flower pollination algorithm for optimizing empirical models. Proposed forecasting models were trained and tested by using historical load consumption and weather temperature data. Obtained results show that, proposed empirical models give promising results on hourly based short-term load forecasting. Proposed semi-quadratic model is having more accurate forecasting values than other models. Best result was obtained for February 2013 with %1,79 forecasting accuracy.

ACKNOWLEDGMENT

This research was supported by Scientific Research Projects Coordination Unit (B.A.P.K.B.) of Kırıkkale University [Project No: 2016/127, 2017].

REFERENCES

- [1] Feinberg E.A. and Genethliou D., “Chapter 12 Load forecasting”, Applied Mathematics

- [2] for Power Systems, pp.269-282. <http://www.ams.sunysb.edu/~feinberg/public/lf.pdf>
- [3] Fan S. and Hyndman R.J., “Short-Term Load Forecasting Based on a Semi-Parametric Additive Model,” IEEE Trans. Power Systems, vol.27, no.1, pp.134-141, 2012
- [4] Hippert H.S., Pedreira C.E. and Souza R.C. “Neural Networks for Short-Term Load Forecasting: A Review and Evaluation”, IEEE Trans. Power Systems, vol.16, no.1 pp. 44-55, 2001
- [5] Mbamalu G.A.N. and El-Hawary M.E., “Load forecasting via suboptimal seasonal autoregressive models and iteratively reweighted least squares estimation,” IEEE Trans. Power Systems, vol.8, no.1, pp. 343–348, 1993.
- [6] Yang H.T. and Huang C.M., “A new short-term load forecasting approach using self-organizing fuzzy ARMAX models,” IEEE Trans. Power Systems, vol.13, no.1, pp. 217–225, 1998.
- [7] Douglas A.P., Breipohl A.M., Lee F.N. and Adapa R., “The impact of temperature forecast uncertainty on bayesian load forecasting,” IEEE Trans. Power Systems, vol.13, no.4, pp. 1507–1513, 1998.
- [8] Sadownik R. and E.P. Barbosa, “Short-term forecasting of industrial electricity consumption in Brazil,” J. Forecast., vol.18, pp. 215–224, 1999.
- [9] Charytoniuk W., Chen M.S. and Van Olinda P., “Nonparametric regression based short-term load forecasting,” IEEE Trans. Power Systems, vol.13, no.3, pp. 725–730, 1998.
- [10] Harvey A. and Koopman S.J., “Forecasting hourly electricity demand using time-varying splines,” J. American Stat. Assoc., vol.88, no.424, pp. 1228–1236, 1993.
- [11] Taylor J.W. and Majithia S., “Using combined forecasts with changing weights for electricity demand profiling”, J. Oper. Res. Soc., vol.51, no.1, pp. 72–82, 2000.
- [12] Mamlook R., Badran O. and Abdulhadi E., “A fuzzy inference model for short-term load forecasting”, Energy Policy vol. 37, no.4, pp.1239–1248, 2009
- [13] Pandian S.C., Duraiswamy K, Rajan C.C.R and Kanagaraj N, “Fuzzy approach for short term load forecasting”, Electr Power Syst Res vol.76 no.(6–7), pp.541–548, 2006
- [14] Aggarwal S, Kumar M, Saini LM and Kumar A, “Short-term load forecasting in deregulated electricity markets using fuzzy approach”, J Eng. Technol, vol.1, no.1, pp.24–31, 2011
- [15] Ying L.C., Pan M.C., “Using adaptive network based fuzzy inference system to forecast regional electricity loads”, Energy Convers Manag., vol.49, no.2, pp.205–211, 2008
- [16] Hassan S., Khosravi A., Jaafar J. and Khanesar M. A., “A systematic design of interval type-2 fuzzy logic system using extreme learning machine for electricity load demand forecasting”, Electrical Power and Energy Systems, vol.82, pp.1–10, 2016



- [17] Chaturvedi D.K., S.O. M. “Short-Term Load Forecasting Using Fuzzy Logic and Wavelet Transform Integrated Generalized Neural Network”, *Electrical Power and Energy Systems*, vol.67, pp.230-237, 2015.
- [18] S. Li, P. L. G. “Short-term load forecasting by wavelet transform and evolutionary extreme learning machine”, *Electric Power System Research*, vol.122, pp. 96-103, 2015
- [19] Yukseltan E., Yucekaya A. and Bilge A.H., “Forecasting electricity demand for Turkey: Modeling periodic variations and demand segregation”, *Applied Energy*, vol.193, pp. 287–296, 2017
- [20] Çevik H.H. and Çunkaş M., “Short-term load forecasting using fuzzy logic and ANFIS”, *Neural Computing and Applications*, vol. 26, no.6, pp.1355–1367, 2015.
- [21] Esener I., Yuksel T. and Kurban M., “Short-term load forecasting without meteorological data using AI-based structures”, *Turkish Journal of Electrical Engineering & Computer Sciences*, vol.23, pp.370-380, 2015.
- [22] Yang X.-S., *Nature-Inspired Optimization Algorithms*, Londra: Elsevier, 2014.



CHARACTERIZATION OF VOLATILE COMPOUNDS OF SHADE-DRIED LAVENDER (*LAVANDULA STOECHAS*) FLOWERS BY PURGE & TRAP TECHNIQUE

Onur Sevindik¹, Ahmet Salih Sonmezdag², Gamze Guclu¹, Hasim Kelebek³, Serkan Selli*¹

¹ Department of Food Engineering, Faculty of Agriculture, Cukurova University, 01330 Adana, Turkey

² Department of Gastronomy and Culinary Arts, Faculty of Fine Arts, Gaziantep University, 27310 Gaziantep, Turkey

³ Department of Food Engineering, Faculty of Engineering and Natural Sciences, Adana Science and Technology University, Adana, Turkey

*Corresponding Author: sselli@cu.edu.tr

ABSTRACT

Lavender (*Lavandula stoechas*), an evergreen medicinal and aromatic plant (MAP) which is one of the well-known member of Lamiaceae family. Owing to its imposing colour, redolent aroma and salubrious properties, lavender has stood always as a conspicuous plant throughout the history. Moreover, there exist some proofs demonstrating the therapeutic usage of lavender by antique Romans and Greeks. These peculiarities provided a wide usage to *Lavandula* genus in food and cosmetic industry. Distribution of *Lavandula* species has expanded in all over the world, particularly in the Mediterranean basin. Apart from its essential oil, shade-dried flowers of lavender have long been used as a fragrance. Although, there are many of comprehensive studies focused on the volatiles of lavender essential oil, only a few numbers of researches exist on the aroma profile of shade-dried flowers and leaves of lavender. The present study was organised to identify and quantify aroma compounds of shade-dried lavender flowers by the isolation of its aromatic extract by means of purge & trap method. A total of 32 aroma compounds were detected including dominantly terpenes followed by volatile phenols, esters, a furanoid, a lactone, an alcohol and an aldehyde. Among all aroma compounds, camphore was found as the most abundant aroma compound in shade-dried lavender flowers, having a 40.6 % of total aroma concentration.

Keywords: Aroma, *Lavandula stoechas*, lavender, purge and trap extraction

1. INTRODUCTION

The medicinal & aromatic plants (MAPs) are gaining an increasing trend due to their extensive usage area in several sectors such as food & flavouring, cosmetic, pharmaceutical, and therapeutic. Lavender (*Lavandula stoechas*), an evergreen MAP, which is one of the well-known member of Lamiaceae family. This MAP is known as its hardy structure, lush growth, and high sustainability. The Spain, France, Japan and England are the spearheading countries for the cultivation and exportation of this specie [1]. Although the production of lavender and its derived products mostly concentrated in Mediterranean basin, the largest market of these goods take place in the USA followed by Japan. Many types of lavender herb are highly used in cosmetic industry owing to their aromatic leaves, flowers, and their essential oils. Many goods in the cosmetic industry have long been utilizing lavender such as; soap, lotion, shower gel, shampoo, detergent, cologne, air fresheners, perfumes and etc. Moreover, it has mentioned in the literature that lavender essential oil can be used as a prophylactic or as a topical treatment against surface infections in the alternative medicine. The expansion of the use of lavender essential oil is also increased by the growing demand of utilizing natural and healthy products in the scope of food industry. A number of studies exhibited its high antioxidant capacity [2], antimicrobial impact [3], antifungal activity [4] and also its usage in variety of foods as a flavouring agent such as, ice cream, herb tea, confectionery and honey. Therefore, as a natural food additive and a preservative, lavender has long been used on the purpose of food preservation. Another usage area of lavender is aromatherapy [5] which has become more of an art than a science owing to have a huge marketing opportunity.

Lavandula stoechas is the most common specie of the lavender grown in Mediterranean basin and its salubrious and redolent essential oil has been studied in plenty of researches. As a result of secondary plant metabolisms, unique aroma lavender emerges mainly consisting of terpenes such as camphor and fenchone.

One of the most important aspect for such medicinal and aromatic plants is the odour quality related to aroma compounds which play key roles to attract consumer preferences. Many of MAPs being utilised as flavouring for food and beverages. Lavender is also can be listed as a natural food flavouring agent. Although, some of studies have focused on the aroma profile of essential oil extracted from lavender [6,7] aroma profile of shade dried flowers and flower buds of lavender has not been deeply investigated yet.

At present, various aroma extraction techniques utilizing in order to perform better qualitative and quantitative surveys. A plenty of aromatic substances exist with a various polarity and volatility in the lavender. Therefore, they can be found in different concentrations in the matrix. The most critical steps of aroma analysis can be counted as the sample preparation, decision of correct extraction methodology and its optimization. The present study was organized to isolate aroma compounds of shade-dried lavender leaves by purge and trap technique and investigating the total aroma profile by means of GC-MS system.

2. MATERIAL AND METHODS

2.1. *Samples and Chemicals*

Commercial samples (1 kg) of dried lavender (*Lavandula stoechas*) (origin: Turkey) was obtained from a local herbalist supplier, in Gaziantep, Turkey in July, 2016. The herbs were identified by the Faculty of Agriculture, University of Cukurova. The moisture content of the herb was 3.7-4.5% (dry basis). Water used in this study was purified by a Millipore-Q system (Millipore Corp., Saint-Quentin, France). The standard volatile compounds were purchased from Sigma-Aldrich (Steinheim, Germany). Dichloromethane, sodium sulfate and 4-nonanol were obtained from Merck (Darmstadt, Germany). Dichloromethane was freshly distilled prior to use.

2.2. *Extraction of Volatile Compounds*

Volatiles of herb was extracted by purge and trap system which comprise a flow-meter which control a nitrogen source and connected to splitter system to divide the flow in several channels in order to purge three samples at the same time. Lichrolut EN tubes obtained from Merck was used as an adsorbent which is one of most the appropriate sorbents for volatile compounds extraction with respect to the previous research [8]. The herb samples was previously mortared and placed into a 20 mL vial then the sample was pre-incubated at optimized purging temperature (60 °C) for 10 minutes. The process was applied for 90 minutes with a nitrogen flow of 500 mL/min. After purging, the volatiles held in the cartridge were eluted with dichloromethane. The elute was dried by anhydrous sodium sulphate, the pooled organic extract was concentrated to 5 mL in a Kuderna Danish concentrator fitted with a Snyder column at 40°C (Supelco, St Quentin, France) and then to 0.5 mL under a gentle flow of nitrogen. Extracts were then stored at -20°C in a glass vial equipped with a Teflon-lined cap until analysis. Extraction was carried out in triplicate.

2.3. *Representativeness test for aromatic extract*

Sample preparation and presentation.

Lavender was evaluated using the descriptive and preference tests according to Poste et al. [9]. The panel was composed of ten assessors (seven females and three males between 20 and 45 years old) from Cukurova University, Food Engineering Department. The assessors were previously trained in sensory evaluation techniques. In the present study, we used a cardboard smelling strip (reference 7140 BPSI, Granger-Veyron, Lya, France) for the checking representativeness of the shade-dried lavender aromatic extract obtained purge and trap extraction technique. Three grams of fined samples were placed in 15 mL brown coded flask as a reference for representativeness tests. Aromatic extract obtained from dichloromethane was adsorbed onto a cardboard smelling strip. After 1 min (the time necessary for solvent evaporation) the extremities of the strips were cut off, then placed in dark coded flasks (15

mL) and presented to the panel after 15 min. All the samples were assessed at room temperature (20 °C) in neutral conditions. Similarity and intensity tests Similarity and intensity tests were performed to demonstrate the closeness between the odour of the extracts and the lavender. These test procedures were well documented in our previous study [10].

2.4. GC-FID, GC-MS Analysis of Volatile Compounds

Agilent 6890 chromatograph interfaced with flame ionization detector (FID) and Agilent 5973-Network-mass selective detector (MSD) (Wilmington, USA) constituted the gas chromatography (GC) system. DB-Wax column (30 m length x 0.25 mm i.d. x 0.5 μ m thickness, J&W Scientific Folsom, USA) were used to separate volatile compounds. 3 μ L of extract was injected in pulsed splitless (40 psi; 0.5 min) mode. Injector and FID detectors were set at 270°C and 280°C, respectively. The flow rate of carrier gas (helium) was 1.5 mL min⁻¹. The conditions of the oven program of the DB-Wax column was 50°C to 250°C at 4°C/min, 10 min hold. As for the mass-selective detector, the identical oven program was used. The MS (electronic impact ionization) conditions were as follows: ionization energy of 70 eV, mass range m/z of 30-300 a.m.u., scan rate of 2.0 scan s⁻¹, interface temperature of 250 °C, and source temperature of 180°C. The volatile compounds were analyzed in full scan mode and assigned by comparison of their retention index and their mass spectra on the DB-Wax column with those of a commercial spectra database (Wiley 6, NBS 75k) and the instrument's internal library made through the aforementioned laboratory researches. After identification, internal standard method with 4-nonanol was used to determine the mean value of volatile compounds and mean values (μ g 100g⁻¹ dry weight; dw) of the triplicate of GC analyses were calculated for each sample. By using n-alkane (C8–C32) series, retention indices of the compounds were calculated [10,11].

3. RESULTS AND DISCUSSION

An aromatic extract of shade-dried lavender obtained by purge and trap aroma extraction technique displayed an identical aroma to the original odor of lavender, when a drop of the aromatic extract was assessed on a cardboard smelling strip (7140 BPSI, Lysas, France). A certain amount of aromatic extract injected into GC-MS system to perform a sensitive identification and quantification of each aroma compounds. Identified volatiles and their linear retention indices determined on the DB-WAX column are given in Table 1.

According to results obtained in the present study, various aroma compound groups identified in the aromatic extract of lavender herb including terpenes, alcohols, esters, furanoids, lactones, and volatile phenols. A total of 32 compounds were identified in the total aroma profile lavender. Terpenes were the most dominant aroma group as constituting the 90.47% of the overall aroma concentration. MAPs are well known with their pleasant odors, spicy tastes

or to show pharmacological activities mainly due to the specialties of those terpene compounds. However, producing purposes and biological functions of these compound have not been completely investigated. Many herbs generate terpenes so as to charm insects for pollination or to protect herbs from being eaten by animals [12]. Among terpenes, camphor, fenchone and, camphene were the three most abundant compounds and their relative percentage concentrations were found as 32578 µg/kg, 23679 µg/kg and, 4139 µg/kg, respectively. Similarly to *Lavandula stoechas*, terpenes were also dominant compounds of MAPs such as *Salvia officinalis*, *Lavandula angustifolia*, and *Mentha asiatica* [8]. An enzyme, terpene synthases, is directly responsible for the production of these volatile terpenes. On the other hand, they could also be formed by the modification of the main skeletons of terpene made by terpene synthases by hydroxylation, dehydrogenation, acylation, and other reactions [13].

Esters were the other important class of the aroma compounds in the *Lavandula stoechas*. Esters compounds have a very wide range of odor and flavouring effects and there are over 200 of these compounds permitted for use in foods. Moreover, these compounds are widely distributed in the essential oils and in some instances represent the major constituent. Generally, ester compounds are responsible for the mature and fruity notes [14]. Bornyl acetate and linalyl acetate were identified and quantified ester compounds in the herb. These esters are significant compounds in the perfume industry and are found in large amounts in various plants [15].

Apart from the terpenes and esters, three volatile phenols, a furanoid, a lactone and, an aldehyde were found in shade-dried *Lavandula stoechas*. Among these volatiles, 5-ethenyldihydro-5-methyl-2-furanone is also known as lavender lactone which is also known as dihydro-5-methyl-5-vinylfuran-2-one, γ -vinyl- γ -valerolactone, 4-methyl-4-hydroxy-5-hexenoic acid lactone. This lactone mainly emerges as an oxidation metabolite of linalool oxide (furanoid) (Gottlieb *et al.*, 1978), and it has cited as a lactone of lavender essential oil in the literature [16].

Table 1. Volatile compounds of *Lavandula stoechas*

No	LRI*	Compounds	Concentration (µg/kg) #	Identification [§]
1	1045	α -pinene	2151	LRI,MS,std
2	1057	camphene	4139	LRI,MS,std
3	1131	verbenene	1136	LRI,MS,tent
4	1138	1,5,8- <i>p</i> -menthatriene	502,0	LRI,MS,tent

5	1205	<i>dL</i> -limonene	395,3	LRI,MS,std
6	1234	<i>p</i> -cymene	715,8	LRI,MS,std
7	1422	fenchone	23679	LRI,MS,std
8	1480	(<i>Z</i>)-linalool oxide (Furanoid)	1487	LRI,MS,std
9	1518	camphor	32578	LRI,MS,std
10	1570	linalool	966,0	LRI,MS,std
11	1578	linalyl acetate	572,0	LRI,MS,std
12	1586	pinocarvone	546,1	LRI,MS,tent
13	1589	<i>D</i> -fenchyl alcohol	479,0	LRI,MS,std
14	1592	bornyl acetate	4143	LRI,MS,std
15	1610	myrtenal	509,3	LRI,MS,tent
16	1635	5-ethenyldihydro-5-methyl-2-furanone	246,3	LRI,MS,tent
17	1651	(<i>E</i>)-pinocarveol	493,1	LRI,MS,tent
18	1663	(<i>E</i>)-verbeneol	1557	LRI,MS,std
19	1699	<i>L</i> -verbenone	579,8	LRI,MS,std
20	1718	<i>p</i> -mentha-1,5-dien-8-ol	61,8	LRI,MS,std
21	1728	<i>D</i> -carvone	556,1	LRI,MS,std
22	1729	epoxylinolol	200,0	LRI,MS,std
23	1757	Myrtenol	208,4	LRI,MS,std
24	1782	γ -cadinene	112,9	LRI,MS,std
25	1838	(<i>E</i>)-carveol	371,0	LRI,MS,std
26	1842	<i>p</i> -cymene-8-ol	294,7	LRI,MS,std
27	1846	(<i>E</i>)-calamenene	88,1	LRI,MS,tent
28	1996	filifolide A	65,0	LRI,MS,tent
29	2083	<i>p</i> -cresol	39,7	LRI,MS,std
30	2153	thymol	100,2	LRI,MS,std



31	2210	carvacrol	543,2	LRI,MS,std
32	2218	α -cadinol	650,2	LRI,MS,std
		Total	80166,6	

* LRI, linear retention index calculated on DB-WAX capillary column

Concentration: Results are the means of three repetitions as $\mu\text{g kg}^{-1}$ dw

§ Identification: Methods of identification; LRI (linear retention index), MS tent. (tentatively identified by MS), Std (chemical standard); When only MS or LRI is available for the identification of a compounds, it must be considered as an attempt of identification. nd (not detected).

4. CONCLUSION

In this study, the main object was to identify and quantify the aroma compounds of *Lavandula stoechas*, a member of *Lamiaceae* plant family, widely grown and also cultivated in Turkey. A total of 32 aroma compounds were identified in shade-dried leaves of this MAP including, mainly terpenes, esters, volatile phenols, an aldehyde, a lactone, an alcohol and a furanoid. Terpene compounds were determined as the main chemical group among the identified aroma compounds and followed by esters. 23 terpene compounds were identified in the sample camphor, fenchone, and camphene were the most important terpenes detected in lavender.

REFERENCES

- [1] K.L. Adam, 2006. Lavender Production, Products, Markets, and Entertainment Farms. *ATTRA*. Retrieved November, 5.
- [2] L.T. Danh, N.D.A. Triet, J. Zhao, R. Mammucari and N. Foster, 2012. Antioxidant activity, yield and chemical composition of lavender essential oil extracted by supercritical CO₂. *The Journal of Supercritical Fluids*. 70 27 - 34.
- [3] J.F. Martucci, L.B. Gende, L.M. Neira and R.A. Ruseckaite, 2015. Oregano and lavender essential oils as antioxidant and antimicrobial additives of biogenic gelatin films. *Industrial Crops and Products*. 71 205 - 213.
- [4] T. Moon, H.M.A. Cavanagh and J.M. Wilkinson, 2004. Lavender as an antibacterial essential oil-are all lavenders equal. *AICA National Conference*. 46.
- [5] L.A. Snow, L. Hovanec and J. Brandt, 2004. A controlled trial of aromatherapy for agitation in nursing home patients with dementia. *The Journal of Alternative and Complementary Medicine*. 10(3) 431 - 437.
- [6] M. Moss, J. Cook, K. Wesnes and P. Duckett, 2003. Aromas of rosemary and lavender essential oils differentially affect cognition and mood in healthy adults. *International*



- Journal of Neuroscience*. 113(1) 15-38.
- [7] M.M. Won, E.J. Cha, O.K. Yoon, N.S. Kim, K. Kim and D.S. Lee, 2009. Use of headspace mulberry paper bag micro solid phase extraction for characterization of volatile aromas of essential oils from Bulgarian rose and Provence lavender. *Analytica Chimica Acta*. 631(1) 54 - 61.
- [8] A.S. Sonmezdag, H. Kelebek and S. Selli, 2017. Identification of aroma compounds of Lamiaceae species in Turkey using the purge and trap technique. *Foods*. 6 1 – 9.
- [9] L.M. Poste, 1991. Laboratory methods for sensory analysis of food, Canada. *Department of Agriculture*.
- [10] A.S. Sonmezdag, H. Kelebek and S. Selli, 2016. Characterization of aroma-active and phenolic profiles of wild thyme (*Thymus serpyllum*) by GC-MS-Olfactometry and LC-ESI-MS/MS. *Journal of Food Science and Technology*. 53 1957-1965.
- [11] A.S. Sonmezdag, H. Kelebek and S. Selli, 2016. Characterization and comparative evaluation of volatile, phenolic and antioxidant properties of pistachio (*Pistacia vera* L.) hull. *Journal of Essential Oil Research*. 1-9.
- [12] E. Breitmaier, 2006. Terpenes: Importance, general structure, and biosynthesis. *Flavors, Fragrances, Pharmaca, Pheromones*. 1-9.
- [13] N. Dudareva, E. Pichersky and J. Gershenzon, 2004. Biochemistry of plant volatiles, *Plant Physiology*. 135 1893-1902.
- [14] G. Reineccius, 2005. Flavor chemistry and technology. *CRC press*.
- [15] H. Casabianca, J. Graff, V. Faugier, F. Fleig and C. Grenier, 1998. Enantiomeric distribution studies of linalool and linalyl acetate. A powerful tool for authenticity control of essential oils, *Journal of High Resolution Chromatography*. 21 107-112.
- [16] R. Timmer, R. Ter Heide, P.J. De Valois and H.J. Wobben, 1975. Analysis of the lactone fraction of lavender oil (*Lavandula vera* DC). *Journal of Agricultural and Food Chemistry*. 23(1) 53-56.



ASSESSMENT OF GENETIC DIVERSITY OF *PSEPHELLUS AUCHERIANUS* COMPLEX IN TURKEY USING SSR MARKERS

Meryem BOZKURT

Department of Biology, Selçuk University, Turkey.

(E-mail: mbozkurt@selcuk.edu.tr)

Corresponding Author's e-mail: mbozkurt@selcuk.edu.tr

ABSTRACT

This study is the first report informing about the genetic diversity of species belonging to *Psephellus aucherianus* complex via microsatellite (SSR) markers. This complex includes three endemic species which are consisting of *Ps. aucherianus* (DC.) Boiss., *Ps. yusufeliensis* O. Tugay and Uysal and *Ps. sintenisii* (Freyn) Ertuğrul and Uysal (spec. and comb. nova). All of these species are evaluated under seriously threat in Red List Data Book. According to IUCN categories, *Ps. aucherianus* was reported as "Endangered (EN)" and *Ps. yusufeliensis* and *Ps. sintenisii* were reported as "Critically Endangered (CR)". Knowledge of the levels of genetic diversity is important for designing conservation strategies for endemic species so as to guarantee sustainable survival of populations. Therefore, the aim of this study was to investigate population structure by estimating genetic diversity within and between locally endemic populations. To determine the genetic diversity of the species, 96 individuals from six populations were assessed by using four SSR markers. However, only 13D10 primer was answered to our all populations. This primer was polymorphic, and it were detected 36 alleles across the populations. Conclusively, our results indicated that there was the presence of a correlation between the level of genetic differentiation and geographical distance and they had been effective in differentiation of populations. We found very pleasing in terms of the species conservation that the high genetic diversity was detected at both the population and relatively species level. Apart from this, *Ps. sintenisii* is seen very close to the populations of *Ps. aucherianus* as connected with geographical closeness contrast to *Ps. yusufeliensis*. Therefore, we can concluded that only one locus or primer can be used especially to make genetically a characterization above one species and its populations but certainly is not suggest for geographically overlapping close taxa or their populations.

Keywords: Conservation, endemic species, genetic diversity, population genetics, Turkey.

1. INTRODUCTION

Turkey is one of the most significant places in the World for plant genetic resources: it is located on three phyto-geographical regions; Euro-Siberian, Mediterranean, and Irano-Turanian. Therefore, it is not surprising that Turkey have highly biodiversity. It has a unique combination of diverse geographical and climatic condition that have given rise to a large number of rare and endemic species. Turkish Flora includes many narrow and local endemic species and many of them are known only from type localities. One of the most important main problem and the main risk for Turkish Flora are lack of data about the population structures of endemic species, in particularly genetic interactions among species and their populations.

The genus *Psephellus* Cass. includes around 100 species and is distributed mainly in western Siberia, Turkey, Iran, Caucasus, Ukraine, and Crimea. In Turkey, *Psephellus* is represented by 37 taxa according to the latest revision and national checklist [1, 2]. This complex consists of three endemic species which are *Ps. aucherianus* (DC.) Boiss., *Ps. yusufeliensis* O. Tugay and Uysal and *Ps. sintenisii* (Freyn) Ertuğrul and Uysal (spec. and comb. nova, unpublished). All of these species are evaluated under seriously threat in Red List Data Book [3]. According to IUCN categories, *Ps. aucherianus* was reported as "Endangered (EN)" and *Ps. yusufeliensis* and *Ps. sintenisii* were reported as "Critically Endangered (CR)" [4]. Information about genetic diversity is very important for designing conservation strategies for endemic species, because they are commonly characterized by low levels of genetic diversity [5, 6]. The development of molecular genetic methods for answering questions on the diversity has been helped define strategies for conservation programs. Among various molecular methods, microsatellites are known as simple sequence repeats (SSR) and particularly preferred for plant conservation studies, because they are codominant and widely distributed in the genome [7]. Furthermore, they are characterized by high polymorphism and a high number of alleles per locus. In natural plant populations, microsatellites have great potential for helping to understand what determines patterns of genetic diversity, especially when used nuclear SSR markers because of more variable. Therefore, SSRs have been used in studies of plant genetic diversity such as Asteraceae [8]. However, they are highly species-specific and have to be isolated de novo for most species [9, 10]. The process of SSR isolation is expensive and time consuming. Therefore, the use of primer sequences developed for one species (source species) into others (target species) is desirable in terms of cost-efficiency [8]. The success rate of microsatellite cross-species amplification has directly been correlated to the evolutionary distance between the source species and the target species [11, 12, 13]. López-Vinyallonga *et al* (2011) were checked the some SSR primers to determine genetical construction of *Centaurea* species and finally they reported that this primers would be very useful and cheaper to make genetical characterization in *Centaurea* species. Therefore, we decided the using of this marker and interested primers for genetical characterization of *Psephellus aucherianus* complex.

Taking into account all these considerations, the aim of this study was:

To test the transferability of four nuclear microsatellite markers previously developed for *Centaurea corymbosa*.

To investigate population structure by estimating genetic diversity within and between locally endemic populations.

2. MATERIAL AND METHODS

Plant material

A total of 96 individuals, which corresponds to 6 populations of *Ps. aucherianus* complex, were collected across 3 provinces in Turkey; Erzincan, Erzurum, and Artvin respectively (Table 1; Figure 1) and sampled leaves dried in silica gel.

Table 1. The populations investigated belonging to *Psephellus aucherianus* complex

Populations and its codes	Taxa	Locality
Population Salihli (PAUM)	<i>Psephellus sintenisii</i>	Erzincan; Kemaliye yolu-Salihli çimento geçidi, 1506 m, 39° 21' 348" - 38° 28' 062", serpantin yamaçlar, KE-4125, 04.06.2011.
Population Bağıştaş (PSAU)	<i>Ps. aucherianus</i>	Erzincan; İliç-Kemaliye arası, Bağıştaş yukarısı, 1130 m, 39° 25' 738"-38° 26' 626", KE-4124, Kalker kayalıklar meşelik, linear yapraklı, 04.06.2011.
Population Dutluca (PADU)	<i>Ps. aucherianus</i>	Erzincan; Kemaliye-Dutluca geçidi, batı yamaçlar (1 km), 1520-1600 m, kırmızı topraklı, meşe açıklıkları, taşlık alanlar, KE-4690, 05.07.2012.
Population Eriç (PSER)	<i>Ps. aucherianus</i>	Erzincan; Kemah, Eriç Köyü güneyi, 1265-2000 m, meşe açıklıkları, taşlık bayırlar, 39° 51' 157" - 39° 49' 616" K, 38° 87' 711" - 38° 87' 543" D, KE-4664, 04.07.2012.
Population Yusufeli (PYUS)	<i>Ps. yusufeliensis</i>	Artvin; Yusufeli-Sarıgöl çıkışı, 625 m, 40° 49' 296" - 41° 32' 844", kaya üzeri, KE- 4237-TU-DU, 31.05.2011.
Population Tortum	<i>Ps. yusufeliensis</i>	Erzurum; Tortum Şelale girişi, 1008 m, 40° 39' 650" - 41° 39' 800", çalılık kumlu tepeler, KE- 4334-TU-DU, 03.06.2011.

(PYFS)		
--------	--	--



Figure 1. The geographical distribution of populations belonging to *Psephellus aucherianus* complex

DNA isolation and amplification conditions

We used at least 16 individuals per population when possible, accounting for a total of 96 individuals from six populations. Total genomic DNA was extracted by the 2X CTAB method as previously described by Doyle and Doyle (1987) and modified by Soltis *et al.* (1991) and Cullings (1992) for silica gel-dried leaves. DNA quality was checked on a 1% agarose gel. For amplification of the three endemic species, we carried out a preliminary test using four SSR markers developed for *Centaurea corymbosa* [16]. Microsatellite locus (13D10) was amplified using FAM fluorescently labeled forward primers as explained in Merle *et al.* in all the studied species.

Data analysis

Software GENETIX [18] and GENEPOP [19] were used for estimating genetic diversity parameters at both species and population levels: observed heterozygosity (H_o); expected heterozygosity (H_e); and (f) inbreeding coefficient (F_{IS}) by the method of Weir & Cockerham (1984). Nei's (1978) unbiased genetic distances were calculated for all population pairs and used to construct a phylogenetic tree (UPGMA). The Factorial Correspondence Analysis (FCA) was performed to visualize the individuals in multidimensional space and to discover the relationships within and among individuals of different species. FCA was computed using GENETIX program.

3. RESULTS AND DISCUSSION

The studied locus (13D10) was polymorphic for all studied populations. We detected a total of 36 alleles, ranging between 11 (Population Salihli; PAUM) and 17 (Population Tortum; PYFS). Population Salihli showed the lowest value of expected heterozygosity (PAUM: $H_e = 0.8730$), whereas population Eriç harboured the highest expected heterozygosity value (PSER: $H_e = 0.9141$; Table 2). Although the genetic diversity of species in small populations is

lower than large populations because of genetic drift and inbreeding [22, 23], the high genetic diversity has been reported in some taxa, such as *Centaurea horrida* ranging from $H_e = 0.7-0.9$ [24] and *Centaurea nivea* $H_e = 0.6$ [25]. The least variable species was *Ps. sintensisii* ($H_e = 0.8730$), whereas the highest genetic diversity was shown by *Ps. aucherianus* ($H_e = 0.9141$; Table 2). Our results generally supported that some rare and endangered species can maintain high levels of genetic diversity [26-30]. The locus showed significant deviations from H-W equilibrium expectations ($P < 0.05$); accordingly, whereas F_{IS} values at population Tortum (PYFS: -0.1034) was negative value, *Ps. sintensisii* (PAUM: 0.3135) was positive value and significantly different from zero (Table 2), which can be attributed to inbreeding and/or to the occurrence of null alleles [31]. According to our dataset, whereas frequency of null alleles is negligible for PSAU (NA: 0.0348 , $r < 0.05$), it is moderate for PAUM (NA: 0.1293 , $0.05 \leq r < 0.20$) [32] and the presence of null alleles might have caused the loss of heterozygosity (F_{IS} : 0.3135) in *Ps. sintensisii* [33, 34]. Our results indicated that there was the presence of a correlation between the level of genetic differentiation and geographical distance and they had been effective in differentiation of *Ps. aucherianus* populations. A relatively high degree of genetic differentiation was detected among Yusufeli (PYUS) and Tortum (PYFS) populations (F_{ST} : 0.0865). This situation can be explained with population Yusufeli tightened in a narrow valley. Thus, a taxonomic assessment was not made at the species level by the genetic differentiation values. According to FCA graphic (Figure 2), individuals of populations belonging to three species are grouped together indicating clear admixture. Population Tortum have wider distribution and this population has a higher level of variation (~35%) compared to other populations (12%), this circumstance is consistent with the detected heterozygote excess (F_{IS} : -0.1034).

Table 2. Main parameters of genetic diversity for each population computed for the studied polymorphic loci.

Codes of Populations	PAUM	PSER	PSAU	PADU	PYFS	PYUS
sample size (N)	16	16	16	16	16	16
mean number of alleles per locus (A)	11	16	12	15	17	14
unbiased expected heterozygosity (He)	0.8730	0.9141	0.8945	0.8906	0.8809	0.8828
observed heterozygosity (Ho)	0.6250	0.9375	0.8125	1.0000	1.0000	1.0000
the frequency of null alleles (NA) (*confidence interval 0.0250-0.9750)	0.1293*	0.0000	0.0348*	0.0000	0.0000	0.0000
Inbreeding coefficient; (F_{IS}) P<0.05 (*)	0.3135*	0.0066	0.1236	- 0.0909	- 0.1034*	- 0.1009
P-val (F_{IS})	0.0000	0.4685	0.0605	0.7916	0.0190	0.0564
Standard deviation (F_{IS})	0.0000	0.0541	0.0133	0.0347	0.0006	0.0007

	PAUM	PSER	PSAU	PADU	PYFS	PYUS	Nei's unbiased
F_{ST}							measures of genetic distance (above the diagonal) (Nei, 1978).
(below the diagonal) P<0.05(*)	PAUM*	0.487	0.083	0.171	1.278	1.472	
	PSER*	0.0283	0.776	0.364	1.522	1.798	
	PSAU*	0.0013	0.0354	0.650	1.402	1.440	
	PADU*	0.0122	0.0240	0.0387	1.295	2.852	
	PYFS*	0.0671	0.0603	0.0641	0.0667	2.574	
	PYUS*	0.0707	0.0630	0.0640	0.0830	0.0865	



the species conservation and they could be trying in the next population studies of species taking place within Centaureinae.

ACKNOWLEDGMENT

This work is part of my PhD thesis. This research was supported by Selçuk University (BAP project number: 11101036) and I thanks them for financial support. I thanks Dr. Tuna UYSAL and Dr. Kuddisi ERTUĞRUL for plant collecting and species identification and I would also like to thanks Dr. Tuna UYSAL for many valuable suggestions that greatly improved the manuscript.

REFERENCES

- [1] K. Ertuğrul, *Psephellus* Cass. In: Güner A, Aslan S, Ekim T, Vural M, Babaç MT, editors. Türkiye Bitkileri Listesi (Damarlı Bitkiler). İstanbul, Turkey: Nezahat Gökyiğit Botanik Bahçesi ve Flora Araştırmaları Derneği Yayını 190–192 (in Turkish), 2012.
- [2] K. Ertuğrul and T. Uysal, 2013. The Revision of the genus *Psephellus* Cass. (Compositae) in Turkey. *TUBITAK project* (109T958).
- [3] IUCN, Species Survival Commission, IUCN Red List Categories: Version 3.1, Gland, Switzerland, 2008.
- [4] M. Bozkurt, 2015. *Determination Of The Genetic Variation In Populations Belonging To Psephellus aucherianus (DC.) Boiss. (Asteraceae) Complex Species*. PhD Thesis, Department of Biology, Graduate School of Natural and Applied Sciences, Selcuk University, Turkey.
- [5] N.C. Ellstrand and D.R. Elam, 1993. Population genetic consequences of small population size: implications for plant conservation. *Annual Review of Ecology, Evolution, and Systematics* 24(1) 217 - 242.
- [6] M.A. Gitzendanner and P.S. Soltis, 2000. Patterns of genetic variation in rare and widespread plant congeners. *American Journal of Botany*. 87(6) 783-792.
- [7] F. M. Alves, M. I. Zucchi, A.M.G. Azevedo-Tozzi, A.L.B. Sartori and A.P. Souza, 2014. Characterization of microsatellite markers developed from *Prosopis rubriflora* and *Prosopis ruscifolia* (Leguminosae– Mimosoideae), legume species that are used as models for genetic diversity studies in Chaquenian areas under anthropization in South America. *BMC Research Notes*. 7: 375.
- [8] S. López-Vinyallonga, J. López-Alvarado, TH. Constantinidis, A. Susanna and N. Garcia-Jacas, 2011. Microsatellite cross-species amplification in the genus *Centaurea* (Compositae). *Collectanea Botanica*. 30: 17-27.



- [9] L. Zane, L. Bargelloni, and T. Patarnello, 2002. Strategies for microsatellite isolation: a review. *Molecular Ecology*. 11(1) 1-16.
- [10] J. Abdelkrim, B.C. Robertson, J.A.L. Stanton, N.J. Gemmell, 2009. Fast, cost-effective development of species-specific microsatellite markers by genomic sequencing. *BioTechniques* 46: 185-191.
- [11] C.R. Primmer, J.N. Painter, M.T. Koskinen, J.U. Palo and J. Merilä, 2005. Factors affecting avian cross-species microsatellite amplification. *Journal of Avian Biology*. 36 (4) 348 - 360.
- [12] T. Barbara, C. Palma-Silva, G.M. Paggi, F. Bered, M.F. Fay and C. Lexer, 2007. Cross-species transfer of nuclear microsatellite markers: potential and limitations. *Molecular Ecology*. 16 (18) 3759-3767.
- [13] N.S. Maduna, C. Rossouw, R. Roodt-Wilding and A.E. Bester-van der Merwe, 2014. Microsatellite cross-species amplification and utility in southern African elasmobranchs: A valuable resource for fisheries management and conservation. *BMC Research Notes*. 7: 352.
- [14] J.J. Doyle and J.L. Doyle, 1987. A rapid DNA isolation procedure for small quantities of fresh leaf tissue. *Phytochem Bull Bot Soc Am* 19: 11-15.
- [15] K.W. Cullings, 1992. Design and testing of a plant-specific PCR primer for ecological and evolutionary studies. *Molecular Ecology*. 1 (4) 233-240.
- [16] H. Fréville, E. Imbert, F. Justy, R. Vitalis and I. Olivieri, 2000. Isolation and characterization of microsatellites in the endemic species *Centaurea corymbosa* Pourret (Asteraceae) and other related species. *Molecular Ecology*. 9 (10) 1671-1672.
- [17] H. Merle, I. Segura, A. Garmendia, and M. Ferriol, Isolation and characterization of polymorphic microsatellite markers for *Centaurea aspera* L. and *Centaurea seridis* L. (Asteraceae). *Molecular Ecology Resources*.
- [18] K. Belkhir, P. Borsa, L. Chikhi, N. Raufaste, and F. Bonhomme, GENETIX 4. 05, Logiciel sous Windows™ pour la génétique des populations (Laboratoire Génome, Populations, Interactions, CNRS UMR 5000, Université de Montpellier II, (1996–2004).
- [19] M. Raymond and F. Rousset, 1995. GENEPOP (version 1.2): population genetics software for exact tests and ecumenicism. *Journal of Heredity*. 86 (3) 248 - 249.
- [20] B.S. Weir and C.C. Cockerham, 1994. Estimating F-statistics for the analysis of population structure. *Evolution*. 38 (4) 1358 - 1370.
- [21] M. Nei, 1978. Estimation of average heterozygosity and genetic distance from a small number of individuals. *Genetics*. 89 (4) 583 - 590.



- [22] Y. Willi, J. Van Buskirk and A.A. Hoffmann, 2006. Limits to the adaptive potential of small populations. *Annual Review of Ecology, Evolution, and Systematics*. 37 (1) 433 - 458.
- [23] Li YY, Guan SM, Yang SZ, Luo Y, Chen XY. 2012. Genetic decline and inbreeding depression in an extremely rare tree. *Conservation Genetics* 13 (2) 343 - 347.
- [24] G. Mameli, R. Filigheddu, G. Binelli and M. Meloni, 2008. The Genetic Structure of the Remnant Populations of *Centaurea horrida* in Sardinia and Associated Islands. *Annals of Botany* 101 (5) 633–640.
- [25] E. Çağlar, 2010. *The Determination Of Genetic Diversity Of Centaurea nivea By Using Microsatellit Based Markers*. Master of Science Thesis, Anadolu University, Turkey.
- [26] M. Rossetto, P.K. Weaver and K.W. Dixon, 1995. Use of RAPD analysis in devising conservation strategies for the rare and endangered *Grevillea scapigera* (Proteaceae). *Molecular Ecology*. 4 (3) 357 - 364.
- [27] X.Q. Ci, J.Q. Chen, Q.M. Li and J. Li, 2008. AFLP and ISSR analysis reveals high genetic variation and inter-population differentiation in fragmented populations of the endangered *Litsea szemaonis* (Lauraceae) from Southwest China. *Plant Systematics and Evolution*. 273 (3-4) 237 - 246.
- [28] S.P. Gordon, C.M. Sloop, H.G. Davis and J.H. Cushman, 2012. Population genetic diversity and structure of two rare vernal pool grasses in central California. *Conservation Genetics*. 13 (1) 117 - 130.
- [29] X.F. Zhao, Y.P. Ma, W.B. Sun, X. Wen and R. Milne, 2012. High genetic diversity and low differentiation of *Michelia coriacea* (Magnoliaceae), a critically endangered endemic in southeast Yunnan, China. *International Journal of Molecular Sciences*. 13 (4) 4396 - 4411.
- [30] F.Q. Wu, S.K. Shen, X.J. Zhang, Y.H. Wang and W.B. Sun, 2015. Genetic diversity and population structure of an extremely endangered species: the world's largest *Rhododendron*. *AoB Plants* 7: plu082; doi:10.1093/aobpla/plu082.
- [31] E.E. Dakin and J.C. Avise, 2004. Microsatellite null alleles in parentage analysis. *Heredity*. 93 (5) 504 - 509.
- [32] M.-P. Chapuis, A. Estoup, 2007. Microsatellite Null Alleles and Estimation of Population Differentiation. *Molecular Biology and Evolution*. 24(3) 621 - 631.
- [33] M.W. Bruford, C. Ciofi and S.M. Funk, 1998. Characteristics of microsatellites. In *Molecular Tools for Screening Biodiversity: Plants and Animals*; Karp, A., Isaac, P.G., Ingram, D.S., Eds.; Chapman & Hall: London, UK, 202 - 205.
- [34] Q.F. Geng, J. Liu, L. Sun, H. Liu, Y. Ou-Yang, Y. Cai, X.S. Tang, H.W. Zhang, Z.S. Wang, and S.Q. An, 2015. Development and characterization of polymorphic microsatellite markers (SSRs) for an endemic plant, *Pseudolarix amabilis* (Nelson) Rehd. (Pinaceae). *Molecules*. 20 (2) 2685 - 2692.



INVESTIGATION OF PHYSICAL AND CHEMICAL PROPERTIES OF DRINKING WATER OF IGDİR UNIVERSITY SEHİT BÜLENT YURTSEVEN CAMPUS

Bingul Z.*¹, Ozturk E.², Yigit A.³ and Turhan Irak Z.⁴, Altikat A⁵.

^{1,4} Environmental Engineering Department, Engineering Faculty, Iğdir University,
TURKIYE.

(E-mail: zuleyha.bingul@igdir.edu.tr, zeynepsilanturhan@hotmail.com)

^{2,3} Research Laboratory Application and Research Center, Iğdir University, TURKIYE.

(E-mail: kimyagerhan@hotmail.com, kimyagerabo@hotmail.com)

⁵ Civil Engineering Department, Engineering Faculty, Iğdir University, TURKIYE.

(E-mail: aysun.altikat@igdir.edu.tr)

Corresponding Author's e-mail: zuleyha.bingul@igdir.edu.tr

ABSTRACT

The waters that are collected at soil depths depend on the geological conditions and flow continuously from an outlet point spontaneously are defined as spring water. These waters are generally used for drinking, using and irrigation water purposes. Population growth, rapid urbanization, mixing of domestic-industrial and agricultural wastes with water without any treatment are causing pollution of water resources. The fact that these waters used for drinking purposes are subject to physical, chemical and biological pollution for various reasons affect the health of people as much as the quality of drinking water. For this reason, as in many other countries, the physical, chemical and microbiological qualities of spring waters in our country have been determined by statutes and standards.

In Iğdir University Bülent Yurtseven Campus, the water taken from the three well goes to the main distribution depot with the pump. In campus area, there are totally 5948 people with a



total of 5002 students studying in different units, 738 academic, administrative and auxiliary staff, and a total of 208 relatives of employees settling in 12 lodging buildings. In this study; in order to determine the characteristics of the wells used as drinking water in the university campus, it is aimed to examine in terms of physical and chemical quality parameters of water and to be evaluated within the scope of Regulation on Waters for Human Consumption (RWHC) of the obtained results. In order to observe the seasonal changes in the parameters, water analysis measurements will be routinely made by the Research Laboratory Application and Research Center of Iğdir University. According to the physical analysis of the water samples taken from the main depot in the university campus, color is characteristic of drinking water, turbidity, electrical conductivity and pH parameters are below the limit values of the regulation. As a result of the chemical analyzes of the water samples, phosphate, fluoride, sulfate, nitrate, nitrite, nickel, lead and cadmium values were determined to be below the limits of the related regulation.

Keywords: Drinking water, Iğdir University, quality parameters, water supply, water quality.

1. INTRODUCTION

Water, which is at the forefront of the basic needs of man and all other living things, is an indispensable source of life's existence and continuation. On natural conditions, water contain different substances according to where they live and they are characterized according to these substances. The physical, chemical and biological characteristics of the water determine their qualities in terms of drinking and use [1, 16, 22]. Drinking and using water should be odorless, colorless, clear and refreshing, do not include disease-causing microorganisms, there should be no harmful chemical substances in health, must be suitable for their intended use and should not be aggressive [12].

Water resources can be examined in two classes, groundwater and surface waters. The quality of groundwater does not show large changes over time. Groundwater's color grades and turbidity are low. Surface water are waters taken from rivers, lakes and dams, which are usually contaminated with the reason of urbanization and industrialization resulting from excessive population growth and need to be improved through treatment.

Water is a very suitable environment for some disease-causing organisms. The water used for drinking is exposed to physical, chemical and biological pollution for various reasons; it affects people health as much as the quality of drinking water. In the developing world, it is estimated that approximately 80% of all diseases are caused by inadequate water and sanitary conditions. Every year more than 5 million people, more than half of whom are children, lose their lives due to water pollution. For this reason, when providing the water needs of the community, the amount of water at the source to be selected should be sufficient and the water quality should be acceptable [15].

The treatment process to be applied for adapting the water taken from a source to the usage purposes depends on the properties of the water source. The waters of some sources are very well characterized and can be supplied to the drinking water network with simple disinfection. Some sources of water require many treatment processes such as accumulation, coagulation, flocculation, filtration, and disinfection, as they are poorly watered, for example, when water is taken from contaminated rivers. Therefore, various parameters in the water source should be measured at specific time intervals and compared with the accepted drinking water standards and it should be determined which parameters should be improved [12].

The physical, chemical and microbiological qualities of spring water have been determined by statutes and standards in our country as well as in many countries in order to protect human health by determining water cleaning and potability requirements. Parallel to the European Union Drinking Water Directive published in 1998, the "Regulation on Waters for Human Consumption" (RWHC) was published in the Official Gazette dated 17.02.2005 and numbered 25730 in our country. According to this regulation; drinking and using water; are defined as waters used for the preparation, processing, storage and marketing of foodstuffs and other human consumption products, in general, for drinking, cooking, cleaning and other domestic purposes, irrespective of origin, originally provided, or purified, whether supplied from source or distribution network, and which provide physical, chemical and microbiological parameter values in accordance with the regulation and which are not provided for commercial sale. With this regulation, it is aimed to ensure the quality standards of waters by conforming to the technical and hygienic conditions of the waters used for human consumption purposes.

In this study, it was aimed to observe in the physical and chemical quality parameters of the well water used as drinking water in Iğdır University Şehit Bülent Yurtseven Campus, to determine physical and to evaluate the obtained results by taking into consideration the related regulations.

2. MATERIAL AND METHOD

2.1. Material

Drinking water of Iğdır University Şehit Bülent Yurtseven Campus was used as material in this study. In campus area, there are totally 5948 people with a total of 5002 students studying in different units, 738 academic, administrative and auxiliary staff, and a total of 208 relatives of employees settling in 12 lodging buildings.

The average water consumption of the people living in the campus is 40 tons/h. The drinking water of Iğdır University Şehit Bülent Yurtseven Campus is provided from the wells. A total of 25.4 liters of water is drawn from three wells and delivered to the main distribution depot with pumps. The first well is located at 1744 meters from the main distribution site, the second well is at 2000 meters and the third well is at 1370 meters. The volume of the main

distribution deposit is 500 m³ and the disinfection process is also done here. Disinfected water is given to the residences with charming transmission without waiting.

2.2. Method

In this study, samples of drinking water were taken from the main distribution store. Analyzes of pH and electrical conductivity were made in the field and immediately with a multi-parameter. Nitrite, nitrate, fluoride and phosphate analyzes were measured by ion chromatography (DIONEX ICS-5000⁺EG). Analyzes of cadmium, iron, boron, manganese, arsenic, aluminum, chromium, copper, lead and nickel were carried out in the samples in ICP-MS (Agilent 7700).

3. RESULTS AND DISCUSSION

According to Article 6 of the Regulation on Waters for Human Consumption [19], it is obligatory that the waters are healthy and clean. If water does not contain substances, micro-organisms and parasites in quantities and concentrations that constitute a potential hazard to human health, conforms to the parameter values determined for quality standards, monitoring, disinfection and analysis features are appropriate, the quality of the treatment, equipment and materials is assured, it is considered to be healthful and clean.

The results of the analysis of well water used as drinking and using water in Iğdir University Şehit Bülent Yurtseven Campus and the standard values required for drinking water according to the Regulation on Waters for Human Consumption [19] and Turkish Standards Institute (TS266) are given in Table 1. The appropriateness of well water for drinking water has been evaluated within the scope of these regulation.

pH indicates the concentration of active H⁺ ion in the water. The amount of carbonate, bicarbonate and carbon dioxide dissolved in the water at the pH of the water is also affected. Chemical reactions in the water and for biological life are important factors. The increase or decrease of pH in water affects the toxicity of certain compounds [18, 20]. According to the RWHC and TS 266, drinking water should be between pH 6.5-9.5. The pH value of the drinking water analysis results is 7.3 and it is within the pH range stated in the regulation.

Table 1. Drinking water analysis results and standard values

Parameter	Unit	RWHC	TS 266	Analysis Result
pH		6.5-9.5	6.5-9.5	7.3
Electrical conductivity	µs/cm	2500	2500	273
Nitrate	mg/L	50	50	20.63

Nitrite	mg/L	0.5	0.5	<0.09
Fluoride	mg/L	1.5	1.5	0.37
Phosphate	mg/L	-	-	25.58
Iron	µg/L	200	200	67.914
Manganese	µg/L	50	50	1.338
Arsenic	µg/L	10	10	5.71
Boron	mg/L	1	1	<0.5
Cadmium	µg/L	5	5	<1.5
Aluminum	µg/L	200	200	<5
Chromium	µg/L	50	50	<5
Copper	mg/L	2	2	0.005
Lead	µg/L	10	10	<3
Nickel	µg/L	20	20	<3

Electrical conductivity is an indicator of total dissolved solids in water and is expressed in microsiemens/cm ($\mu\text{S}/\text{cm}$). Conductivity level is $2500 \mu\text{S} / \text{cm}$ at 20°C in regulation [11]. Drinking water electrical conductivity value is $273 \mu\text{S} / \text{cm}$ and below the limit value.

Nitrate and nitrite are indications of bacterial contamination in the aquatic environment. In recent years, due to population growth and industrialization, the likelihood and quantity of these substances in the water has increased. Ammonium concentrations in drinking water probably indicate a fresh fecal contamination, a sign of health hazard, and the presence of nitrate indicates an outdated contamination and possibly a less harmful condition. Nitrate is harmless to adults and can always be found in the waters. However, continuous drinking of water containing more than 20 mg of nitrate in litter causes acute and chronic poisoning in humans and methemoglobinemia in babies younger than 6 months [2]. The nitrate and nitrite values of the samples analyzed in this work are below the limits of the relevant regulation.

When fluoride is taken at the appropriate amount, it prevents tooth decay, it helps bone development. For this reason, fluoride is recommended for children's drinking water. However, prolonged exposure to fluoride in large quantities leads to fluorosis and severe skeletal problems. The amount of fluoride in the water is very important when considering

both benefits and losses. According to Regulation on Waters for Human Consumption and Turkish Standards Institute (TS 266), the maximum fluoride concentration to be found in drinking water is 1.5 mg/L [4]. Fluoride concentration in drinking water analysis of Iğdir University Şehit Bülent Yurtseven Campus was measured as 0.37 mg/L and below the limit value.

Phosphates in water resources can be found either as a result of contact with minerals originating from natural sources or as a result of human activities such as fertilizer use, sewerage and industrial discharges. Phosphorus is an inorganic element of bones and teeth and therefore is a necessary element for the human body. The daily phosphorus requirement is the same as the calcium requirement, and the highest amount that can be taken is 800 mg / L. WHO and USEPA have not established a limit value for human health due to the low quantities of phosphorus in water resources [9]. The phosphate value of the drinking water analysis results is 25.58 mg/L.

In drinking water sources, the iron (II) salts are in an unstable structure, passing into the form of dissolving iron (III) hydroxide and rusting in the form of rust silt. Iron can also cause undesirable bacterial growth in the water network (iron bacteria) and formation of deposits in the form of a slurry coating in the pipes [9]. The iron limit value in regulation is 200 µg/L and the drinking water analysis value is 67.914 µg/L.

Manganese is one of the most common metals in the earth's structure, often associated with iron. But the concentrations in the water are lower than iron. Although it is possible to determine a limit value at 0,4 mg/L concentration for health [21], there is no need to set a limit value for health since manganese in drinking water sources are generally well below these concentrations and the acceptability of the water by the consumer (taste, stain, accumulation in pipelines, etc.) is below this concentration. However, as a result of manganese uptake at high concentrations, adverse physiological effects, especially neurological effects can be observed [13]. The manganese value of the samples analyzed in this work are below the limits of the relevant regulation.

Arsenic is a naturally occurring element with wide distribution on earth. Arsenic is a toxic substance and the degree of toxicity depends on the chemical and physical shape of the arsenic compounds, the presence of the elements that affect the reaction in the food, the amount of ingested, age and sex. Due to the carcinogenic effect of arsenic compounds, the maximum arsenic concentration that can be tolerated in drinking waters is legally regulated. Considering the effects of arsenic on human health, World Health Organization (WHO) made regulations on the amount of arsenic in the water in 1993 and reduced the arsenic limit to 10 µg/L [3]. The arsenic limit value in Regulation on Waters for Human Consumption is 10 µg/L and the drinking water analysis value is 5.71 µg/L.

Boron can be seen primarily in underground waters by natural means such as rocks containing borate and borosilicate and draining from soil [8]. The borate concentration in surface water is mainly due to wastewater discharges and this is caused by household cleaning products, which also decreases the incidence in water resources due to reduced use [21]. Drinking water containing boron mineral in high proportion can cause some discomforts in the digestive system. It also causes growth and swelling in the liver [10]. In our study, boron was found below 0.5 mg/L.

Cadmium is usually found below 1 µg/L in uncontaminated natural water resources [21]. Underground waters have higher concentrations than superficial waters. Very high levels of cadmium, taken with drinking water, irritate the nose, vomiting and diarrhea can sometimes lead to death [7]. The cadmium value is below the limits of the relevant regulation.

Since the solubility of aluminum at the neutral pH level is low, the concentration of dissolved aluminum in water resources is often low and usually ranges from 0.001-0.05 mg/L. Aluminum concentration is rapidly increasing below pH 4.5 and above pH 7.5. In the acidic water, values ranging from 0.5-1 mg/L is seen. In acid mine drainage, more extreme values such as 90 mg/L concentrations can be seen. Aluminum on certain concentrations in drinking water can cause color and odor formation. When the dissolved aluminum concentration in water exceeds 0,2 mg/L, depending on the pH, the aluminum hydroxide in the network collapses in white gelatinous form, causing the water to become milky [17]. The drinking water analysis value is below 5 µg/L.

It is found as chromium(III) and chromium(VI) in the nature. Chromium(III) is the most commonly seen form, and this insoluble state found in many soils and rocks is converted into chromium(III) salts which are soluble in air, oxidation and bacterial activity. Chromium (III) salts, an essential element for humans, are used in catalysts, paint pigments, fungicides, ceramics and glassware as well as in leather tanning. Chromium(VI) is found less frequently in nature and its presence in the water is due to industrial and domestic wastewater discharge. Contrary to chromium(III), an element is not necessary for human beings, but the harmful effects of health are attributed to this form of chromium [18]. The drinking water analysis value is below 5 µg/L.

Copper is found in natural water resources, usually in low concentrations, if there is no contact with metal containing areas. It can be seen as rock erosion or industrial origin in water resources. In treated drinking water, it can be welded copper and brass from pipes. At concentrations above 1 mg/L may cause staining in laundry and sanitary ware; At concentrations exceeding 2.5 mg/L, it gives an unpleasant bitter taste to water [21]. At higher concentrations (4-5 mg/L), the water color can also change [14]. The copper limit value in regulation is 2 mg/L and the drinking water analysis value is 0.005 mg/L.

Lead is found at concentrations of 0.01 mg/L on the surface and underground waters. Although local pollution effect is observed due to industrial or mining origin, usually high

concentrations are due to installation. In the drinking waters generally have values below 5 µg/L. The effects of lead for humans are the same whether inhaled or taken by mouth, and lead poisoning for children and adults primarily affects the nervous system. As a result of exposure to the lead, effects such as weakness in the fingers and ankles, increase in blood pressure and anemia can be seen. High levels of exposure may cause serious damage to the brain and kidneys and even death [6]. Lead concentration in drinking water analysis of Iğdir University Şehit Bülent Yurtseven Campus was measured as <3 mg/L.

Nickel concentrations in rivers and lakes are fairly low and generally less than 10 µg/L [5]. The dissolution of nickel bearing rocks can also be found in some of the underground waters. However, it is primarily present as plumbing and pipe welds in the drinking water. The nickel value is below 3 µg/L.

As a result, the analysis results of well water used as drinking water in the university campus are below the limit values stated in the regulation and it is considered to be safe drinking water in terms of physical and chemical properties.

REFERENCES

- [1] Ağaoğlu, S., Ekici, K., Alemdar, S., Dede, S., 1999. A study on the Microbiological, Chemical and Physical Quality of Spring Waters in Van Region , Van Medical Journal: 6 (2): 00-00, 30-33.
- [2] Ağaoğlu, S., Alişarlı M., Alemdar, S., Dede, S., 2007. The Determination of Nitrate and Nitrite Contents of Drinking Water in the Region of Van, Van Veterinary Journal, 18(2):17-24.
- [3] Alpaslan, M.N., Dölgen D., Boyacıoğlu, H., Sarptaş H., 2010. Arsenic removal from drinking water by chemical methods, ITU Journal-Water Pollution Control Cilt:20, Sayı:1, 15-25.
- [4] Altinkale, Demer, S ve Memiş, Ü., 2011. Investigation of different fluoride contents of drinking waters in Isparta City Center, Ekology, 20 (79):77-82.
- [5] ATSDR-Agency for Toxic Substances and Disease Registry, 2005. Public Health Statement-Nickel, Atlanta: U.S. Department of Health and Human Services.
- [6] ATSDR-Agency for Toxic Substances and Disease Registry, 2007. Public Health Statement-Barium, Atlanta: U.S. Department of Health and Human Services.
- [7] ATSDR-Agency for Toxic Substances and Disease Registry, 2012. Public Health Statement-Cadmium, Atlanta: U.S. Department of Health and Human Services.
- [8] Çöl, M., Çöl, C., 2003. "Environmental Boron Contamination in Waters of Hisarcik Area in the Kutahya Province of Turkey", Food and Chemical Toxicology, Cilt 41.
- [9] De Zuane, J., 1990. "Handbook of Drinking Water Quality", (2nd edition), ABD: John Wiley & Sons Inc.



- [10] Demirtaş, A., 2010. Significance of Boron For Human Nutrition and Health, Journal of Agricultural Faculty of Atatürk University, 41 (1), 75-80.
- [11] Dönderici, Z.S., Dönderici, A. ve Başarı, F., 2010. An Investigation on the Physical and Chemical Quality of Spring Waters, Turkish Bulletin of Hygiene and Experimental Biology, 67(4): 167-172.
- [12] Eroğlu, V., 1995. Purification of Water, Istanbul Technical University, Faculty of Civil Engineering, İstanbul.
- [13] Gray, N.F., 2005. "Water Technology-An Introduction for Environmental Scientists and Engineers", 2nd edition., Elsevier Science & Technology Books.
- [14] Gray, N.F., 2008. "Drinking Water Quality-Problems and Solutions", 2nd edition, New York: Cambridge University Press.
- [15] Karpuzcu, M., 1991. Environmental Pollution and Control, Boğaziçi University, Institute of Environmental Sciences, İstanbul.
- [16] Karpuzcu, M., 2005. Water Supply and Environmental Health, Gebze Institute of Technology, İstanbul.
- [17] Oğuz, T.C., 2015. Common Water Quality Problems in Drinking Water Treatment and Solution Suggestions for its Treatment, Expertise Thesis, Ministry of Forestry and Water Affairs.
- [18] Patır, B., Güven, A.M. ve Arslan, A., 1992. Investigations on Hygienic Qualities of Drinking and Using, Welding, Well and Lake Waters in Elazığ Region, Fırat University Medical Journal of Health, 6, 1-2: 127-134.
- [19] RWHC, 2005. Regulation on Waters for Human Consumption, Official Newspaper, 25730, 17.02.2005.
- [20] Tuluk, B., Kayserili Orhan, F. ve Kaşali, K., 2017. An investigation on physical, chemical and microbiological quality of drinking water in Erzurum city, J Turgut Ozal Med. Cent. 24(1): 25-30.
- [21] World Health Organization-WHO. (2011). "Guidelines for Drinking Water Quality". 4th edn. Geneva: World Health Organization.
- [22] Yardımcı, N., (1994), "Su Getirme", Atatürk Üniversitesi, Mühendislik Fakültesi, İnşaat Mühendisliği Bölümü, Erzurum.



IMPROVING WATER LEACHING RESISTANCE OF FIRE RETARDANTS IN WOOD

Suat ALTUN

Department of Industrial Design Engineering, Technology Faculty, Karabuk University,
TURKEY.

Corresponding Author's e-mail: saltun@karabuk.edu.tr

ABSTRACT

Wood is a combustible material and needs to be protected against fire. Most of fire retardants are not resistant to leaching. The aim of this study was to increase the resistance of these chemicals to leaching in order to improve the fire resistance of wood. For these purpose Scots pine (*Pinus sylvestris* L.) and Chestnut (*Castanea sativa* Mill) wood impregnated with 3 % aqueous solutions of boric acid, zinc chloride and aluminum chloride at 60 °C by using vacuum- press impregnation method according to instruction of the ASTM D1413-07 standard. Leaching resistance of the samples post esterified with propionic anhydride (propionylation treatment) were determined. Thermogravimetric analysis was applied according to the ASTM E1131-03 standard in order to determine the thermal properties of these samples. For propionylation treatment, amount of leachant was decreased in parallel with weight percent gain after propionylation. The highest leaching resistance was determined in chesnut and aluminum chloride. According to thermogravimetric analysis propionylation treatment affected the fire resistance property of wood negatively although decreased the leaching of impregnation chemicals.

Keywords: Chestnut; Impregnation; Propionylation; Scots pine.

2. INTRODUCTION

Wood has many inherently good properties, such as renewability, wide availability, low cost, thermal and sound insulation, and a high strength to weight ratio which make it a preferred building material. Wood also possesses some properties that can be regarded as disadvantages. One of the significant problems is its combustibility. The fire resistance of wood can be improved by treating wood with fire retardants. Most of the fire retardants used

are effective in reducing different reaction to fire parameters of wood such as ignitability, heat release and flame spread. Unfortunately, most of the fire retardants are not durable in exterior applications. The durability of fire retardant treatments, when exposed to humid conditions, is closely linked to the water solubility of the chemicals used [1].

Borates have been used widely as wood preservatives and have several advantages in addition to imparting flame retardancy, providing sufficient protection against wood destroying organisms, having a low mammalian toxicity, and low volatility. However, boron compounds are susceptible to leaching under certain conditions, as they are not chemically fixed within the wood [2].

Aluminium chloride and zinc chloride are inorganic metal compounds, which have fire-retarding effects [3]. But, it was indicated that metal ions leach easily from the treated wood and metal ions containing preservatives could not protect wood at exterior conditions as long as expected [4]. Because of their negative effects on strength and hygroscopicity, waterborne preservative use declined during the first half of the 20th century. However, with increased environmental awareness of potential mammalian effects associated with the use of oil-type preservatives rekindled an interest in waterborne preservatives, especially the leach-resistant waterborne preservatives [5].

Limitation of water-impregnating chemicals contact in the cell wall through low water absorption is expected to limit chemical leaching [6]. Chemicals have the ability to increase the water repellency and react with cell wall components, such compounds can be used for limiting impregnation release from treated wood [7]. Many polymers, resins and water repellents have been tested for their ability to reduce impregnation chemical leachability, increase dimensional stability, and provide high biological and fire resistance [8].

Esterification of wood cell wall by using anhydrides is one of the ways to make wood more hydrophobic. Acetylation has been the most studied method for this purpose [9-13]. Acetylation method gives a by-product that introduces an acidic condition to the wood resulting in strength loss and acidic corrosion of the metal fasteners used in the acetylated wood. Because of weaker acidity of propionic acid than that of acetic acid, propionic anhydrides can be expected to be less harmful to wood when used as modifiers [14].

The main purpose of this study was to increase the resistance of waterborne fire retardant chemicals to leaching to improve the fire resistance of wood. To achieve this purpose, Scots pine (*Pinus sylvestris* L.) and Chestnut (*Castanea sativa* Mill) woods impregnated with 3 % aqueous solutions of boric acid, zinc chloride and aluminum chloride were post-treated with propionic anhydride. The effects of propionylation on the leaching resistance and thermal behaviour of impregnated woods were investigated.

2. MATERIAL AND METHODS

Materials

Scots pine (*Pinus silvestris* L.) and Chestnut (*Castanea sativa* Mill.) were used in this experiment. Nondeficient, proper, knotless, and normally grown wood materials were selected. As fire retardant impregnating chemicals, zinc chloride ($ZnCl_2$) [15], boric acid (H_3BO_3) [16], and aluminum chloride ($AlCl_3 \cdot 6H_2O$) [17]; propionic anhydride ($C_6H_{10}O_3$) [18] for chemical modification were used. All the chemicals were purchased from Yildiz Chemical Co. in Turkey.

Preparation of samples and treatment process

Samples were cut into dimensions of $20 \times 20 \times 20$ mm (R \times T \times L) for the treatments and test. All the samples acclimatized at a temperature of 20 ± 3 °C and a relative humidity (RH) of 65% before further treatments. Air-dry samples were treated by vacuum-pressure method according to ASTM D 1413-07 [19] standard. 3 % aqueous solutions having temperature of 60 °C were used. The samples were weighed before impregnation and placed in a vacuum chamber. Impregnation was conducted at 3 bar pressure for 5 min after pre-vacuum period (620 mm-Hg, 30 min). After the internal pressure was decreased to atmospheric pressure, impregnation solution was unloaded. The retention for each impregnation chemicals was calculated as following:

$$R = (G \times C/V) \times 10 \text{ (kg.m}^{-3}\text{)} \quad (1)$$

where $G = T_2 - T_1$, T_1 is the sample weight before impregnation (g), T_2 is the sample weight after impregnation (g), V is the volume of sample (cm^3), and C is the concentration of solution (%).

Propionylation treatment was conducted as post-treatment to prevent leaching of fire retardants. According to the results of pre-experiments, the process of the propionylation used was described in Figure 1. The weight percent gain (WPG) of the samples was calculated according to the following equation:

$$WPG = \frac{m_i - m_o}{m_o} \times 100 \quad (2)$$

where m_o is the oven-dry weight of the samples before the propionylation in grams and m_i is the oven-dry weight of the samples after the propionylation in grams.

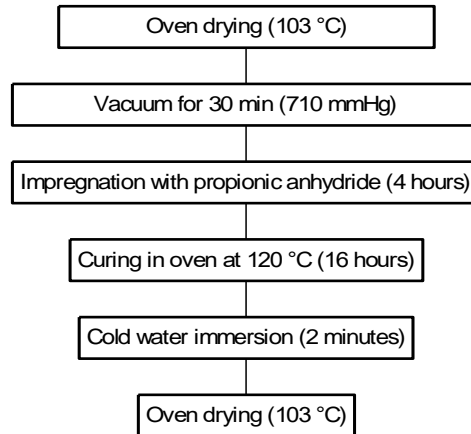


Figure 1. Process of propionylation of pre-impregnated wood samples

The leaching procedure was conducted in water as described by Baysal and Yalınkılıç [20]. Ten specimens were immersed in a beaker containing 800 ml distilled water and stirred with a magnetic stirrer (400–500 rpm) at room temperature for 8 h, followed by drying at 60 °C for 16 h. This cycle was repeated 10 times. After each leaching period the water was exchanged with fresh water. The amount of leachant L was calculated from the difference of the oven-dried weight after treatment and oven-dried weight after leaching as following:

$$L = [(W_{oi} - W_{of}) / W_{oi}] \times 100 (\%) \quad (3)$$

where W_{oi} is the oven-dried weight of treated wood after propionylation treatment and W_{of} is the oven-dried weight of treated wood after leaching.

A thermogravimetric analysis (TGA) instruments Labsys TGA simultaneous TG-DTA apparatus was employed for the thermogravimetric tests. The test was carried out according to ASTM E1131-03 [21]. High purity argon was used for the tests at a flow rate of 150 mL.min⁻¹. The argon was purged for 20 min, before starting the heating program, to establish an inert environment. The sample mass was 15 mg. The experiments started with a drying session (up to 30 °C). The subsequent thermal decomposition was carried out from 30 °C up to 500 °C at a heating rate of 10 °C.min⁻¹. Temperature of rapid pyrolysis and total weight loss (%) at 500 °C were determined.

3. RESULTS AND DISCUSSION

Some properties of the impregnated samples, impregnation solutions and the amounts of retention are given in Table 1. The amounts of retention in Scots pine were higher than that in chestnut in the case of all three chemicals. Because of higher porosity and permeability of Scots pine than that of chestnut, these samples absorbed more impregnation solution. As reported by Yalınkılıç [22] that aluminum chloride is a good fire retardant but impregnation with it is difficult, retention of aluminum chloride solution was a little bit lower than that of others. The highest retention (16.1 kg/m³) was determined in Scots pine impregnated with

boric acid. This amount was much higher than the boric acid retention reported by Özçifçi [23] (1.96 kg/m³) and by Keskin [24] (3.38 kg/m³).

Table 1. Determined properties of impregnated samples

Wood species	Impregnation chemical	C (%)	pH	Post treatment	D _{RM} (g/cm ³)	P (%)	R (kg/m ³)	WPG (%)	L (%)
Scots pine	Boric acid	3	5.2	-	0.521	65.2	16.1	-	4.1
				Pr	0.504	66.4	15.7	1.51	5.6
	Zinc chloride	3	5.5	-	0.525	65.0	15.3	-	6.6
				Pr	0.508	66.2	15.8	8.76	5.6
	Aluminium chloride	3	2.6	-	0.511	65.9	11.3	-	6.7
				Pr	0.541	63.9	11.5	17.67	1.5
Chestnut	Boric acid	3	5.2	-	0.685	54.3	9.9	-	2.2
				Pr	0.703	53.2	10.3	4.70	2.1
	Zinc chloride	3	5.5	-	0.693	53.8	9.6	-	4.0
				Pr	0.696	53.6	9.9	19.87	0.9
	Aluminium chloride	3	2.6	-	0.687	54.2	7.2	-	4.5
				Pr	0.712	52.5	7.1	15.99	0.8

D_{RM}:Air-dry densities; P:Porosity; R:Amount of retention; WPG:Weight percent gain; L: Amount of leachant; Pr:Propionylation

Propionylation treatment was conducted to prevent leaching of the impregnation chemicals. The highest WPG value (19.87%) was determined in chestnut samples pre-impregnated with zinc chloride. Also, high WPG values were determined in the samples pre-impregnated with aluminum chloride (15.99 % - 17.67 %). WPG of the samples pre-impregnated with boric acid after propionylation were lower than the others. Although Le Van [25] had achieved only 4% WPG in propionylation of pendorasa pine, Li et al. [26] reported similar WPG (17.2 %) with this study in propionylation of poplar.

WPG of the chestnut was higher than that of Scots pine. According to Minato and Ogura [27], degrees of esterification reaction depends on the number of accessible OH groups. Also, Tserki et al. [28] indicated that hemicelluloses are more susceptible to esterification than

cellulose. While the pentosane content of pine is 11 %, it is 19.7% in chestnut. Besides, because of the amount of cellulose is quite similar in both pine and chestnut (approximately 42%) [29], chestnut which has the higher density has more accessible OH groups than that of Scots pine. Therefore, it can be said that propionylation of chestnut gave higher WPG.

WPG values in samples pre-impregnated with zinc chloride and aluminum chloride were quite high compared to samples impregnated with boric acid. Hafizoğlu [29] indicated that chemicals such as strong acids, bases and some salts which are break the hydrogen bonds between the cellulose microfibrils in the crystalline zone could be used to increase the number of accessible OH groups before the chemical modification of wood. So, high acidity of aluminum chloride (ph 2.6) could lead the breakage of hydrogen bonds and increase the number of accessible OH groups. Thus, it increased the degrees of propionylation reaction in both scots pine and chestnut. Low WPG values in samples impregnated with boric acid could be explained by the incompatibility of boric acid with anhydrides and potassium [16]. Boric acid may interrupt the propionylation reaction.

The test conducted to determine the effect of propionylation on leaching of impregnation chemical showed that leaching from Scots pine was higher than that of chestnut. Leaching from relatively permeable species is more than that of impermeable species due to higher water penetration into the wood [30]. Also, higher porosity and the impregnation retention of Scots pine must have contributed this results. Propionylation decreased significantly leaching from samples impregnated aluminum chloride. The amount of leachant was determined as 1.46% and 0.84% in Scots pine and chestnut, respectively. Leaching from propionylated chestnut pre-impregnated with zinc chloride was also very low (0.9%) although there was not any difference in the case of Scots pine. Propionylation did not affect the leaching from samples impregnated with boric acid. These results were in parallel with the results of WPG values. The higher WPG in propionylation led the lower leaching. Limitation of water-impregnating chemicals contact in the cell wall through low water absorption is expected to limit chemical leaching [6]. The higher degrees of propionylation reaction made the wood more hydrophobic thus prevented water from penetrating into the wood. Therefore, propionylation decreased the leaching.

The pyrolytic behavior of wood is the overall behaviors of the three components, which makes it extremely complicated. However, the thermal degradation of wood is affected to a large extend by cellulose [31]. Effects of impregnation and the propionylation as the post-treatment on the thermal properties of wood was determined via thermogravimetric analysis (TGA). The total weight loss (WL) and the maximum pyrolysis temperature (Tmax) values of the samples were given in Table 2 and Figure 2.

All the three impregnation chemicals used had a reducing effect on the total weight loss. Also, they reduced the rapid pyrolysis temperatures. Consistent with the results obtained, Le Van et al. [32] reported that especially the flame retardants reduced the rapid pyrolysis temperature

and increased the amount of char formation. Studies have shown that the amount of combustible gas decreases when the amount of char formation increases [31, 32]. The lowest temperature of rapid pyrolysis and total weight loss (52.1 %) was determined in Scots pine impregnated with zinc chloride. Zinc chloride and boric acid had a similar effect on the total weight loss and temperature of rapid pyrolysis. It can be said that these results were better than the results reported by Rowell and LeVan-Green [33] and Wang et al. [34]. Impregnation with aluminum chloride did not affect the results as much as impregnation with the others.

Table 2. Results of thermogravimetric analysis

Wood species	Impregnation chemical	Post-treatment	WL (%)	Tmax (°C)
Scots pine	Unimpregnated (U)	-	67,3	359
		Pr	74,2	367
	Boric acid (BA)	-	53,5	332
		Pr	66,3	328
	Aluminum chloride (AC)	-	60,3	328
		Pr	68,4	342
	Zinc chloride (ZC)	-	52,1	271
		Pr	60,9	271
Chestnut	Unimpregnated (U)	-	66,9	351
		Pr	73,2	361
	Boric acid (BA)	-	57,4	312
		Pr	68,0	324
	Aluminum chloride (AC)	-	70,4	332
		Pr	69,4	340
	Zinc chloride (ZC)	-	61,5	311
		Pr	65,8	308

WL: Total weight loss; Tmax: Temperature of rapid pyrolysis; Pr: Propionylation

Although propionylation decreased the leaching of the impregnation chemicals, it increased the total weight loss and rapid pyrolysis temperature of all treatments in both Scots pine and Chestnut compared to control samples. Consistent with this result, Li et al. [26] indicated that acetylation and propionylation did not have a fire retarding effect. The weight increase achieved by the propionylation was the result of the attachment of the propionyl group which is a completely organic structure consisting of carbon, hydrogen and oxygen to the wood material in the substitution reaction. At high-temperature, CO₂ and CO were released by completely burning of the components in this organic structure. For this reason, the propionylation increased the total weight loss of the wood material.



4. CONCLUSION

Propionylation was carried out to increase the resistance of the fire-retardant chemicals to leaching to improve the fire resistance of wood. It reduced the amount of leachant in both Scots pine and chestnut except the samples impregnated with boric acid. The amount of leachant in Scots pine was higher than that of chestnut due to Scots pine's lower density and higher permeability. Substitution reaction of propionyl groups with the OH groups made the wood more hydrophobic and it prevented the chemicals in the cell wall and lumens from water leaching. Leaching decreases obtained was quite high especially in the samples pre-impregnated with aluminum chloride.

Although propionylation decreased the leaching in both samples impregnated with zinc chloride and aluminum chloride significantly, it did not contribute the fire-retardant effects of these chemicals. Further, it increased the total weight loss and the temperature of rapid pyrolysis of the impregnated samples. Therefore, it should not be used with the fire retardants. It may be used with other impregnation solutions which have acidic character to prevent from leaching them. It is also not recommended to use the propionic anhydride with the boron compounds because of incompatibility of these chemicals.

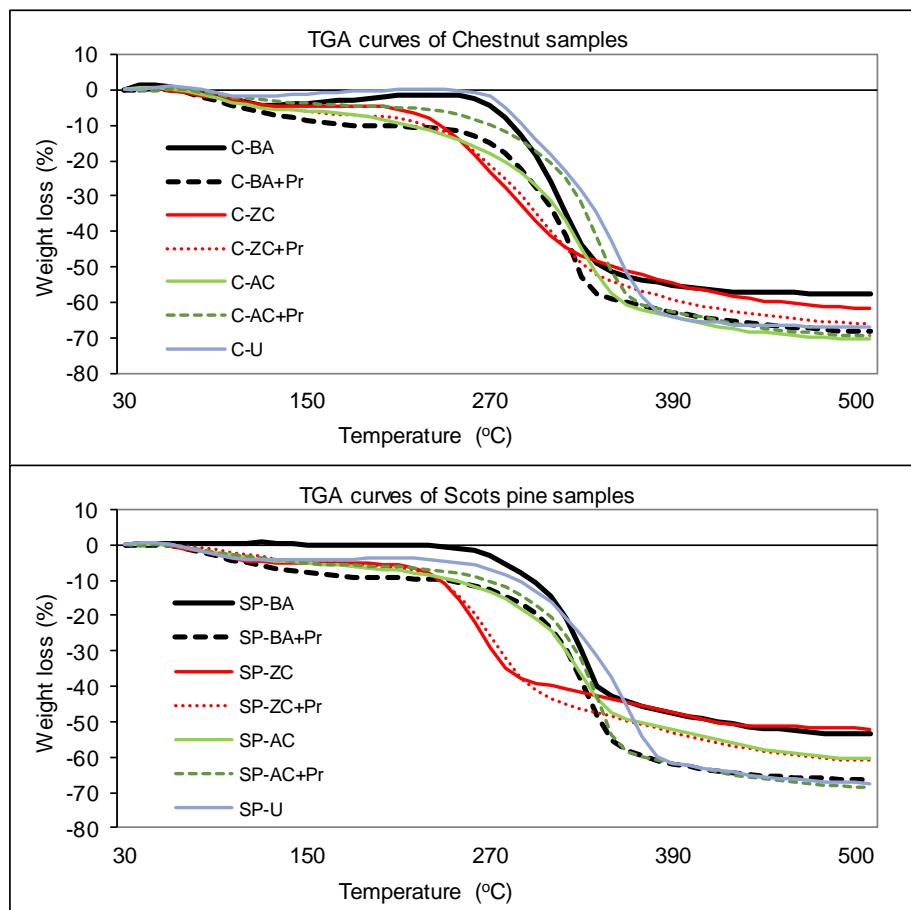


Figure 2. TGA curves of the samples impregnated and propionylated

ACKNOWLEDGMENT

This work was supported by Scientific Research Projects Coordination Unit of Karabük University. [Project Number: KBÜBAP-17-YD-351].

REFERENCES

- [1] B. Östman, A. Voss, A. Hughes, P.J. Hovde, O. Grexa. 2001. Durability of fire retardant treated wood products at humid and exterior conditions review of literature. *Fire Mater.* 25: 95-104.
- [2] E. Baysal, M.K. Yalınkılıç, M. Altınok, A. Sönmez, H. Peker, M. Çolak. 2007. Some physical, biological, mechanical, and fire properties of wood polymer composite (WPC)



- pretreated with boric acid and borax mixture. *Construction and Building Materials*. 21: 1879-1885.
- [3] S. Aslan, Ağaç Zararlıları Koruma ve Emprenye Teknikleri, Küçük ve Orta Ölçekli Sanayi Geliştirme ve Destekleme İdaresi Başkanlığı, Ankara, 272, 1998.
- [4] H. Yamaguchi. 2002. Low molecular weight silicic acid–inorganic compound complex as wood preservative. *Wood Sci. Technol.* 36: 399-417.
- [5] J.E. Winandy, Effects Of Waterborne Preservative Treatment On Mechanical Properties: A Review”, Ninety-First Annual Meeting of the American Wood-Preservers' Association Marriott Marquis Hotel New York, New York May 21-24, 1-18 (1995).
- [6] M. K Yalınkılıç, 2000. *Improvement of boron immobility in the borate-treated wood and composite materials*. Ph.D. Thesis, Kyoto University, Japan
- [7] S.N. Kartal, W. Hwang, A. Yamamoto, M. Tanaka, K. Matsumura, Y. Imamura, 2007. Wood modification with a commercial silicon emulsion: Effects on boron release and decay and termite resistance. *International Biodeterioration & Biodegradation*, 60:189–196.
- [8] E. Baysal, A. Sönmez, M. Çolak, H. Toker, 2006. Amount of leachant and water absorption levels of wood treated with borates and water repellents. *Bioresource Technology*. 97: 2271 - 2279.
- [9] C.A.S. Hill, D. Jones, 1999. Dimensional Changes in Corsican Pine Sapwood due to Chemical Modification with Linear Chain Anhydrides. *Holzforschung*. 53: 267–271.
- [10] E. Obataya, M. Sugiyama, T. Bunichiro, 2002. Dimensional stability of wood acetylated with acetic anhydride solution of glucose pentaacetate. *J Wood Sci*. 48:315-319.
- [11] N.S. Çetin, N. Özmen, P. Tingaut, G. Sebe, 2005. New transesterification reaction between acetylated wood and tetramethoxysilane: A feasibility study. *European Polymer Journal*. 41: 2704–2710.
- [12] A.N. Papadopoulos, C.A.S. Hill, A. Gkaraveli, 2004. Analysis of the swelling behaviour of chemically modified softwood: A novel approach. *Holz Roh Werkst*. 62: 107–112.
- [13] C. Sander, E.P.J. Beckers, H. Militz, W. Veenendaal, 2003. Analysis of acetylated wood by electron microscopy. *Wood Sci Technol*. 37: 39–46.
- [14] J.Z. Li, T. Furuno, S. Katoh, T. Uehara, 2000. Chemical modification of wood by anhydrides without solvents or catalysts. *J Wood Sci*. 46:215-221.
- [15] Merck Chemicals “*Chem./Phys.Info – Zinc chloride*” Merck KGaA 108816, Darmstadt Germany, 1-6, 2006.



- [16] Merck Chemicals “*Chem./Phys.Info – Boric acid*” Merck KGaA 100765, Darmstadt Germany, 1-5, 2007.
- [17] Merck Chemicals “*Chem./Phys.Info – Aluminum chloride hexahydrate*” Merck KGaA 101084, Darmstadt Germany, 1-6, 2003.
- [18] Merck Chemicals “*Chem./Phys.Info – Propionic anhydride*” Merck KGaA 800608, Darmstadt Germany, 1-6, 2003.
- [19] *ASTM Standard D1413-07e / Standard test methods for wood preservatives by laboratory soil-block cultures*, 2007. American Society for Testing and Materials, Philadelphia, PA.
- [20] E. Baysal, M.K. Yalınkılıç, 2005. A new boron impregnation technique of wood by vapor boron of boric acid to reduce leaching boron from wood. *Wood Science and Technology*. 39: 187–198.
- [21] *ASTM Standard E1131-03, Standard test methods for wood compositional analysis by termogravimetry*, 2003. American Society for Testing and Materials Philadelphia, PA.
- [22] M.K. Yalınkılıç, 1993. *Ağaç Malzemenin Yanma, Higroskopisite ve Boyutsal Stabilite Özelliklerinde Çeşitli Emprenye Maddelerinin Neden Olduğu Değişiklikler ve Bu Maddelerin Odundan Yıkanabilirlikleri*, Doçentlik Tezi, KTÜ Orman Fakültesi, Trabzon.
- [23] A. Özçifçi, 2001. *Emprenye edilmiş lamine ağaç malzemelerin teknolojik özellikleri*, Ph.D. Thesis, Graduate School of Natural and Applied Sciences, Gazi University, Ankara, Turkey.
- [24] H. Keskin, 2007. Effects of Impregnation Materials on Combustion Properties of Laminated Veneer Lumber Obtained from European Oak (*Quercus petraea* Liebl.) and Lombardy Poplar (*Populus nigra* L.). *Journal of Applied Polymer Science*. 105:1766–1773.
- [25] S.L. LeVan, Chemistry of Fire Retardancy, The Chemistry of Solid Wood, Advances in Chemistry Series 207, In Rowell, R.M., ed., American Chemical Society; Chapter 14, Washington, DC, 175-210, 531-574, 1984.
- [26] J.-Z. Li, T. Furuno, S. Katoh, 2001. Preparation and Properties of Acetylated and Propionylated Wood-Silicate Composites. *Holzforschung*. 55: 93–96.
- [27] K. Minato, K., Ogura, 2003. Dependence of reaction kinetics and physical and mechanical properties on the reaction systems of acetylation I: reaction kinetic aspects. *J Wood Sci*. 49:418-422.



- [28] V. Tserki, N.E. Zafeiropoulos, F. Simon, C. Panayiotou, 2005. A study of the effect of acetylation and propionylation surface treatment on natural fibers. *Composites: Part A*. 36:1110–1118.
- [29] H. Hafızođlu, Orman Ürünleri Kimyası Ders Notları, Cilt 1, Odun Kimyası, K.T.Ü. Orman Fak. Yayın No: 52, Trabzon, 4-11, 22-82, 1982.
- [30] A. Kılıç, 1998. *Ağaç türlerine göre suda çözünen emprenye maddelerinin yıkanma özellikleri*, MSc Thesis, Graduate School of Natural and Applied Sciences, Zonguldak Karaelmas University, Bartın, Turkey.
- [31] M. Gao, C.Y. Sun, C.X. Wang, 2006. Thermal degradation of wood treated with flame retardants. *Journal of Thermal Analysis and Calorimetry*. 85(3) 763-769.
- [32] S.L. LeVan, R.J. Ross, J.E. Winandy, 1990. *Effects of fire retardant chemicals on bending properties of wood at elevated temperatures*. Res.Pap. FPL-RP-498. Madison, WI: U.S.
- [33] R.M. Rowell, S.L. LeVan-Green, Thermal properties, Handbook of Wood Chemistry and Wood Composites, In Rowell, R.M., ed., Taylor&Francis, Florida, Chapter 6, 121-139, 2005.
- [34] Q. Wang, J. Li, J.E. Winandy, 2004. Chemical mechanism of fire retardance of boric acid on wood. *Wood Science and Technology*. 38: 375-389.



ENERGY AND EXERGY ANALYSIS OF AN ORGANIC RANKINE CYCLE USING DIFFERENT WORKING FLUIDS FROM WASTE HEAT RECOVERY

E. Ozdemir*¹ and M. Kilic²

¹ Uludag University, Yenisehir Ibrahim Orhan of Vocational School, Department of Machine, Bursa, TURKEY.

(E-mail: esraozdemir@uludag.edu.tr)

² Uludag University, Engineering Faculty, Department of Mechanical Engineering, Bursa, TURKEY.

(E-mail: mkilic@uludag.edu.tr)

Corresponding Author's e-mail: esraozdemir@uludag.edu.tr

ABSTRACT

Energy and energy conservation are vital issues for all countries of the world. Because of this reason, making more efficient energy use and energy production from using low-grade waste heat sources are significant. The Organic Rankine Cycle, which uses an organic fluid instead of water-steam as a working fluid, is a power generation cycle. The working principal of an organic Rankine cycle is similar to the common vapor Rankine cycle. In this study, the energy and exergy analysis of organic Rankine cycle is performed for different dry working fluids which are R600a, R600, R245fa, R123 and R113. The organic Rankine cycle's performance parameters are evaluated depending on varied evaporation temperatures and the inlet temperatures of the waste hot fluid. Results show that the best performance parameters which are thermal efficiency, exergy efficiency, net power and lower total irreversibility, are calculated for the R600a working fluid at the evaluations of both the increment of the evaporation temperature and the increment of the inlet temperature of waste hot fluid.

Keywords: Energy; Exergy; Organic Rankine Cycle; Working Fluid.



1. INTRODUCTION

Nowadays, energy has become a major issue in ensuring that countries provide a competitive advantage. The technological innovations, increasing the permeability of international borders, capital mobility and development of communication cause increasing the amount and speed of energy use. For this reason, energy saving and making more efficient use of energy is a vital matter for the world development due to many environmental impacts and energy shortage. In recent years, the global warming has compelled the energy planners to develop a new energy conversion technology which produces electricity without causing environmental pollution.

One of the most important ways to transform on large scale thermal energy into power is the steam Rankine cycle. Water is used as a working fluid in this cycle. There are several advantages for water using as working fluid. These are very good thermal/chemical stability; owing to very low viscosity, less pumping work required; owing to high latent and specific heat, good energy carrier; non-toxic; non-flammable and no threat to the environment and cheap and abundant [1]. However, many problems are encountered when using water as a working fluid: need of superheating to prevent condensation during expansion, risk of erosion of turbine blades, excess pressure in the evaporator, complex and expensive turbines [2]. Because of these reasons, water is used in high temperature applications and large centralized systems. An organic or non-conventional working fluid, which has higher molecular mass and lower ebullition/critical temperature than water, is more suitable in small and medium scale power plants and low temperature applications. This technology is “Organic Rankine Cycles”.

The organic Rankine cycle (ORC) is established for converting heat to electricity. The most important feature of an ORC is its capability of utilization of various kinds of low-grade heat sources for power generation [3]. Owing to its low operating temperature, an organic Rankine cycle can suitably recover heat from various sources. Useable heat resources in ORC are solar energy, geothermal energy, biomass products, surface seawater and waste heat from various thermal processes.

An Organic Rankine Cycle (ORC) has several advantages over conventional steam power plant: less heat is needed during the evaporation process; the evaporation process takes place at lower pressure and temperature; the expansion process ends in the vapor region and hence the superheating is not required and the risk of blades erosion is avoided; the smaller temperature difference between evaporation and condensation also means that the pressure drop/ratio will be much smaller and thus simple single stage turbines can be used [1].

The challenges, when ORC is used in a process, are of low thermal efficiency, limited ways to improve the work output, selection of working fluids matching to available heat source and sink temperatures and their effects up on environment [3].

The performance of an ORC system is strongly related to the working fluid. The working fluid determines thermal efficiency, safety, stability, environmental impact and economic profitability of the system in an ORC. In recent years, working fluid selection for ORC has drawn significant attention. Different performance evaluation criteria lead to different optimum working fluids. For this reason, a reasonable evaluation criterion is the key issue for working fluid selection.

Many studies on ORC have been presented in the literature. For example, Liu *et al.* [4] used total heat-recovery efficiency and heat availability instead of thermal efficiency as the evaluation criteria to optimize the working fluid and operating conditions for organic rankine cycle. Chen *et al.* [5] compared the system performance between a supercritical Rankine cycle using CO₂ as working fluid and a subcritical ORC using R123 as working fluid. Kanoglu and Bolatturk [6] assessed the thermodynamic performance of the Reno (Nevada, USA) binary plant. This plant uses geothermal fluid at 158 °C and isobutene as working fluid. Roy *et al.* [3] analyzed non-regenerative organic Rankine cycle, based on the parametric optimization, using R-12, R-123, R-134a and R-717 as working fluids superheated at constant pressure. Gao *et al.* [7] analyzed the performance of supercritical ORC driven by exhaust heat using 18 organic working fluids. Wang *et al.* [8] analyzed a double Organic Rankine Cycle for discontinuous waste heat recovery. Wang *et al.* [9] optimized the working fluid and parameters of ORC system with simulated annealing algorithm. They compared results for 13 working fluids. Kaska [10] analyzed a waste heat driven organic Rankine cycle and assessed performance of the cycle and pinpoint sites of primary exergy destruction using actual plant data. Imran *et al.* [11] assessed the economic assessment of greenhouse gas (GHG) reduction through waste heat recovery using organic Rankine cycle (ORC). Zhu *et al.* [12] assessed the performances of ORC under saturated expansion using organic organic and isentropic fluids, and under superheated expansions using organic wet fluids.

The brief review above shows that the types of working fluids have a significant influence on the performance of ORC. In this paper, with the light of studies in literature, the energy and exergy analysis of subcritical organic Rankine cycle is performed for different dry working fluids which are R600a, R600, R245fa, R123 and R113. The organic Rankine cycle's performance parameters are evaluated depending on varied evaporation temperatures and the inlet temperatures of the waste hot fluid. The exergy efficiency, thermal efficiency, the total-heat-recovery efficiency, the irreversibility rate, the net power, the evaporation pressure, the outlet temperature of waste hot fluid or the evaporation temperature are calculated with the various evaporation temperatures and the inlet temperatures of the waste hot fluid. Results from the analyses show that both evaporation temperature and the inlet temperature of hot

fluid have significant effect on the performance parameters of an ORC. Also the R600a working fluid produces higher thermal efficiency, exergy efficiency, net power and lower total irreversibility rate under accepted conditions in compared with other working fluid.

2. MATERIAL AND METHODS

Basic Organic Rankine Cycle

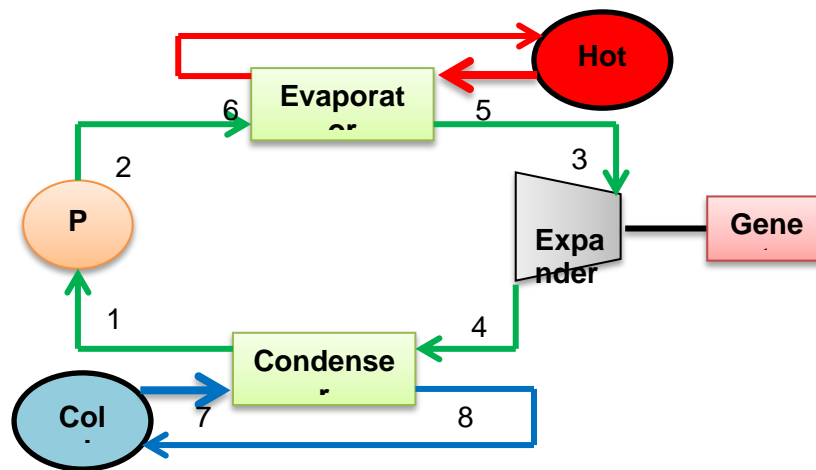


Figure 1. Schematic diagram of organic Rankine cycle

The schematic of a simple ORC system is shown in Figure 1. It includes four components: evaporator, expander, condenser and pump. An ORC is composed of four phases:

- 1-2: Pressure increase in the condensate in the feed pump from pressure p_1 to p_2 .
- 2-3: Isobaric heating, evaporation and overheating of the working medium in the steam generator (evaporator) at pressure $p_2 = p_3$.
- 3-4: Expansion of the vapor working medium in an expansion machine (e.g. a turbine) from pressure p_3 to p_4 .
- 4-1: Isobaric heat release, complete condensation and possible under-cooling of the working medium in the condenser at pressure $p_4 = p_1$.

Working fluids for ORC's are categorized in three groups based on their slope of saturation vapour curves in T-s diagram. The fluids having positive slope are dry fluids ($ds/dT > 0$). The fluids having negative slope are wet fluids ($ds/dT < 0$). The fluids having nearly infinitely large slopes are isentropic fluids ($ds/dT=0$).

In this study, R600a, R600, R245fa, R123 and R113 dry fluids are selected as the working fluids. Table 1 shows the thermo-physical properties of the selected fluids. It can be seen from Tab. 1 that R600a has the lowest value of critical temperature. It is followed by R600, R245fa, R123 and R113 respectively.

Table 1. Thermo-physical properties of the selected fluids [13]

Parameters	R600a	R600	R245fa	R123	R113
Molecular mass (g/mol)	58,12	58,12	134,05	152,93	187,38
Maximum temperature (K)	575,00	575,00	440,00	600,00	525,00
Maximum pressure (MPa)	35,00	12,00	200,00	76,00	200,00
Critical point temperature (K)	407,70	425,00	427,01	456,70	487,10
Critical point pressure (MPa)	3,63	3,80	3,65	3,66	3,39
Critical point density (kg/m ³)	225,50	228,00	519,43	550,00	560,00
Boiling point temperature (°C)	-11,68	-0,5273	15,18	27,78	47,59

System Description and Modelling

The analysis of an ORC based on thermodynamic laws and the energy, exergy analyses were performed for the working fluids investigated. For simplicity, the following assumption were made:

- ✓ All processes are operating at steady state.
- ✓ The thermal and friction losses in the pipes are negligible.
- ✓ The kinetic and potential energy changes are negligible.
- ✓ Pressure drops of working fluid in the evaporator and condenser is neglected.
- ✓ There are only two pressures: an evaporating pressure p_e and a condensing pressure p_c .
- ✓ The inlet temperature of hot waste fluid in evaporator is 130 °C.
- ✓ The isentropic efficiency of turbine and the pump are 0.80.
- ✓ Atmospheric condition is taken as 100 kPa and 293.15 K.
- ✓ The mass flow rate and the specific heat capacity of the waste hot fluid are 1 kg/s and 1 kJ/kgK respectively.
- ✓ The minimum temperature difference in the evaporator is 5 K.
- ✓ The cooling medium temperature T_L is 293.15 K.

For any steady state control volume, by neglecting the potential and kinetic energy changes, general expression of mass, energy and exergy balance equations is that:

$$\text{Mass balance equation: } \sum \dot{m}_{in} = \sum \dot{m}_{out} \quad (1)$$

$$\text{Energy balance equation: } \dot{E}_{in} = \dot{E}_{out} \quad (2)$$

$$\dot{Q} + \dot{W} = \sum \dot{m}_{out} h_{out} - \sum \dot{m}_{in} h_{in} \quad (3)$$

$$\text{Exergy balance equation: } \sum \dot{E}x_{in} - \sum \dot{E}x_{out} - \dot{E}x_d = \Delta \dot{E}x_s \quad (4)$$

$$\text{Where for a steady-state system, } \Delta \dot{E}x_s \text{ is zero. } \dot{E}x_{in} = \dot{E}x_{out} \quad (5)$$

$$\dot{E}x_{heat} + \dot{W} = \dot{E}x_{out} - \dot{E}x_{in} + \dot{I} \quad (6)$$

where, subscripts in and out represent the inlet and exit states, \dot{Q} is heat input, \dot{W} is work input, $\dot{E}x$ is exergy rate and \dot{I} is the irreversibility rate.

Process 1-2 (pump):

$$\text{The isentropic efficiency: } \eta_p = (h_{2s} - h_1)/(h_2 - h_1) \quad (7)$$

$$\text{The pump power: } \dot{W}_p = \frac{\dot{m}_{wf}(h_{2s} - h_1)}{\eta_p} = \dot{m}_{wf}(h_2 - h_1) \quad (8)$$

$$\text{The irreversibility of the pump: } \dot{I}_p = (\dot{E}_1 - \dot{E}_2) + \dot{W}_p = T_0 \Delta S_p \quad (9)$$

Process 2-3 (evaporator):

During the above heat exchange, the temperature of hot fluid decreases from T_5 to T_6 . The specific heat capacity C_p of the hot fluid at constant pressure is assumed to be constant.

$$\text{The evaporator heat rate: } \dot{Q}_e = \dot{m}_{wf}(h_3 - h_2) = \dot{m}_{hf}(h_5 - h_6) \quad (10)$$

$$\dot{Q}_e = \dot{m}_{hf} C_p (T_5 - T_6) \quad (11)$$

$$\text{The irreversibility of the evaporator: } \dot{I}_e = T_0 \dot{m}_{wf} \left[(s_3 - s_2) - \frac{2(h_3 - h_2)}{(T_5 + T_6)} \right] \quad (12)$$

Process 3-4 (expander):

$$\text{The isentropic efficiency: } \eta_t = (h_3 - h_4)/(h_3 - h_{4s}) \quad (13)$$

$$\text{The expander power: } \dot{W}_t = \dot{m}_{wf}(h_3 - h_{4s})\eta_t = \dot{m}_{wf}(h_3 - h_4) \quad (14)$$

The irreversibility of the turbine:
$$\dot{I}_t = (\dot{E}_3 - \dot{E}_4) - \dot{W}_t = T_0 \Delta S_t \quad (15)$$

Process 4-1 (condenser):

The condenser heat rate:
$$\dot{Q}_c = \dot{m}_{wf}(h_4 - h_1) \quad (16)$$

The irreversibility of the condenser:
$$\dot{I}_c = T_0 \dot{m}_{wf} \left[(s_1 - s_4) - \frac{(h_1 - h_4)}{T_L} \right] \quad (17)$$

The net power output:
$$\dot{W}_{net} = \dot{W}_t - \dot{W}_p \quad (18)$$

The thermal efficiency (η_{th}) of the ORC is the ratio of the net power output to the heat input.

It can be expressed as:
$$\eta_{th} = \frac{\dot{W}_{net}}{\dot{Q}_e} = \frac{\dot{W}_t - \dot{W}_p}{\dot{Q}_e} \quad (19)$$

The exergy destruction rate of ORC:
$$\dot{I}_{cycle} = T_0 \dot{m}_{wf} \left[-\frac{2(h_3 - h_2)}{(T_5 + T_6)} - \frac{(h_1 - h_4)}{T_L} \right] \quad (20)$$

The exergy efficiency of ORC:
$$\eta_{exe} = \frac{\dot{W}_{net}}{\dot{W}_{net} + \dot{E}_d} = \frac{\dot{W}_{net}}{\dot{Q}_e \left(1 - \frac{2T_L}{(T_5 + T_6)} \right)} \quad (21)$$

The total heat-recovery efficiency, defined as the ratio of net power to the available energy in ideal case [14]:
$$\eta_r = \frac{(T_5 - T_6)}{(T_5 - T_0)} \eta_{th} \quad (22)$$

3. RESULTS AND DISCUSSION

3.1 The analysis of various evaporation temperatures

The evaporation temperature and the inlet temperature of waste hot fluid effect the performance analysis of an Organic Rankine cycle. Therefore, we focused on two variables in this study. Firstly, the evaporation temperature was increased from 70 °C (333.15 K) to 110 °C (378.15 K) with a 5 °C and then the exergy efficiency, thermal efficiency, the total-heat-recovery efficiency, the irreversibility rate, the net power, the outlet temperature of waste hot fluid and the evaporation pressure were calculated for the various evaporation temperatures.

The inlet temperature of the waste hot fluid was 130 °C (403.15 K). It was assumed that the condensation pressure and temperature is constant at 100 kPa and 293.15 K.

According to the analysis, the thermal efficiency, the outlet temperature of waste hot fluid and the evaporation pressure increase when the evaporation temperature increases for the R600a working fluid. Nevertheless, the total heat-recovery efficiency, the total cycle the irreversibility rate, the net power decrease with the evaporation temperature. The exergy efficiency is parabolic-like function with evaporation temperature.

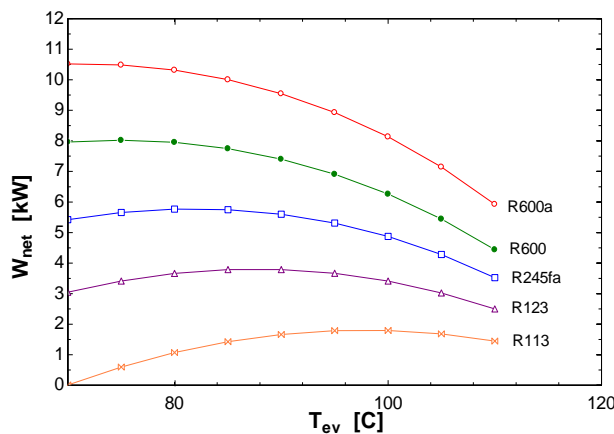


Figure 2. Comparison of the net power irreversibility rate

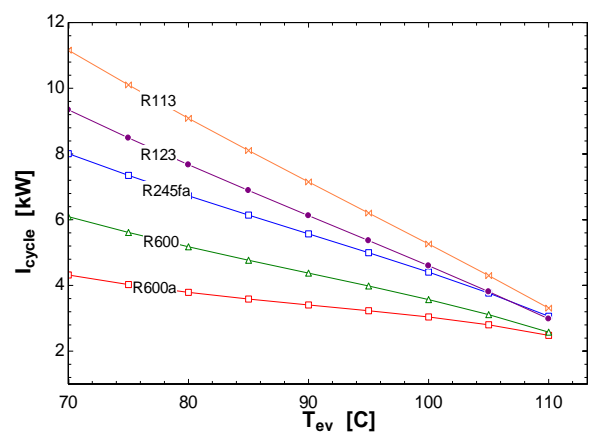


Figure 3: Comparison of the

When compared the net power of the working fluids, according to Fig.2 for all of the working fluids, the net power increases before and then decreases with the increase of the evaporation temperature. In addition, the highest net power is obtained for the R600a working fluid with 10,52 kW. This is followed by R600, R245fa, R123 and R113 respectively.

Results from Figure 3 show that total irreversibility rate or exergy destruction decreases with evaporation temperature. The minimum total irreversibility rate is obtained for the R600a working fluid. Also, it is calculated in analysis that the components with greater exergy destructions to lower one are evaporator, expander, condenser and pump.

According to Figure 4, when the evaporation temperature increases in the analysis of ORC, the outlet temperature of hot fluid increases dramatically for all of the working fluids. Otherwise the lowest values are calculated for the R600a working fluid. In other words, the R600a organic fluid benefits from the heat of the waste hot fluid to use in the evaporator.

According to the results of calculations, Figure 5 shows that the evaporation temperature has important effect on the evaporation pressure which increase with evaporation temperature. In addition, the increase of evaporation pressure effects the energy and exergy efficiency of ORC. It can be seen that from Figure 6, the highest evaporation pressure value are calculated for R600 a working fluid which followed by R600, R245fa, R123 and R113.

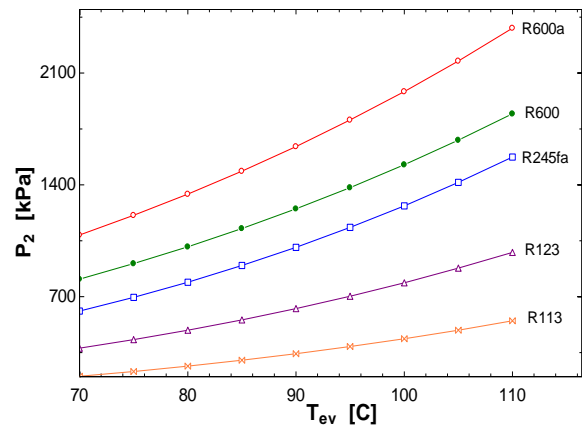
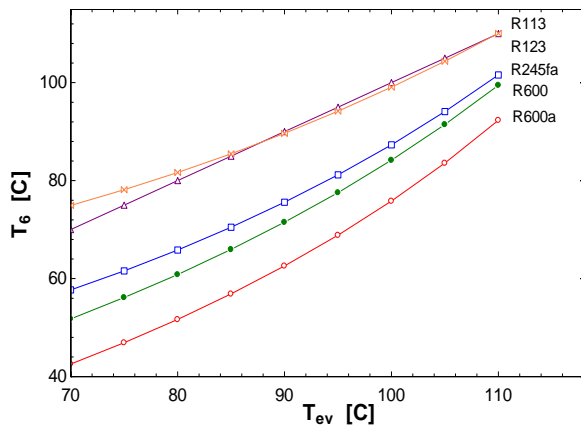


Figure 4. Comparison of the outlet temperature of hot fluid pressure

Figure 5. Comparison of the evaporation pressure

Figure 6 and Figure 7 show the comparison of the exergy efficiency and thermal efficiency for organic working fluids. The working fluids with greater both exergy efficiency and thermal efficiency to lower one are R600a, R600, R245fa, R123 and R113. When the thermal efficiency is evaluated with the net power (Fig.3), the thermal efficiency increases with the increment of the net power however the net power decreases, the thermal efficiency still increases which shows that the effect of the increase of evaporation temperature on the decrease of the heat absorbed by the working fluid (Q_{ev}) is greater than on the decrease of the net power (W_{net}).

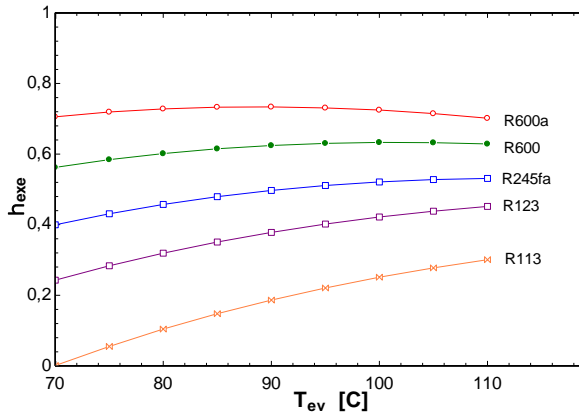


Figure 6. Comparison of the exergy efficiency

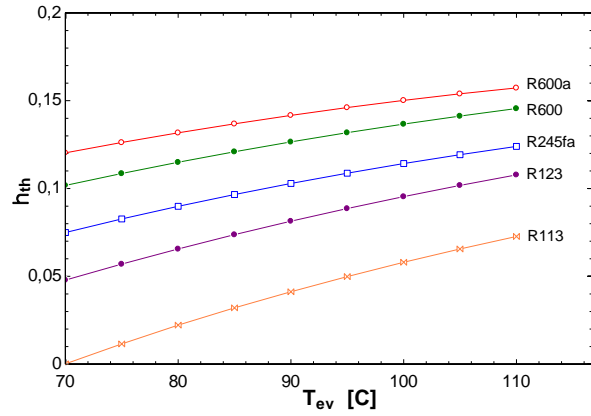


Figure 7. Comparison of the thermal efficiency

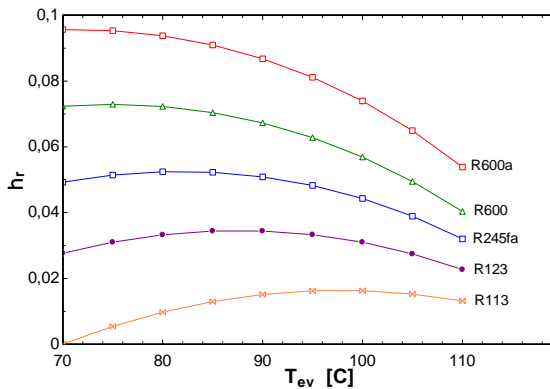


Figure 8. Comparison of the total heat-recovery efficiency

The total heat-recovery efficiency which has the same trend with the net power is calculated in its higher value for R600a working fluid as shown in Figure 8. As Equation (22), Figure 4 and Figure 8 are commented together, it can be seen that the increase of the outlet temperature of the hot fluid is more effective than the increase of the thermal efficiency on the total heat-recovery efficiency.

3.2 The analysis of various inlet temperatures of hot fluid

After the evaporation temperature has been examined, the effect of the various inlet temperatures of hot fluid on the performance of an ORC is evaluated in this section. The evaporation temperature was assumed to be 70 °C (353.15 K). The outlet temperature of the hot fluid was increased from 100 °C (373.15 K) to 140 °C (413.15 K) with a 5 °C and then the exergy efficiency, the total-heat-recovery efficiency, the irreversibility rate, the net power and the outlet temperature of waste hot fluid were calculated for the various inlet temperatures. It was assumed that the condensation pressure and temperature is constant at 100 kPa and 293.15 K.

According to the analysis, the thermal efficiency and the evaporation pressure did not change with the inlet temperature of hot fluid. In addition, the exergy efficiency, the outlet temperature of waste hot fluid and the evaporation pressure decrease when the inlet temperature of hot fluid increases for all of the working fluids. On the other hand, the total heat-recovery efficiency, the total cycle the irreversibility rate, the net power increase with the inlet temperature of hot fluid.

According to Figure 9 for all of the working fluids, the net power increases with the increment of the inlet temperature of hot fluid. In addition, the maximum net power is obtained in 140 °C for the R600a working fluid with 12,27 kW. This is followed by R600, R245fa, R123 and R113 respectively.

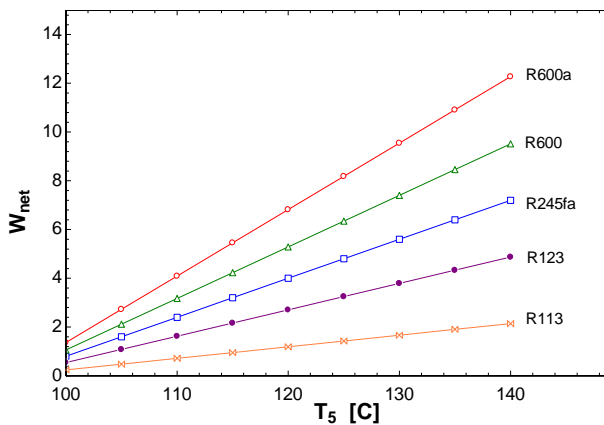


Figure 9. Comparison of the net power

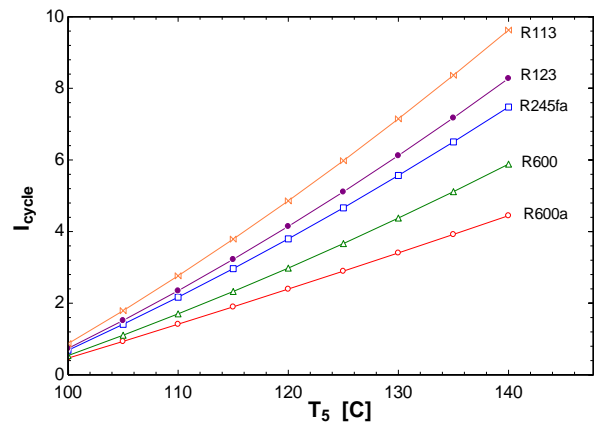


Figure 10. Comparison of the total irreversibility rate

Results from Figure 10 show that total irreversibility rate or exergy destruction increases with the inlet temperature of the hot fluid. The minimum total irreversibility rate is calculated for the R600a working fluid. The value of the total exergy destruction is calculated as be 0,46 kW and 4,45 kW at the inlet temperature of hot fluid 100 °C and 140 °C respectively.

As compared the outlet temperature of hot fluid for the working fluids, when the inlet temperature of hot fluid increases in the analysis of ORC, the outlet temperature of hot fluid decreases significantly for all of the working fluids as shown in Figure 11. Otherwise the lowest values of the outlet temperature of working fluid are calculated for the R600a working

fluid. In other words, the R600a organic fluid benefits more from the heat of the waste hot fluid to use in the evaporator.

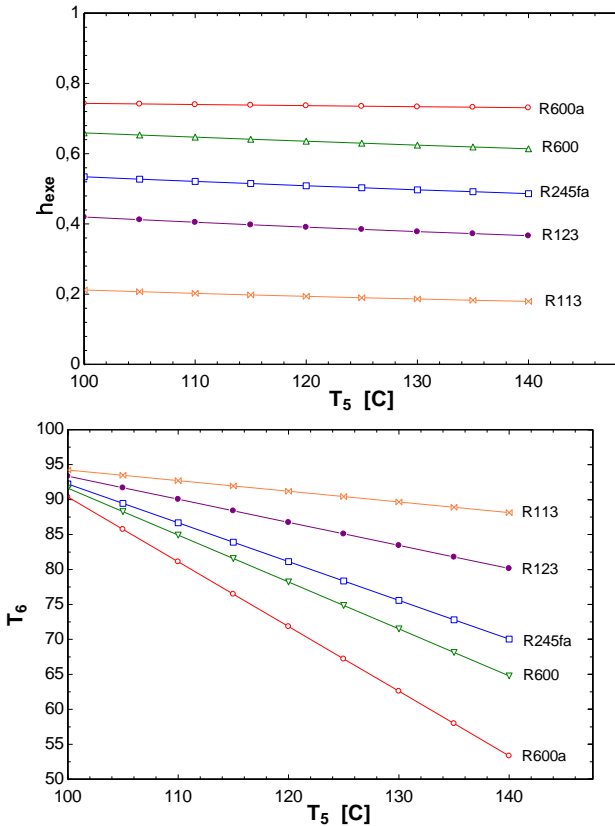


Figure 11. Comparison of the outlet temperature of hot fluid **Figure 12.** Comparison of the exergy efficiency

According to Figure 12, the exergy efficiency reduces with the growth of the outlet temperature of hot fluid. When the equation (21) and Figure 12 are commented, it can be shown that the effect of the inlet heat in evaporator on the exergy efficiency is greater than the effect of the increment of the net power on the exergy efficiency. In addition, the highest exergy efficiency is calculated as be 21,18% at the inlet temperature of 100 °C for the R600a.

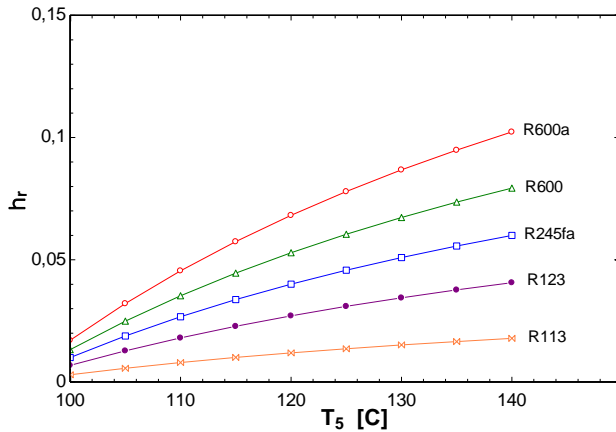


Figure 13. Comparison of the total heat-recovery efficiency

The total heat-recovery efficiency which increases with the growth of the outlet temperature of hot fluid, is calculated in its the maximum value for R600a working fluid as shown in Figure 13. As Equation (22) and Figure13 are commented together, it can be said that the increase of the inlet temperature of the hot fluid is effective on the total-heat recovery efficiency because of the stability of the thermal efficiency.

4. CONCLUSION

The selection of working fluids according to appropriate evaporation temperature and the inlet temperature of the hot waste fluid have a significant influence on the performance of an ORC. The working fluid of an ORC determines thermal efficiency, safety, stability, environmental impact, and economic profitability of the system. So, in this paper, an ORC with the subcritical and saturated expansion is analysed based on thermodynamic theory. The results obtained from the calculations are compared for five types of working fluids which are R600a, R600, R245fa, R123 and R113. According to analysis, the best performance parameters which are thermal efficiency, exergy efficiency, net power and lower total irreversibility, are calculated for the R600a working fluid at the evaluations of both the increment of the evaporation temperature and the increment of the inlet temperature of waste hot fluid.

REFERENCES

- [1] B.F. Tchanche, G. Lambrinos, A. Frangoudakis, G. Papadakis, 2011. Low-grade heat conversion into power using organic Rankine cycles-A review of various applications, *Renewable and Sustainable Energy Reviews*. 15 3963–79.
- [2] E. Wali, 1980. Optimum working fluids for solar powered Rankine cycle cooling of buildings. *Solar Energy*. 25 235–241.



- [3] J.P. Roy, M.K. Mishra, A. Misra, 2011. Performance analysis of an organic Rankine cycle with superheating under different heat source temperature conditions. *Applied Energy*. 88, 2995–3004.
- [4] B.-T. Liu, K.-H. Chien, C.-C. Wang, 2004. Effect of working fluids on organic Rankine cycle for waste heat recovery. *Energy*. 29 (8) 1207–1217.
- [5] Y. Chen, P. Lundqvist, A. Johansson, P.A. Platell, 2006. Comparative study of the carbon dioxide transcritical power cycle compared with an organic Rankine cycle with R123 as working fluid in waste heat recovery. *Applied Thermal Engineering*. 26, 2142–2147.
- [6] M. Kanoglu, A. Bolatturk, 2008. Performance and parametric investigation of a binary geothermal power plant by exergy. *Renewable Energy*. 33, 2366–2374.
- [7] H. Gao, C. Liu, C. He, X. Xu, S. Wu, Y. Li, 2012. Performance analysis and working fluid selection of a supercritical organic rankine cycle for low grade waste heat recovery. *Energies*. 5, 3233–3247.
- [8] D. Wang, X. Ling, H. Peng, 2012. Performance analysis of double organic Rankine cycle for discontinuous low temperature waste heat recovery. *Applied Thermal Engineering*. 48, 63–71.
- [9] Z.Q. Wang, N.J. Zhou, J. Guo, X.Y. Wang, 2012. Fluid selection and parametric optimization of organic Rankine cycle using low temperature waste heat. *Energy*. 40, 107–115.
- [10] O. Kaska, 2014. Energy and exergy analysis of an organic Rankine for power generation from waste heat recovery in steel industry. *Energy Conversion and Management*. 77, 108–117.
- [11] M. Imran, B. Park, H. Kim, D. Lee, M. Usman, M. Heo, 2014. Thermo-economic optimization of regenerative organic Rankine cycle for waste heat recovery applications. *Energy Conversion and Management*. 87, 107–118.
- [12] Q. Zhu, Z. Sun, J. Zhou, 2015. Performance analysis of organic Rankine cycles using different working fluids. *Thermal Science*. 19, 179–191.
- [13] http://www.coolprop.org/fluid_properties/PurePseudoPure.html#thermodynamic-properties-of-fluid, (Date accessed: 28.05.2017)
- [14] B.-T. Liu, K.-H. Chien, C.-C. Wang, 2004. Effect of working fluids on organic Rankine cycle for waste heat recovery. *Energy*. 29 (8), 1207–1217.



FINDING THE OVERLAPPING MODULES IN WEIGHTED COMPLEX NETWORKS

Yılmaz Atay*¹, Murat Aslan² and Halife Kodaz³

^{1, 2, 3} Department of Computer Engineering, Selcuk University, Konya, TURKEY

E-mail: {yilmazatay, murataslan, hkodaz}@selcuk.edu.tr

Corresponding Author's e-mail: yilmazatay@selcuk.edu.tr

ABSTRACT

There are some sub-object clusters that can be considered as significant in real networks. The objects in these clusters are called nodes and can be revealed using a number of properties in graph theory. The subgroups that may be meaningful in graphs are called communities or network modules. In some cases, it is possible that the same node can exist in two or more subsets, which is called overlapping in the literature. In our study, artificial algae algorithm is used to detect overlapping modules in weighted complex networks. This algorithm has been proposed by inspiration from the characteristics and living behavior of moving micro algae, and recently many areas have been used. The proposed algorithm has been modeled as an optimization problem for determining the overlapping modules and develops algae in population as candidate solutions. Since there is a discrete structure of the focused problem, a number of revisions have been made to the algorithmic structure of artificial algae algorithm which is suitable for continuous problems. The most suitable candidate in all candidate solutions suggests clustering that provides most meaningful sub-clusters for the entire network. In this study, it is aimed to find overlapping network modules in various real networks used as test data in the literature. The detailed analysis of the results from tests made is given in the section of the experimental results. The success of the proposed artificial algae algorithm that could be properly applied in finding overlapping communities/modules has been shown by comparing with the results of other algorithms.

Keywords: Artificial Algae Algorithm, Community Detection, Overlapping, Network Modules, Weighted Complex Networks

1. INTRODUCTION

The complex networks can be modeled by graphs. These obtained models provide us very important information. The complexity of relationships in networks might bring out very difficult graph structures. For this reason, the need for algorithms which provide analysis of graphs is increased by time. Examples of these complex structures include the internet and the world wide web, citation networks, social networks, and biological and biochemical networks of various kinds [1]. Objects and connections in networks are presented with vertices and edges, respectively. Normally, graphs which are used to represent the given network types are referred to as the simplest form of undirected and unweighted networks. But networks that model real-world systems are complex structures with various weights. Therefore, various studies have been recently carried out for the analysis of weighted networks [2-6]. Some subnetworks that are found in complex networks and can be considered meaningful are referred to as community structures [7]. When the studies given the references are examined, a network analysis has been carried out by revealing the various sub-structures which may be meaningful. The extraction of these substructures is easier in normal (undirected and unweighted) networks than that in weighted networks. This study focuses on the identification of the communities in weighted networks. Thus, this difficult problem is considered as an optimization problem and a new algorithm is suggested for its solution. In addition, this study focuses on the determination of overlapping modules as well as the detection of meaningful sub-structures from weighted networks.

For non-overlapping cases, while each vertex is contained in a single group, in the case of overlapping, one or more vertices can be found in the same group/groups [2]. An example related to overlapping communities is shown in Figure 1.

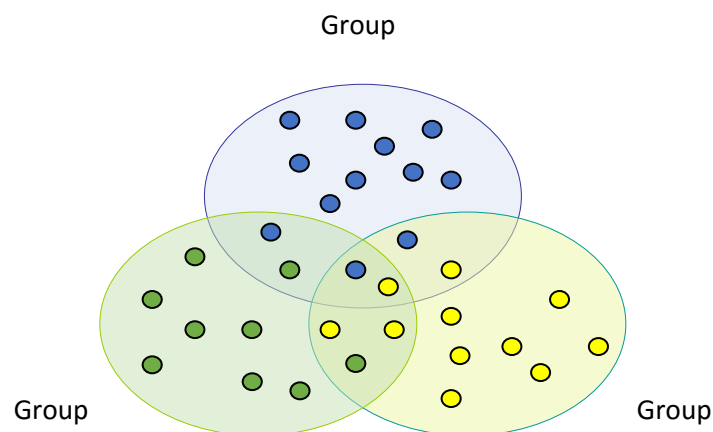


Figure 1. A grouping sample of vertices in the overlapping communities.

Figure 1 shows three different groups that form a representative network —Groups A, B and C. The small blue, green, and yellow shapes in the groups represent the nodes/vertices in the network. These nodes are normally located in a single group in non-overlapping situations but when this figure is examined, it can be seen that two green, three blue, and four yellow nodes are in similar groups. Including of these nodes in the specified groups should be done according to certain conditions. These conditions depend on that it is used suitable approaches for optimal placing the nodes into one or more groups. Therefore, it has been used to a novel bio-inspired meta heuristic optimization algorithm [8] to detect the overlapping communities in weighted networks in this study.

1.1. Community detection and the formulation definition

Communities express the sub-graphs obtained by certain features such as the number of edges, the density of weights, the number of vertices and the adjacency relationship in any networks. While nodes of a specific community have the maximum interaction with the other nodes in own community, they do not have any interaction or they have quite little interaction with the nodes of the other communities.

The modularity is one of the most popular fitness functions known in the literature. The concept of modularity was introduced in 2004 [9]. This function is based on maximization of the relationships of the members with each other in the obtained communities, and minimization of the relationships of these members with the members of the other communities. The evaluation function obtained by this way is based on a non-random and mathematical model. The most basic modularity function Q_{Basic} is given in Equation 1 [7, 9]

$$Q_{Basic} = \sum_{i=1}^k (e_{ii} - a_i^2) \quad (1)$$

Where e_{ii} indicates the edge probabilities of the binary vertices, a_i demonstrates the fraction of edges that have at least one endpoint within the group (% edges with at least 1 end in module i).

For a more general modularity function, when an example network is represented with graph structure, the acquired community structures can be considered as the sub-graphs that have the qualities and the quantities such as the maximum common properties, the number of interaction, the positional similarity. While the vertices which are the members of these structures have the maximum relationships or common properties with the nodes in its own community (inside of the community), they have the minimum relationships or

common properties with the nodes in the other community (outside of the community). Groups of people who have strong relationship in social environments, colonies of living creatures which feed on each other are located in the same community in the environmental areas, and clusters of computers which have the maximum data exchange and the maximum collaboration that they from each other are located in the same community in the computer networks can be given as examples related to the community detection problem [10].

Let the given graph structure $G(V, E)$ represents sample network, and G , V and E represent the given graph, the set of the vertices and the set of edges, respectively.

$$V = \{v_i | i = 1, 2, 3 \dots n\} \text{ and } E = \{e_j | j = 1, 2, 3 \dots m\}$$

i , j , n and m represent the indexes of the vertices, the index of the edge, the number of the total vertices and the number of the total edges, respectively. Additionally, suppose that adjacency matrix Adj which demonstrates the relationships between the members of clusters E and V with $n \times n$ dimensions are defined. Adj is generated by Equation 2 [20].

$$Adj_{(i,j)} = \begin{cases} 1 & \text{if node } i \text{ and node } j \text{ are connected,} \\ 0 & \text{otherwise.} \end{cases} \quad (2)$$

Q which represents the modularity fitness function for graph G is given in Equation 3.

$$Q = \frac{1}{2 \times m} \sum_{ij} \left(Adj_{(i,j)} - \frac{k_i \times k_j}{2 \times m} \right) \times \delta(C_i, C_j) \quad (3)$$

Q refers to the objective function to be maximized. While $Adj_{(i,j)}$ represents the adjacency matrix of graph G , m indicates the number of the total edges in the network and it is computed using the formula given in Equation 4. k_i and k_j describe degrees of the i^{th} and j^{th} vertex, respectively, and k_i is calculated according to Equation 5. C_i and C_j indicate the community which the vertex i and j belongs to, respectively. $\delta(C_i, C_j)$ expresses the function which indicates whether the vertices i and j take part in the same community or not. $\delta(C_i, C_j)$ creates the output according to Equation 6.

$$m = \frac{1}{2} \sum_{ij} Adj_{(i,j)} \quad (4)$$

$$k_i = \sum_j Adj_{(i,j)} \quad (5)$$

$$\delta = \begin{cases} 1 & \text{if } C_i = C_j \\ 0 & \text{if } C_i \neq C_j \end{cases} \quad (6)$$

We have used a modified version of the function given in Equation 3 for detection of overlapping communities [2]. The given Q_o in Equation 7 is the modified function for finding overlapping communities in weighted networks.

$$Q_o = \frac{1}{2 \times m} \sum_c \sum_{ij} \left(Adj_{(i,j)} - \frac{k_i \times k_j}{2 \times m} \right) \times \alpha(C_i, C_j) \quad (7)$$

$$\alpha(C_i) = \frac{k_i}{\sum_c k_{Ci}} \quad \text{and} \quad k_{Ci} = \sum_{v \in C} w_{iv} \quad (8)$$

While the first of the formulas given in Equation 8 may be used to determine the possible subgroup of the current node, the second formula is used to calculate the weight.

2. MATERIAL AND METHODS

The adaptation of the Artificial Algebra Algorithm to the problem of overlapping community detection in weighted networks and the adjustments related to the tests of the algorithm on various real-world data are described.

The algorithm

The paper [8] was published that presents a novel bio-inspired meta heuristic *artificial algae algorithm* (AAA) by Uymaz et al. This algorithm is inspired by the living behaviors of micro algae and uses algae to survive by identifying and moving to the suitable environment and reproduce the next generation. AAA is based on three processes called “Evolutionary Process”, “Adaptation” and “Helical Movement” [8]. In the evolutionary process, when the algal colonies have enough light, algal cells in these colonies grow and reproduce themselves to generate two new algal cells similar to the real mitotic division. In the second process "adaptation", algal colonies, which cannot grow sufficiently in an environment, try to adapt themselves to the environment. The last process "helical movement" is a process which update of algal colonies. In this process, only 3 algal cells of each colony are modified [8, 11]. The basic operating steps of *artificial algae algorithm* used in this study are given in Figure 2.

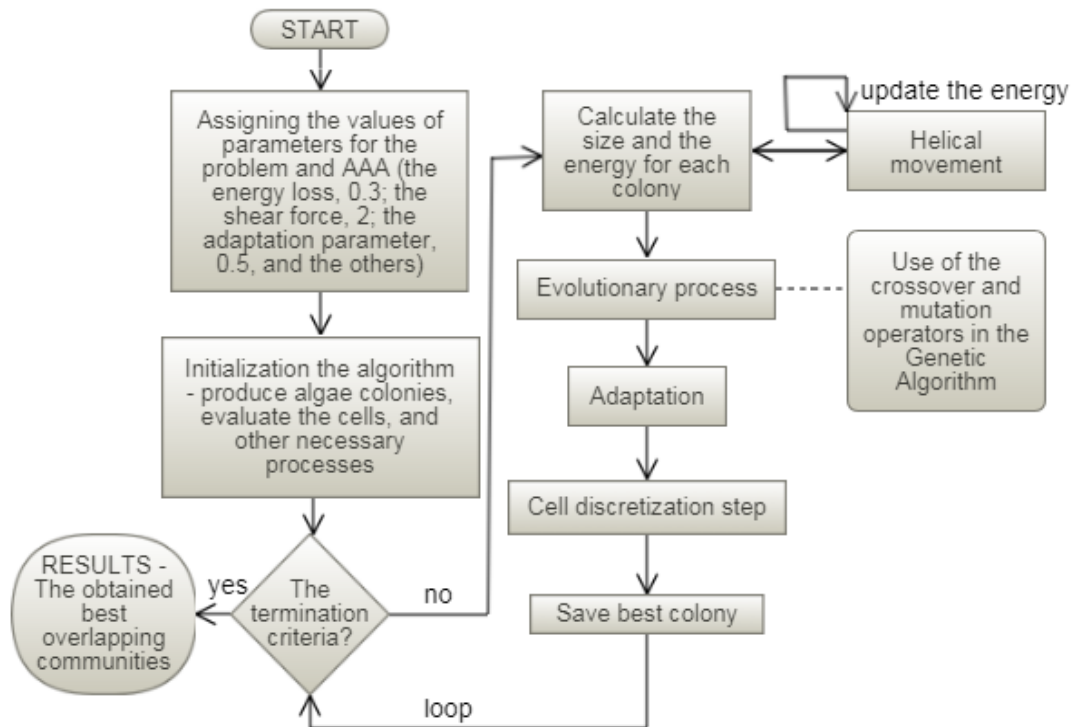


Figure 2. The basic operating steps of artificial algae algorithm selected in this paper.

The general working steps of AAA were used to obtain overlapping communities. Evolutionary and adaptation processes were used to develop algal cells in the colonies. The crossover and mutation procedures of Genetic Algorithm have been incorporated into Artificial Algae Algorithm to achieve appropriate solutions. In this paper, the algorithm is adapted to the community detection problem which is a discrete problem. This process is performed in cell discretization step.

In the first step of the study, the values of the specific parameters for both the problem and the algorithm are determined. In the second step, the algae in the colonies representing the population of the algorithm are generated and the fitness values are calculated according to Equation 7. The stopping condition in Figure 2 is the maximum number of cycles. According to this criterion, the algorithm runs in the order of the size-energy calculation, helical movement, crossover-mutation operations, adaptation, discretization and determination of the most suitable colony. When the termination criterion of AAA is satisfied, a list in which the most appropriate communities in the given network are identified is obtained. According to this list, overlapping communities also provide connected node clusters (overlapping nodes).



Experiment data and the parameters

The maximum generation number, the number of algae in the colonies, the number of execution have been determined as 1000, 100, and 20, respectively. The other parameters values have been assigned as default according to the standard genetic algorithm and artificial algae algorithm. The experimental studies were carried out on a computer which has ~16384 MB Memory, Intel Core i7-4700HQ, ~2.4GHz Processor, and Windows 10 operating system.

The algorithm has been tested on two real-world networks. These networks are Zachary's Karate Club and Dolphin Social Network. The brief description of each network is as follows. The Zachary's Karate Club [12, 13] has 78 interactions (edges) among 34 members (nodes) and the nodes represent members of a university club in the US, and edges show ties between two members of the club. This club was modeled as a network structure in the 1970s. Dolphin Social Network [14] is a social interaction network which consists of frequent associations between 62 dolphins in a community living off Doubtful Sound, New Zealand. The relationships between dolphins were established by observation of statistically significant frequent association. This network has 62 nodes and 159 edges (undirected).

3. RESULTS

In this section, this study is presented the test results of the proposed algorithm with the aim of detecting overlapping communities from weighted networks. Table 1 shows the obtained best modularity values according to the formula in Equation 8, the number of communities, and overlapping nodes.

Table 1. The test results of AAA on two real-world networks.

<i>Networks</i>	<i>Q_o values</i>	<i>No. of communities</i>	<i>The overlapping nodes</i>
Zachary's Karate Club	0.421	2	node—10
Dolphin Social Network	0.548	4	nodes—3, 40, and 62

The best modularity value is 0.421 obtained after 20 runs in the tests performed on Zachary's Karate Club network. This network has been divided into two communities by the algorithm and it has been understood that node-10 is included in both groups. In the network shown in Figure 3, node 10 is shown with a blue circle. This node is labeled as overlapping node according to the test results of the algorithm.

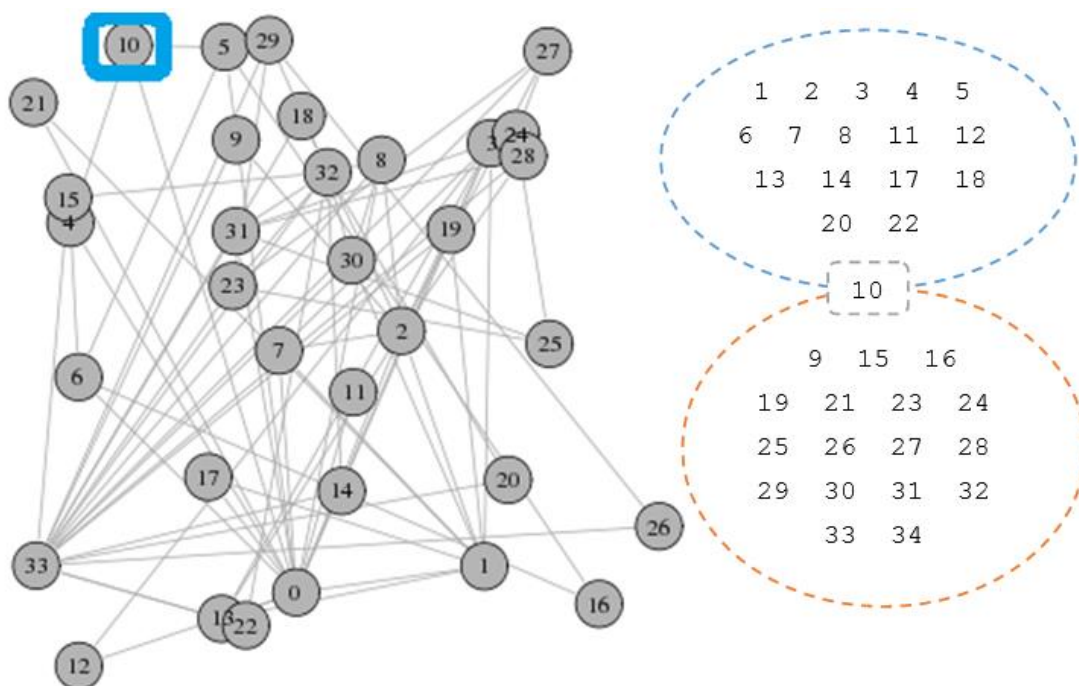


Figure 3. The obtained nodes in the overlapping communities of Zachary's Karate Club.

According to the results of the experiments on Dolphin Social Network, this network is divided into four communities. The proposed algorithm has reached 0.548 modularity value for 20 runs on this network. According to this value, three nodes are determined as overlapping nodes. These are nodes 3, 40, and 62.

4. CONCLUSION

In this study, a novel bio-inspired artificial algae algorithm is proposed for the detection of meaningful subgroups in weighted networks. The subgroups identified in this study are overlapping communities. The detection of such communities is more difficult and more



complex than the detection of other subgroups. For this reason, both the feasibility and the success of the proposed methods are very important. For this purpose, the new meta-heuristic algorithm proposed in this study has achieved similar results to other successful meta-heuristic algorithms. Due to the original mechanism of the proposed algorithm is compatible with continuous problems; the algorithm has been adapted to discrete problems so that overlapping communities can be initially applied. In addition, the crossover and mutation operators of the genetic algorithm have been also included in the mechanism of artificial algae algorithm. The test studies of the algorithm were carried out on two real networks. The obtained results are presented in Table 1 and Figure 3.

ACKNOWLEDGMENT

This study was supported by Selcuk University—Academic Staff Training Program Coordination Unit (OYP Program, project number: 2013–OYP–057).

References

1. Newman, M.E.J., Analysis of weighted networks. *Physical Review E*, 2004. 70(5).
2. Chen, D.B., et al., Detecting overlapping communities of weighted networks via a local algorithm. *Physica a-Statistical Mechanics and Its Applications*, 2010. 389(19): p. 4177-4187.
3. Li, S.D. and S. Ge, Overlapping Local Community Detection in Directed Weighted Networks. 2014 IEEE 17th International Conference on Computational Science and Engineering (CSE), 2014: p. 1196-1200.
4. Lou, X.Y. and J.A.K. Suykens, Finding communities in weighted networks through synchronization. *Chaos*, 2011. 21(4).
5. Ghaffaripour, Z., A. Abdollahpouri, and P. Moradi, A Multi-objective Genetic Algorithm for Community Detection in Weighted Networks. 2016 Eighth International Conference on Information and Knowledge Technology (Ikt), 2016: p. 193-199.
6. Fan, Y., et al., Accuracy and precision of methods for community identification in weighted networks. *Physica a-Statistical Mechanics and Its Applications*, 2007. 377(1): p. 363-372.
7. Newman, M.E.J., Fast algorithm for detecting community structure in networks. *Physical Review E*, 2004. 69(6).
8. Uymaz, S.A., G. Tezel, and E. Yel, Artificial algae algorithm (AAA) for nonlinear global optimization. *Applied Soft Computing*, 2015. 31: p. 153-171.



9. Newman, M.E.J. and M. Girvan, Finding and evaluating community structure in networks. *Physical Review E*, 2004. 69(2).
10. Atay, Y., et al., Community detection from biological and social networks: A comparative analysis of meta heuristic algorithms. *Applied Soft Computing*, 2017. 50: p. 194-211.
11. Uymaz, S.A., G. Tezel, and E. Yel, Artificial algae algorithm with multi-light source for numerical optimization and applications. *Biosystems*, 2015. 138: p. 25-38.
12. Zachary, W.W., An information flow model for conflict and fission in small groups. *Journal of anthropological research*, 1977. 33(4): p. 452-473.
13. Zachary's Karate Club Network, [cited: 05.03.2017], Available from (web page): <http://networkdata.ics.uci.edu/data/karate>.
14. Lusseau, D., et al., The bottlenose dolphin community of Doubtful Sound features a large proportion of long-lasting associations - Can geographic isolation explain this unique trait? *Behavioral Ecology and Sociobiology*, 2003. 54(4): p. 396-405.



COLOUR FEATURE-BASED CLASSIFICATION OF WHEAT GRAIN USING ANN WITH BAYESIAN REGULARIZATION LEARNING ALGORITHM

A. Kayabasi^{*}, B. Yildiz, K. Sabanci, E. Yigit, A. Toktas, M. Tekbas

Karamanoğlu Mehmetbey University, Engineering Faculty, Department of Electrical and Electronics Engineering, TURKEY

(ahmetkayabasi@kmu.edu.tr, beratyildiz@kmu.edu.tr, kadirsabanci@kmu.edu.tr, enesyigit@kmu.edu.tr, atoktas@kmu.edu.tr, mustafatekbas@kmu.edu.tr)

Corresponding Author's e-mail: ahmetkayabasi@kmu.edu.tr

ABSTRACT

In this paper, a color feature-based classification of the wheat grains into bread and durum using artificial neural network (ANN) model with bayesian regularization (BR) learning algorithm is presented. Images of 200 wheat grains are taken by a high resolution camera in order to generate the data set for training and testing processes of the ANN-BR model. Data of 3 main colour features (R, G and B) for 200 wheat grains (100 for durum and 100 for bread) are acquired for each grain using image processing techniques (IPTs). Features of R, G and B are separately determined by taking arithmetic average of the pixels within each grain. Several colour features of R/TRGB, G/TRGB, B/TRGB, R-G, G-B and R-B where TRGB is the total of R+G+B are reproduced. Then ANN-BR model input with the 9 colour parameters are trained through 180 wheat grain data and their accuracies are tested via 20 data. The ANN-BR model numerically calculate the outputs with mean absolute error (MAE) of 0.0060 and classify the grains with accuracy of 100% for the testing process. These results show that the ANN-BR model can be successfully applied to classification of wheat grains.

Keywords: Classification, wheat grains, image processing technique, artificial neural network, bayesian regularization learning algorithm



1. INTRODUCTION

Classifying of agricultural products is very important for economic reasons. The wheat grains with different quality are used in making bread, pasta and cakes which are end products. The quality of wheat grain is related to the amount of protein it possesses. Durum wheat has more protein than the bread wheat. The bread wheat grains mixing into durum grains lead to a reduction in its protein content. Therefore, classification of wheat grains is very important to increase the quality and decrease the cost. Image processing techniques (IPTs) can be employed to classify the products through the visual features. Furthermore, artificial intelligence techniques (AITs) are integrated to the IPTs for classification applications [1-2]. Artificial neural network (ANN), support vector machine (SVM), adaptive neuro-fuzzy inference system (ANFIS), decision tree (DT), K-nearest neighbors (KNN),

Naive Bayes (NB) and discriminant analysis (DA) are the most used AITs for classifying agricultural products[3-7]. Over a last decade ANN which is widely used AIT model adopts remarkable importance in classification of agricultural grains due to its fast and accurate modeling.

Several works for classifying of various agricultural products have been studied in the literature. Berman et al. classified wheat grains using near infrared hyperspectral image analysis [8]. The efficiencies of the cotton seeds were appointed by classifiers depending on DT and multilayer perceptron (MLP) by Jamuna et al. [9]. In classification of the wheat and barley seeds, DA and KNN were used to form a classifier [10]. Progressive analysis and meta-multiclass method were employed to classify the wheat grains by Zapotoczny [11]. A study using classifiers and ultraviolet visible spectrophotometry conducted to classify the spice through the KNN [12]. Prakash et al. studied the classification of objects for machine vision implementations with classifier algorithms of the KNN and Naive Bayes [13]. ANN and ANFIS were utilized to classify rice grains into five species with respect to the morphologic features [14]. A MLP-based ANN was modeled by Muñoz-Valencia et al. for classification of coffee grains according to their mineral content [15]. The ANN with the NB was designed by De Oliveira et al. for classification of green coffee grains into four group [16]. It is seen that those proposed classifiers varied among the used techniques, the features of products taken into account and the classification accuracy. Some of them might be difficult to implement while several took into account fewer parameters in classification. Therefore, their mean errors concerning the accuracy of the classification maintained limited.

In this study, a model using ANN with bayesian regularization (BR) [17] learning algorithm is designed to classify wheat grains into bread or durum according to their colour features with high accuracy. The ANN-BR model is built on feed forward back propagation (FFBP) based on multilayer perceptron (MLP). 3 colour features (R, G and B) of 200 wheat grains are acquired for each grain through IPTs for input ANN-BR model. The feature data of 180 grains and 20 grains which are uniformly selected from the total number of 200 grains are respectively employed to train and test the accuracy of the model. The ANN-BR model correctly classifies the wheat grains into durum and bread with 100 % for the training and testing process.

3. IMAGE PROCESSING TECHNIQUE

In this section, images are taken and they are imposed to the IPTs to acquire data related to the colour features of the wheat grains in order to the ANN-BR model as illustrated in Figure 1. A setup including a computer, a camera and a box arranged by camera holder and a strip LED lighting is used in order to obtain the images. The camera is Logitech C920 CCD having specifications of full HD (1080p), 15 MP, H.264 encoding, Carl Zeiss optics. The photographs are taken by the camera fixed at 35 cm height from the wheat at the bottom of the box which is closed and self-illuminated. The inside of the box is covered with black background.

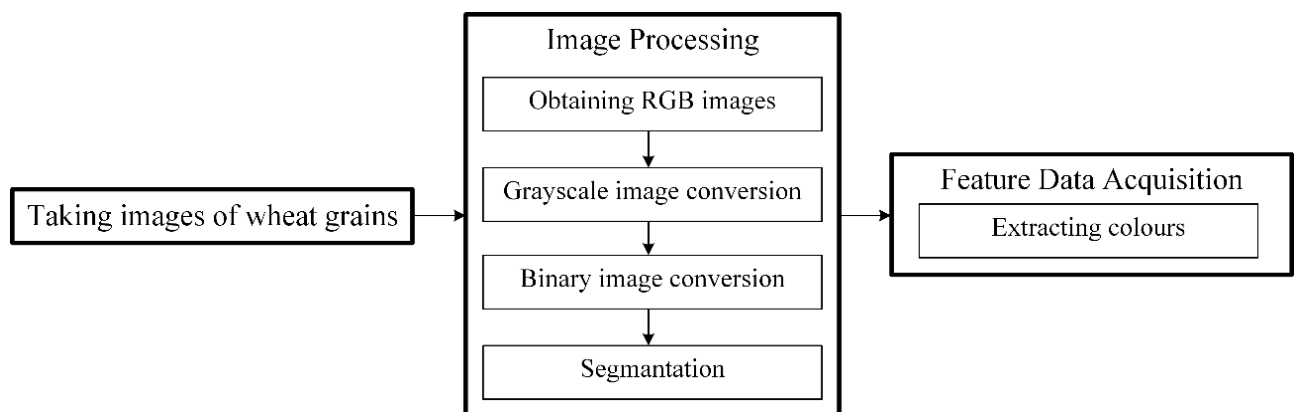


Figure 1. Flowchart of extracting colour features

The images of the wheat grains for bread and durum taken by the camera are illustrated in Figure 2. The bread wheat grain is close to yellow in color, while the durum wheat grain is darker yellow. Therefore features related to color is considered in this study to model a classifier based on IPT. In order to acquire feature data of the wheat grains (cultivated in

Konya, Turkey) for classification, photographs of 100 bread wheat grains (Figure 3(a)) and 100 durum wheat grains (Figure 3(b)) are taken with the high-resolution camera.

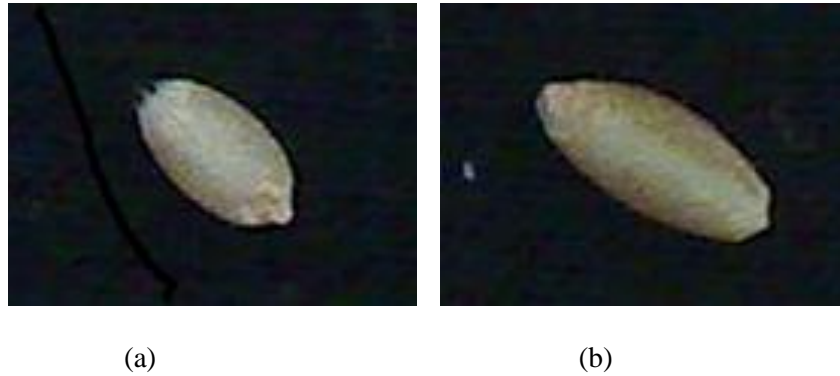


Figure 2. The images of the grains for a) bread wheat, b) durum wheat

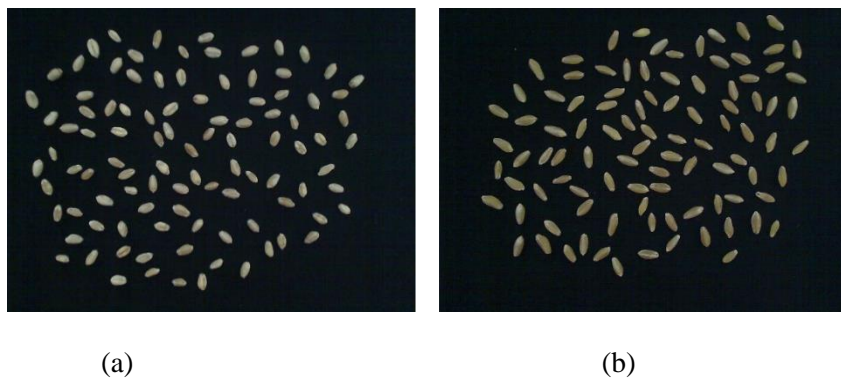


Figure 3. The RGB images of 100 grains for a) bread wheat, b) durum wheat

The IPTs are conducted through MATLAB[®] software to acquire the feature data. Firstly, the RGB level of the each pixel in the images are determined. These images are then converted to grayscale format as shown in Figure 4a and 4b. Secondly, the grayscale images seen from Figure 4c and 4d are converted to binary images (black/white) using Otsu's method [18] in accordance with threshold values of 0.30588 and 0.25882 for bread and durum grains, respectively. Thus the noise of each image is eliminated using morphological process. Thirdly, the each grain's position is fixed and they are tagged according to its position through segmentation process.

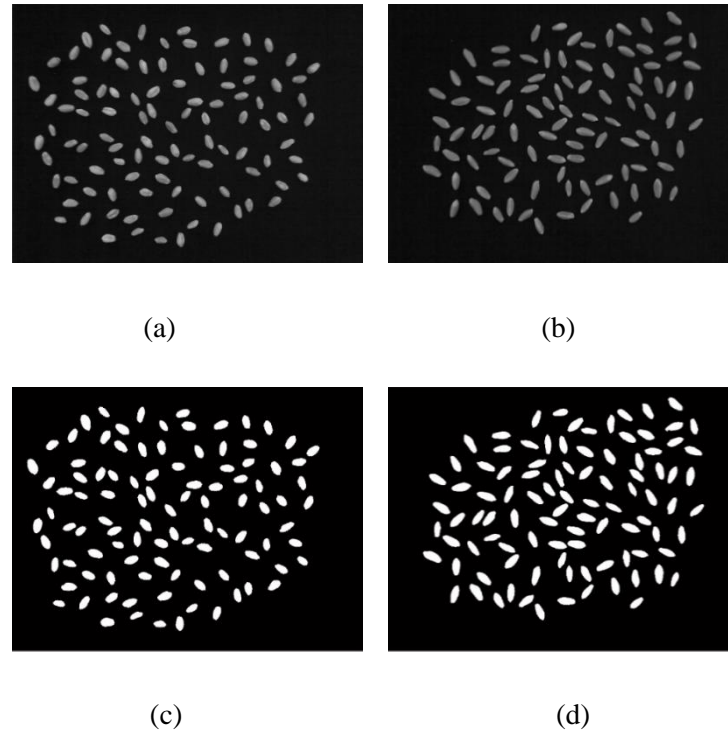


Figure 4. The images of 100 grains for a) grayscale of bread wheat, b) grayscale of durum wheat a) binar images of bread wheat, b) binar images of durum wheat (originally given in Figure 3)

4. DATA ACQUISITION

The visual data related to colour features of each grain is extracted to constitute data set (Table 1). R, G and B in Table 1 are separately determined by taking arithmetic average of the pixels within each grain. Likewise, several colour features of R/TRGB, G/TRGB, B/TRGB, R-G, G-B and R-B where TRGB is the total of R+G+B are reproduced. Colors features of the wheat grains are considered in this study to ANN-BR model.

Table 1. The main and reproduced color feature data

Input data	Input #	Colour
Main data	3	R, G, B
Reproduced data	6	R/TRGB, G/TRGB, B/TRGB, R-G, G-B, R-B

In Figure 5, 3D scattering of the grains are illustrated to show how durum and bread grains discriminate among each other according to the mentioned colour features. R, G, B from the colour is considered for examining their behavior. It is seen that from the Figure 5 the durum and bread grains cluster distinctly on opposite sides with respect to visual features of colour. This results demonstrate that the durum and bread grains have different features according to colour. Therefore, these colour features can be successfully utilized to classify the wheat grains.

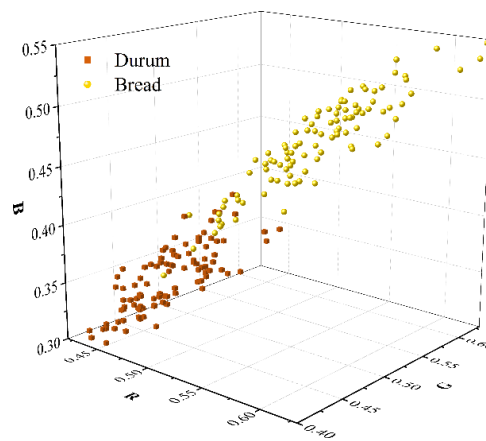


Figure 5. 3D scattering of 100 durum and 100 bread grains according to colour features of R, G and B

5. THE ANN-BR MODEL

Different learning algorithms are used for ANN networks. Some famous type of different backpropagation learning algorithms are Levenberg-Marquardt (LM), Bayesian regularization (BR), cyclical order incremental update (COIU), Powel-Beale conjugate gradient (PBCG), Fletcher-Powel conjugate gradient (FPCG), Polak-Ribiere conjugate gradient (PRCG), one step secant (OSS) and scaled conjugate gradient (SCG) [17]. In this study, the BR algorithm was used in ANN model as learning algorithm. LM and BR are able to obtain lower mean squared errors than any other algorithms for functioning approximation problems. LM was especially developed for faster convergence in backpropagation algorithms. BR learning algorithm updates the weight and bias values according to the LM optimization and minimizes a linear combination of squared errors and weights. It also modifies the linear combination so that at the end of training the resulting network has good generalization qualities.

Training Process of ANN-BR Model

The main and reproduced color feature data (R, G, B, R/TRGB, G/TRGB, B/TRGB, R-G, G-B and R-B) of the wheat grains were given as inputs and their respective classification results of IPT were given as output to the ANN-BR model. While 180 of 200 data set of wheat grains were employed for training process. After several trials, ANN-BR model based on MLP having one input layer with nine neurons, one hidden layer with five neurons and one output layer with one neuron was constructed, as shown in Figure 6. “Tangent sigmoid” function is used for input and hidden layers while “purelin” function is utilized for output layer. The parameters of the ANN-BR model used in this work are listed in Table 2. The training results are checked according to the following mean absolute error (MAE),

$$MAE = \frac{\sum |Target - Output|}{\text{Number of grains}} \quad (1)$$

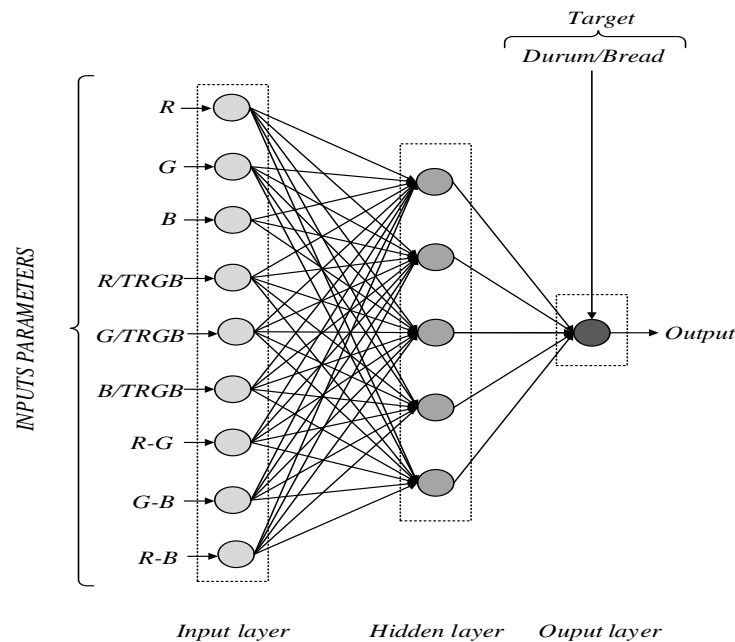


Figure 5. The ANN-BR model for classification of the wheat grains into bread or durum

Table 1. The parameters used to set the ANN model

Parameter	Set type/value
Number of epochs	500
Seed value	1239411541
Minimum gradient descent	10^{-10}
Momentum parameter (μ)	0.00015
μ increment value	5
μ decrement value	0.15
Maximum μ value	10^{10}

Testing Process of ANN-BR Model

The testing data including 9 colour features of 20 grains (10 bread wheat grains and 10 durum wheat grains) and their testing results are tabulated in Table 2 and Table 3, respectively. As illustrated Table 3, while the number of “1” is assigned to specify durum grains, “2” is appointed to define the bread grains as targets of the ANN-BR model. The ANN-BR model proposed in this study accurately classifies 14 grains with 0 (zero) and 6 grains with very small absolute errors. It demonstrates that the proposed IPT based ANN-BR model can be successfully utilized to classify the wheat grains.

Table 2. The colour features of wheat grains used for testing process

Grain #	Colour features								
	R	G	B	R/TRGB	G/TRGB	B/TRGB	R-G	G-B	R-B
1	0.46401	0.46110	0.37554	0.35675	0.35451	0.28873	0.00291	0.08556	0.08847
2	0.44629	0.42667	0.31442	0.37586	0.35933	0.26480	0.01963	0.11225	0.13187
3	0.45408	0.43612	0.32905	0.37243	0.35770	0.26988	0.01796	0.10707	0.12503
4	0.47520	0.45899	0.38777	0.35947	0.34720	0.29333	0.01622	0.07122	0.08744
5	0.49530	0.46130	0.36418	0.37500	0.34927	0.27573	0.03399	0.09712	0.13111



6	0.49414	0.47737	0.38694	0.36375	0.35141	0.28484	0.01677	0.09043	0.10720
7	0.49538	0.48514	0.40774	0.35684	0.34946	0.29370	0.01024	0.07741	0.08765
8	0.42867	0.41413	0.30537	0.37335	0.36069	0.26596	0.01454	0.10876	0.12331
9	0.46764	0.46611	0.36868	0.35905	0.35788	0.28307	0.00153	0.09743	0.09896
10	0.49530	0.46130	0.36418	0.37500	0.34927	0.27573	0.03399	0.09712	0.13111
11	0.54295	0.55344	0.49124	0.34198	0.34860	0.30942	0.01050	0.06220	0.05170
12	0.56097	0.56472	0.49251	0.34666	0.34898	0.30435	0.00375	0.07222	0.06847
13	0.54778	0.53283	0.45383	0.35699	0.34725	0.29576	0.01495	0.07899	0.09395
14	0.50643	0.49885	0.41525	0.35651	0.35117	0.29232	0.00758	0.08361	0.09119
15	0.57530	0.57505	0.49077	0.35055	0.35040	0.29904	0.00025	0.08428	0.08453
16	0.53829	0.54708	0.48991	0.34171	0.34729	0.31100	0.00879	0.05718	0.04838
17	0.55437	0.54975	0.47757	0.35049	0.34757	0.30194	0.00463	0.07217	0.07680
18	0.53307	0.55278	0.48354	0.33967	0.35223	0.30810	0.01971	0.06925	0.04954
19	0.53343	0.54038	0.47404	0.34463	0.34912	0.30626	0.00695	0.06634	0.05939
20	0.52088	0.54294	0.46972	0.33966	0.35405	0.30630	0.02207	0.07322	0.05116

Table 3. The testing results of classifying the wheat grains with the ANN-BR model

Grain #	Result			
	IPT Results	ANN-BR Results	Absolute Errors	Classification
1	1	1	0	Durum
2	1	1	0	Durum
3	1	1	0	Durum
4	1	0.9810	0.0190	Durum
5	1	0.9994	0.0006	Durum
6	1	1	0	Durum
7	1	1.0342	0.0342	Durum
8	1	1	0	Durum
9	1	1	0	Durum
10	1	0.9994	0.0006	Durum
11	2	2	0	Bread
12	2	2	0	Bread
13	2	2	0	Bread
14	2	2.0580	0.0580	Bread
15	2	2	0	Bread
16	2	2	0	Bread
17	2	2	0	Bread
18	2	2	0	Bread
19	2	2	0	Bread
20	2	2	0	Bread
MAE			0.0060	

Accuracy	100%
----------	------

6. CONCLUSION

In this article IPT based ANN-BR model is proposed for accurate classification of the wheat grains into bread and durum. The ANN-BR model based upon the MLP with three layers is designed for this purpose. 3 main and 6 reproduced colour features are acquired for 100 bread and 100 durum wheat grains. The ANN-BR model is trained with 180 grains and its accuracy is tested through 20 grains of 200 wheat grains data. The ANN-BR model classify the wheat grains with the MAE of 0.0060 for testing process. The ANN-BR model correctly classifies the wheat grains into durum and bread with 100 % for the training and testing process. The proposed method can be easy integrated to the industry to automatically classify the agricultural grains.

REFERENCES

- [1] K. Mollazade, M. Omid and A. Arefi, 2012. Comparing data mining classifiers for grading raisins based on visual features. *Computers and Electronics in Agriculture*, 84 124–131.
- [2] C. Sungur and H. Ozkan, 2015. A real time quality control application for animal production by image processing 95. *Journal of the Science of Food and Agriculture*. 95 2850–2857.
- [3] X. Yu, K. Liu, D. Wu and Y. He, 2012. Raisin quality classification using least squares support vector machine (LSSVM) based on combined color and texture features. *Food and Bioprocess Technology*, 5 (5) 1552–1563.
- [4] B.G. Hu, R.G. Gosine, L.X. Cao and de C.W. Silva, 1998. Application of a fuzzy classification technique in computer grading of fish products. *IEEE Transactions on Fuzzy Systems*, 6 (1) 144–152.
- [5] Y. Al Ohali, 2011. Computer vision based date fruit grading system: Design and implementation 23. *Journal of King Saud University-Computer and Information Sciences*. 23 29–36.



- [6] R.P. Gálvez, F.J.E. Carpio, E.M. Guadix and A. Guadix, 2016. Artificial neural networks to model the production of blood protein hydrolysates for plant fertilization 96. *Journal of the Science of Food and Agriculture*. 96 207–214.
- [7] J. Pet'ka, J. Mocak, P. Farkaš, B. Balla and M. Kováč, 2001. Classification of Slovak varietal white wines by volatile compounds 81. *Journal of the Science of Food and Agriculture*. 81 1533–1539.
- [8] M. Berman, P.M. Connor, L.B. Whitbourn, D.A. Coward, B.G Osborne and M.D. Southan, 2007. Classification of sound and stained wheat grains using visible and near infrared hyperspectral image analysis 15. *Journal of Near Infrared Spectroscopy*. 15 351–358.
- [9] K.S. Jamuna, S Karpagavalli, P. Revathi, S. Gokilavani and E. Madhiya, 2010. Classification of Seed Cotton Yield Based on the Growth Stages of Cotton Crop Using Machine Learning Techniques. *International Conference on Advances in Computer Engineering*, 312–315.
- [10] F. Guevara-Hernandez and J. Gomez-Gil, 2011. A machine vision system for classification of wheat and barley grain kernels 9. *Spanish Journal of Agricultural Research*. 9 672–680.
- [11] P. Zapotoczny, 2011. Discrimination of wheat grain varieties using image analysis: morphological features. *European Food and Research Technology*, 769–779.
- [12] C.V. Di Anibal, I. Ruisánchez, M. Fernández, R. Forteza, V. Cerdà and M.P. Callao, 2012. Standardization of UV–visible data in a food adulteration classification problem. *Food Chemistry*, 2326–2331.
- [13] J.S. Prakash, K.A. Vignesh, C. Ashok and R. Adithyan, 2012. Multi class Support Vector Machines classifier for machine vision application. *In Machine Vision and Image Processing (MVIP)*, 197–199.
- [14] A.R. Pazoki, F. Farokhi and Z. Pazoki, 2014. Classification of rice grain varieties using two Artificial Neural Networks (MLP and Neuro-Fuzzy) 24. *Journal of Animal and Plant Sciences*. 24 336–343.
- [15] R. Muñoz-Valencia, J.M. Jurado, S.G. Ceballos-Magaña, Á. Alcázar and J. Hernández-Díaz, 2014. Characterization of Mexican coffee according to mineral contents by means of multilayer perceptrons artificial neural networks 34. *Journal of Food Composition and Analysis*. 34 7–11.
- [16] E.M. De Oliveira, D.S. Leme, B.H.G. Barbosa, M.P. Rodarte and R.G.F.A. Pereira, 2016. A computer vision system for coffee beans classification based on computational intelligence techniques 171. *Journal of Food Engineering*. 171 22–27.



- [17] M. Zandieh, A. Azadeh, B. Hadadi and M. Saberi, 2009. Application of neural networks for airline number of passenger estimation in time series state. *Journal of Applied Science*, 9 (6) 1001–1013.
- [18] N. Otsu, 1979. A Threshold Selection Method from Gray-Level Histograms, *IEEE Transactions on Systems, Man, and Cybernetics*, 9 (1) 62–66.



PHOTOVOLTAIC (PV) COVERED ELECTRICITY DEMAND OF A BUILDING WITH NON-OPTIMAL INCLINATION AND ORIENTATION

Rustu Eke*¹, Cihan Demircan²

¹ Mugla Sıtkı Koçman University Clean Energy Research & Development Centre and Photovoltaic Material and Device Laboratory Department of Physics, Mugla, TURKEY
(E-mail: erustu@mu.edu.tr)

² Mugla Sıtkı Koçman University Graduate School of Natural and Applied Sciences and Clean Energy Research & Development Centre Mugla, TURKEY

Corresponding Author's e-mail: erustu@mu.edu.tr

ABSTRACT

The first BIPV system of Turkey was installed on the façade and two towers of the Staff's Block of Educational Faculty building of Mugla Sıtkı Koçman University in February 2008. The PV system covers 405m² (60°tilted surface and two vertical towers on east and west sides of the building) with single and triple junction amorphous thin film photovoltaic modules. The total installed power of the BIPV system is 40.3 kWp. Total cumulative produced electricity of the system from the start up during 200 months is exceeding 280.000 kWh. In this study, the electricity demand of the building is monitored with network analysers and PV data is collected with a Sunlog data logger. It is found that in clear days in summer, PV covers approximately 45% or electricity demand of the building at weekend also the PV modules has a non-optimal inclination and orientation. Daily power and electricity demands are also analysed.

Keywords: BIPV, cover ratio, electricity demand.



1. INTRODUCTION

The global PV market has experienced a significant progress in the recent years and 50% growth in the year 2016 alone and the worldwide cumulative PV installed capacity is realized more than 303GWp with one year installed 76.6GW. Furthermore, it is expected that this figure will exceed 500GWp by the year 2019 [1]. Turkey has installed 571 MW of new solar PV capacity in 2016, making it the best year for the country's solar sector. 2017 is expected to be equally good, while a few worrying signs are on the horizon from 2018 onwards. According to data published by Turkey's ministry of energy and natural resources, the country added 571 MW of new solar PV systems in 2016, up from a cumulative 248.8 MW of solar PV capacity in the end of 2015. This is a 230% year-on-year growth [2].

Over the last three decades world energy demands have shown a consistently growing trend, with primary energy growing by 89.5% and CO₂ emissions by 79% in the 1973–2006 period. Global greenhouse gas emissions are increasing rapidly and, in May 2013, CO₂ levels in the atmosphere exceeded 400 parts per million for the first time in several hundred millennia. Despite positive developments in some countries, global energy-related CO₂ emissions increased by 1.4% to reach 31.6 gigatonnes (Gt) in 2012, a historic high [3]. Buildings are responsible for a considerable share of energy consumption, and will play a growing role in the energy demands of emerging economies in the next decades. Buildings are typically responsible for 40% of the total primary energy consumption in the US, the European Union and also in developing countries [4,5]. Most public buildings are typically large and there are free spaces for the integration of photovoltaic modules. Building-integrated photovoltaics (BIPV) use the building envelope to incorporate solar cells that convert sunlight directly into electricity, and we argue that they are not only the ultimate showcase for this clean, renewable and benign energy generation technology, but represent a perfect application of on-site energy production as well. Furthermore, on-site BIPV generation avoids the need of voltage step-up and step-down typical of centralised generation and transmission and distribution (T&D) systems, as well as all the associated hardware and losses. The building's electrical installation itself can be used as the interface between the PV modules and the public distribution grid. Energy demands in buildings can be either reduced by the implementation of energy efficiency strategies, or met by on-site generation. Yun and Steemers have recently demonstrated the effectiveness and implications of applying PV to facades [6].

In warm and sunny climates, large-area public and commercial buildings operating mostly during daytime hours present electricity demands that are dominated by computers and air-conditioning loads, which present a good match with solar radiation availability [7-10]. BIPV installations present the distinct advantage of generating power close to the point of use, avoiding transmission and distribution investments, and the associated losses. Furthermore, because they are integrated onto a building's roof and/or façade, there are no extra surface area requirements for BIPV power plants. These PV modules can be regarded as roofing and

façade building elements, and should become a more widespread energy generation alternative in the near future, as PV manufacturing costs decline and photo generated electricity becomes competitive with conventional generation technologies. It has been previously shown how BIPV can assist distribution utility daytime peaking feeders in peak-shaving under different environments [7-9,11,12].

In many studies thermal and photovoltaic performances of BIPV systems are analysed [13-20]. In a typical office building in Brazil, it was demonstrated that over 50% of the energy demands can be supplied by solar energy [21-26].

In this work, we analyse the particular characteristics of a public buildings; due to the distinct characteristics of the building envelope in various buildings, BIPV systems can represent an interesting alternative to assist in covering their energy demands.

PV and also BIPV have great potential to contribute to electricity production in the urban environment of the south of Turkey. Muğla Sıtkı Koçman University has been involved in R&D for PV materials and systems since 1996. Currently Muğla Sıtkı Koçman University Clean Energy R&D Centre is one of the leading establishments in the field having the largest PV park with many different demonstration photovoltaic power systems (PVPSs) in the main campus. With the installed PVPS, Muğla Sıtkı Koçman University covers approximately 4% of the electricity demand of the main campus. The first and largest BIPV application of Turkey was installed on the façade and the two towers of the “Staff Block Education Faculty’s buildings which is formerly an administration building of Muğla Sıtkı Koçman University (Figure 1) [15].



Figure 1. Muğla Sıtkı Koçman University BIPV System.

Although maximum annual performance of grid-connected PV is usually obtained with modules tilted at an angle equal to the site latitude, facing the equator, this building was oriented with 30° south-east facing (Figure 2).

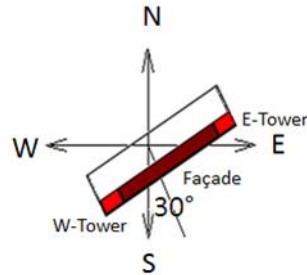


Figure 2. Orientation of the building

The total installed power of the BIPV system is 40.3kWp. Two different types of photovoltaic technology is used in this application. On the façade, triple junction amorphous modules with two different nameplate power is used and totally 405 m² of the facade is covered. And the modules were installed using specially designed mounting units with 60° tilt angles and 25 cm apart from the building for the ventilation. The 30.15 kWp PVPS on the façade was connected to the campus grid with four 6 kW three phase inverters. On the towers located on the east and West side of the building, single junction amorphous silicon modules were installed vertically and 10 cm apart from the walls. The 10.24 kWp PVPS cover 136 m² surface areas on the two towers and the systems are connected to the campus grid with two 5 kW single phase inverters [15].

The main purpose of the study is analysing the one-year period electricity demands of the building and the rate of covering this demand by PV. Electricity cover ratio of a system is generally obtained by the ratio of the electricity produced from the system and the total electricity demand which is given as:

$$\text{Power Cover Ratio} = \frac{AC, PV \text{ output power in kW}}{AC, \text{Actual total power demand in kW}} = \frac{P_{inv}}{P_{inv} + P_{grid}} \quad (1)$$

$$\text{Electricity Cover Ratio} = \frac{\text{daily PV electricity in kWh}}{\text{daily total Demand in kWh}} \quad (2)$$

The results are shown in this paper which is obtained in July 2013.

Monitoring

The electricity demand of the building is monitored with three network analyser (Figure 3) and PV data is collected with a Sunlog data logger (Figure 4). Network analysers collect electrical parameters in 5 seconds intervals. Solar and PVPS electrical data is collected in 15 minutes intervals.



Figure 3. Network analyzer used for measuring the electricity demand of the building.



Figure 4. Data logging unit for PV system.

PERFORMANCE ANALYSIS

The building is facing to an open area, so there is no shading obstacle except strings shading and a tree. Daily power curves of the PV systems on the building are also measured and a typical daily power distribution of the BIPV system is given in Figure 5. Because of the facing of the building (30° east from south) and different daylight saving time there is an obvious shift from the solar noon.

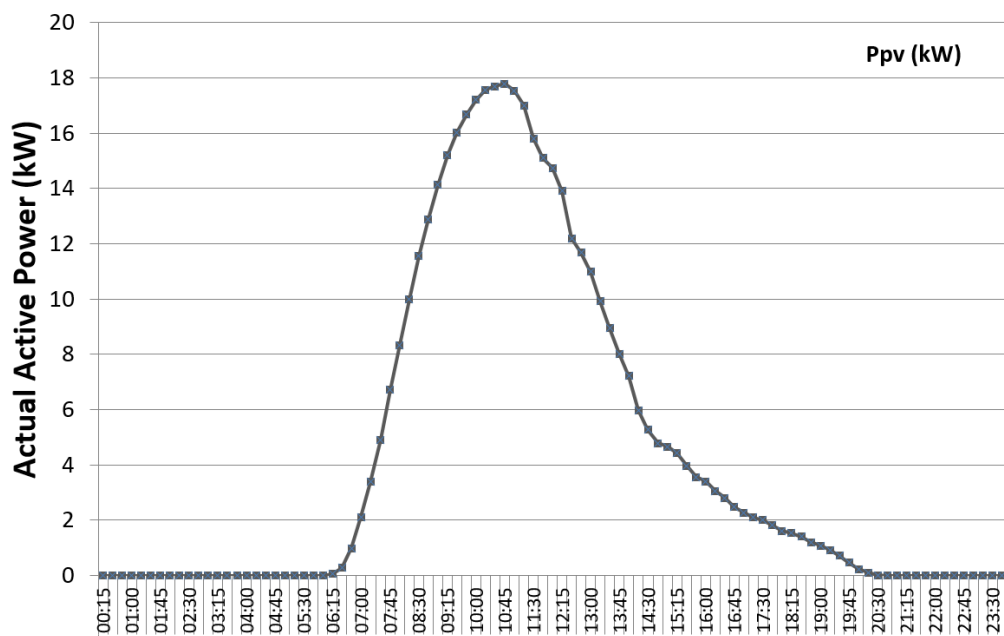


Figure 5. Daily BIPV power in a clear sky day

Cumulative produced electricity of the BIPV system from the start up is exceeding 280.000 kWh (between July 2008 and July 2017). BIPV system's daily average electricity produced and fed to grid is about 90 kWh (70 kWh façade and 20 kWh east and west towers). Maximum actual produced power by BIPV is measured as 29 kW in December 2010 but now the maximum actual power decreased and it was measured as 18 kW in July 2013 and 17 kW in July 2017.

With the help of the network analysers the electricity demand of the building can be determined. The power consumption of the building depends on the loads used by the staff working in the building and it varies between 10 kW and 41 kW as shown in Figure 6.

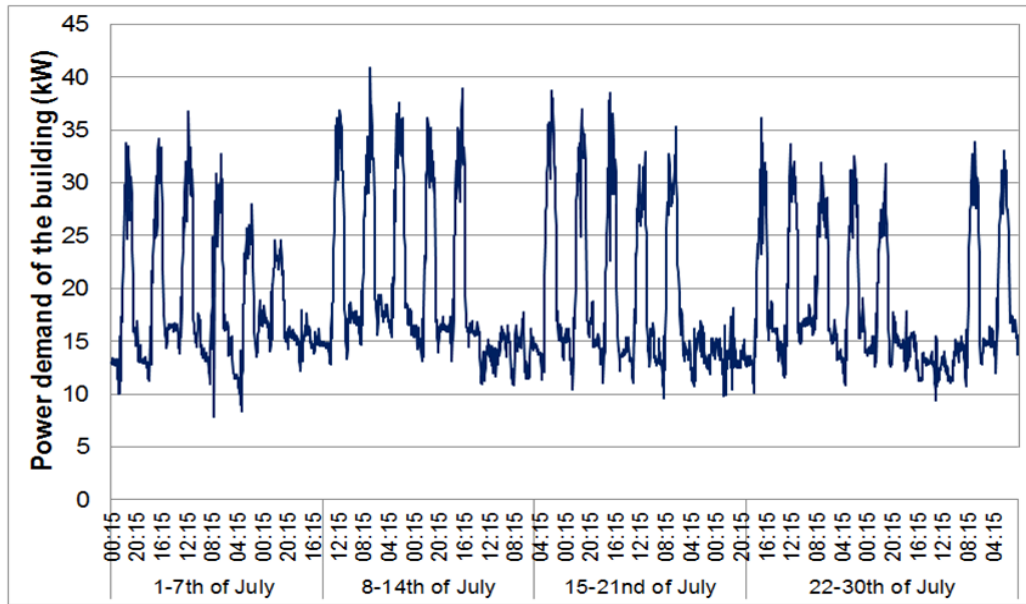


Figure 6. Daily power consumption of the BIPV system in July.

Power demand of the building can be analysed in two sections as for weekdays and weekends. The average daily power consumption of the BIPV system for weekdays and weekend in July are shown in Figure 7. In weekdays, staffs are working in their offices so electricity consumption increases between 8.30 am and noon. In lunch break demand decreases dramatically. Afternoon power demand is decreased up to evening hours and only some loads like surrounding lights are active at nights.

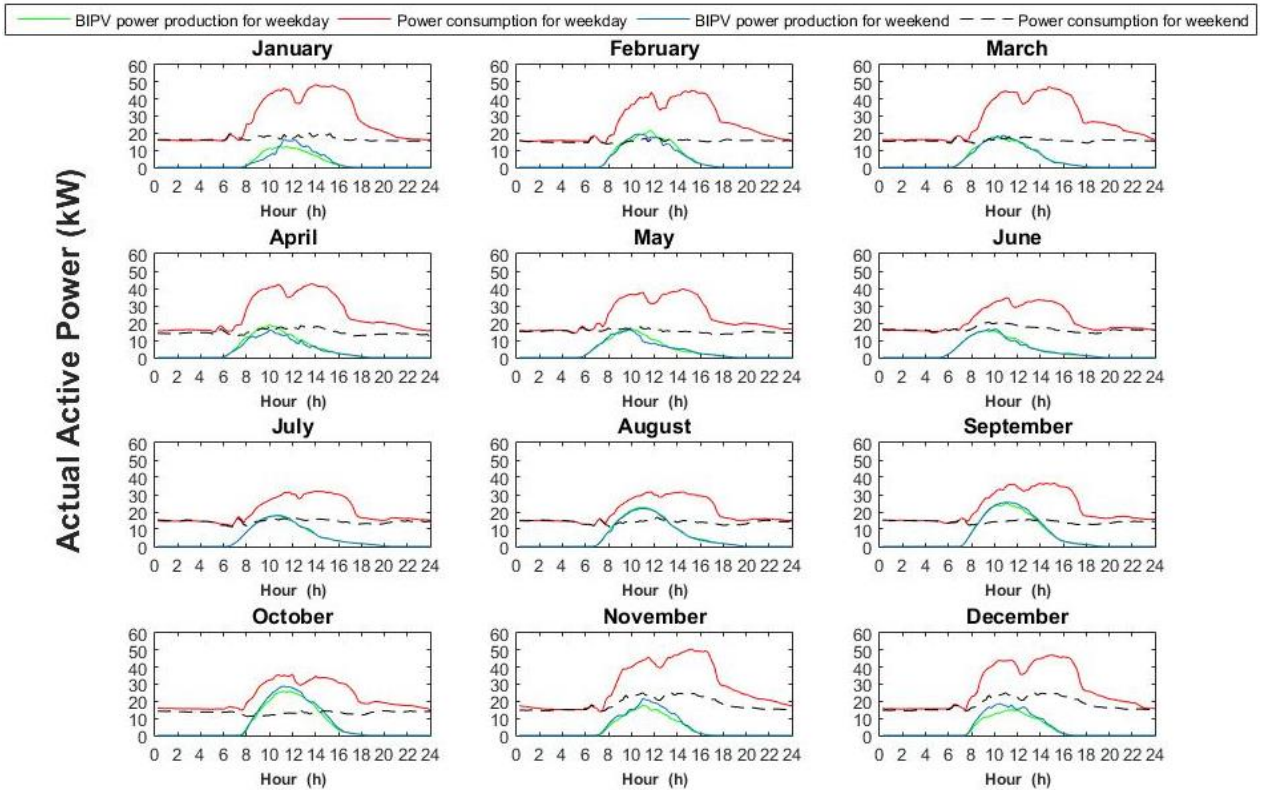


Figure 7. Monthly Average daily actual power of the building in weekdays and weekends.

It can be easily seen from Fig 7 that PV electricity covers some part of the electricity demand of the building P_{tot} is the total power demand, P_{PV} is the total power output of the PV system and P_{grid} is the net electricity purchased from the grid.

Therefore BIPV system's total cover ratio at the weekdays is about 20% and at the weekends is about 29%. Calculated monthly average daily and hourly power cover ratios of the produced electricity using (2) is shown in Figure 8. The calculated cover ratios are sketched for weekday and weekend periods. As it is clear from the figure, electricity cover ratio of the BIPV system is less than generally 20% but at weekends the calculated cover ratio increases and it exceeds 35% in clear sky days. Only in the first weekend of July there was a common exam in the University Campus so some of the staff worked in their offices after exam and increased the electricity demand of the building.

In weekdays Power cover ratio reaches 60% round 10am and for weekend averages power cover ratio reaches 110% between 10 and 11am. Cover ratio over 100% means production covers the total demand and the rest is used in the other units connected to the grid.

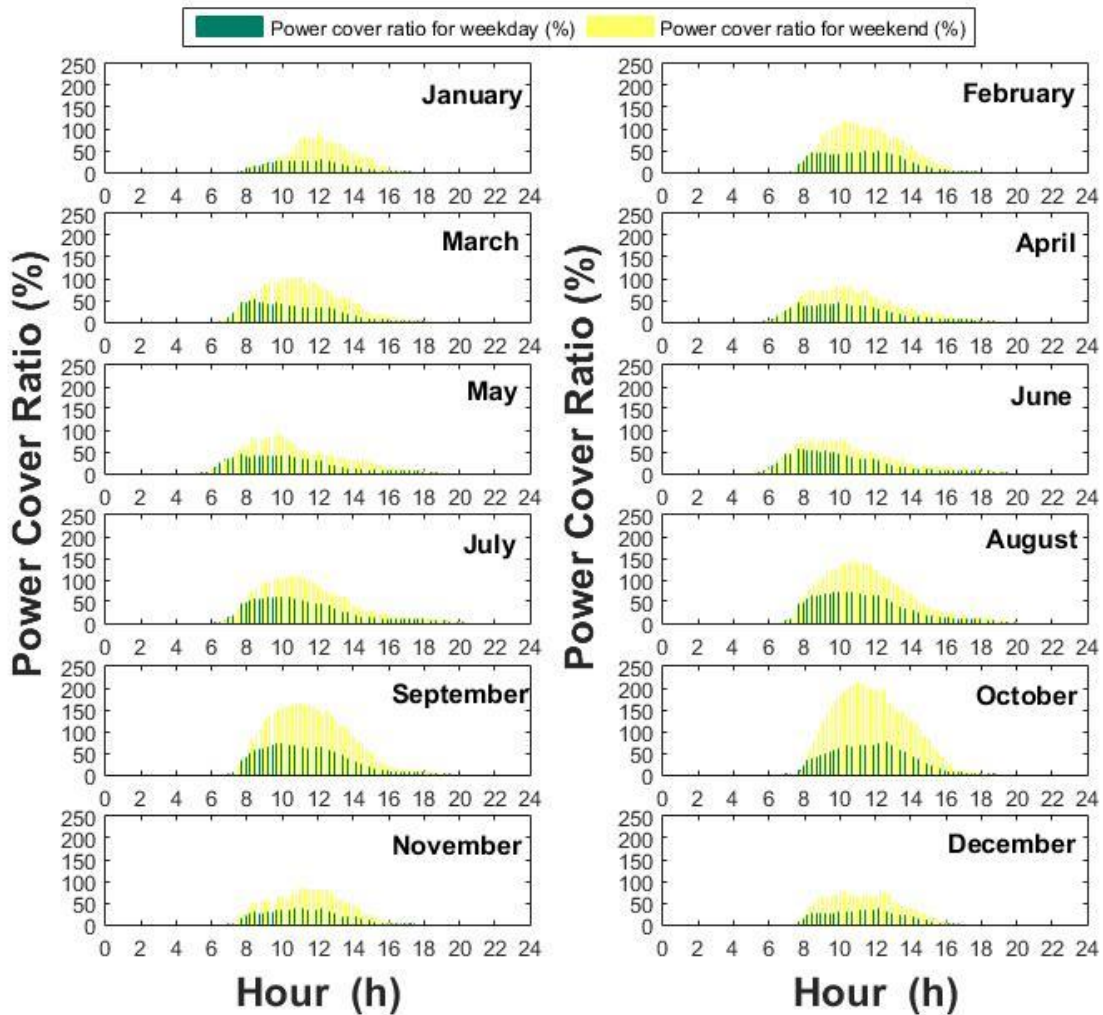


Figure 8. Monthly average daily and hourly power cover ratios of the produced electricity.

CONCLUSIONS

BIPV system's daily produced energy is about 90 kWh (70 kWh façade and 20 kWh east and west towers). Maximum actual produced power by BIPV is about 18 kW. The monitoring results showed that the electricity cover ratio varies in weekdays and weekends. Therefore, BIPV systems cover 20% at the weekdays and 30% at the weekends electricity demand of the building. Daily total consumed energy at the weekdays is about 485 kWh and at the weekends



is about 340 kWh. In weekdays power cover ratio reaches 60% round 10am and for weekend averages power cover ratio reaches 110% between 10 and 11am. BIPV system's average electricity cover ratio at the weekdays is about 20% and at the weekends is about 29%. The total cumulative electricity produced and used from the loads during 200 months is over 280000kWh and monthly total profile is shown in Figure 9 where the decrease comes from the shading effect because of the trees and leafs in south part of the building.

This study shows that public building envelopes like this University building, can host considerably large on-site PV modules that can represent important contributions to the local distribution utilities. The building envelope can accommodate the PV modules, and the building's electrical installation can provide the interface between the PV system and the utility's distribution network, resulting in a strategically sited, virtually zero-area, clean and renewable power plant.

Strategically sited PV systems can contribute to alleviate urban distribution networks, shifting demand peaks when there is a good match between loads and the solar radiation resource. We have shown how a building-integrated photovoltaic system (with approximately 40kWp) can contribute to both the public building and the local distribution utility in a metropolitan environment in a warm and sunny climate. Since a considerable fraction of the local distribution feeder load is due to the building under analysis, the BIPV system can contribute in reducing the feeder's peak.

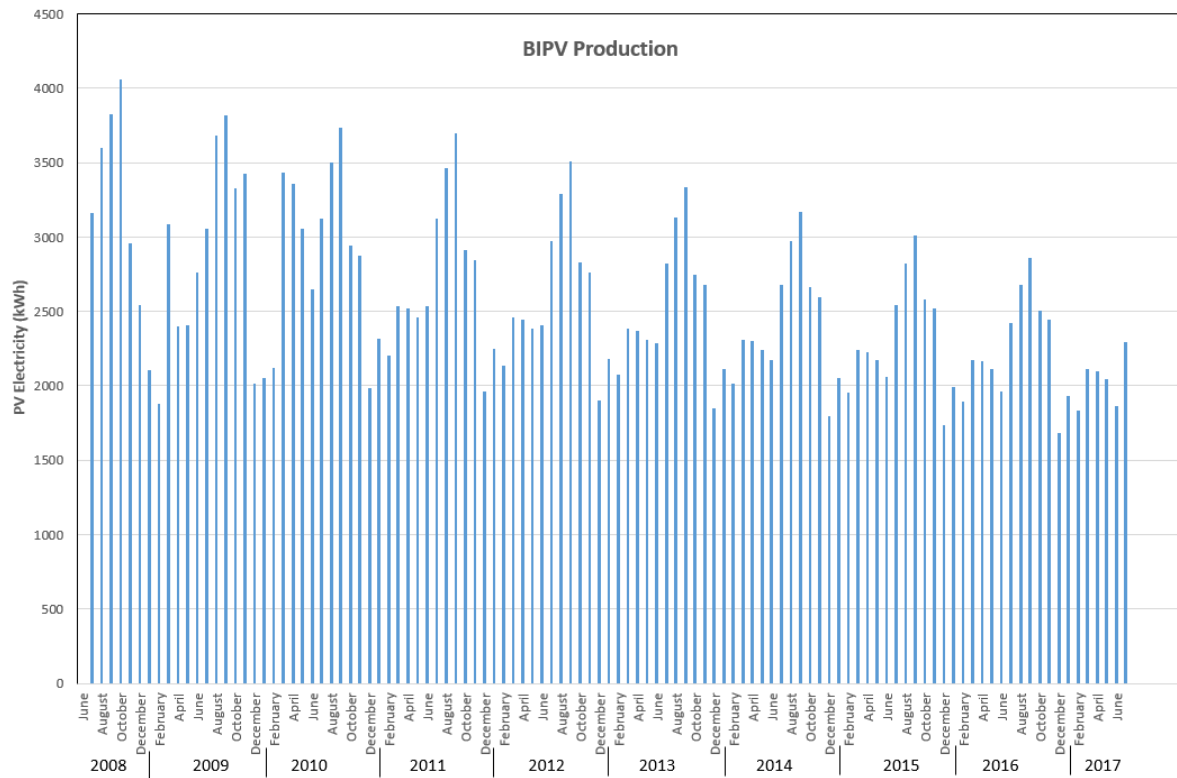


Figure 9. Monthly total electricity from the BIPV system.

While not all of the BIPV system's nominal capacity can be regarded as dispatchable energy, due to the solar resource intermittency, a considerable fraction of the installed PV power can be relied on for peak-shaving.

ACKNOWLEDGEMENT

This work was supported by Mugla Sıtkı Kocman University Scientific Research Projects (BAP) with the codes 08/10 and 12/107. Some part of this study is presented in Second International Conference on Water, Energy and the Environment Kusadası, Turkey September 21-24, 2013.



REFERENCES

- [1] S.P. Europe, “Global market for solar power 2015-2019” European Photovoltaic Industry Association, Brussels, Tech. rep. 2015.
- [2] I. Tsagas, PVmagazine. <https://www.pv-magazine.com/2017/02/27/turkey-adds-571-mw-of-solar-pv-in-2016/> February 2017. [accessed March 2017]
- [3] IEA Annual Energy Outlook 2013, Special report. Available from: <http://www.iea.org/publications/freepublications/publication/English.pdf> [accessed January 2015]
- [4] S. Baden, P. Fairey, P. Waide, J. Laustsen 2006. Hurdling financial barriers to low energy buildings: experiences from the USA and Europe on financial incentives and monetizing building energy savings in private investment decisions. In: Proceedings of the 2006 ACEEE Summer Study on Energy Efficiency and Buildings, American Council for an Energy Efficiency Economy, Washington DC, USA.
- [5] H.S. Geller, Energy Revolution: Policies for a Sustainable Future. Island Press, Boulder, CO, USA, 2002.
- [6] G.Y. Yun and K. Steemers, 2009. Implications of urban settings for the design of photovoltaic and conventional façades. *Solar Energy* 83(1): 69–80.
- [7] A.Y. Al-Hasan, A.A. Ghoneim and A.H. Abdullah, 2004. Optimizing electrical load pattern in Kuwait using grid connected photovoltaic systems. *Energy Conversion and Management* (45): 483–494.
- [8] N. Kellow, D. Jarrar, 1994. Design of a solar air-conditioning system for peak electrical load shaving. *Energy Conversion and Management* 32: 169–181.
- [9] R. Rüther, P.J. Knob, J.C. da Silva, S.H. Rebechi, 2008. Potential of building integrated photovoltaic solar energy generators in assisting daytime peaking feeders in urban areas in Brazil. *Energy Conversion and Management* 49: 1074–1079.
- [10] R. Rüther, P. Braun, 2009. Energetic contribution potential of building-integrated photovoltaics on airports in warm climates. *Solar Energy* 83: 1923–1931.
- [11] J.C. Hernández, A. Medina and F. Jurado, 2008. Impact comparison of PV system integration into rural and urban feeders. *Energy Conversion and Management* 49: 1747–1765.
- [12] T. Muneer, M. Asif, J. Kubie, 2003. Generation and transmission prospects for solar electricity: UK and global markets, *Energy Conversion and Management* 44: 35–52.



- [13] M. Castro, A. Delgado, F.J. Argul Colmenar, F. Yeves, J. Peire, 2005. Grid-connected PV buildings: analysis of future scenarios with an example of Southern Spain. *Solar Energy* 79(1): 86–95.
- [14] R. Charron and A.K. Athienitis, 2006. Optimization of the performance of double-façades with integrated photovoltaic panels and motorized blinds. *Solar Energy* 80(5): 482–491.
- [15] R. Eke and A. Senturk, 2013. Monitoring the performance of single and triple junction amorphous silicon modules in two building integrated photovoltaic (BIPV) installations. *Applied Energy* 109:154–162.
- [16] D. Infield, L. Mei and U. Eicker, 2004. Thermal performance estimation for ventilated PV facades. *Solar Energy* 76(1–3): 93–98.
- [17] D.H.W. Li, G.H.W. Cheung, J.C. Lam. 2005. Analysis of the operational performance and efficiency characteristic for photovoltaic system in Hong Kong. *Energy Conversion and Management* 46: 1107–1118.
- [18] J.D. Mondol, Y.G. Yohanis, B. Norton. 2007. Comparison of measured and predicted long term performance of grid a connected photovoltaic system. *Energy Conversion and Management* 48: 1065–1080.
- [19] M. Oliver and T. Jackson. 2001. Energy and economic evaluation of building-integrated photovoltaics. *Energy* 26: 431–439.
- [20] M. Ordenes, D.L. Marinoski, P. Braun, R. Rüther. 2007. The impact of building-integrated photovoltaics on the energy demand of multifamily dwellings in Brazil. *Energy and Buildings* 39: 629–642.
- [21] P. Braun and R. Rüther, 2010. The role of grid-connected, building-integrated photovoltaic generation in commercial building energy and power loads in a warm and sunny climate. *Energy Conversion and Management* (51): 2457–2466.
- [22] C.S. Jardim, R. Rüther, I.T. Salamoni, T.S. Viana, S.H. Rebechi, P. Knob. 2008. The strategic siting and the roofing area requirements of building-integrated photovoltaic solar energy generators in urban areas in Brazil. *Energy and Buildings* 40: 365–370.
- [23] T. Miyazaki, A. Akisawa, T. Kashiwagi. 2005. Energy savings of Office buildings by the use of semi-transparent solar cells for windows. *Renewable Energy* 30: 281–304.
- [24] R. Rüther, J. del Cueto, G. Tamizh-Mani, A.A. Montenegro, S. Rummel, A. Anderberg, B. von Roedern, 2008. Performance test of amorphous silicon modules in different climates – year four: progress in understanding exposure history stabilization effects, In: 33rd IEEE Photovoltaic Specialists Conference, San Diego, USA, 304–307.



- [25] J. Urbanetz, C.D. Zomer, R. Rüther, 2011. Compromises between form and function in grid-connected, building-integrated photovoltaics (BIPV) at low-latitude sites. *Building and Environment* 46: 2107-2113.
- [26] C.D. Zomer, M.R. Costa, A. Nobre, R. Rüther, 2013. Performance compromises of building-integrated and building-applied photovoltaics (BIPV and BAPV) in Brazilian airports. *Energy and Buildings* 66: 607–615.



AN APPROACH BASED ON RECURSIVE LARGEST FIRST (RLF) ALGORITHM TO SOLVING THE GRAPH COLORING PROBLEM USING A HYBRID SELECTION STRATEGY

Murat Aslan¹, Yilmaz Atay*²

^{1,2} Department of Computer Engineering, Engineering Faculty, Selcuk University, Konya, Turkey

(murataslan@selcuk.edu.tr, yilmazatay@selcuk.edu.tr)

Corresponding Author's e-mail: yilmazatay@selcuk.edu.tr

ABSTRACT

Graph Coloring Problem (GCP) relates to the coloring the adjacent vertices or edges by different colors using a minimum number of different colors. The objective of the vertex or edge coloring is to color the entire graph without conflicts. Coloring a graph using the least possible number of colors expresses chromatic number for that graph. If the number of vertices or the complexity of the edges connection in a graph increases, the success of reaching the chromatic number will be different for each algorithm. Hence, GCP is known as the NP-hard problem. In this study, we propose an approach based on Recursive Largest First (RLF) algorithm to solving the GCP using a hybrid selection strategy for determining the vertex to be selected for coloring process which obtained from some greedy heuristic algorithms selection strategies. This strategy has been defined by combining the strategies given as the vertex degree, the number of adjacent vertices colored with different colors for every uncolored vertex and the number of uncolored adjacent vertices for every uncolored vertex. The proposed algorithm was tested on some benchmark graphs presented by DIMACS and the results were compared with the Degree of Saturation (DSATUR), RLF, Largest Degree Ordering (LDO), Incident Degree Ordering (IDO), Welsh Powel (WP) and First Fit (FF) algorithms considering executing times and the minimum number of colors algorithms find. The results demonstrated that the proposed algorithm obtained effective results for benchmark graphs presented by DIMACS. As a result, when the experimental results are

taken into consideration, it is understood that the proposed algorithm provides an approach that can be successfully applied to the solution of GCP.

Keywords: *Chromatic number, graph coloring algorithms, graph coloring problem, NP-hard*

1. INTRODUCTION

The problem of graph Coloring (GCP) is a problem that adjacent regions in a map can be colored using at least minimum different colors come up with by Francis Gutrie [1]. GCP is applied to the different real world problems such as frequency assignment problems [2], map-coloring problems [3], timetable scheduling problems [4, 5], Sudoku problem [6], register allocation problems [7] and printed circuit testing problem [8] in recent years. GCP consists of two types of coloring approaches as vertex or edge coloring. The target of these two types of coloring approach is colored whole vertices or edges in a graph using least possible different colors. Naturally, for graph coloring problem, it is expected that if a graph colored correctly it could have no conflict vertices or edges [9].

V is a set of vertices (nodes) and E is a set of edges for an undirected $G = (V, E)$ graph. If a graph is colored using at least a number of different colors provided that adjacent vertices or edges do not receive the same color is called k -colorable graph. It is mean that, if a graph is colored using with k colors, it could not be colored with $(k-1)$ colors [10]. The least number of different colors used for coloring all vertices or edges a graph is called *chromatic number* and it is demonstrated (G).

If the number of vertices or edges in a graph increases, the complexity of the graph also increases. There is a direct relationship between complexity and the number of nodes or edges. Increasing the complexity of the graph makes difficult to color the graph using minimum number of different colors. As a result, it is quite difficult for each algorithm to reach the chromatic number for formed complex graph problems. Because of its complicated nature GCP is known as the Np-hard problem [11]. Researchers are searching for new solutions because of the different approaches are found different solutions for the same problem. In this context, many various algorithms have been proposed in the literature for the solution of GCP. Some of the fastest and most effective algorithms are greedy heuristic algorithms which developed specifically for the GCP. Greedy heuristic algorithms provide a quick solution because they color the nodes with a problem-based approach. However, since greedy heuristics do not provide a general approach for every graph coloring problems, they

could not reach the chromatic number for each problem. Greedy algorithms provide effective solutions for problems with fewer nodes in general. Local search algorithms and metaheuristic algorithms can obtain pretty successful results for the solution of complex graphs [12].

Many different methods have been proposed in the literature for the solution of graph coloring problem. First Fit (FF) [13], Sequential Graph Coloring Heuristic Algorithm (SGCHA) [14], Largest Degree Ordering (LDO) [13], Degree of Saturation (DSATUR) [15], Welsh and Powell (WP) [16], Incidence Degree Ordering (IDO) [13] and Recursive Largest First (RLF) [17] algorithms are some of the greedy heuristic algorithms proposed in the literature for solution of the GCP. Some local search algorithms which have been applied to the GCP are Tabu Search (TS) [18] and Simulated Annealing (SA) [19] algorithms. Genetic Algorithm (GA) [20], Particle Swarm Optimization Algorithm [21], Gravitational Swarm Intelligence (GS) [22], Cultural Algorithm (CA) [14], Shuffled Frog Leaping Algorithm (SFLA) [23] and Cuckoo (COA) Algorithm [12] are some of the metaheuristic algorithms which have been applied to the GCP.

In the scope of this study, we proposed a new approach to making some changes on effective greedy algorithm's RLF. A new selection method called DegreeOfSelection (DegS) has been proposed by combining different selection methods, for the process of selecting the vertex for coloring. Graph Coloring Problem is explained in section 2. In section 3, graph coloring algorithms and the algorithm proposed in this study are detailed. Experimental results are given in section 4 and the last section of this study is contained information about the conclusions and future studies.

2. GRAPH COLORING PROBLEM

For an undirected $G = (V, E)$ graph V is a set of nodes and E is a set of edges. $V = \{v_1, v_2, v_3, v_4, v_5, v_6, v_7, v_8\}$ and $E = \{e_1, e_2, e_3, e_4, e_5, e_6, e_7, e_8, e_9, e_{10}, e_{11}, e_{12}, e_{13}, e_{14}\}$ are vertices and edges of graph is given in Fig. 1.

Adjacent nodes must have least one edge connection between each other. When we examine Fig. 1, we can see that v_3 and v_4 nodes are adjacent nodes, but because of the no edge connection between v_3 and v_8 they are not adjacent nodes. The color set used for coloring nodes of graph G is shown as $C = \{1, 2, \dots, k\}$.

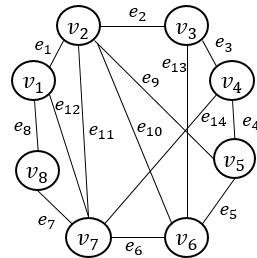


Figure 1. An example graph

In terms of achieving the minimum number of colors for a graph, selection order and color of vertices are very important criteria. If the graph is not colored with a certain coloring strategy, the cost will probably be increased because of unnecessary color have been used. So increased cost is not requested characteristic in Graph coloring. Due to the significance of the color and coloring sequence of the vertex, there are different selection methods proposed in the literature to find a minimum number of different colors for a graph. The degree of vertices is one of the most important feature of vertex selection for coloring process and the degrees of vertices is shown $Deg(v)$. Adjacency matrix is used for calculate the degrees of vertices. Unless otherwise noted, the degree of a vertex is equal to number of adjacent vertices for an undirected and unweighted graph [10]. Eq. 1 is used to create the adjacency matrix for the graph G.

$$Adj = \begin{cases} 1, & \text{there is edge connection between } v_i \text{ and } v_j \\ 0, & \text{there is no edge connection between } v_i \text{ and } v_j \end{cases} \quad (1)$$

The degrees of vertices of the graph given in Fig.1 is shown in Table 1. The adjacency matrix given in Eq. 1 is used to calculate the degrees of vertices.

Table 1. Degrees of vertices

Vertex	v_1	v_2	v_3	v_4	v_5	v_6	v_7	v_8
Deg (v)	3	5	3	3	3	4	5	2

Increasing the number of vertices in a graph or the complexity of the edges connections make it difficult to color the entire graph with least different colors. Therefore to obtain an acceptable solution for complex graphs, the coloring method is being quite important. In the

next section, there will be given information about some graph coloring approaches and the algorithm proposed in this study. Due to every coloring algorithm has a unique coloring approach, the color of the vertices probably will be different for each algorithm.

3. GRAPH COLORING ALGORITHMS

First fit algorithm

The FF algorithm selects the vertices from the first vertex to last vertex in the set of V sequentially and colors the nodes. During the coloring process, tries to give the appropriate color to selected vertex starting from the first color in the set $c = \{1, 2, \dots, k\}$. According to the FF algorithm, the order of the selecting vertices and the colors given to the vertices are given in Fig. 2. s indicates selection order of vertex, v indicates selected vertex and c indicates the color of vertex.

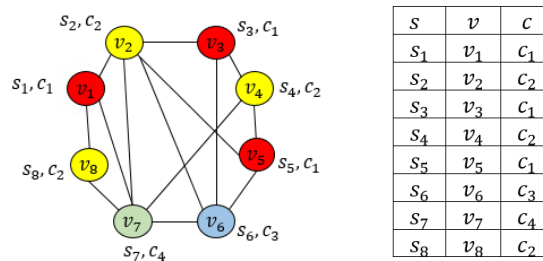


Figure 2. Steps of the FF algorithm

Welsh and Powell algorithm

For each step of the algorithm, the colors in the set of colors given as $c = \{1, 2, \dots, k\}$ are selected as the active color by the sequentially. The following steps are executed while coloring the vertices with the selected color;

Step 1: The uncolored vertex which has most adjacent is colored with the active color.

Step 2: The adjacent vertices of the colored vertex are deleted from the set of vertices because of they cannot be colored with the same color.

Step 3: If there is least one vertex in the set of the vertices can be colored, the uncolored vertex which has most adjacent is colored with the active color and returned to Step 2.

Step 4: If there is least one uncolored vertex is exist, the next color in the color set is selected as the active color and return to Step 1.

The selected order of colored vertices and the colors are given to them are given in Fig 3. While the FF algorithm used 4 colors, the WP algorithm just used 3 colors for the same graph.

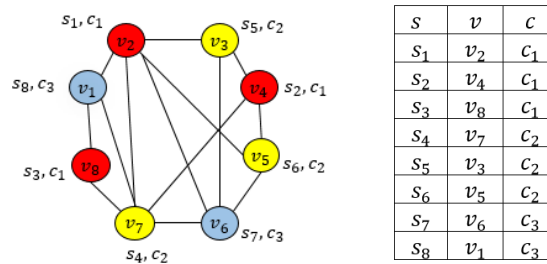


Figure 3. Steps of the Welsh Powell algorithm

Largest degree ordering algorithm

At each step of the algorithm just only one vertex is colored. At the beginning of the algorithm, the degrees of vertices is calculated for every vertex. The degree of every vertex is given in Fig 1 are shown in Table 1. Then, at each step of the algorithm, the uncolored vertex which has the largest degree is selected for coloring process. Take into account the colors of the adjacent of the selected vertex; the appropriate color starting from the first color in the color set $c = \{1, 2, \dots, k\}$ is given to selected vertex. The algorithm is continued to work until all vertices are colored correctly. If the graph is given in Figure 1 is being colored with LDO algorithm, the following results will be obtained.

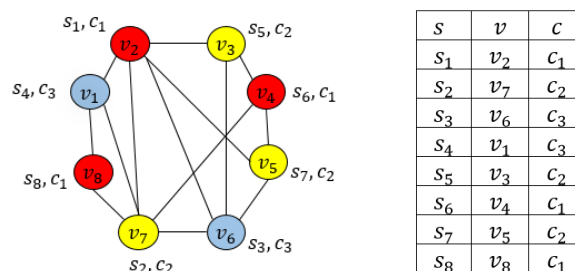


Figure 4. Steps of the LDO algorithm

Incidence degree ordering algorithm

The degree of every uncolored vertex is calculated. Only just one vertex is colored at each step of the algorithm. In the first step, the uncolored vertex which has a maximum number of adjacent is selected and colored with the first color in the color set given as $c = \{1, 2, \dots, k\}$. In the other steps of the algorithm;

Step 1: The uncolored vertex with the largest number of the colored adjacent vertices is selected for the next coloring process. If there is more than one vertex that satisfies this condition, the first vertex in the set of the uncolored vertices with the largest number of the colored adjacent vertices with the highest degree from those vertices is selected for coloring.

Step 2: The first appropriate color (except adjacent vertices colors) in the color set is given to selected vertex.

Step 3: If there is least one uncolored vertex in graph, go to Step 1. If not, the algorithm is terminated.

The colors of colored vertices and the selecting order of them are given in Fig. 5 for IDO algorithm.

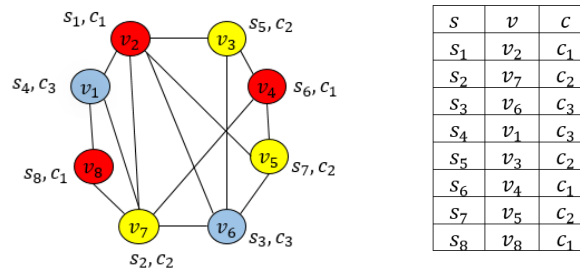


Figure 5. Steps of the IDO algorithm

Degrees of saturation algorithm

The degrees of every uncolored vertex are calculated. Only just one vertex is colored at each step of the algorithm. For the first step, the uncolored vertex which has a maximum number of adjacent is selected and colored with the first color in the color set given as $c = \{1, 2, \dots, k\}$. In the other steps of the algorithm;

Step 1: The uncolored vertex with the largest number of colored adjacent vertices which colored with a different color is selected for the next coloring process. If there is more than one vertex that satisfies this condition, the first vertex of the highest degree from those vertices is selected for coloring.

Step 2: The first appropriate color (except adjacent vertices colors) in the color set is given to selected vertex.

Step 3: If there is least one uncolored vertex, go to Step 1. If not, the algorithm is terminated.

If DSATUR algorithm is used for the graph which is given Fig. 1, the results obtained from DSATUR are shown in Fig. 6.

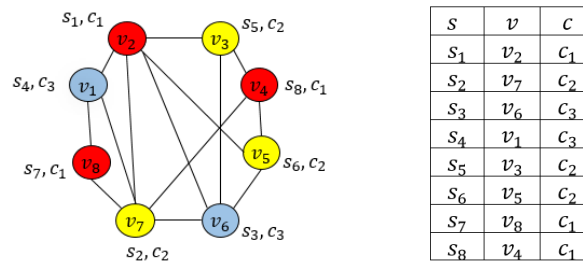


Figure 6. Steps of the DSATUR algorithm

4.1. Recursive largest first algorithm

For each step of the algorithm, the colors in the set of colors given as $c = \{1, 2, \dots, k\}$ are selected as the active color by the sequentially. The aim of RLF is to use the same color for coloring maximum number of different vertices. Thus, when all vertices are colored, the minimum number of different colors will be used. The following steps are executed while coloring the vertices with the selected color;

Step 1: The uncolored vertex that has the largest degree is selected.

Step 2: The selected vertex is colored with the active color. Then, in order to determine the vertices which can be colored with the same color, the selection strategy proposed in RLF is applied as follows;

S1: For the coloring process, vertices that are adjacent to the colored vertex are being found from the adjacency matrix ($U = \{u_1, u_2, \dots, u_t\}$). And also, non-adjacent vertices of the colored vertex are being found too (V').

S2: All vertices in the set of V' are be visited. And then, the number of adjacent vertices for each vertex in V' with vertices in U are be calculated. The uncolored vertex that has the largest adjacent vertices in V' with vertices in U is to colored with active color.

S3: The colored vertex and its adjacent vertices are deleted from the set V' and added to the set U .

S4: If the set of V' is not empty, then go to S2.

Step 3: If there is least one uncolored vertex is exist, the next color in the color set is selected as the active color and return to Step 1. If not, the algorithm is terminated. The Steps of the RLF algorithm and the results obtained from RLF are shown in Fig. 7.

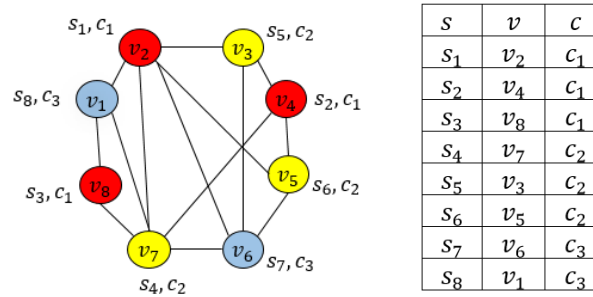


Figure 7. Steps of the RLF algorithm

Proposed algorithm

The proposed algorithm in this study based on RLF strategy. Some changes have been made in Step 1 and Step 2 of the RLF algorithm. A new strategy for vertex selection has been proposed. The proposed vertex selection strategy is as follows;

- An array named *DegreeOfSelection* ($DegS$) is defined for calculate the selection probability of every uncolored vertices for coloring.
- The initial value for each vertex in $DegS(v)$ is set to 0.
- The vertex degree of each vertex in the set $DegS(v)$ is calculated and then the $DegS(v)$ value of the vertex or vertices with the largest vertex degree is increased by one.
- The $DegS(v)$ value of the vertices with the largest number of uncolored adjacent vertices is increased by one.
- The $DegS(v)$ value of the every uncolored vertex which has the largest number of adjacent vertices with colored in different colors is increased by one.

Thus, the $DegS(v)$ values of vertices are being calculated for select the vertex for coloring. The modification for Step 1 of RLF is as follows; In the original RLF, the "vertex with the largest vertex degree" is selected for the coloring. But, in proposed algorithm, only for the first coloring process the uncolored vertex with the largest vertex degree is selected for coloring. When Step 1 is run again in algorithm, the uncolored vertex which $DegS(v)$ value is the largest is selected for coloring.

The second modification in the algorithm is made on S2 of step 2. Normally in RLF, in step S2 the vertex with the largest adjacent vertices in V' is colored with the active color. In the

proposed algorithm, in the case that there are more than one vertices that satisfy this condition; the $DegS(v)$ values for the vertices with the largest adjacent vertices in V' are calculated. Then the vertex with the least $DegS(v)$ value is selected for coloring.

Only two changes have been made in the working steps of the RLF algorithm. The obtained results are detailed in the next section. The proposed algorithm is applied to the graph given in Fig. 1. The results obtained from Proposed Algorithm (PA) are shown in Fig. 8.

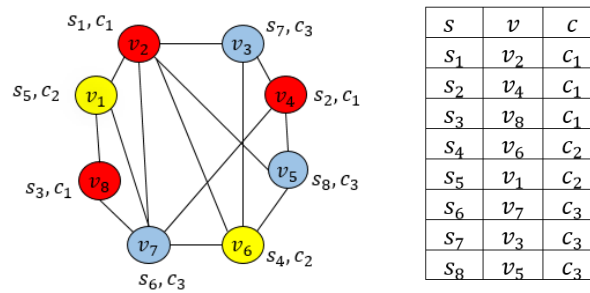


Figure 8. Steps of the proposed algorithm

4. EXPERIMENT RESULTS

The algorithm proposed in this study and other graph coloring algorithms have been tested on some benchmark graphs proposed by DIMACS [24]. All algorithms were tested under the same conditions. DIMACS graphs are important to compare algorithms to find that which algorithm is better for coloring. The obtained results from DSATUR, RLF, LDO, IDO, WP, FF and Proposed Algorithm were compared with time in second and minimum color number. The algorithms are written and run in Matlab 2010a. For experiments we used a computer has Intel i7 2.60 GHz processor and 24 GB DDR3 RAM. The DIMACS Benchmark graphs used for experiments in this study are given in Table 2. The *graph* column shows the number of the graph, *Name* column related graph name, *V* is number of vertices, *E* is number of edges, *Density* column shows density of edges, $\chi(G)$ indicates the chromatic number or the best known result of the graph.

Table 2. Benchmark graphs used in experiments (* means that chromatic number is unknown).

Graph	Name	V	E	Density	$\chi(G)$	Graph	Name	V	E	Density	$\chi(G)$
G1	DSJC125.1*	125	736	0,09	5	G19	queen10_10*	100	2940	0,59	11

G2	DSJC125.5*	125	3891	0,50	17	G20	queen11_11	121	3960	0,55	11
G3	DSJC125.9*	125	6961	0,89	44	G21	queen12_12*	144	5192	0,50	13
G4	DSJC250.1*	250	3218	0,10	8	G22	queen13_13	169	6656	0,47	13
G5	DSJC250.5*	250	15668	0,50	28	G23	queen14_14*	196	8372	0,44	16
G6	DSJC250.9*	250	27897	0,03	72	G24	queen15_15*	225	10360	0,41	16
G7	r125.1	125	209	0,03	5	G25	flat300_20	300	21375	0,48	20
G8	r125.1c	125	7501	0,97	46	G26	flat300_26	300	21633	0,48	26
G9	r125.5	125	3838	0,50	36	G27	flat300_28	300	21695	0,48	28
G10	r250.1	250	867	0,03	8	G28	le450_5c	450	9803	0,10	5
G11	r250.1c	250	30227	0,97	64	G29	le450_5d	450	9757	0,10	5
G12	miles750	128	2113	0,26	31	G30	le450_15b	450	8169	15	15
G13	miles1000	128	3216	0,40	42	G31	le450_25a	450	8260	0,08	25
G14	miles1500	128	5198	0,64	73	G32	le450_25b	450	8263	0,08	25
G15	queen6_6	36	290	0,4	7	G33	fpsol2.i1	496	11654	0,09	65
G16	queen7_7	49	476	0,40	7	G34	fpsol2.i2	451	8691	0,09	30
G17	queen8_8	96	1368	0,30	9	G35	fpsol2.i3	425	8688	0,10	30
G18	queen9_9	81	1056	0,33	10						

DSJC series graphs created by David Johnson are known difficult Benchmark graphs [12]. The *DSJC125.5* graph is an example of a random graph. The first parameter (125) of this graph is indicates the number of vertices number, and the second value (5) indicates that the edge density is 50%. *r125* and *r250* graphs are random geometric graphs created by Michael Trick [25]. On *Leighton* graphs, the number of vertices is equal to 450 and *le450_5c* is a one of the *Leighton* graph. The first parameter of this graph shows the number of vertices and the second parameter shows the chromatic number of this graph [17]. *Miles* graphs were created by Donald Knuth to show cities within a specific area of the US map. *Miles* graphs were created by drawing an edge between two cities located at a certain distance [26, 27]. *Queen* graphs are known chessboard graphs. On the *Queen's* graphs, the selected vertex is adjacent with the vertex in same row, column or diagonal. So selected vertex can not take the color of the vertex in same row, column or diagonal [27]. The *fpsol* graphs are graphs of the register allocation problem that created by Gary Lewandowski [25]. *Flat* graphs are created by Culberson and in flat graphs, the first parameter is the number of vertices and the second parameter is the chromatic number [19].

Table 3. The number of minimum colors found by the algorithms

Graph	$\chi(G)$	PA	RLF	DSATUR	WP	IDO	LDO	FF	Graph	$\chi(G)$	PA	RLF	DSATUR	WP	IDO	LDO	FF
G1	5	6	6	6	7	7	7	8	G19	11	13	13	14	17	17	17	16
G2	17	20	21	22	23	25	23	26	G20	11	14	14	15	17	18	17	17
G3	44	47	49	51	53	54	53	56	G21	13	15	15	16	19	20	19	20
G4	8	10	10	10	11	12	11	13	G22	13	16	16	17	23	22	23	21
G5	28	34	35	37	41	40	41	43	G23	16	17	17	19	25	24	25	23
G6	72	83	84	92	93	95	93	99	G24	16	18	18	21	25	26	25	25
G7	5	5	5	5	5	5	5	5	G25	20	37	38	42	44	45	44	47
G8	46	47	47	46	47	48	47	51	G26	26	38	39	41	45	48	45	45
G9	36	39	38	38	39	39	39	44	G27	28	39	38	42	45	48	45	46
G10	8	8	8	8	8	8	8	9	G28	5	5	5	10	12	12	12	17
G11	64	65	67	65	68	67	68	76	G29	5	5	6	12	14	13	14	18
G12	31	31	31	31	32	31	32	34	G30	15	16	17	16	18	18	18	22
G13	42	42	42	42	43	43	43	44	G31	25	25	25	25	26	25	26	28
G14	73	73	73	73	73	73	73	76	G32	25	25	25	25	25	25	25	27
G15	7	8	8	9	9	10	9	11	G33	65	65	65	65	65	65	65	65
G16	7	9	9	11	12	12	12	10	G34	30	30	30	30	30	30	30	30
G17	9	10	11	12	13	15	13	13	G35	30	30	30	30	30	30	30	30
G18	10	12	12	13	15	15	15	16									

The number of colors that the algorithms find for each graph are given in Table 3 and computation time in seconds for this algorithm are given in Table 4. All algorithms reach chromatic numbers for *fpsol2* and *r125* graphs. When Table 4 is examined it is seen that WP algorithm is the fastest algorithm that finds the results. However, it is seen that WP algorithm has not found the chromatic number for many graphs. 35 benchmark graphs were used in the experiments. But, Wp algorithm just finds the chromatic number of 7 graphs which used in the experiments. The second fastest algorithm is the FF algorithm. Yet, the most inefficient algorithm among these algorithms is the FF algorithm. It has found the chromatic numbers for just 4 graphs. For other graphs, FF is generally found the number of color far from chromatic

numbers. The LDO algorithm is also one of the algorithms that find the results quickly. However, the LDO algorithm has reached the chromatic number for only 7 graphs. The IDO algorithm has reached chromatic numbers for 9 graphs. But, when running times in seconds are examined it is slower than Wp, RLF, FF and LDO algorithms. When Table 3 is analysed, it is seen that the DSATUR algorithm obtained quite successful results for 16 graphs. On the other hand, when Table 4 is analysed, it is understood that DSATUR algorithm is the slowest algorithm among these algorithms if the algorithms compared each other about competition times. For *r125.1c* graph, only DSATUR algorithm has reached $\chi(G)$. When algorithms are evaluated in terms of competition times and performance, the RLF algorithm is quite successful. RLF generally finds the chromatic numbers or near to chromatic numbers for test graphs. RLF has found successful results for 24 test graphs. No algorithm has found the chromatic number for the *queen* graphs. However, if Table 3 is analyzed it is realized that RLF algorithm and PA generally find out the best results. According to Table 3, it is understood that the PA finds out the best results for 32 test graphs if PA is compared with the other graph coloring algorithms. PA is not very fast algorithm when it's competition time is analyzed according to the Table 4. In addition, PA just only faster than DSATUR algorithm. The main reason why PA running slow when it is compared the other graph coloring algorithms is due to need more calculations for the process of determining the vertex to be selected for the coloring. No algorithm has reached $\chi(G)$ for *queen8_8*. But, PA is obtained the best results among of the algorithms which used in this study. According to Table 3, the best results for *le450* graphs are obtained from the PA. When all experimental results are evaluated together, it is seen that the most successful algorithm among these algorithms is the proposed algorithm in this study.

Table 4. The competition time in seconds for algorithms

Graph	PA	RLF	DSATUR	WP	IDO	LDO	FF	Graph	PA	RLF	DSATUR	WP	IDO	LDO	FF
G1	0,0355	0,0096	0,0445	0,0008	0,0202	0,0031	0,0018	G19	0,0423	0,0056	0,2388	0,0004	0,1585	0,0034	0,0030
G2	0,1009	0,0094	0,3795	0,0006	0,2797	0,0070	0,0064	G20	0,0700	0,0067	0,3790	0,0005	0,3438	0,0052	0,0051
G3	0,3238	0,0091	0,8916	0,0014	0,6657	0,0122	0,0110	G21	0,1101	0,0095	0,5768	0,0006	0,4772	0,0073	0,0065
G4	0,1409	0,0319	0,2815	0,0006	0,2198	0,0093	0,0074	G22	0,1479	0,0133	0,8133	0,0008	0,6626	0,0110	0,0103
G5	0,6842	0,0257	3,0125	0,0014	2,1033	0,0277	0,0280	G23	0,2179	0,0197	1,2280	0,0010	0,9793	0,0138	0,0122
G6	2,5448	0,0100	7,7768	0,0024	5,8030	0,0591	0,0579	G24	0,3105	0,0251	1,5767	0,0014	1,3685	0,0163	0,0161
G7	0,0827	0,0110	0,0223	0,0003	0,0165	0,0036	0,0022	G25	1,3339	0,0357	4,8681	0,0021	3,5845	0,0405	0,0416
G8	0,3792	0,0112	0,9970	0,0019	0,8333	0,0119	0,0127	G26	1,4203	0,0359	5,0414	0,0018	3,7282	0,0404	0,0404
G9	0,1700	0,0049	0,3696	0,0008	0,3175	0,0077	0,0075	G27	1,4154	0,0357	5,0572	0,0018	3,6039	0,0465	0,0407
G10	0,1519	0,0380	0,0524	0,0010	0,0326	0,0053	0,0033	G28	0,8128	0,1240	1,4864	0,0018	0,9637	0,0267	0,0265
G11	2,3824	0,0067	8,8824	0,0019	8,0142	0,0495	0,0522	G29	0,8110	0,1193	1,4355	0,0028	0,9814	0,0287	0,0260
G12	0,1161	0,0081	0,4499	0,0008	0,2973	0,0067	0,0062	G30	0,6575	0,0924	1,1130	0,0019	0,7351	0,0309	0,0249
G13	0,2215	0,0064	0,8157	0,0012	0,5640	0,0093	0,0094	G31	0,7528	0,0753	1,1708	0,0017	0,7743	0,0313	0,0250
G14	0,5738	0,0067	1,6821	0,0025	1,2087	0,0169	0,0166	G32	0,8231	0,0855	1,1462	0,0018	0,7805	0,0282	0,0268
G15	0,0082	0,0015	0,0366	0,0002	0,0169	0,0007	0,0007	G33	4,9318	0,1171	1,9623	0,0032	1,3161	0,0484	0,0377
G16	0,0105	0,0016	0,0602	0,0003	0,0310	0,0011	0,0010	G34	2,0915	0,0651	1,2621	0,0015	0,8170	0,0352	0,0311
G17	0,0187	0,0033	0,0894	0,0003	0,0638	0,0018	0,0012	G35	1,9559	0,0584	1,2676	0,0018	0,8601	0,0337	0,0296
G18	0,0350	0,0035	0,1495	0,0005	0,0926	0,0028	0,0024								



5. CONCLUSION AND DISCUSSION

The obtained results showed that the proposed algorithm finds out acceptable results for the solution of benchmark graphs presented by DIMACS. According to the experimental results, the proposed algorithm is a feasible approach for the GCP. PA is more successful than the other algorithms when the performance of greedy algorithms is evaluated about the find the minimum colors for graphs. According to the experimental results, it is understood that PA is quite successful in terms of competition times and performance. However, the disadvantage of PA is run slower when compared to RLF. When PA's results for Benchmark graphs are evaluated, it can be concluded that PA can be applied to real world problems. PA generally is found the chromatic numbers for test graphs. The performance of the PA can be improved in subsequent studies.

REFERENCES

- [1] Fritsch, R. and G. Fritsch, *The Four-Color Theorem: History, Topological Foundations, and Idea of Proof*, translated by J. Peschke. 1998, Springer.
- [2] Hale, W.K., *Frequency assignment: Theory and applications*. *Proceedings of the IEEE*, 1980. 68(12): p. 1497-1514.
- [3] Gwee, B.-H., M.-H. Lim, and J.-S. Ho. *Solving four-colouring map problem using genetic algorithm*. in *ANNES*. 1993.
- [4] Chmait, N. and K. Challita, *Using Simulated Annealing and Ant-Colony Optimization Algorithms to Solve the Scheduling Problem*. *Computer Science and Information Technology*, 2013. 1(3): p. 208-224.
- [5] Dowsland, K. and J. Thompson, *Ant colony optimization for the examination scheduling problem*. *Journal of the Operational Research Society*, 2005. 56(4): p. 426-438.
- [6] Ono, S., et al. *Difficulty estimation of number place puzzle and its problem generation support*. in *ICCAS-SICE, 2009*. 2009. IEEE.
- [7] Chow, F.C. and J.L. Hennessy, *The priority-based coloring approach to register allocation*. *ACM Transactions on Programming Languages and Systems (TOPLAS)*, 1990. 12(4): p. 501-536.
- [8] Garey, M., D. Johnson, and H. So, *An application of graph coloring to printed circuit testing*. *IEEE Transactions on circuits and systems*, 1976. 23(10): p. 591-599.



- [9] Gross, J.L. and J. Yellen, Graph theory and its applications. 1998: CRC press.
- [10] West, D.B., Introduction to graph theory. Vol. 2. 2001: Prentice hall Upper Saddle River.
- [11] Garey, M.R. and D.S. Johnson, Computers and Intractability: A Guide to the Theory of NP-completeness. 1979, WH Freeman and Company, New York.
- [12] Mahmoudi, S. and S. Lotfi, Modified cuckoo optimization algorithm (MCOA) to solve graph coloring problem. Applied soft computing, 2015. 33: p. 48-64.
- [13] Al-Omari, H. and K.E. Sabri, New graph coloring algorithms. American Journal of Mathematics and Statistics, 2006. 2(4): p. 739-741.
- [14] Abbasian, R., M. Mouhoub, and A. Jula. Solving Graph Coloring Problems Using Cultural Algorithms. in FLAIRS Conference. 2011.
- [15] Brélaz, D., New methods to color the vertices of a graph. Communications of the ACM, 1979. 22(4): p. 251-256.
- [16] Welsh, D.J. and M.B. Powell, An upper bound for the chromatic number of a graph and its application to timetabling problems. The Computer Journal, 1967. 10(1): p. 85-86.
- [17] Leighton, F.T., A graph coloring algorithm for large scheduling problems. Journal of research of the national bureau of standards, 1979. 84(6): p. 489-506.
- [18] Blöchliger, I. and N. Zufferey, A graph coloring heuristic using partial solutions and a reactive tabu scheme. Computers & Operations Research, 2008. 35(3): p. 960-975.
- [19] Yilmaz, B., A novel meta-heuristic for graph coloring problem: simulated annealing with backtracking, in The graduate school of natural and applied science. 2011, Yeditepe University: The graduate school of natural and applied science, İstanbul.
- [20] Glass, C.A. and A. Prügel-Bennett, Genetic algorithm for graph coloring: exploration of Galinier and Hao's algorithm. Journal of Combinatorial Optimization, 2003. 7(3): p. 229-236.
- [21] Agrawal, J. and S. Agrawal, Acceleration Based Particle Swarm Optimization for Graph Coloring Problem. Procedia Computer Science, 2015. 60: p. 714-721.
- [22] Ruiz, I.R. and M.G. Romay, Gravitational swarm approach for graph coloring, in Nature Inspired Cooperative Strategies for Optimization (NICSO 2011). 2011, Springer. p. 159-168.



- [23] Aslan, M., An approach based on shuffled frog leaping algorithm for vertex coloring problem in graphs, in The graduate school of natural and applied science. 2017, Selcuk University: The graduate school of natural and applied science, Konya.
- [24] Trick, M. Graph Coloring and its Generalizations. 2017 Access Date: 15 May 2017]; Available from: <http://mat.gsia.cmu.edu/COLOR08/INSTANCES/>.
- [25] Johnson, D.S. and M.A. Trick, Cliques, coloring, and satisfiability: second DIMACS implementation challenge, October 11-13, 1993. Vol. 26. 1996: American Mathematical Soc.
- [26] Knuth, D.E., The Stanford GraphBase: a platform for combinatorial computing. Vol. 37. 1993: Addison-Wesley Reading.
- [27] Mehrotra, A. and M.A. Trick, A column generation approach for graph coloring. *informatics Journal on Computing*, 1996. 8(4): p. 344-354.



EFFECT OF SURFACE ROUGHNESS ON WETTABILITY OF ADHESIVE ON WOOD SUBSTRATES

H. Yorur*¹, A. M. Erer² and S. Oğuz³

¹ Huseyin YORUR' Forest Faculty, Karabük University, TURKEY.

(E-mail: huseyinyorur@karabuk.edu.tr)

² A. Mustafa ERER' Science Faculty, Karabük University, TURKEY.

(E-mail: merer@karabuk.edu.tr)

³ Serkan OĞUZ' Science Faculty, Karabük University, TURKEY.

(E-mail: soguz78@gmail.com.tr)

Corresponding Author's e-mail: huseyinyorur@karabuk.edu.tr

ABSTRACT

In this study, the relationship between the surface roughness and the wettability of adhesive were investigated at room temperature on wood substrates (Pine, Beech and Fir). Wood substrates was prepared (longitudinal, radial and tangential surface directions). All the substrates were conditioned at 20±2 °C and 65±5% relative humidity. To measure the surface roughness of wood substrates, the Mitutoyo SJ301 surface roughness measuring device was used. Contact angles of adhesive were measured by using of the sessile drop method. As a result, it was observed that the wetting angle decreased with increasing surface roughness. Thus, the wettability of surfaces observed that strongly affected by surface roughness.

Keywords: Wettability, Contact angle, Surface roughness, Wood substrate, Surface direction

1. INTRODUCTION

It is very important to relate to the surface of the materials used for adhesive and top surface treatment for joining and protecting the wood materials used in the industry. Wood material has hygroscopic and anisotropic structure. Due to its anisotropic structure, the behaviors it shows in the direction of longitudinal, radial and tangent are different. Wetting and surface roughness are among the most important factors affecting properties of these related materials such as adhesion, impregnation and surface treatment.

Wettability is often evaluated by measuring the contact angle of a droplet on various substrates [1]. The wettability of a liquid in contact with a surface material plays a crucial role in many industrial implement, such as adhesion, coating and painting. To evaluate the wettability, the simplest and most common method is contact angle measurements on substrates [2]. The wettability can be influenced by various parameters such as porosity, surface roughness, heterogeneity and wood surface direction, etc. [3]. The effect of surface roughness on wettability have been studied by many researchers; Erer, Mantanis, Piao, Büyüksarı [4, 5, 6, 7]. Thus, the measurement of contact angel gives a prediction on wetting behavior. To determine the wettability of wood substrates by PVAc glue, young's equation is conventionally is used;

$$\theta = \frac{\gamma_{sg} - \gamma_{sl}}{\gamma_{lg}} \quad (1)$$

where γ_{sg} , γ_{sl} and γ_{lg} are the interfacial tensions, θ is contact angle in degree [8].

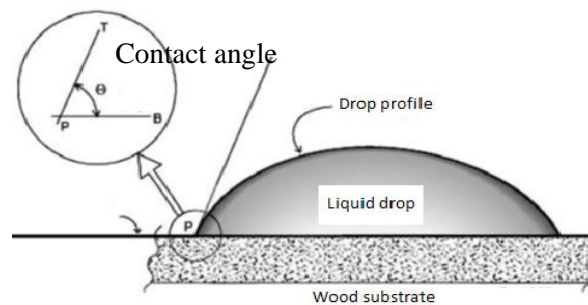


Figure 1. Profile of drop

Figure 1. Liquid drop section [4]

Young's equation is suitable for an ideal surface, which is flat, perfectly smooth and chemically homogeneous [9]. For a rough and nonideal surface (Fig 2), the true wetting area is greater than its geometric area, and wetting properties of the surface are directly proportional to surface roughness [10]. The relationship between surface roughness and wettability was described already in 1936 by Wenzel who specified that adding surface roughness will increase the wettability caused by the chemistry of the surface [10].

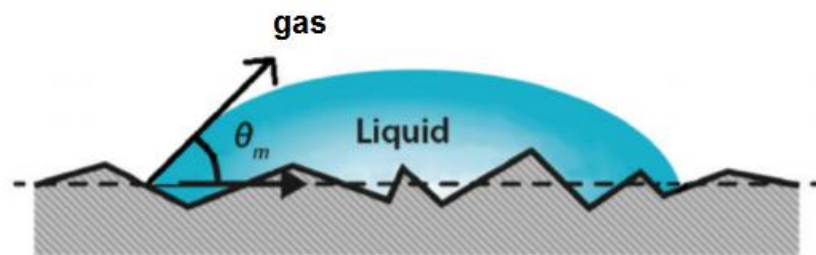


Figure 2. Apparent or measured contact angle on rough (Wenzel) surface [11]

Consequently, contact angle on a rough surface is different from the contact angle on an ideal surface, it is called the apparent contact angle. According to be hydrophilicity (<90) or hydrophobicity (>90), the apparent contact angle of a rough solid surface is either smaller or greater than the contact angle of the ideal system [12]. On a hydrophilic surface such as wood, more roughness often means a larger surface area for liquid to spread [6].

2. MATERIAL AND METHODS

In this study, PVAc basis glue (Concentration: 1.1 g / cm³, viscosity: 13,000 - 17,000 mPa.s, pH value at 20°C: 2,8) and air dried(65% relative humidity) and cut at various surface direction (Longitudinal, tangential and radial) wood substrate (Scotch Pine, Oriental Beech and Uludağ Fir) were chosen to measure the contact angle with sessile drop technique. By means of this technique, PVAc basis glue was dropped on wood substrate at room temperatures. Dynamic contact angle measurements were made with on 50(width) x 50(length) x 10(height) mm samples of wood. Casio Pro EX-F1 (1200 fps) Model camera used to catch views of drops at the 5th, 10th, 15th, 30th, 60th, 90th, 120th, and 150th seconds and these images were transferred into AutoCAD 2010 to measure contact angles of each drop from the right and left profiles. As a result of these processes repeated three times for room temperature, mean angle values were calculated and new diagrams were drawn through the Sigma Plot 12.0 Software. For measuring the surface roughness of wood substrates, according to DIN 4768 standard [13] by using stylus type profilometer the Mitutoyo SJ-301 surface roughness measuring device was used. For the surface roughness measurement, the

needle scanning length was selected as 4 mm and the scanning speed as 0.5 mm/s. Measurements were applied perpendicular to the fiber direction. Ten samples were used from each group for the Surface roughness measurements. The arithmetical average of surface roughness(Ra) and maximum roughness(Ry) values were determined.

3. RESULTS AND DISCUSSION

Experimental investigation of the wettability of wood surfaces has been performed by sessile drop technique. Surface roughness influence on the wetting properties has been evaluated by contact angle measurement analysis. Values of measured contact angle can be strongly affected by the surface roughness [14].

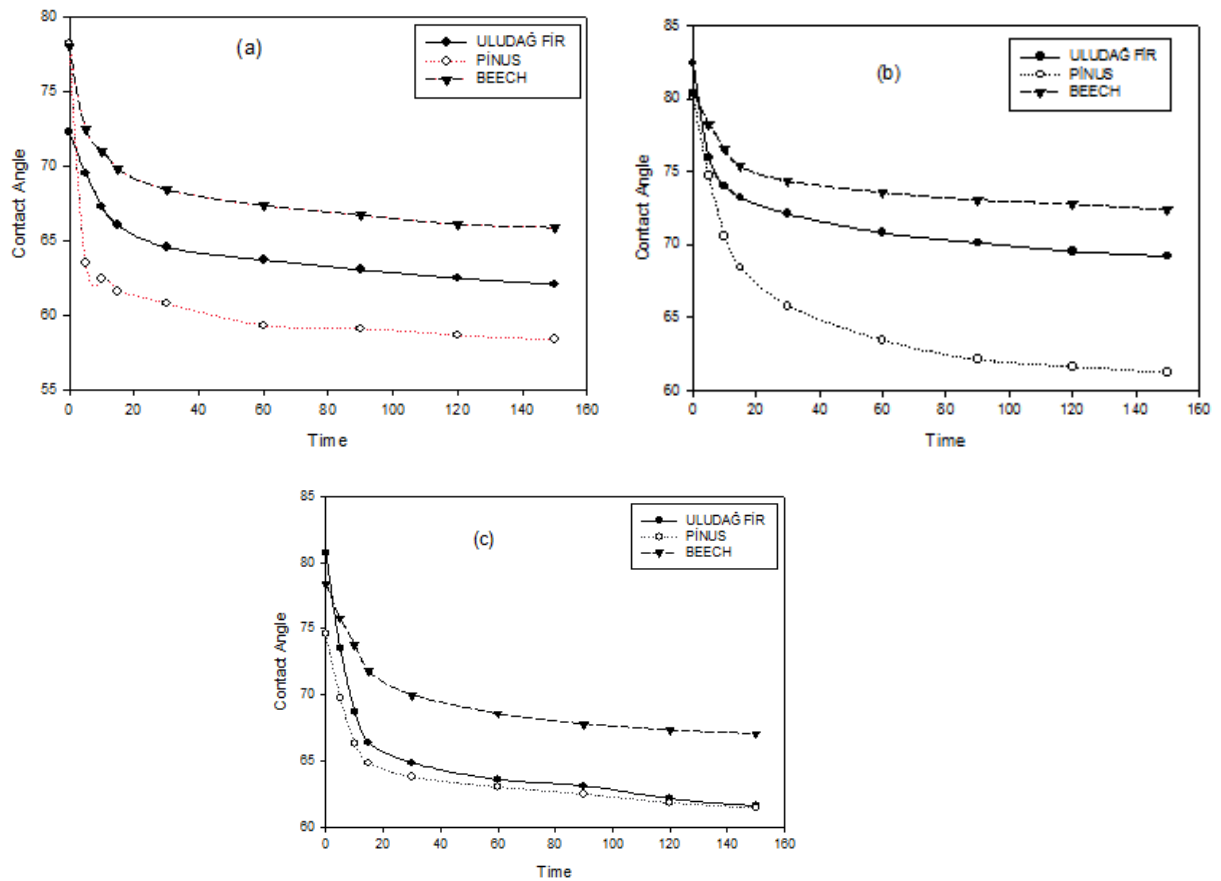


Figure 3. Time dependence of the contact angle of PVAc glue on wood substrates at various surface directions for (a) Tangential, (b) Radial and (c) Longitudinal.

According to the contact angle measurement results; Fig.3 (a-c) exhibit the relationship between the contact angle and the time at room temperature that the contact angle decreases with time exponentially for all surface directions and substrates. The values of contact angle show the degree of wettability [15]. Figure 4 shows the relationship between contact angle surface roughness for three surface directions and air-dried wood substrates which are Fir, Beech and Pine.

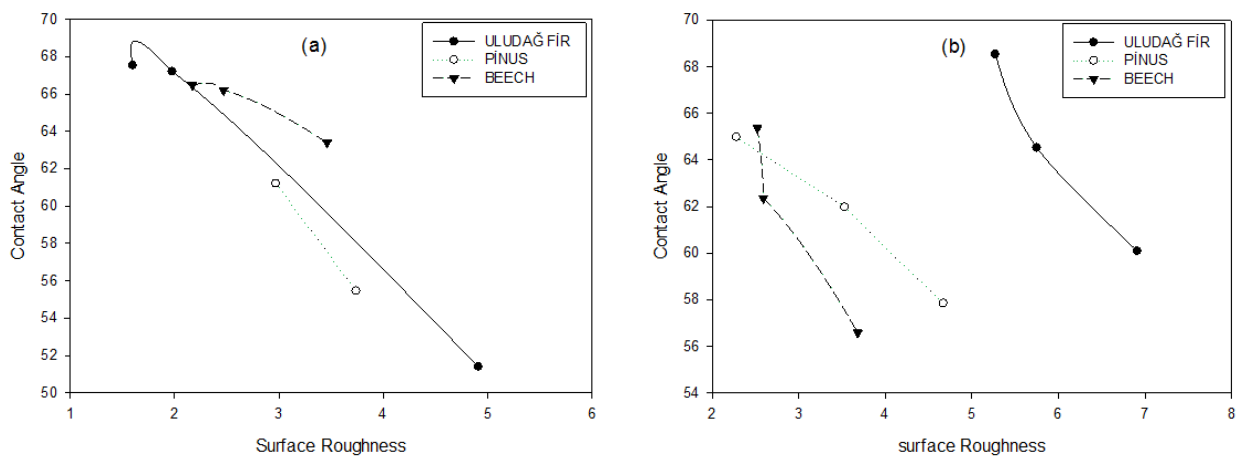


Figure 4. The change in the contact angle values with the surface roughness at various surface directions for (a) Tangential, (b) Radial.

For all directions in wood surface, a decrease in contact angle was observed with increasing surface roughness. According to these results, the effect of the surface roughness on the contact angle was determined.

5. CONCLUSION

6.

Accordingly, the contact angle values decrease while the surface roughness values increase.

From the presented studies, the following conclusions can be produced;

- 1- Roughness has a strong influence on wettability of wood surface.
- 2-Similar influence of surface roughness has been found for different tested wood substrate (Pine, Beech and Fir).



3-The data obtained from experimental studies were tested both surface direction (Tangential, Radial and Longitudinal) and wood type (Pine, Beech and Fir) and a strong agreement was observed between the results.

ACKNOWLEDGMENT

(This work was supported by Scientific Research Projects Coordination Unit of Karabük University. Project Number: KBÜ/BAP-17-YD-349).

REFERENCES

- [1] S.Q. Shi, D.J. Gardner, 2001. Dynamic adhesive wettability of wood. *Wood Fiber Sci* 33(1):56-68.
- [2] K.L. Mittal, (Ed.) 2006. *Contact angle, wettability and adhesion* (Vol. 4). CRC Press.
- [3] T.F. Shupe, C.Y. Hse, E.T. Choong, L.H. Groom, 1998. Effect of wood grain and veneer side on loblolly pine veneer wettability. *Forest Prod J* 48(6):95-97.
- [4] A.M. Erer, 2011. *Investigations of the wetting properties of binary lead free solder alloy(Sn-Ag) system on Cu substrate*, PhD Thesis, Department of Physics, Graduate School of Natural and Applied Sciences, Bülent Ecevit University, Turkey.
- [5] G. I. Mantanis, R.A. Young, 1997. Wetting of wood. *Wood science and Technology*, 31(5), 339-353.
- [6] C. Piao, J.E Winandy, T.F. Shupe, 2010. From hydrophilicity to hydrophobicity: A critical review: Part I. Wettability and surface behavior. *Wood and Fiber Science*, 42(4), 490-510.
- [7] Ü. Büyüksarı, T. Akbulut, C.Guler, N. As, 2011. Wettability and surface roughness of natural and plantation-grown narrow-leaved ash (*Fraxinus angustifolia* Vahl.) wood. *BioResources*, 6(4), 4721-4730.
- [8] H.Y. Erbil, 2006. *Surface chemistry of solid and liquid interfaces*. Blackwell, Oxford.



- [9] A. Marmur, 2009. Solid-surface characterization by wetting. *Annu Rev Mater Res* 39:473-489.
- [10] R.N. Wenzel, 1936. “Resistance of solid surfaces to wetting by water”, *Industrial and engineering chemistry* 28 988.
- [11] A. Marmur, 2006. “Soft contact: Measurement and interpretation of contact angles”, *Soft Matter* 2 12.
- [12] T. Onda, S. Shibuichi, N. Satoh, K. Tsujii, 1996. Super-water-repellent fractal surfaces. *Langmuir*, 12(9), 2125-2127.
- [13] Dln 4768, 1990. *Determination of values of surface roughness parameters Ra, Rz, Rmax using electrical contact instruments, concepts and measuring conditions*, Deutsches Institut für Norming, Berlin, Germany.
- [14] K.J. Kubiak, M.C.T Wilson, T. G. Mathia, P. Carval, 2011. Wettability versus roughness of engineering surfaces. *Wear*, 271(3), 523-528.
- [15] L. Zang, Z. Yuan, H. Xu, and B. Xu, 2011. Wetting process and interfacial characteristic of Sn–3.0 Ag–0.5 Cu on different substrates at temperatures ranging from 503K to 673K. *Applied Surface Science*, 257(11), 4877-4884.



Classification of Bread and Durum Wheat Using ELM and ANN

K. Sabanci*, M. F. Aslan, E. Yigit, A. Kayabasi, A. Toktas, H. Duysak

Karamanoğlu Mehmetbey University, Engineering Faculty, Department of Electrical and Electronics Engineering, TURKEY

(kadirsabanci@kmu.edu.tr, mfatihhaslan@kmu.edu.tr, enesyigit@kmu.edu.tr, ahmetkayabasi@kmu.edu.tr, atoktas@kmu.edu.tr, huseyinduysak@kmu.edu.tr)

Corresponding Author's e-mail: kadirsabanci@kmu.edu.tr

ABSTRACT

Wheat is the most important food source in the worldwide. Classification of wheat grains is very important in terms of quality, health and cost. In this study, classification of two types wheat grains into bread and durum was carried out. Number of the wheats used in classification is 200. The species of wheat grains in this dataset are bread and durum and these species have equal samples in the dataset as 100 instances. Seven features, including width, height, area, perimeter, roundness, width and perimeter/area, were extracted from each wheat grains. For training and testing data, these seven features were used as input. Classification was conducted by Artificial Neural Network (ANN) and Extreme Learning Machine (ELM) artificial intelligence techniques. Then the performances of models are compared. The dataset was divided into two group as training and testing with the ratio of 70% and 30%. The program is written in Matlab GUI environment. High accuracy values were obtained with both these methods. As a result of the study, the accuracy of training was calculated as 97.14% for training, 1.3 seconds for training duration and 97.89% for testing accuracy. These values were calculated for ELM, the training accuracy rate was 93.57%, the training duration was 0.0575 seconds and the testing accuracy rate was 96.79%. As it is clear from the values, the accuracy values of both models are close to each other.

Keywords: Artificial Neural Network, Classification, Extreme Learning Machine, Wheat Grains



1. INTRODUCTION

Wheat is the most important food source around the worldwide. It is a basic nutrient used in the production of flour and fodder. It is one of the most basic foodstuffs for people to feed. And it is the raw material of bread and macaroni. In terms of planting area and production amount in Turkey, wheat is the most prevalent feeder [1]. On average 40% of Turkey's daily food needs are covered by wheat products [2]. Therefore, wheat is an important food source in terms of production and consumption. Studies on the quality and cost of wheat are of great importance. For the production of bread and macaroni bread and durum wheat varieties are used. Because, the quality of wheat affect the quality of the flour used in bread and macaroni. The mixing of wheatgrass causes both the quality of the macaroni to decrease and the cost of the seed to increase. Therefore, both wheat varieties need to be classified precisely. At this point, quality and cost for bread and macaroni reach the desired level [3].

It is very important to determine the quality of the products in the marketing of wheat products. Protein is the most important factor affecting the quality of wheat varieties. For this reason, it is necessary to classify wheat varieties and to use each wheat varieties to produce suitable crops. Therefore, the classification of wheat varieties is important both for producers and consumers due to the quality of the crop. Traditional classification methods are both slow and difficult. Furthermore, the results obtained from the classification are not at the desired level. For this reason, such classification processes have been carried out automatically by computer-aided systems in recent years. In this way, faster and more reliable results are obtained [4].

Many works have been done up to now to automatically classify grain products. In the study of Olgun et al., the Dense Scale Invariant Features (DSIFT) method was used for feature extraction. The features obtained from this feature detector are classified by Support Vector Machines (SVM). In this study there are 40 classes and 160 properties of each class are obtained. As a result, an accuracy rate of 88.3% was obtained [5]. In a study by Taner et al., An ANN model was developed to classify durum wheat varieties. As the input parameters, thousand kernel weight, geometric mean diameter, sphericity, grain volume, surface area, volume weight, specific gravity, porosity and color output parameter were used. For the M-1 model, the R2 value was found to be 99.99%, the RMSE value was 0.00074 and the mean relative error value was 0.009%. All the results obtained with the M-1 model were found to be compatible with the actual data [1]. Babalik et al. have worked on determining the vitreous of durum wheat using image processing techniques [6]. Hernandez and Gil used discriminative analysis and K-nearest neighborhood algorithms in the classification of wheat and barley seeds and obtained successful results [7]. Pazoki et al. used adaptive networks based on fuzzy neural networks and fuzzy logic systems, which are artificial intelligence techniques, in the classification of rice grain. The morphological and morphological characteristics of the rice

grains were applied as an input to the net and they made five kinds of rice classification [8]. In the application of Abdullah and Quteishat, the proposed system aims to classify three different wheat seeds. The proposed system uses Multilayer Artificial Neural Networks for classification. Features given as input to ANN system are area, minor axis length, main axis length, equivalent diameter, environment and entropy. The features obtained from image processing. Experimental results show that the proposed classification system is able to classify wheat seeds with a test accuracy of approximately 95% [9]. In the study performed by Yasar et al., the types of wheat seeds were classified by ANN approach. The ANN system used 7 inputs, 10 hidden neurons and one output. Kama, Rosa and Canadian wheat varieties were analyzed by measuring the geometrical properties obtained by X-ray technique. The properties obtained are area, environment, core length, asymmetry coefficient, compactness. As a result of the ANN, the train result was 99.99% and the test result was 99.78% in the regression process of 210 data [10]. Finally, Bagheri and Nikparast mentioned the significance of computer-based seed identification in the revision study and the various studies made in this subject. For artificial learning, they describe the use of morphological features such as shape, size, color and texture in the identification of seeds, as well as the approaches used for seed identification [11].

The above-mentioned studies were performed by using image processing. Computer aided systems were used in this study. Classification of two different wheat species was performed by using image processing techniques. The classification process was performed with a program prepared in the Matlab GUI interface. 200 wheat grains were used in classification process. With the help of image processing techniques, seven features were extracted from each wheat grains. Width, height, area, perimeter, roundness, width//height and perimeter/area were used as input for training and testing. Classification of wheat grains was carried out the ANN and ELM models. Then the performances of these methods are compared with each other.

2. MATERIAL AND METHODS

Obtaining Data and Production of Pictures

Within the scope of the project bread and durum wheat varieties grown in Konya region have been provided. A mechanism has been established to obtain the shape characteristics of these wheat grains (width, height, area, perimeter, roundness, width//height and perimeter/area). Computer, camera, box and lighting system are used in this system. The computer has an Intel Core i7 CPU with 3.1 GHz and 8 GB DDR3 RAM. The camera is full HD with 15 MP resolutions. The designed apparatus is shown in Fig. 1.



Figure 1. System designed to produce images

Image Processing and Future Extraction

Using the apparatus shown in Fig. 1, RGB images of 200 wheat grains (100 for bread and 100 for durum) were obtained. These images were then digitized.

Image features were obtained using image processing techniques. For this reason, each image obtained is converted from RGB color space to gray color space. Then, the threshold value was determined with the Otsu method [12] to obtain a black and white image. Thus, each wheat image is transformed into binary values (black (0) - white (1)). Morphological operations [13] were applied to these images to reduce noise. Then, each wheat grain was counted and the properties of each of these wheat grains were extracted. These features are given as input to ANN and ELM methods. The images obtained by image processing techniques are shown in Fig. 2.

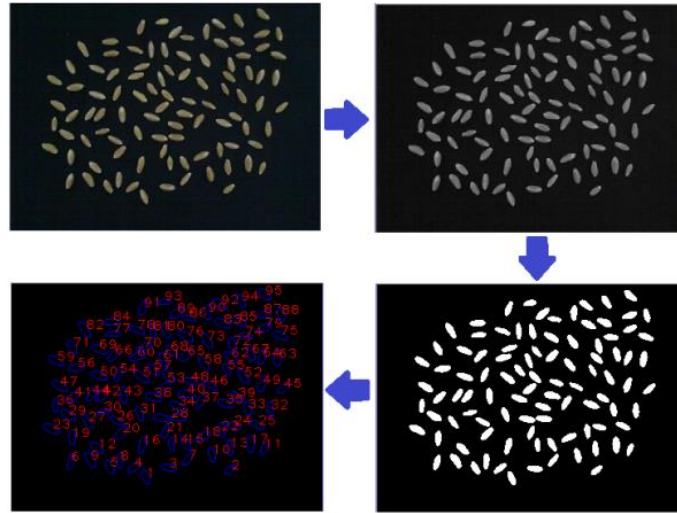


Figure 2. Steps of image processing techniques

Matlab Graphical Interface (GUI)

Matlab is a software development tool designed for the analysis and solution of technical calculations and mathematical problems. Matlab GUI is an interface that allows the user to interact with the program by using visual objects (button, edit text, static text, etc.). In this study, the accuracy values of ANN and ELM models were obtained using a GUI interface and graphically plotted. The prepared GUI interface is shown in Fig. 3.

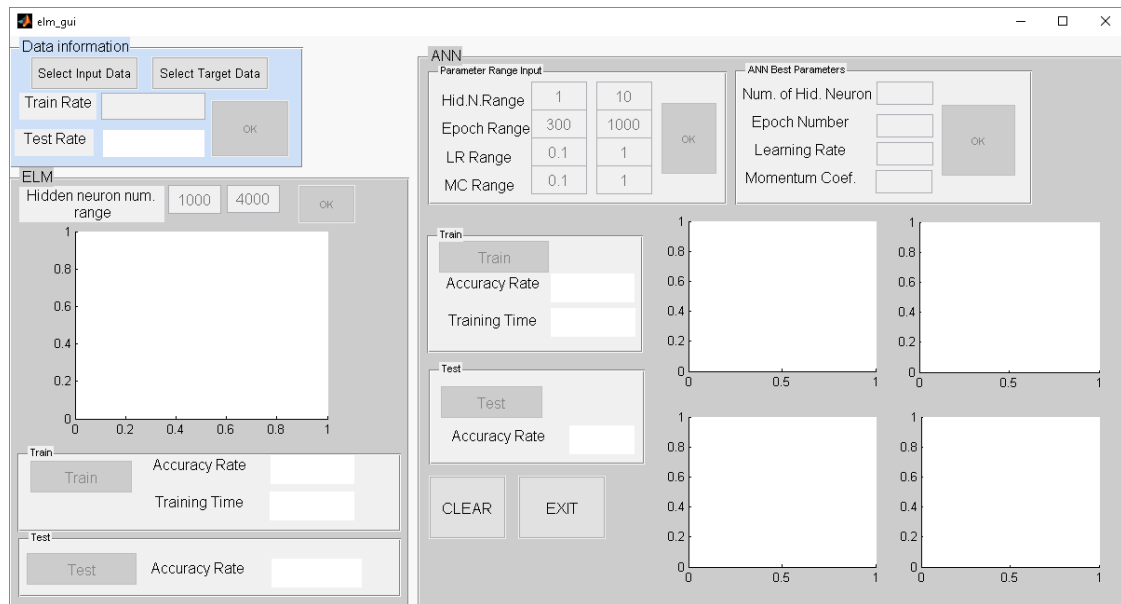


Figure 3. Designed GUI interface

Artificial Neural Network

ANN is a research field of artificial intelligence technique. Processing of information in ANN is performed through neurons. The neurons are connected to each other by weighted connections (see Fig. 4). An ANN basically consists of an input layer, a hidden layer, and an output layer. Input data is applied directly to the input layer, that is, the number of input neurons must be equal to the number of each different input sample. Then, this data passes from operations such as addition, multiplication and activation function reaching the output layer. Finally, these data are given directly to the output layer. More than one hidden layer can be used in ANN depending on transaction complexity. One hidden layer was used in our work. The basic structure of ANN is presented in Fig. 4 and each circle represents a cell.

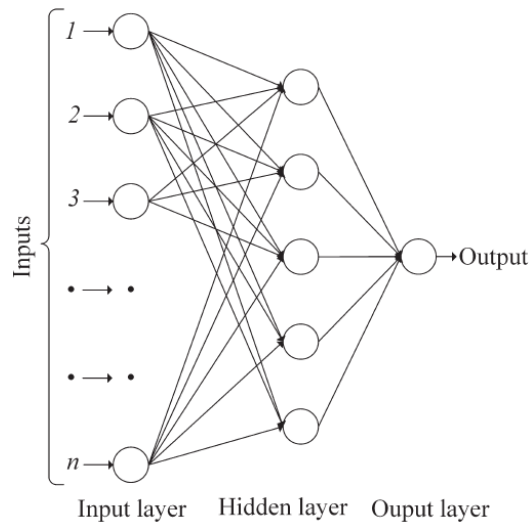


Figure 4. ANN structure

In our study, as input data, the width, height, area, perimeter, roundness, width//height, and perimeter/area properties obtained from each bucket were used. For training and testing data, these seven features were used as input. 70% of the wheat dataset were used as training data and 30% were used as testing data. As a target data, each kind of wheat was used.

Extreme Learning Machines

In this article, ELM, which is the supervised learning method, is used for wheat classification.

This section will briefly discuss the ELM method introduced by Huang et al. [14]. This method is used in classification and regression processes. It is a method that allows extremely fast training and testing operations. It does not have limitations like learning rate, local minimum, moment coefficient, as in ANN. It has advantages over other methods in terms of fastness and high accuracy.

ELM actually has an ANN network structure with a single hidden layer (see Fig. 5). Weights and thresholds are assigned randomly, as in ANN. These weights are not changed afterwards. Operations are performed according to the initial weights and threshold values.

Inputs in the ELM are features derived from the data available. The data used as the output is also the target data. Since the weights are also randomly assigned, the main purpose here is to find the Beta coefficient (see Fig. 5). Beta coefficients are generated during the train phase and then the same coefficient is used during the test phase. Moore-Penrose generalized inverse is used to find beta coefficients [14]. As a result of obtaining the Beta coefficients, the network becomes trained. That is, there is no iterative calculation in the ELM. For this reason, it has a great advantage in terms of train speed.

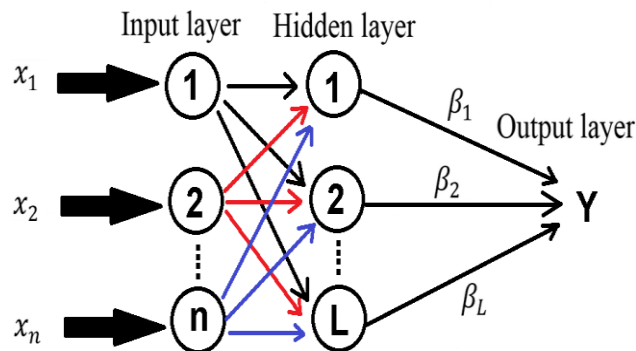


Figure 5. ELM structure

3. RESULTS AND DISCUSSION

In this study, classification of two different types of wheat, bread and durum wheat were carried out. The features obtained from image processing are used for classification. The classification process was performed with a program prepared in the Matlab GUI interface. The wheat grain dataset consists of two equal group as bread and durum and each group has 100 instances. With the help of image processing techniques, seven properties were obtained from each wheat: width, height, area, perimeter, roundness, width/height and perimeter/area. For training and testing data, these seven features were used as input. Classification was performed using ANN and ELM. Then the performance of these artificial intelligence techniques are compared with each other. 70% of the wheat dataset were allocated for training and 30% for testing. The prepared GUI interface and result values are shown in Fig. 6.

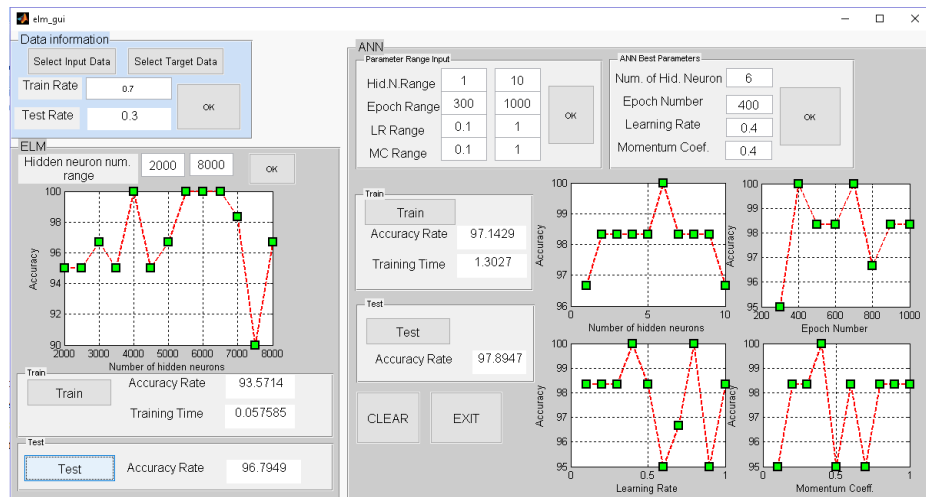
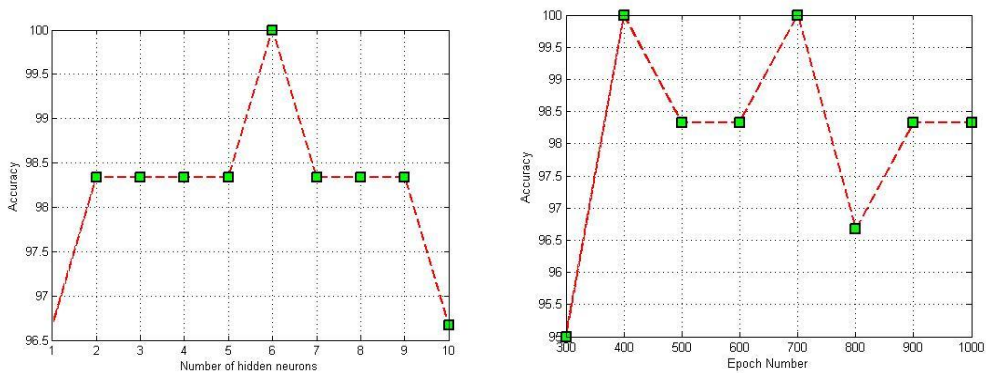


Figure 6. Designed GUI and accuracy values

More than one hidden layer can be used in ANN depending on transaction complexity. One hidden layer was used in our work. In ANN there are parameters directly affecting the performance of the system. By changing these parameters, it is tried to create systems with least faults. These parameters are learning rate, momentum coefficient, number of hidden neuron, and iteration number. In our work, the range of these values is entered into the GUI interface, and the best accuracy values are calculated. Then, the average accuracy value is obtained by taking the average of these accuracy values. Fig. 7 graphically shows the accuracy values obtained by changing these values within a certain range.



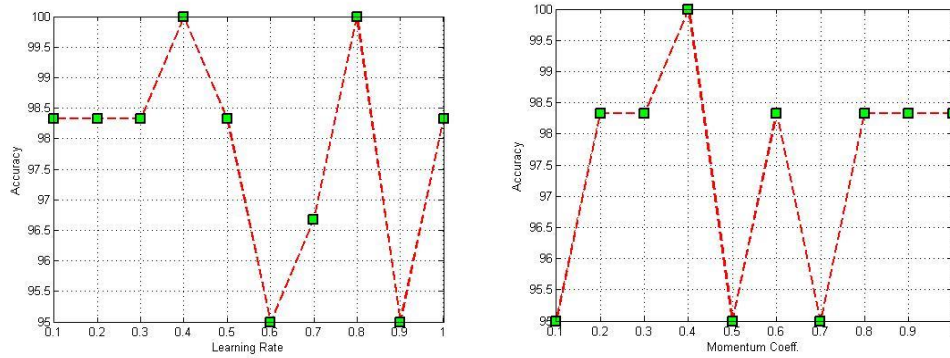


Figure 7. Accuracy values according to changing parameters for ANN

In the ELM method, there are no parameter limitations as in ANN. Because ELM is not a method based on iteration. Beta values are calculated directly, without iteration. The number of hidden neurons is the factor that affects performance in the ELM method. The accuracy graph obtained by changing the number of hidden neurons within a certain range is shown in Fig. 8. When the graphs were examined, high accuracy values were obtained with both learning methods. Then, the average accuracy values were obtained by averaging the accuracy values.

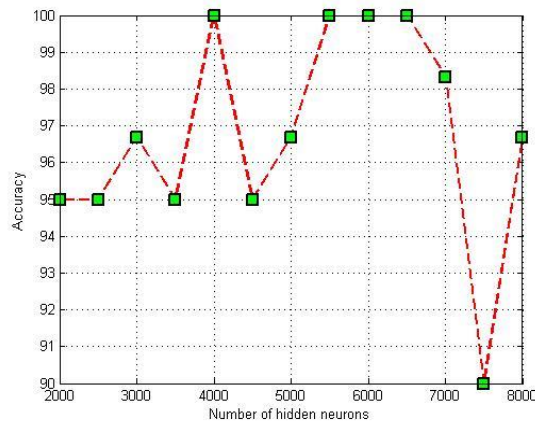


Figure 8. Accuracy values according to number of hidden neurons for ELM



4. CONCLUSION

As a result of the study, in the classification process with ANN, the training accuracy rate was 97.14%, the training duration was 1.3 seconds and the test accuracy rate was 97.89%. These values were calculated for ELM, with a training accuracy rate of 93.57%, a training time of 0.0575 seconds and a test accuracy rate of 96.79%. As it is clear from the values, the accuracy values of both learning algorithms are close to each other. More accurate values were obtained by ANN method. Nevertheless, ELM has a great advantage over time in terms of ANN.

REFERENCES

- [1] A. Taner, A. Tekgüler, H. Sauk, 2015. Classification of durum wheat varieties by artificial neural networks. *Anadolu Tarım Bilimleri Dergisi*, 30 (1) 51-59.
- [2] Anonymous, 2008. <http://www.fao.org>.
- [3] K. Sabanci, A. Toktas, and A. Kayabasi, 2017. Grain classifier with computer vision using adaptive neuro-fuzzy inference system. *Journal of the Science of Food and Agriculture*, doi:10.1002/jsfa.8264.
- [4] A. Pourreza, H. Pourreza, M. H. Abbaspour-Fard, H. Sadrnia, 2012. Identification of nine Iranian wheat seed varieties by textural analysis with image processing. *Computers and Electronics in Agriculture*, 83 102-108.
- [5] M. Olgun, A. O. Onarcan, K. Ozkan, S. Isik, O. Sezer, K. Ozgisi, N. G. Ayter, Z. B. Basciftci, M. Ardic, O. Koyuncu, 2016. Wheat grain classification by using dense SIFT features with SVM classifier. *Computers and Electronics in Agriculture*, 122 185-190.
- [6] A. Babalik, F. M. Botsali, 2010. Yapay Sinir Ağı ve Görüntü İşleme Teknikleri Kullanarak Durum Buğdayının Camsılığının Belirlenmesi. *Selçuk-Teknik Dergisi*, 163-174.
- [7] F. Guevara-Hernandez, J. Gomez-Gil, 2011. A machine vision system for classification of wheat and barley grain kernels. *Spanish Journal of Agricultural Research*, 9 (3) 672-680.



- [8] A. R. Pazoki, F. Farokhi, Z. Pazoki, 2014. Classification of rice grain varieties using two artificial neural networks (MLP and Neuro-Fuzzy). *The Journal of Animal & Plant Sciences*, 24 (1) 336-343.
- [9] N. A. Abdullah and A. M. Quteishat, 2015. Wheat Seeds Classification using Multi-Layer Perceptron Artificial Neural Network. *International Journal of Electronics Communication and Computer Engineering*, 6 (2) 306-309.
- [10] A. Yasar, E. Kaya, and I. Saritas, 2016. Classification of Wheat Types by Artificial Neural Network. *International Journal of Intelligent Systems and Applications in Engineering*, 4 12-15.
- [11] A. Bagheri and Y. Nikparast 2017. Seed Identification by Artificial Vision: A Review. *Biological, Environmental and Agricultural Sciences*, 1 (1) 28-32.
- [12] N. Otsu, 1979. A threshold selection method from grey-level histograms. *IEEE Transactions on Systems, Man, and Cybernetics*, 9 (1) 62-66.
- [13] W.M. Hafizah and E. Supriyanto 2012. Automatic generation of region of interest for kidney ultrasound images using texture analysis. *International Journal of Biology and Biomedical Engineering*, 6 (1) 26-34.
- [14] G. B. Huang, Q. Y. Zhu and C. K. Siew, 2004. Extreme Learning Machine: A New Learning Scheme of Feedforward Neural Networks. *IEEE*, 985-990.



Engineering Materials For The Improvement Of Thermal Comfort During Immersion

Vesna Marija Potočić Matković^{*1}, Ivana Salopek Čubrić² and Goran Čubrić³

^{1,2,3} University of Zagreb, Faculty of Textile Technology, CROATIA.

(E-mail: marija.potocic@ttf.hr, ivana.salopek@ttf.hr, goran.cubric@ttf.hr)

Corresponding Author's e-mail: marija.potocic@ttf.hr

ABSTRACT

A wetsuit is a garment worn by divers, surfers, windsurfers, canoeists, and others engaged in different water sports. Considering the characteristics, such suits must be soft, elastic, of high tensile strength, strong tear resistance and with optimal thermal protection. In this investigation, thermography is used to measure changes in upper body temperature of divers wearing thick neoprene diving suit. According to the results, highest body skin temperature before immersion was recorded in central upper chest body zone, then in left and right upper chest. Highest temperature drop was recorded in the first 5 minutes of immersion in water, especially in a zone of neck. After 25 min of immersion, lowest skin temperature was recorded in the zone of neck and it was 17% lower than before immersion. The outcomes of research will facilitate the process of designing wetsuits in order to increase/decrease thermal insulation in the zones that are identified and finally to maintain optimal thermal comfort.

Keywords: textile; neoprene; thermography; comfort.

[2]. Neoprene's burn point is around 260°C [3]. There is no hazard in skin contact, no toxic effects are known, it is stable under normal temperature und pressures.

It was widely used in aircraft and automobile parts, sports equipment, thermal insulation materials, biomedical materials and the insulating layer of microelectronic circuits and other areas [4]. Neoprene foam can be produced in either closed-cell or open-cell form. The closed-cell form is waterproof, less compressible and more expensive. The open-cell form can be breathable. The insulation properties depend on bubbles of nitrogen gas enclosed within the material, which reduce its ability to conduct heat (fig. 1).

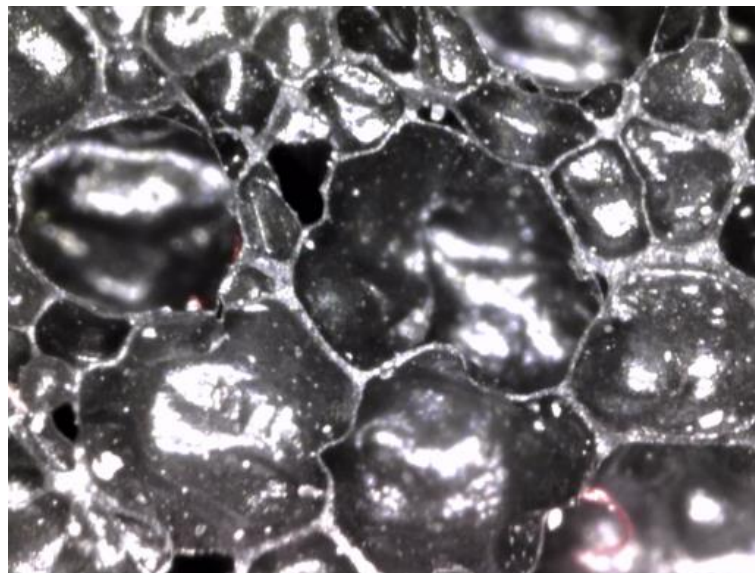


Figure 1. Bubbles enclosed within the neoprene material

The bubbles also give the wetsuit a low density, providing buoyancy in water. Regular neoprene foam is soft and stretchable, ozone resistant. Neoprene developed for deep sea diving is more compression resistant. Neoprene foam with heaviest density, hardness and higher strength is used for boots, orthopaedic and sport support products. Fire retardant neoprene is used for life jackets. Lighter and more stretchable than regular neoprene is used for surfing and triathlon suits [2]. Therefore neoprene sheet intended for wetsuit can have

density of 0,15 to 0,25 g/cm³, tensile strength of 0,5 to 13,0 MPa and elongation from 100% up to 800%.

2. DIVING SUITS AND HEAT TRANSFER

Wetsuits are designed to protect divers from underwater environment and to reduce the thermal shock that may happen during the stay in the cold water. The clothing plays important role in the maintenance of heat balance because it modifies the heat loss from the skin surface [5]. Normally, heat transfer between the human body and environment is regulated by the following mechanisms: conduction, convection, radiation and evaporation. When the human body is in the water, two among defined mechanisms play the most important role – conduction and convection. Conduction is probably the most common mechanism of heat transfer that regularly occurs in the nature and appears between objects that are in direct contact. When the body is immersed, the heat transfer by conduction occurs between the and surrounding water. In comparison to the air, the thermal conductivity of water is 25 times greater. Water also has ability to absorb body heat approximately 3500 times greater than air of the same volume [6]. In the water, the heat transfer trough convection is caused by currents or due to movements through the water. It also needs to be pointed out that the heat transfer by convection is significantly higher in windy conditions and when waves are intensive. Finally, evaporation also contributes as a mass transfer by convection [6].

The normal temperature of the human body, that is maintained trough the mechanism of thermoregulation, is in the range 36.5 to 37.5 °C. In the cold conditions, like those that are normal for divers, the human body dissipates more heat than it absorbs. When the core temperature drops below 35.0 °C, the of the body is in the condition of mild hypothermia. Such condition should be treated with warm clothing, physical activity and warm drinks. The following stage of hypothermia is called moderate hypothermia and it should be treated using intravenous fluid. The most complicated type of hypothermia is called severe and it requires cardiopulmonary resuscitation, extracorporeal membrane oxygenation and even use of cardiopulmonary bypass [7].

Wetsuits are typically worn where the temperature of water is in the range 10-25°C. They provide thermal protection that depends of the level of fit, meaning that suit that is too loose on the body may not be thermally efficient. Such suits have some additional limitations among which should be pointed out the fact that water can enter the suit and increase the level of thermal discomfort. Wetsuits are made of neoprene in different thicknesses. There is a number of different wetsuits suits, but generally, suits can be divided into the following groups:

- Semi-dry suits and

- Hot water suits.

The temperature range for semi-dry suits is within 10-20°C. The advantage of such suits is the fact that suits are equipped with seals that limit the volume of water that enters into the suit and retain it for a while between the body and suit. The retained water is warmed, so diver, although in wet condition, does not suffer from cold. Semi-dry suit is produced of thick neoprene.

Hot water suits are similar to wetsuits, but they do not fit perfectly, as the wetsuits usually do. Normally, they are produced of foamed neoprene.

Additionally, during the immersion, divers may also use the dry suits and dive skins. For the most extreme conditions, dry suits are recommended. The temperature range for such suits is between -2 and + 15 °C. The construction of neoprene dry suit provides certain insulation even if the suit floods completely [8].

Dive skins are normally used where the water temperature is higher than 20.0 °C, so in comparison to other suits, they provide restricted thermal protection. For some divers, it is common to wear such suit under a wetsuit what provides additional wear comfort and maintains optimal thermal protection [9]. Dive skin suits are produced of elastane yarns.

Taking all into account, there is a significant challenge for engineers and designers to design diving suit that will be at the same time waterproof, with optimal fit and thermal comfort.

3. PERFORMANCE OF DIVING SUITS: THERMAL PROTECTION MEASUREMENTS

For the last decades, different testing methods for measurement of wetsuits and their thermal characteristics have been studied by scientists. Generally, the methods can be divided into two main groups:

- a) method for measurement using thermal manikins (i.e. objective method)
- b) wear trials using human participants.

Due to the fact that the measurements of wetsuits should be performed in real-life conditions, the use of thermal manikins has certain advantage. Namely, when compared with human trials, the most important advantage is the fact that thermal manikins can be used in extreme conditions that can harm participants and are considered to be unethical to use in human trials. Among these conditions are exposure to toxic and corrosive chemical environments, flash fires, hot liquids and hot water, extremely cold water and extreme weather conditions, etc

[10]. Among other advantages, it should be pointed out that thermal manikin can act as a standardized subject [10]. The table 1 gives overview of some main characteristics of two thermal manikins – submersible thermal manikin NEMO and thermal manikin TIM.

Recently, a number of investigations focused at the differences between manikin and humans have been conducted. Still, there is very limited research that will make attempt to address inter-manikin differences and manikin-human correlation in order to help to understand measurement differences and provide appropriate recommendation for the development of applicable standards for suits [11]. Among such investigations should be pointed out the pilot study that made the comparison of measurements using two manikins (NEMO and TIM) and wear trials. In the study, the heat losses (expressed as local heat transfer coefficients or local insulation values) were compared for two manikins and two human subjects wearing immersion suits with three different levels of closed cell foam insulation in two floatation positions. The results of study indicated that the variation in local heat transfer coefficients was likely due to the effects of differences in fit, folds or wrinkles in the suit materials, and was essentially random. According to the authors, these random differences then tended to average out in the calculation of the overall resistance. Finally, it is concluded that the heat loss from the manikins was a good representation of the heat loss from humans [11]. Other investigations were focused on human trials wearing wetsuits. Hall et al. compared performance and body temperature of triathletes swimming in water at 14°C with and without wetsuit. Four athletes out of ten were unable to complete swimming without wetsuit. Also, there was a significant difference in linear temperature rate change and total temperature rate change between swimming without and with wetsuit [13].

Table 1. Comparison of thermal manikins [11, 12]

	NEMO	TIM
Surface area, m ²	1.86	1.80
Height, mm	1770	1778
Weight, kg	70.0	94.5
Number of zones	23	15

Shell material	Aluminium	Aluminium
Power	60Hz electrical power	AC -
Producer	Measurement Technology Northwest (USA)	CORD Group (Canada)

Pavlik et al. also tested wetsuits on triathletes. They claim that wearing a wetsuits improves the swimmer performance [14]. The results of Tomakawa et al. suggest that wearing of wetsuit improve swimming performance and propulsion efficiency and, at the same time reduces energy consumption in swimming portion [15]. Prado et al. investigated the effects of wearing a wetsuit on resting cardiovascular measures. They observed that mean arterial pressure was greatest when the smallest wetsuits was worn (compared to swimming without wetsuit), [16]. Maraboti et al. also evaluated the possible cardiovascular and respiratory effect but in dry conditions. They observed a significant decrease in heart rate and cardiac output and a significant increase in total peripheral resistances [17].

Some researchers investigated wearer satisfaction when wearing diving suits. Kim et al. analyzed 15 items measuring importance of wetsuits and concluded that for female and older divers functional performance of wetsuits is more important than for male and younger divers [18].

4. METHODE USED IN STUDY

Infrared thermography is gaining popularity among the researchers in various fields. In the field of textiles, the potential of thermography is used to observe the production process, material properties, clothing comfort, failure and product development [19, 20].

In this investigation, thermography is used to observe the changes in body temperature of divers wearing neoprene diving suit immersed in sea water. For the measurement is used thermal camera FLIR E5 [21]. The specifications of used camera are given in the Table 1.

Table 2. IR camera specifications [20]

Imaging and Optical Data	
IR Resolution	120 × 90
MSX Resolution	320 × 240
Thermal Sensitivity	<0.10°C
Field of View	45° × 34°
Detector	Uncooled Microbolometer
Screen	3.0 in. 320 × 240 color LCD
Frame Rate	9 Hz
Analysis	
Image Modes	IR image, visual image, MSX, thumbnail gallery
(MSX)	IR image with enhanced detail presentation
Temperature Range	0° to 150°C (Standard Range is -20°C to +250°C (-4°F to +482°F))
Emissivity Correction	Variable from 0.1 to 1.0

The observed body zones of divers are neck, right shoulder, right upper chest, central upper chest, left upper chest and left shoulder. The zones are defined on the basis of body mapping proposed by Smith & Havenith [22] and shown on the figure 2. The temperature of skin for

each observed body zone is recorded after different intervals of immersion in water, i.e. 5, 10, 15 and 25 minutes.

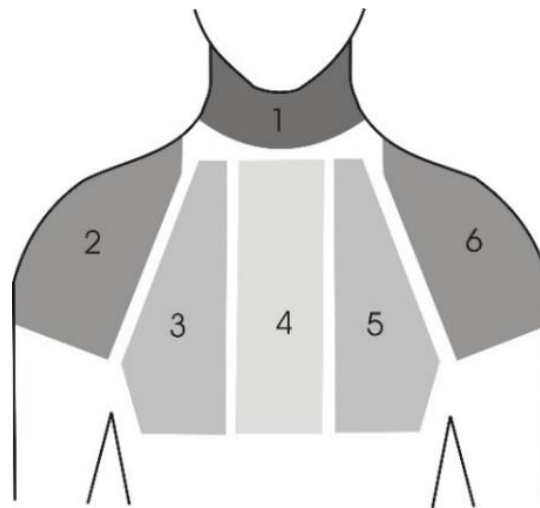


Figure 2. Observed body zones

5. RESULTS AND DISCUSSION

In the results section are presented results of measurement on male diver who was wearing 7 mm thick neoprene diving suit. Temperature of water during all cycles of immersion was 18,4 °C. The thermogram of diver's upper body taken before the before immersion is given in fig. 3.

The figure 4 gives the overview of temperatures recorded after 5, 10, 15 and 25 min of immersion in the water, for each observed body zone.

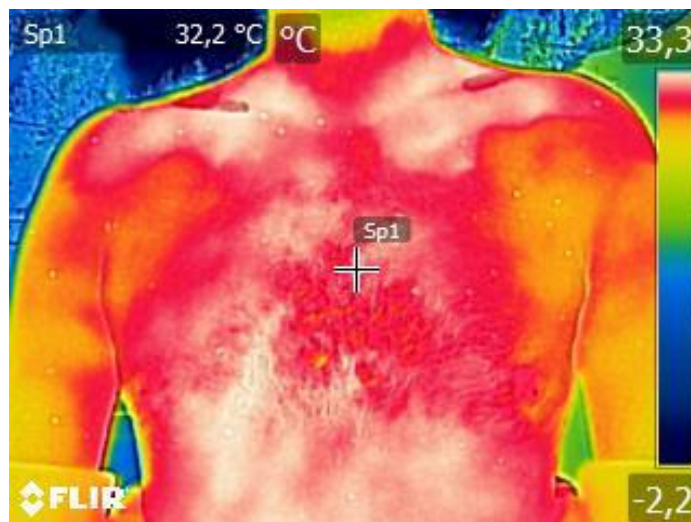


Figure 3. Thermal image of diver

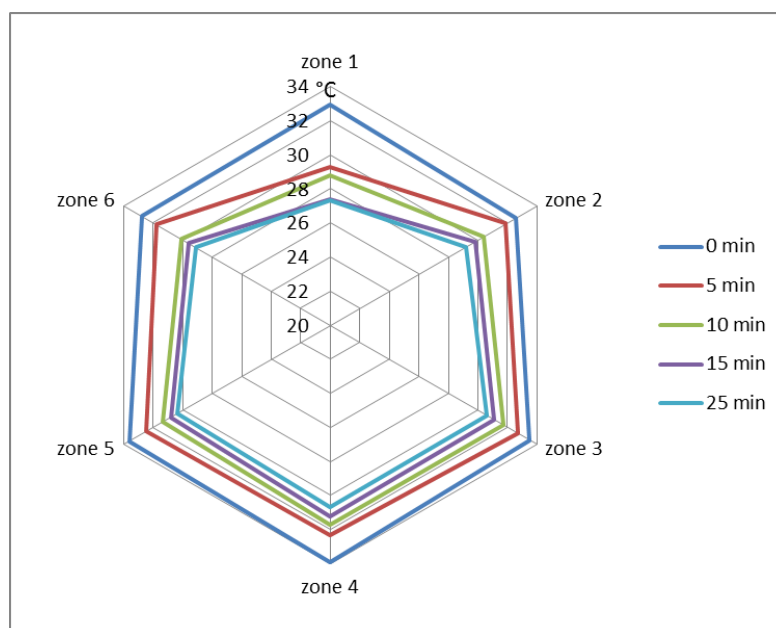


Figure 4. Distribution of temperatures



6. CONCLUSION

Before immersion, highest body skin temperature was recorded in a central upper chest body zone, then in left and right upper chest, neck, while lower temperatures were recorded in left and right shoulders (fig.4).

Highest temperature drop was recorded in a first 5 minutes of immersion in water, especially in a zone of neck. It has to be noted that neck was the only zone uncovered by diving suit.

After 25 minutes of immersion, the lowest skin temperature was recorded in the zone of neck - 27,3 °C, what is 17% lower than before immersion (fig. 4, zone 1). Highest skin temperature, after 25 min of immersion in the water, was recorded in a central upper chest body zone - 30,7 °C, what is 9,4 % lower than before immersion (fig. 4, zone 4).

The outcomes of research will facilitate the process of designing wetsuits in order to increase/decrease thermal insulation in the zones that are identified and finally to maintain optimal thermal comfort.

Future investigations will include measurement of temperature drop in observed body zones caused by immersions in different water temperatures and by wearing neoprene wetsuits of different thicknesses.

ACKNOWLEDGMENT

The research is supported by University of Zagreb.

REFERENCES

- [1] Neoprene (CR) chemical compound, Available at <https://www.britannica.com/science/neoprene>. Retrieved July 6, 2017.
- [2] M. H. Yeh, W. S. Hwang and L. R. Cheng, 2007. Microstructure and mechanical properties of neoprene–montmorillonite nanocomposites, *Applied Surface Science*, 253, 4777–4781.
- [3] Neoprene, Available at <https://en.wikipedia.org/wiki/Neoprene>. Retrieved July 6, 2017.
- [4] W. Yiming *et al.*, 2011. *Study of High-Performance Chloroprene Sponge in Diving Suit Application*, Proceedings of a meeting 2011 International Conference on Future Computer Science and Education, Xi'an, China.
- [5] B. Mijović, Z. Skenderi and I. Salopek, 2009. Comparison of Subjective and Objective Measurement of Sweat Transfer Rate, *Collegium antropologicum*, 33 (2) 315-320.



- [6] M.A. Lang and R. Robbins, Scientific diving under ice: a 40-year bipolar research tool, *The international polar year science 2007–2008*. Smithsonian Institution Scholarly Press, Washington DC, 2007.
- [7] D.J. Brown *et al.*, 2012. Accidental hypothermia, *The New England Journal of Medicine*. 367 (20) 1930–1938.
- [8] D.F. Brewster and J.A. Sterba, 1988. *Market Survey of Commercially Available Dry Suits*, US Naval Experimental Diving Unit Technical Report, NEDU-3-88
- [9] Ecostinger, What is the difference between stinger suit, dive skin, wetsuit, drysuit and dive suit, Available at <http://www.ecostinger.com/blog/what-is-the-difference-between-stinger-suit-dive-skin-wetsuit-drysuit-and-dive-suit/>. Retrieved July 5, 2017.
- [10] H. Zang and G. Song, 2014. Performance of immersion suits: A literature review, *Journal of Industrial Textile*. 44 (2) 288-306.
- [11] L. Mak, *et al.*, 2010. *Thermal protection measurement of immersion suit comparison of two manikins with humans pilot*, Technical Report, no. TR-2010-06, National Research Council, Canada
- [12] Measurement Technology Northwest: Submersible thermal Manikin, MTNW, Seattle, 2016.
- [13] J. Hall *et al.* 2015. Thermal response of triathletes to 14°C swim with and without wetsuits. *Extreme Physiology & Medicine*. 4 (1)
- [14] J.Pavlik, M. Pupiš and R. Pavlović, 2015. Variability of swimming performance depending on the use of wetsuits. *Research in Physical Education, Sport & Health*. 4 (2) 51-55.
- [15] M. Tomikawa, Y. Shimoyama and T. Nomura, 2008. Factors related to the advantageous effects of wearing a wetsuit during swimming at different submaximal velocity in triathletes, *Journal of Science and Medicine in Sport*. 11 (4) 417-423,
- [16] A. Prado *et al.* 2017. A first look into the influence of triathlon wetsuit on resting blood pressure and heart rate variability, *Biology of Sport*. 34 (1) 77-82.
- [17] C. Marabotti, *et al.* 2017. Cardiovascular and respiratory effects of the neoprene wetsuti in non-immersed divers, *Undersea and Hyperbaric Medicine*. 44 (2) 141-147.
- [18] D-E. Kim, D. Michaelson and Y. Ha, 2015. *Selection Criteria for Scuba Driver's Wetsuits*, International Textile and Apparel Association Annual Conference Proceedings, Iowa StateUniversity.



- [19] I. Salopek Čubrić, G. Čubrić and V.M. Potočić Matković, 2016. *Thermography Assisted Analysis of Textile Materials as a Predictor of Human Comfort*, Book of Proceedings of the 6th International Ergonomics Conference ERGONOMICS 2016 - Focus on synergy, Zagreb, Croatian Ergonomics Society.
- [20] I. Salopek Čubrić, G. Čubrić and V.M. Potočić Matković, 2016. *Use of Thermography to Analyse the Influence of Yarn Properties on Fabric Drying*, Book of Proceedings of the 7th International Textile Conference, Tirana.
- [21] Flir, “Flir EX- Series Infrared Cameras with MSX,” available at <http://www.flir.com/instruments/ex-series/>
- [22] C. J. Smith and G. Havenith, 2011. Body mapping of sweating patterns in male athletes in mild exercise-induced hyperthermia, *European Journal of Applied Physiology*. 111 (7) 1391-1404.

3rd International Conference on Science, Ecology and Technology

ICONSETE'2017

Rome, ITALY • August 14-16, 2017



UNIVERSITÀ
degli STUDI
di CATANIA



THE PURSUIT OF HISTORY
International Periodical for
History and Social Research

